2011

In situ Assessment of Support and Drainage for PCC Subbase

La Zhao
Iowa State University

In situ assessment of support and drainage for PCC subbase

by

La Zhao

A thesis submitted to the graduate faculty

In partial fulfillment of the requirements for the degree of

MASTER OF SCIENCE

Major: Civil Engineering (Geotechnical Engineering)

Program of Study Committee:
David J. White, Major Professor
Pavana K.R. Vennapusa
Vernon R. Schaefer
Roy Gu

Iowa State University

Ames, Iowa

2011

TABLE OF CONTENTS

LIST OF TABLES

LIST OF FIGURES

ABSTRACT

Design and maintenance of pavement drainage is critical to ensure the long service life of pavements. A minimum assumed coefficient of saturated hydraulic conductivity (K_{sat}) value of the base materials is used to design the aggregate base/subbase layer geometry (i.e., thickness, width and slop). However, k_{sat} is often a single assumed value used during design and is not field verified. k_{sat} is typically either measured on small volume of material in the lab or estimated by using empirical relationships. Both methods do not adequately capture the field variability.

In this study, a gas permeability test (GPT) device that has been recently designed and fabricated at Iowa State University is used to evaluate the hydraulic conductivity of pavement base materials in the field and laboratory. Field studies were conducted on newly constructed base layers projects in IA, MI and PA. Field testing conducted in MI and PA involved capturing the spatial of fines content and k_{sat} variability over a relatively small area (smaller than 10 m by 10m area). Field testing in Iowa involved evaluating the effect of construction operations for placement or granular base/subbase on fine content, k_{sat}, density and stiffness (i.e., number of passes, compaction using vibration, and static compaction). Laboratory studies were conducted using various materials to validate the gas permeability test (GPT) measurements by conductivity conventional laboratory falling and constant head testing. The difference between in situ and laboratory data was compared to complete the design parameter derivations, and effects of the pavement performance.

Results indicated that GPT is repeatable (k_{sat} of COV $\leq$ 1%) on a series of repeatability tests conducted on a material and has a wide range of k_{sat} values (0.1 to 820 cm/sec).

CHAPTER 1. INTRODUCTION

This chapter presents six sections: industry problem, technical problem, research goals objectives, and the significance of this research. The last section describes the organization of this thesis.

Industry Problem

Pavement drainage layer performance is a critical component for ensuring the longevity of pavements. Pavement design generally addresses the removal of water by incorporating a subsurface drainage system which is composed of a drainable aggregate base/subbase layer and longitudinal/transverse drains. In pavement design, the aggregate base/subbase layer geometry (i.e., thickness, width, and slope) is designed using a minimum assumed coefficient of saturated hydraulic conductivity (ksat) value of the base material. Design engineers typically determine ksat value based on empirical relationships or limited laboratory tests (MEPDG 2004).

White et al. (2004) indicated that the in situ k_{sat} of newly constructed base materials has a coefficient of variation of 50% to 400% which is caused primarily due to segregation of aggregate fines during construction. Despite this high coefficient of variation, current specifications do not require any testing to verify that the drainage design assumptions are met because there are no rapid and repeatable in-situ test methods to measure k_{sat}. Therefore, new rapid and effective in situ testing is needed to measure k_{sat} that allows the construction contractor to check the permeability of pavement base/subbase layers during construction.

Technical Problem

Most quality control and quality assurance testing for permeability of base/subbase layers occurs in the laboratory and not in the field. The k_{sat} value is typically assumed based on historical information, empirical relationships with the material gradation parameters, or limited laboratory testing. But previous studies (e.g., White et al. 2004, 2010) have indicated that conventional constant or falling head vertical flow laboratory testing methods are not suitable for testing drainable base materials and empirical relationships are not highly reliable. There is a need for a new laboratory testing method that can effectively simulate the water flow conditions as it occurs in the field.

To address the need for such a method, an in situ gas permeameter test (GPT) device has recently been designed and fabricated at Iowa State University (White et al. 2010) that perform permeability tests in less than 30 seconds. This device also can be used in the laboratory with low pressure heads (< 25 mm of water) to simulate field conditions. White et al. (2010) conducted validation tests that compared GPT and conventional laboratory tests. The expected benefit of this research is allowing engineers to design for drainage quality by using field verification of hydraulic conductivity.

Research Objectives

The three main aspects that ensure good performance of the drainage layers are: (a) selecting appropriate drainage design input parameters (e.g., k_{sat}); (b) conducting field QC/QA to ensure that the design parameters are met; and (c) following proper construction guidelines to reduce segregation of fines and, in turn, the variability of k_{sat} of the drainage layers.

Given the factors providing a good performance of the drainage layers, the objective of this research is to address these four aspects through the following broad research tasks:

- Build on work conducted for the Iowa DOT research project (White et al. 2004) for development of a portable GPT to determine saturated hydraulic conductivity.
- Validate the gas permeameter test (GPT) measurements.
- Study field construction operation for placement or granular subbase and the relationship between compaction and permeability.
- Evaluate field support and drainage change of newly constructed pavement and compare with design assumption.

Results from this research are expected to provide new insights into pavement drainage layers and new testing methods to effectively measure k_{sat} both in laboratory and in situ .

Significance of the Research

Water in and under roads can reduce the mechanical properties (e.g. stiffness) of aggregates and underlying subgrades layers, thereby speeding up the pavement deterioration and leading to costly maintenance and pavement repair. The following factors are key to ensuring maximum performance of the drainage layers: (a) selecting appropriate drainage design input parameters (e.g., k_{sat}), (b) conducting field QC/QA to ensure that the design parameters are met, and (c) following proper construction guidelines to reduce segregation of fines and, in turn, the variability of k_{sat} of the drainage layers.

Currently, design engineers still use an assumed drainage design value based on empirical relationships or limited laboratory tests. However, empirical relationships apply only to a limited range of in situ conditions and materials and limit number of laboratory tests are not suitable enough to predict the variability of field condition. Therefore, both laboratory and in situ measurements are needed to develop the design parameters.

The GPT device is quick, easy and repeatable to determine the saturated hydraulic conductivity in the actual road condition. Laboratory tests in this study will evaluate a number of pavement foundation materials in several states. The hydraulic conductivity test compares the differences between in situ and laboratory data to complete the design parameter derivations, and affects the pavement performance.

Filed studies were conducted at sites in Michigan and Pennsylvania, to investigate moisture content, density and hydraulic conductivity. Field investigation of construction operation for placement or granular subbase and the relationship between compaction and permeability were conducted on I-35, story county, Iowa. Roller intelligent compaction uses a Caterpillar CS563C smooth drum vibration roller to measure machine drive power (MDP). The machines were equipped with real time kinematic (RTK) global position system (GPS) and on board display and documentation systems (White et al. 2010). Properties of different roller pass were evaluated by conducting testing in conjunction with a variety of in situ testing device to measure moisture content, density, hydraulic conductivity (k_{sat}), California bearing ratio (CBR), shear strength and elastic modulus on untrimmed base, trimmed base and mixture of virgin crushed limestone and RPCC test beds.

Organization of the Document

This thesis is presented in five additional chapters. Chapter 2 presents the background information of permeability of drainage layers. Chapter 3 describes the laboratory and in situ test methods used in this researches study. Chapter 4 describes the index properties of the materials used in this study. Chapter 5 presents the results and analysis of laboratory and field testing. Chapter 6 summarizes the conclusions and offers recommendations for future research.

CHAPTER 2. BACKGROUND/LITERATURE REVIEW

This chapter reviews the literature information of the hydraulic conductivity of pavement foundation materials. The literature review consists of four main parts: importance of drainage in pavement systems; types of drainage layers in pavement systems; drainage design; and laboratory and in situ methods.

Importance of Drainage in Pavement Systems

Ultimately, drainage in pavement systems is important because water in and under roads can reduce the mechanical properties in aggregate and soil layers, thereby speeding up the pavement failure and leading to dangerous conditions. Engineers design pavement systems by considering the region's climate conditions, traffic flow, the kinds of vehicles that will pass through the road, and economic factors (Faífsca 2009).

Providing adequate drainage to pavement systems plays an important role on pavement performance. McAdam (1982) observed that many roads deteriorated rapidly when the subgrade was saturated. Cedergren (1988) stated that good drainage can extend the pavement life three or four times and save billion dollars per year in the United States, alone. Forsyth et al. (1978) estimated that good drainage can improve the service life of asphalt and portland cement concrete (PCC) pavements 33% and 50%, respectively.

Water in pavement systems causes the loss of subgrade support, reduces stiffness in the granular layer, erodes base layers, reduces the pavement service life, and contributes to the debonding of pavement layers (Mallela et al. 2001; Christopher et al. 2006). Therefore, water is one of the principal reasons causing the failure of pavements. There are many papers available in the literature with field case studies where water has contributed or accelerated the pavement deterioration (e.g., Mallela et al. 2001; Christopher et al. 2006; Cedregren 1989). Huang (1993) summarized that when water is entrapped in the pavement structure:

1. The strength of unbounded granular materials and subgrade soils is reduced,
2. Pumping of concrete pavements occurs with subsequent faulting, cracking, and general shoulder deterioration.
3. As moving traffic causes high hydrodynamic pressure, pumping of fines in the base course of flexible pavements may also occur with resulting loss of support.

4. When the depth of frost penetration is higher than the pavement thickness (especially in northern climates), during the frost melting period, frost heave and the reduction of load-carrying capacity occurs as a result of high water table.
5. Water causes differential heaving over swelling soils.
6. When continuous contact with water is of subject, stripping of asphalt mixture and "D" cracking of concrete occurs.

Pavement structures generally consist of three layers: surface course, base/subbase course and subgrade (see Figure 1). Surface course is one or more layers of a pavement structure. Surface layer may consist of either asphalt concrete (AC) (also known as flexible pavement) or Portland cement concrete (PCC) (also known as rigid pavement). A wearing surface provides sufficient smoothness, friction resistance, and sealing or drainage of surface water. (Christopher et al. 2006). Subsurface drainage are used for: (1) lowering the ground water level; (2) intercepting the lateral flow of subsurface water beneath the pavement structural; and (3) removing the water that penetrates the pavement surface (NCHRP 2004).

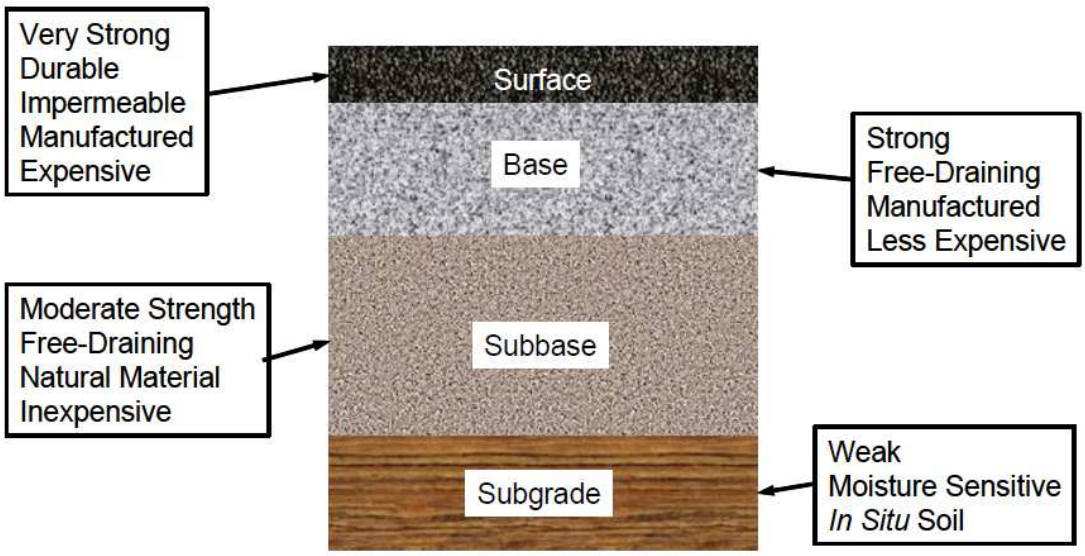

Figure 1. Variation of material quality with depth in a pavement system with idea drainage characteristics (Christopher et al. 2006)

Moisture/drainage problems are among the major distresses in flexible and rigid pavements. Moisture/drainage problems in flexible pavements cause fatigue cracking, rutting, corrugations, bumps, depressions, potholes and roughness. Moisture/drainage

problems in rigid pavements cause fatigue cracking, punch-outs, pumping, faulting, and roughness. Longitudinal cracks and pavement edges in AC cause water penetration into the pavement structure, thus damaging the pavement systems. (Christopher et al. 2006)

In pavement systems, major moisture sources are rain and snow that penetrate through the surface; groundwater fluctuations; meltwater from ice lenses; and water moved from subgrade to base layers by capillary action (Huang, 1993). In addition, high groundwater table is a moisture source for pavement structures and subgrades and it comes laterally from the pavement edges and shoulder ditches. Surface joints, cracks, and shoulder edges also cause rainwater to penetrate into the pavement systems. Sources of moisture in pavement systems are presented in Figure 2.

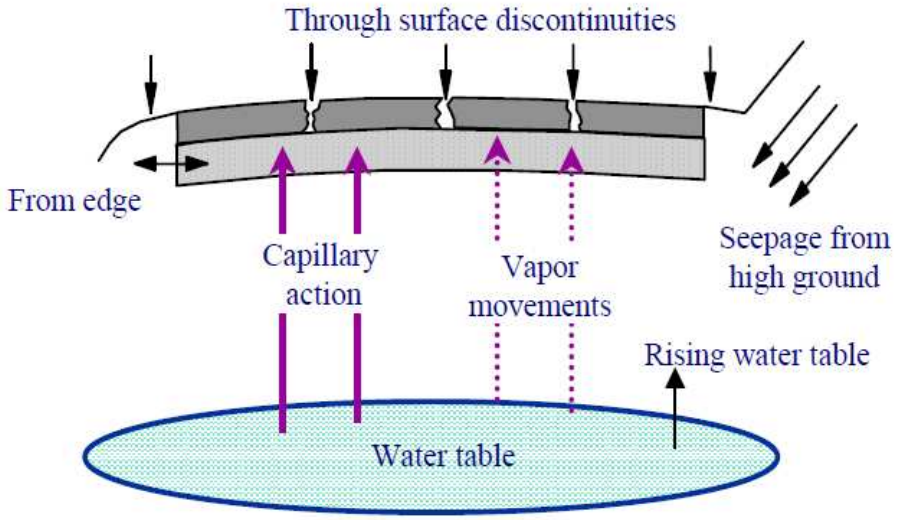

Figure 2. Sources of moisture in pavement systems (Christopher et al. 2006, Mallela et al. 2001)

Drainage design

The purpose of drainage design is to keep the base, subbase, subgrade, and other susceptible paving materials against saturation or even being exposed to constant high moisture level over time (MEPDG, 2004).

Following are the important aspects that require consideration during design and construction for preventing, controlling, or removing moisture penetration into the pavement systems (ACPA 2008b, Christopher et al. 2006, Huang 2000):

1. Prevent moisture penetration in pavement systems.
2. Use materials that are insensitive to the effects of moisture (see Table.1).
3. Incorporate design features to minimize moisture damage.
4. Quickly remove moisture that enters the pavement systems.

To prevent moisture penetration in pavement systems, building cross slope and longitudinal slope are beneficial and effectively sealing pavement joints.

Removal of water in a timely manner is essential for drainage design, therefore appropriate drainage features should be provided. For example, there are different drainage features such as designing under drains and ditches to permanently lower the water table; and permeable bases and edge drains that can rapidly remove the infiltrated water. Pavement base/subbase layers in pavement systems are intended to provide uniform support conditions (with adequate stiffness) along with good drainage characteristics. However, the stiffness and permeability properties of base/subbase layers depend on the material type used. Materials and design features should be insensitive to the effect of moisture. MEPDG (2004) summarized the soil characteristics as pavement materials (see Table 1).

Table 1.Summary of soil characteristics as pavement materials (NCHRP 2004)

Major Divisions	Name	Strength when not subject to frost action	Potential Frost Action	Compressibility & Expansion	Drainage Characteristics
Gravel GW and Gravelly GP Soils	Well–graded gravels or gravel sand mixtures, little or no fines	Excellent	None to very slight	Almost none	Excellent
	Poorly graded gravels or gravel-sad mixtures little or no fines	Good to excellent	None to very slight	Almost none	Excellent
GM	Silty gravels, gravel-sand silt mixture	Good to excellent	Slight to medium	Very slight	Fair to poor
		Good	Slight to medium	Slight	Poor to practically impervious
GC	Clayey gravels, gravel-sand clay mixture	Good	Slight to medium	Slight	Poor to practically impervious
SW	Well-graded sands or gravelly sands, little or no fines	Good	None to very slight	Almost none	Excellent
Sand and SP Sandy	Poorly graded sands or gravelly sands, little or no fines	Fair to good	None to very slight	Almost none	Excellent
	Silty sands, sand – silt mixtures	Fair to good	Slight to high	Very slight	Fair to poor
		Fair	Slight to high	Slight to medium	Poor to practically impervious
Soils	Clayey sands, sand-clay mixtures	Poor to fair	Slight to high	Slight to medium	Poor to practically impervious
Silts& Clay with the Liquid Limit Less than 50	Inorganic silts & very fine sand, rock flour, silty or clayey fine sand or clayey silts with slight plasticity	Poor to Fair	Medium to very very high	Slight to medium	Fair to poor
	Inorganic clays of low to medium plasticity, gravelly clays, sandy clays, silty clays, lean clay	Poor to Fair	Medium to high	Slight to medium	Practically Impervious
	Organic silts & organic silt-clay or low plasticity	Poor	Medium to high	Medium to high	Poor
Silts& Clays with Liquid Limit greater than 50	Inorganic silts, micaceous or diatomaceous fine sand or silty soils, elastic silts	Poor	Medium to very high	High	Fair to poor
	Inorganic clays of high plasticity, fat clays	Poor to Fair	Medium to very high	High	Practically impervious
	Organic clays of medium to high plasticity , organic silts	Poor to very poor	Medium	High	Practically impervious
Highly organic soils	Peat& other highly organic soils	Not suitable	Slight	Very high	Fair to poor

The design of drainage features in pavement systems addresses: (a) the determination of water content expected to penetrate through the pavement systems from various sources as

described above, (b) conducting drainage flow analysis, and (c) determination of drainage capacity of a drainage layer and its geometry (Huang 2000). According to Huang (2000), the design inflow is the sum of the inflows from all sources excluding the outflow through the subgrade soil. Moulton (1980) presented simplified charts to determine the permeability of soil and water table at the boundary which is the outflow through subgrade. Drainage capacity should be designed to make outflow rate greater than the inflow rate so water can be carried out safely from the source to the outlet sites. Drainage capacity is decided based on the collector pipe and drainage layer which have steady-state flow and unsteady-state flow. Baber and Sawyer (in Huang 2000) demonstrated how to calculate the steady-state flow capacity of the drainage layer. Unsteady-state flow capacity is defined by the degree of drainage. It is the ratio of the volume of water drained since the rain stops to the total storage capacity of the drainage layer. Huang (2000) suggested using time for 50% degree of drainage by Casagrande and Shannon (1952). AASHTO 1993 considered the effect of drainage design including the structure layer coefficient (m) on flexible pavements and load transfer coefficient (C_d) on rigid pavements. Those factors are a function of drainage quality and the percentage of time that the pavement structure is near saturation.

$$q = kH(S + \frac{\mathrm{H}}{2\mathrm{L}}) \tag{2.1}$$

Water needs to be removed quickly before any damage occurs. Pavement system design should address the removal of infiltration of free water by vertical flow or lateral subsurface drainage system (Kozeliski 1992). Three critical ways to remove water are layer or blanket, longitudinal drain, and transverse drain (Huang, 1993). Darcy's law governs the moment of water in pavement and it can be applied directly to determine the drainage. Design engineers assume a minimum permeability value in hydraulic design of permeability layer based on the limited laboratory test measurements. Different assumptions and requirements of different design methods are summarized in Table 2. However, none of these methods rely on the field testing to verify if the design assumptions have been met.

Table 2. Permeable coefficient of open graded drainage layer

Design Method	Design value (k_{sat})	
MEPDG 2004 (Recommended Min.)	1000 ft/day	0.35 cm/sec
Christopher et al. (2006) (Recom. Min)	1000 ft/day	0.35 cm/sec
ACPA 2008 (Recommended Target)	50 to 150 ft/day (Max = 350 ft/day)	0.02 to 0.05cm/sec (Max = 0.12cm/sec)

MEPDG (AASHTO 2008) rates the quality of drainage from "excellent" to "poor" depending on the time the drainage layer takes to drain 50% of the water as summarized in Table 3.

Table 3. Permeable base quality of drainage rating based on time taken to drain 50% of the drainable water (after MEPDG)

Quality of Drainage	Time to Drain
Excellent	2 hours
Good	1 day
Fair	7 days
Poor	1 month
Very Poor	Does not drain

MEPDG (2004) software shows a systematic approach to drainage design. The purpose of design is to lead the preparation of cross section with adequate drainage features. A systematic approach for subsurface drainage considerations in new or reconstructed pavement is presented in Figure 3.

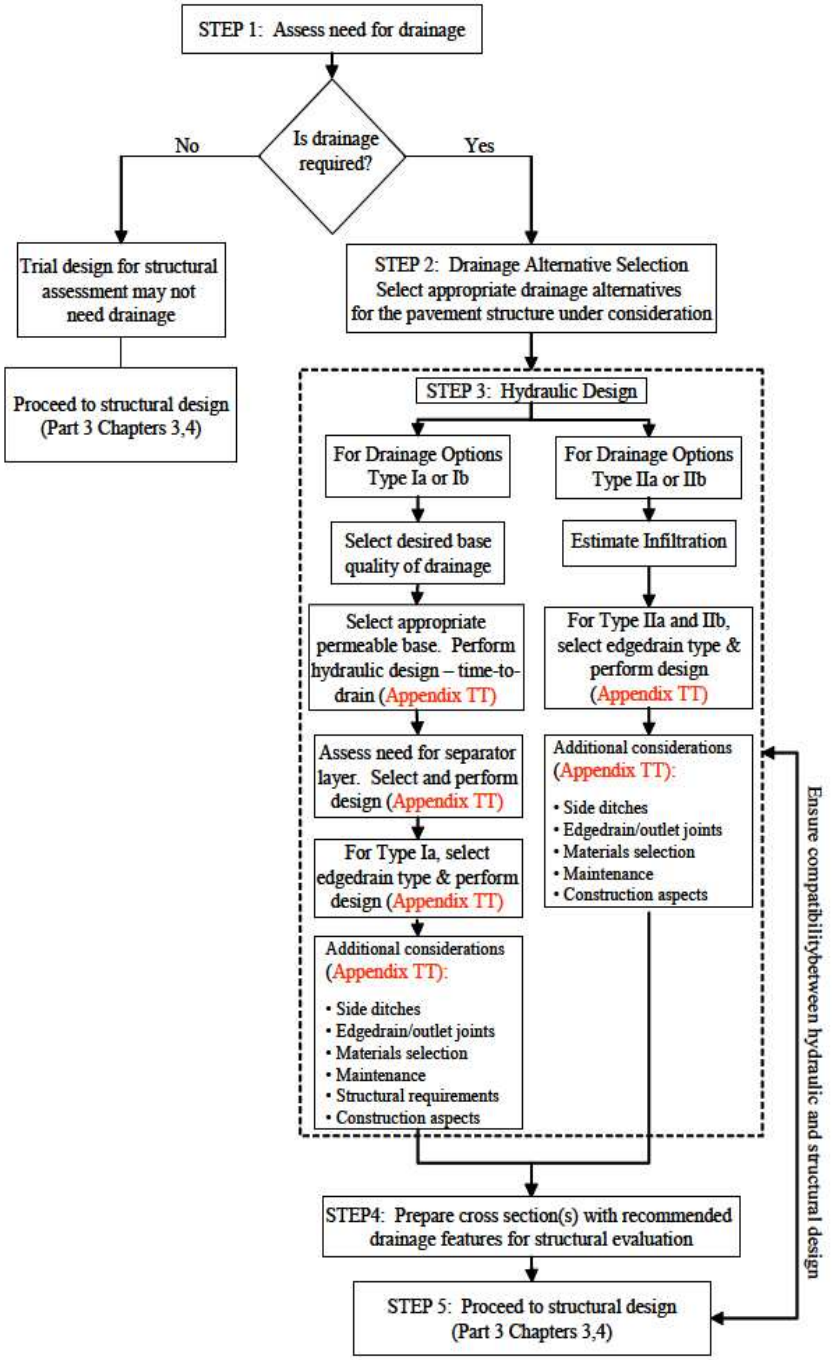

Figure 3. Systematic approach for subsurface drainage considerations in new or reconstructed pavement (MEPDG 2004)

Types of Drainage Layers in Pavements Systems

The prevention of moisture penetration into pavement systems is impractical and expensive. Removing water quickly from pavement systems depends on the permeability of the base, subbase or both (Elsayer et al. 1996). Insensitive materials such as cement treated base, asphalt stabilized base and granular materials with few fines are used for pavement design to prevent the moisture accelerated damage.

Many types of drainage materials or layers have been used to address drainage issues in pavement systems as presented below:

- untreated base/subbase layers
- treated base layers (with cement, asphalt, lime, fly ash, etc.)
- untreated base/subbase layers with geotextiles
- geocomposites

The selection of layers depends on the structural requirements (ACPA, 2008). The advantages and disadvantages of different types of drainage layers in pavement systems are shown in Table 4.

Untreated base/subbase layers

Untreated base/subbase layers are common for roads that are designed for low to medium traffic volumes. Untreated base/subbase layers provide additional strength especially for flexible pavement systems. Untreated base/subbase layers should have the ability to resist deterioration and degradation. Deterioration occurs as a result of the induced moisture including swelling and freeze/thaw. Degradation is erodibility and intrusion of fines.

Dense-graded base generally are not permeable to drain pavement as it is expected. Open-graded base have high permeability, thus it is often selected by design engineers. Cedergren (1988) recommends open grade base course to provide an internal drainage system under pavement to rapidly remove water. Especially, granular base with limited fines of open-grade base has high crushed materials; low fine content is used to combat the effects of moisture. Because water in open-graded materials easily penetrates through materials, and therefore the layer remains saturated for less time. Also, fewer fines mean less material can be ejected through joints and cracks. However, open-graded base has low stability which can result in rutting problems for flexible pavement asphalt concrete (Elsayer et al. 1996). Heavy

traffic loads may cause high hydrodynamic pressure at bearing points and crushed aggregate particles may fall into an open void structure of the permeable subbase, leaving the ends of the slab unsupported (ACPA, 2008b). In untreated base/subbase layers, the infiltration of the subgrade into the subbase and breakdown of the aggregate can lead to pavement failure (e.g., Beckemeyer et al. 2002).

Treated base layer

Treated base generally include cement treated base, lean concrete base (which may include fly ash or slag cement) and asphalt treated base (ACPC 2008). Treated bases provide relatively strong, uniform support and are resistant to erosion. Treated bases also separate water from intruding into the underlying unbound materials. MEPDG (2004) reported that the higher the cement content and compressive strength, the more resistant the material against moisture damage. Therefore, high crushed aggregates are very important to ensure long-term durability. MEPDG (2004) also mention hot-mix asphalt base materials can be effective in minimizing moisture problems in HMA and PCC pavements.

However, water in treated bases can distress pavement systems. For example, water in asphalt-treated bases reduces modulus by 30% and in cement or lime treated bases increases erosion susceptibility (ACPA 2008c).

Untreated base/subbase layers with geotextiles

Geotextiles protect the untreated base/subbase drainage layers from clogging by retaining the subgrade soil fines and allowing free water flow. Geotextiles often use a polymer fiber as raw materials and are usually classified by their manufacturing process as either woven or nonwoven (NCHRP 2004). Nonwoven geotextiles are widely used in subsurface applications because of the excellent filtration and separation characteristics. In addition, nonwoven geotextiles can permit use of a single layer of more economical drainage aggregates. In the later 1970s, geotextiles were successfully used in subdrainage for both groundwater and surface water infiltration (Forsyth 1978). Some detrimental effects come from the water held by capillary forces in soils and aggregates. The aggregate used for drainage must satisfy the filter criteria which consist of the clogging criterion and permeability criterion. According to the clogging criterion, material must be fine enough to avoid the adjacent fine material from piping or migrating into the filter material. The permeability criterion is that the filter

material must be coarse enough to carry water without any significant resistance (Huang, 1993). Clogging Criterion is shown in (2.2):

$$\frac{\text{D15 filter}}{\text{D85 soil}} \leq 5 \tag{2.2}$$

Geosynthetics

Geosynthetics are commonly used in pavement systems for both paved and unpaved roadways. Geosynthetics are planar polymeric materials used to reinforce and/or separate the surrounding soils for creating barriers to water flow in liners, cutoffs, and for improving drainage (NCHPR 2004, Cuelho et al. 2009). Primary function of geosynthtic materials and geosynthetic materials used in transportation show in Table 5 and Table 6.

Geocomposite drainage layers can be placed between the base and the subgrade layers or installed directly beneath the pavement surface as a substitute to a drainable base. Geosynthetics cover different materials including geotextiles, geogrids and geomembranes. Geogrids consist of a regular grid with apertures (large opening) between tensile elements. Apertures are selected based on the gradation of materials, and allow the surrounding soil materials to interlock across the geogrid. Geomembranes are low permeable materials which consist of continuous sheets to retard or prevent fluid. Rough surfaces increase the fraction of the adjacent soil layer. Geonets look similar to geogrids, but individual elements of geonets are at acute angle to each other which is different than geogrids (NCHRP 2004).

Geocomposite materials combine two or more specific types of products and take advantage of multiple benefits. The six functions of geosynthetics are summarized in Table 4. Table 5 shows the most commonly used geosynthetic materials used for transportation. According to these two tables, geotextile and geogrids are the most commonly used materials in transportation. Furthermore, geosynthetics are most commonly used in unpaved roads in the United States (NCHRP 2004). Geocomposites can be beneficial in northern climates to help mitigating the frost/heave effects (Christopher 2001).

Table 4. Different types of drainage layers in pavement systems

Type	Advantage	Disadvantage
Untreated base/subbase	Relatively inexpensive to construct.	Prone to create non-uniform support and permeability conditions due to fines segregation. [a] Generally has low resistance to erosion.
Treated subbases (e.g., cement, asphalt, lime, fly ash)	Provide relatively strong and uniform support conditions, high permeability if open-graded stone is used. Resistant to erosion.	Relatively expensive to construct compared to untreated bases due to material cost and specialized equipment usage.
Untreated base/subbase with geotextile separation layers	Protect base/subbase layers from contamination with fines from the underlying subgrade.[c]	Expensive, disintegrates when exposed to light.
Geocomposites	Can improve drainage of water which through cracks and joints in the pavement surface.	Difficult to maintain the multiple layers.

[a]Vennapusa (2004); [b]ACPA, 2008c; [c]Christopher et al. (2006),

Table 5. Primary functions of geosynthetic materials (NCHRP 2004)

Geosynthetic	Filtration	Drainage	Separation	Reinforcement	Fluid Barrier	Protection
Geotextile	x	x	x	x		x
Geogrid			x	x		
Geomembrane					x	
Geonet		x				
Geocomposites:						
Geosynthetic Clay liner						x
Thin film Geotextile Composite						x
Field coat Geotextile						

Table 6. Geosynthetic materials used in transportation (NCHRP 2004)

General Category	Specific Use
Separation of dissimilar materials	Between subgrade and aggregate base in paved and unpaved roads and airfield Between subgrade and ballast for railroads Between old and new asphalt layers
Reinforcement of weak materials	Over soft soils for unpaved roads, paved roads, airfield, railroads, construction platforms
Filtration	Beneath aggregate base for paved and
Drainage	Drainage interceptor for horizontal flow Drain beneath other geosynthetic systems

Test Methods

In situ testing methods

Many in-situ permeability testing devices have been developed to conduct permeability testing in the field. Table 7 summarizes the characteristics of various in-situ permeability test methods. In this study, to assess the in situ permeability properties, the APT device developed by White et al. (2010) was used.

Table 7. Summary of various in situ permeability testing equipments used in PCC/Asphalt surface and aggregate base/subbase layers (after White et al. 2010)

Device	Perment	Reference
Field permeability testing device	Water	Moulton et al. (1979)
Field permeameter	Water	Clyne et al. (2001)
Dynamic permeability testing device	Water	Standiford (1985)
Dynamic air outflow meter	Air	Standiford (1985)
Air permeameter test device	Air	White et al. (2007)
Gas permeameter	CO_2, Air	White et al. (2010)

Field permeability testing device (FPTD) is used as an in-situ testing device to determine the coefficient of permeability of highway base through field studies. FPTD is reasonable, accurate, reproducible and convenient for subbase courses. The base or subbase thickness ranges from 3 inches (76.2 mm) to 18 inches (457.2 mm). FPTD is a durable and inexpensive device that is easy to operate in fields (Moulton 1979). However, FPTD cannot measure the coefficient of permeability of base and subbase within a practical range. The possible measure range is between 10^{-4} cm/sec and 10 cm/sec.

Minnesota Department of Transportation (Mn/DOT) permeameter is also an in-situ testing device that can obtain the saturated hydraulic conductivity of pavement base materials. Over time, the infiltration rate becomes a steady value, when water infiltrates into a base material under a constant head. Then the steady flow is converted to a saturated

hydraulic conductivity. Mn/DOT permeability requires the base layer to be equal/higher than 6 inches (15 cm) to obtain a reliable estimation of hydraulic conductivity. To avoid the flow rate being too fast or too slow, the saturated hydraulic conductivity ranges between 10^{-5} and 10^{-3}cm/s

Air permeability test (APT) is a nondestructive in situ permeability test that determines the hydraulic conductivity of granular base materials. APT was designed to determine the permeability at very low pressures (less than 25 mm of water pressure), and low flow rates having Reynolds Number (R_e) of less than 2000. Hydraulic conductivity calculations should consider the partial saturation conditions; compressibility and viscosity of air; and the Brook-Corey pore size distribution index. In addition, some material properties including the dry density, degree of saturation, residual saturation, and pore-size distribution index should also be calculated while determining the hydraulic conductivity. The material measurement limit of hydraulic conductivity is equal to or greater than 10^{-2} cm/s (White 2007).

Laboratory testing methods

Traditional laboratory tests that measure permeability include the constant head test and falling head test. Constant head method is applied to determine the coefficient of permeability for laminar flow of water through granular soils. To limit the effect of consolidation during testing, this procedure is limited to disturbed granular soils containing not more than 10% of soil passing the No. 200 sieve. (ASTM D2434-68).

Falling head tests are conducted on all specimen types that have hydraulic conductivity less than 1×10^{-6} m/s. (ASTM D5084-03). In the falling head tests, samples are saturated and water flows through the samples. The changes of the water height are observed over time. Table 8 shows the comparison of different laboratory hydraulic conductivity tests.

Head (1982) developed large scale laboratory permeability test to determine the hydraulic conductivity of aggregate base materials. This test represents more realistic condition for large aggregates compared to the standard laboratory permeability. Jones and Jones (1989) introduced a horizontal permeability test to measure the hydraulic conductivity of aggregate used in the drainage layer. This test shows a reasonable measurement of hydraulic conductivity at various hydraulic gradations, but it is suggested to develop test methods that are more repeatable and reproducible. Similarly, Randolph et al (2000) also developed a

horizontal permeability test to measure the hydraulic conductivity of granular materials. This test measures the head loss and the quantity of water flowing through samples. Darcy's equation is used to determine the hydraulic conductivity.

Table 8. A comparison of different laboratory hydraulic conductivity tests

Test	Advantage	Disadvantage
Falling head test (ASTM D5084-03)	Inexpensive equipment	Does not simulate actual conditions (vertical water flow), applicable only for low permeability soils (silts or clays)
Constant head test (ASTM D2434-68)	Inexpensive equipment	Does not simulate actual conditions (vertical water flow), applicable only for low permeability soils (silts or clays)
Large Scale Aggregate compaction mold permeameter (White et al. 2004)	Uses large scale sample (1 ft diameter x 1 ft height) and accommodates use of aggregate materials with particle sizes up to 1 inch.	Requires lot of water, cumbersome to run the test, and uses relatively high water heads (> 1 ft of water)

CHAPTER 3. METHODS

This chapter summarizes the test methods and standards used to conduct in situ and laboratory test to determine the hydraulic conductivity of pavement foundation layers. In addition to hydraulic conductivity tests, various in situ tests were conducted to evaluate compaction conditions of the subbase materials. Different foundation construction materials collected from five sites in four states were studied (Table 9).

Table 9. Summary of investigated sites and materials

State	Site location	Materials	Date
Michigan	I-94	Existing subbase, base, subgrade	May 27 to June 1,2009
Michigan	I-96	Subbase, subgrade	May 18 to May 20, 2010
Pennsylvania	US-22	Cement-treated base (CTB),asphalt-treated base (ATB),subbase, subgrade	July 27 to 28, 2009
Iowa	I-35	Trimmed and untrimmed recycled concrete, pavement base	August 27, 30 and 31 ,2010

Research Design

In situ tests involved various methods including: (a) spatial northing and easting positions of each test location were determined by global positioning system (GPS) measurements; (b) California bearing ratio and resilient modulus were estimated by dynamic cone penetrometer tests (DCP); (c) Elastic modulus and modulus of subgrade reaction obtained by static plate load test (PLT). (d) saturated hydraulic conductivity (k_{sat}) was calculated according to the gas permeability test device (GPT) data; (e) Moisture content (w%) and dry unit weight (γ_d) were calculated according to the Humboldt nuclear gauge tests; (f) Dynamic elastic modulus ($E_{LWD\text{-}Z23}$) was determined by using a 300 mm diameter plate Zorn light weight deflectometer (LWD); and (g) Caterpillar single drum roller intelligent compaction (IC), operated in low amplitude vibratory and static drum condition.

Laboratory tests were performed on representative sample collected in the field. Index properties were determined to classify the materials. Laboratory permeability tests included large scale aggregate compaction permeameter tests, falling head tests, and constant head

tests. Laboratory soil index properties tests included: Atterberg limits, particle size analysis, specific gravity, and sieve analysis of the aggregates.

In situ Test Methods

In situ tests were applied on pavement foundation study of highway construction in Iowa, Pennsylvania, and Michigan to determine the mechanical properties of materials. The in situ tests and test methods are summarized in Table 10.

Table 10. Summary of devices and methods used for in situ soil testing

Test device	Method followed
Gas permeability test (GPT)	David J. White (2007)
Nuclear moisture-density gauge (NG)	ASTM D2922-05
Minnesota Permeability test	Timothy R. Clyne (2001)
Dynamic cone penetrometer (DCP)	ASTM D6951/D6951M-09
Light weight deflectometer (LWD)	LWD operation Manual (2000)
Plate load test (PLT)	ASTM D1196
Caterpillar IC measurement	Per manufacture guidelines

Gas permeability test

The new self-contained gas permeameter test (GPT) device for quality control (QC) and quality assurance (QA) is to determine the saturated hydraulic conductivity of pavement base layer and subbase layer in the construction sites. The GPT is a ruggedized and repeatable test device for rapid in situ determination of permeability.

The GPT is self contained with two compressed gas cylinders attached to the wheel cart and weighs about 16 kg (35 lb). GPT also can connect to the air compressor in the field. To easily transport and handle the GPT in the field, the unit can be mounted to a wheel cart. GPTs perform more than 50 tests before the cylinders need to be refilled. Figure 4 and Figure 5 show GPT used in the field with air compressor.

Figure 4. Gas permeability test used in the field

Figure 5. Gas permeability test used in the field with air compressor

The gas flow is controlled by using a regulator and a precision orifice. The pressures at the inlet and the outlet of the orifice are monitored using digital pressure transducers and are displayed along with the calculated gas flow rate on a digital display panel. Flow rate is calculated based on pressure measurements at inlet and outlet of orifice. Inlet pressure transducer measurement range is 0 to 1724 kPa (0–250 psi) and the outlet pressure transducer measurement range is 0 to 76 mm (0–3 in.) of water. Four different orifices (Table 11) were used to present the flow pressure conditions of hydraulic conductivity value to satisfy wide

range of materials. Three dimensional (3 D) design drawings of the GPT device and its components are demonstrated in Figure 6.

Table 11. APT model with four different orifices

Types of GPT	Orifice diameter (μm)
GPT(A)	2982.00
GPT(B)	870.95
GPT(C)	293.66
GPT(D)	149.41

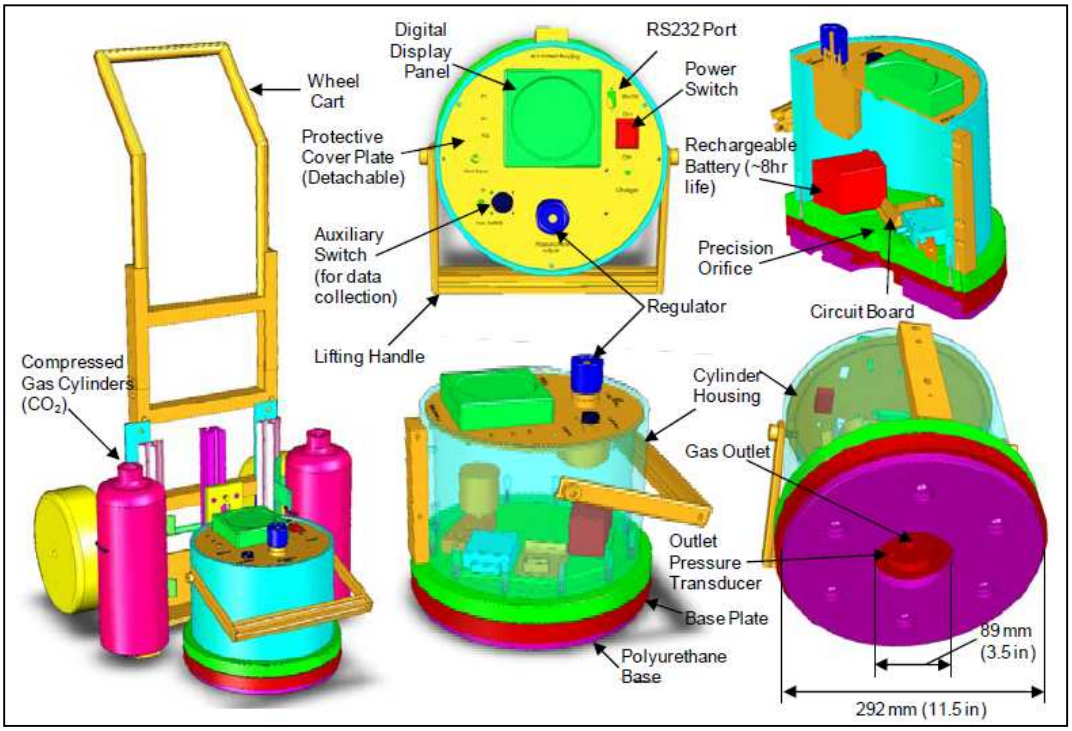

Figure 6. Three-dimensional sketch of the GPT device and components (White et al. 2010)

Saturated hydraulic conductivity calculations

GPT can collect data in the field to produce color-coded spatial maps of hydraulic conductivity. Each test takes less than 30 seconds so multiple tests can be performed quickly in each test location to collect P_0 and Q values. P_0 and Q values are used to calculate k_{sat}

values that range from 10^{-4} to 10 cm/s. An average k_{sat} is calculated for each location and those values are used to draw the spatial maps.

GPT measures gas flow and pressure, Darcy's law is used to calculate the hydraulic conductivity. This equation can apply compressibility of gas, viscosity of gas, and gas flow under partially saturated conditions. Hydraulic conductivity (k) is calculated as follows (NCHRP 2010):

$$k_{sat} = \left[\frac{2\mu_{gas} Q P_1}{r G_o \left(P_1^2 - P_2^2\right)}\right] \times \frac{\rho g}{\mu_{water}\left(1 - S_e\right)^2 \left(1 - S_e^{((2+\lambda)/\lambda)}\right)} \quad \textbf{(3.1)}$$

Where

k_{sat} = saturated hydraulic conductivity (cm/s);

Q = volumetric flow rate (cm^3/s);

P_1 = absolute gas pressure on the soil surface (P_a) P_o 9.81+ 101325;

P_2 = atmospheric pressure (Pa);

r = radius at the outlet (4.45cm);

G_0 = Geometric factor (dimensionless factor)

S_e = effective water saturation (S_e= (S-S_r)/ (1-S_r));

ρ = density of water (g/cm^3);

g = acceleration due to gravity (cm/s^2) and

μ_{water} = absolute viscosity of water (gm/cm-s).

Nuclear gauge

Nuclear gauge is performed following the ASTM D2922-05, *Test Method for Density of Soil and Soil Aggregate In-place by Nuclear Methods (Shallow Depth).* A calibrated nuclear moisture –density gauge (NG) device is used to provide rapid measurements of moisture content and soil dry unit weight. Two values of moisture content and soil dry unit weight are measured in each location and the average value is reported.

Mn/DOT permeability test

Minnesota Department of Transportation (Mn/DOT) permeability test is a quick and simple method for determining the hydraulic conductivity in granular base materials. The

main components of Minnesota permeameter are outer tube, inner tube, air tube, distribution plug and top plug.

The outer tube is 1.71 m (67 in.) long and the diameter is 63.5 mm (2.5 in.). The outer tube is used as a reservoir of water. The inner tube is 1.68 m (66 in.) long and diameter is 31.75 mm (1.25 in.). Two acrylic tubing in the top and bottom of permeameter assist the inner tube in the center of the outer tube. Mylar ruler is taped in the inner tube to read the water flow distance in the permeameter. Minnesota Permeameter shows in Figure 7.

The procedures of this test includes preparing the auger hole, filling the reservoir with water, situating the permeameter in the auger hole, filling water in the tube, and measuring the flow and time. Hydraulic conductivity (k) is calculated as shown below:

$$K_{sat} = \frac{CQ}{2\Pi H^2 (1 + \frac{C}{2}(\frac{a}{H})^2)} \tag{3.2}$$

Where:

K_{sat} = saturated hydraulic conductivity (cm/s);

a = well radius (cm);

H = head of water in the well (cm) and

C = factor is determined by the following equation:

$$C = 0.02(\frac{H}{a})^{(\frac{2}{3})} \tag{3.3}$$

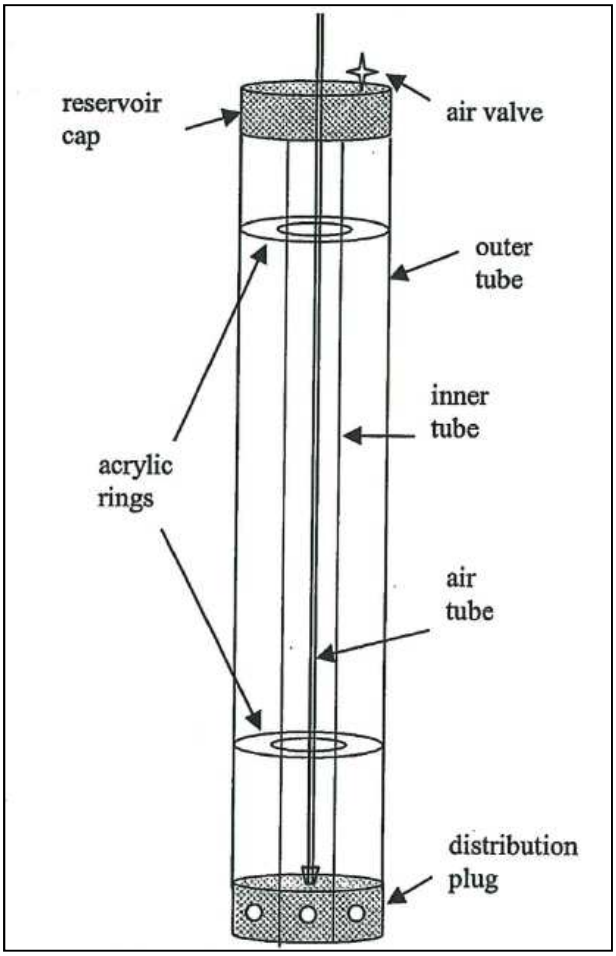

Figure 7. Minnesota Permeameter (Clyne et.al. 2001)

Dynamic cone penetrometer

Dynamic cone penetrometer (DCP) tests were conducted in accordance with the ASTM D6951-03. The DCP works by 8 kg onto a rod with cone trip dropped from a height of 575 mm. DCP recorded by penetration distance for a given number of blows. DCP can be used to estimate the in situ California bearing ratio (CBR) to identify the strata thickness, shear strength of strata, and other material characteristics.

$$CBR = \frac{292}{(DCPI)^{1.12}} \; ; \textit{for all soils except for CH soils or CL soil with CBR} < 10 \qquad (3.4)$$

$$CBR = \frac{1}{(0.017019 * DCPI)^2} \; ; \textit{CL soils with CBR} < 1 \qquad (3.5)$$

$$CBR = \frac{1}{0.002871 * DCPI}; CH\ soils \quad (3.6)$$

$$M_{r\,(DCPI)} = 17.6 * (CBR) * 0.64; \textit{ for all materials}$$

Where: DCPI = dynamic cone penetrometers index (mm/blow)

M_r = resilient modulus (MPa)

Light weight deflectometer

Light weight deflectometer (LWD) can be used to rapidly determine the elastic modulus and performed using the light drop weight tests ZFG2000 by Gerhard Zorn. The LWD device is consisted of a 300 mm diameter plate and 720 mm drop height. LWD tests were performed on a flat area of the material surface. Three seating drops were performed. The three test drops were recorded and the average value was reported. White and Vennapusa (2009) reported that the measuring range of the deflection transducer is 0.2 mm to 30 mm for Zorn LWD. Elastic modules were calculated from the average deflection reading as shown in the equation 4.

The modulus can be determined by using the following equation:

$$ELWD = \frac{(1-\nu^2)\,\sigma_0 \gamma}{d_0} \times f \quad (3.5)$$

where,

E_{LWD} = elastic modulus (MPa);

ν = Poisson's ratio (assumed to be 0.4 for this research);

σ_o = applied stress (MPa);

r = radius of the plate (mm);

d_o = measured settlement (mm);

and f = shape factor that depends on the stress.

Plate load test

Plate load test (PLTs) were performed in accordance with the ASTM D1196. This test was performed on soils and unbound base and subbase materials to determine the shear strength. This test was performed by using a custom apparatus on the Freightliner for the Geotechnical Mobile Laboratory (White and Gieselman 2009). The bearing plate (300 mm

diameter) was directly placed on the subgrade or base layer. The static load was applied on the bearing plate using the weight of track as the reaction force. Deformations were measured by using three 50-mm liner voltage displacement transducers (LVDTs).The average value of three LVDTs was used for calculation. During test, the data logger continuously recorded the load and deformation. Initial (E_{v1}) and reload (E_{v2}) elastic module readings were determined according to the Equation 4. White et al. 2009 stated that the stress and deflection reading of granular materials were taken from 0.2 to 0.4 MPa (29 to 58 psi) and the non-granular subgrade soil were taken from 0.1 to 0.2 MPa (14.5 to 296 psi).

Caterpillar IC measurement (machine drive power)

The Caterpillar IC measurement values were used to indicate the compaction levels of machine drive power (MDP). MDP is based on the rolling resistance of drums to determine the forces acting on the drum and the desired energy to counteract the forces (White et al. 2010). The MDP values were recalculated and referred as MDP*. The Caterpillar IC system (Figure 8) includes an accelerometer, slope sensor, controllers, communication data radio, real-time kinematic (RTK) GPS receiver, on board report system and off board GPS base station (not in the Figure 8).

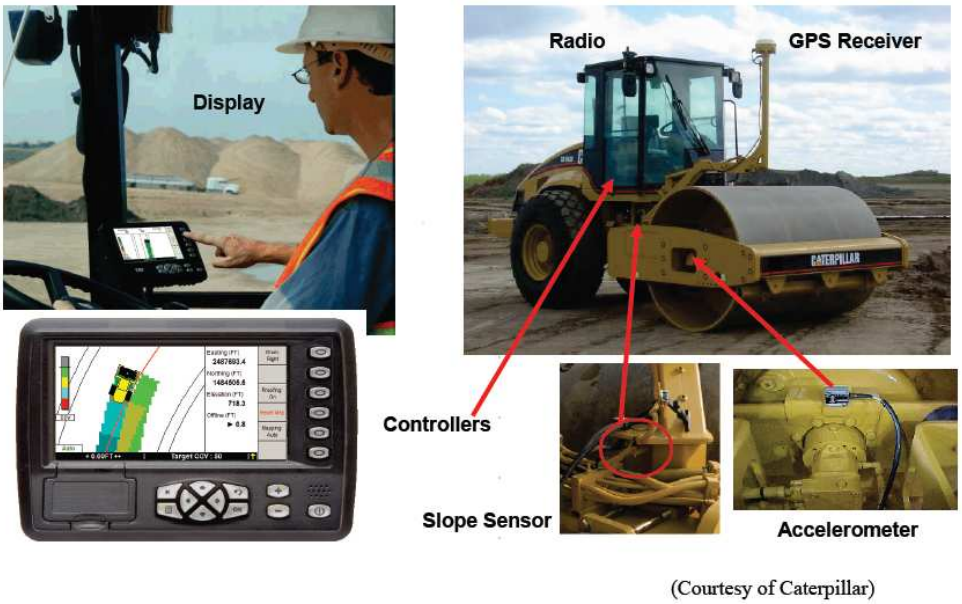

Figure 8. Caterpillar single drum IC system (adopted from FHWA)

Laboratory Tests

Laboratory tests, including the soil index properties tests and permeability tests, are applied on the samples taken from various project sites. Table 12 shows all the tests that were conducted in the laboratory.

Table 12. Laboratory tests methods

Laboratory Test Method	Standard
Large scale aggregate compaction mold permeameter	White et al. 2004
Falling head test	ASTM D5084-03
Permeability of Granular Soils (Constant Head)	ASTM D2434-68
Falling head testing in concrete	—
Atterberg limits test	ASTM D4318–05
Particle-size analysis of soils	ASTM D 422-63
Specific Gravity of Solids by Water Pycnometer	ASTM D854-10
Sieve of Fine and Coarse Aggregates	ASTM C 136-01

Large scale aggregate compaction mold permeameter

Large scale aggregate compaction mold permeameters (LSLP) are used to determine the hydraulic conductivity of aggregate base materials. The components of LSLP are water reservoir tank, compaction and base molds. Water reservoir tank is 32 in. high and the diameter is 11.75 in. Aggregate compaction mold is specially fabricated to 0.3 m (11.8 in.) diameter by 0.3 m (11.8 in.) high. Base mold has a 10 in. diameter butterfly valve attached to the compaction mold. Figure 9 shows the cross–section of the large scale aggregate compaction mold permeameter (Vennapusa 2004).

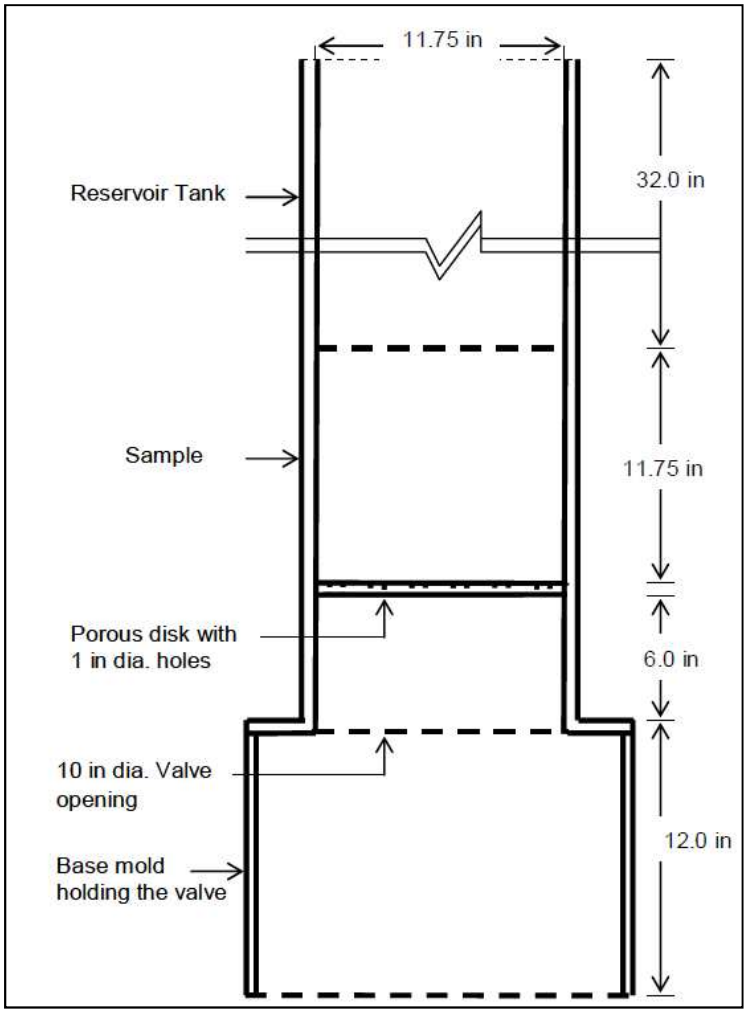

Figure 9. Cross–section of the large scale aggregate compaction mold permeameter (Vennapusa 2004)

The LSLP can be used to conduct two kinds of permeability tests, falling head and constant head tests. In falling head tests, after the sample has been saturated, the decrease in the water level in the reservoir is timed while the water flows through the sample.

In constant heads test, after the sample has been saturated, an inlet flow of water maintains the water level in the reservoir while the water flows through the sample. To fill the known volume, the same steady state flow was used and water quantity (Q) and time (s) was recorded. The LSLP is presented in Figure 10.

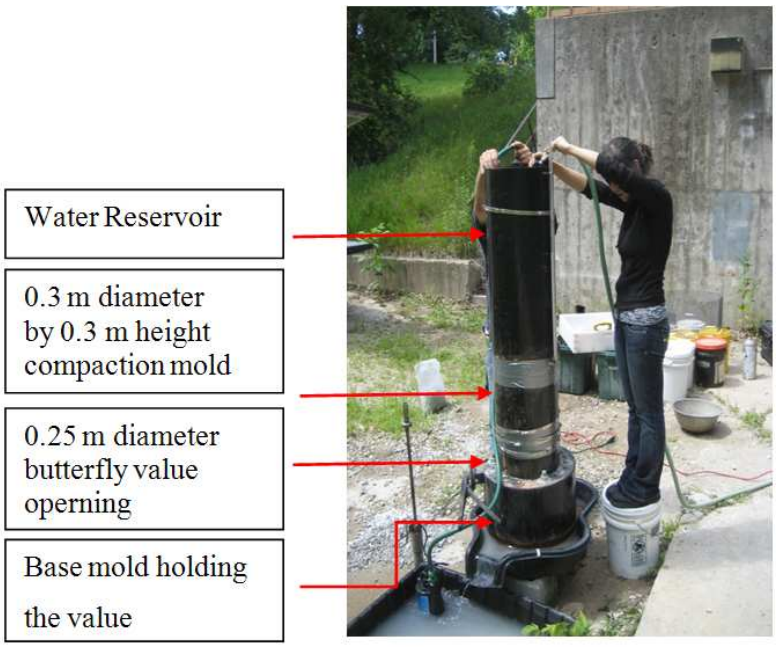

Figure 10. Large scale aggregate compaction mold permeameter

Constant head permeability testing

Constant head testing was performed according to the ASTM D2434, "Standard Method for Permeability of Granular Soils (Constant Head)." This test determines the coefficient of permeability for the laminar flow of water through granular soils. This test requires a specimen cylinder with a minimum diameter that is approximately 8 to 12 times than the maximum particle size. This test can only be used on granular soils that contain less than 10% of soil passing the 75 µm (No. 200) sieve. Darcy's equation is used to calculate the hydraulic conductivity. Hydraulic conductivity (K) is calculated as shown below:

$$K = \frac{QL}{Ath} \tag{3.6}$$

Where

K = coefficient of permeability;

Q = quantity of water discharged;

L = distance between discharged;

A = cross-sectional area of specimen;

t = total time of discharge and

h = difference in head on manometers.

Falling head testing

Falling head testing determines the hydraulic conductivity of granular soils and concrete specimens. Samples are required to be saturated before testing. Then flow through the sample and change in time with head is observed. If this test applied on granular soils, the set up of falling head testing is similar to that of constant head testing.

Falling head testing in pervious concrete treated base (CTB)

Falling head test is also applied on the pervious concrete specimens. Figure 11 shows falling head test used for pervious concrete specimens. The samples were confined in a member and sealed in the rubber sleeve, and surrounded by the adjustable hose clamps. The concrete treated base (CTB) specimens were enclosed in a rubber sleeve and directly attached to the pipe. Flexible sealing gum was used around the top perimeter of the sample to prevent leakage.

Figure 11. Falling Head Permeability Testing of cement treated base

Hydraulic conductivity (k) is calculated as follows:

$$K_{sat} = \frac{A_1 \times L}{A_2 \times t} \ln\left(\frac{H_1}{H_2}\right) \quad (3.6)$$

Where

K = coefficient of permeability. (in./sec);

A_1 = cross sectional area of pipe, (in^2);

L = length of the sample, (in.);

A_2 = cross sectional area of specimen, (in^2);

t = time in second from H_1 to H_2;

H_1 = initial water level, (in.) and

H_2 = final water level, (in.).

The porosity measurements applied in this research followed the Volume Method. The dry condition and immersed condition are required to be measured. Porosity is calculated as presented below:

$$P_{total} = 1 - \frac{W_2 - W_1}{\rho \upsilon} \times 100\% \qquad (3.7)$$

Where

P_{total} = Total porosity, (%);

W_1 = Weight immersed;

W_2 = Dry weight;

V = Normal sample volume based on dimensions of the sample,(ft^3 or m^3) and

ρ = Density of water, (pcf or kg/m^3).

Atterberg limits test

This test is applied by following the ASTM D4318-05 "Standard test methods for liquid limit, plastic limit, and plasticity index of soils." This method can be performed only on the portion of a soil that passes the 425 μm (No.40) sieve. This methods can be applied when pulverize ready which at room temperature or in an oven at a temperature not exceeding 60°C. Liquid limit tests were performed according to method A (Multi-point liquid limit). Atterberg limits are used to classify materials according to the Unified Soil Classification System (USCS) and State Highway and Transportation Officials (AASHTO).

Particle-size analysis of soils

Particle-size analysis of soil is used to determine the distribution of particle sizes in soils. Particle size distribution curves were determined by using 2000g of air-dry sample. The

prepared samples were separated into two portions by using the No.10 sieve. Sieve analysis is performed on the distribution of particle sizes retained on No.10 sieve. Hydrometer analysis is conducted to determine the distribution of particle sizes passing No.10. After the hydrometer reading, the suspension is transferred to a No.200 (75μm) sieve, washed, oven dried, and then sieved through the No. 40 and No.100 sieves.

Specific gravity

Specific gravity test is performed by following the ASTM D854-05. Specific gravity of soil is the ratio of the mass of a unit volume of soil solids to the mass of the same volume of gas-free distilled water at 20°C. This test requires using the helium-pycnometer. Sample used are required to pass the No.10 (2 mm) sieve. Specific gravity is used to calculate the voids ratio, degree of saturation and density of the soil solids. All materials adopted by method B-procedure for oven-dried specimens.

Passing #200 test

Passing #200 tests are performed in accordance with the ASTM C 136-01. This test determines the fine content of samples brought from bag samples. Bag samples of the base materials were obtained from directly beneath the GPT location and transported to the laboratory to determine the fines content (passing No. 200 sieve). The weight of the dry samples was measured, and then washed samples were sieved through the 75μm on No. 200 sieve. Samples were put into an oven at 110±5°C (230+9°F) until it became dry.

Geostatistical Spatial Analysis

Geostatistical methods were used to analyze the correlated hydraulic conductivity and passing # 200 fines content and dry unit weight with moisture content from field sites. Kriged spatial contour maps, experimental semivariogram plots with spatial statistic, and histograms plot with univariate statistics were used to present the field results.

NCHRP (2010) report presents that spatial variability can be assessed and quantified by using the geostatistical semivariogram analyzes. It also can be used as a spatial prediction technique (for predicting values at unsampled locations based on values at sampled locations). The semivariogram $\gamma(h)$ is defined as one-half of the average squared differences

between data values that are separated at a distance h (NCHRP,2010). Figure 12 shows typical semivariogram plot and its characteristics.

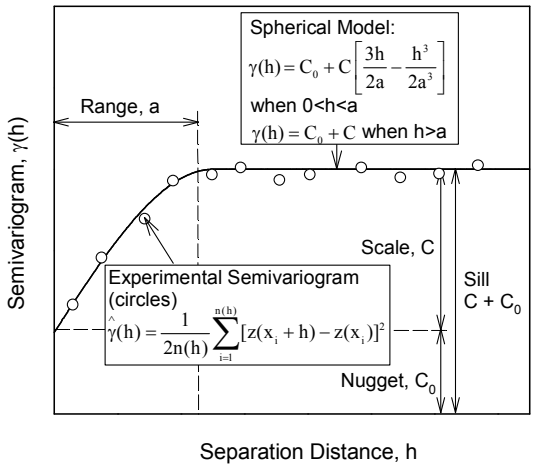

Range: As the separation distance between pairs increase, the corresponding semivariogram value will also generally increase. Eventually, however, an increase in the distance no longer causes a corresponding increase in the semivariogram, i.e., where the semivariogram reaches a plateau. The distance at which the semivariogram reaches this plateau is called as range. Longer range values suggest greater spatial continuity or relatively larger (more spatially coherent) "hot spots".

Sill: The plateau that the semivariogram reaches at the range is called the sill. A semivariogram generally has a sill that is approximately equal to the variance of the data.

Nugget: Though the value of the semivariogram at h = 0 is strictly zero, several factors, such as sampling error and very short scale variability, may cause sample values separated by extremely short distances to be quite dissimilar. This causes a discontinuity at the origin of the semivariogram and is described as nugget effect. (Isaaks and Srivastava, 1989)

Figure 12. Typical semivariogram plot and its characteristics (adapt by NCHRP 2010)

CHAPTER 4. MATERIALS

This chapter describes the index properties of materials collected from investigation at four different field sites. Materials were analyzed both in-situ and in laboratory. The material index properties include gradation, specific gravity, Atterberg limits and classification. Table 13 and Table 14 and Table 15 provide summary of investigated sites and materials.

Table 13. Summary of investigated sites and materials

State	Site location	Materials	Date
Michigan	I-94	Existing subbase, base, subgrade	May 27 to June 1,2009
Michigan	I-96	Subbase, subgrade	May 18 to May 20, 2010.
Pennsylvania	US-22	Cement-treated base (CTB),asphalt-treated base (ATB),subbase, subgrade	July 27 to 28, 2009
Iowa	I-35	Trimmed and untrimmed recycled concrete, pavement base	August 27, 30 and 31, 2010

Table 14. Description and source of materials in the lab

Material	Description	Lab/Field Study	Source
Sand 1	Concrete sand	Lab	Hallet Materials, Ames, IA
Sand 2	ASTM 20/30 silica sand	Lab	-
WLS-IA	Well-graded crushed limestone	Lab	Martin Marietta Materials, Ames, IA
PG	Open grade pea gravel	Lab	Hallet Materials, Ames, IA
SGB	Small glass beads (0.75 mm spheres)	Lab	-
LGB	Large glass beads (1 mm spheres)	Lab	-
OLS-IA	Open-graded crushed limestone	Lab	Martin Marietta Materials, Ames, IA
OLS-63	Open-graded crushed limestone	Lab	Hwy 63, New Hampton, IA

Table 15. Description and source of materials in the lab and field

OS-MI	Open-graded slag	Lab and Field	I-94, St. Clair and Macomb, MI
# 57-PA	AASHTO #57 crushed limestone	Lab and Field	SR-22, Clyde, PA
OLS -PA	Open-graded crushed limestone	Lab and Field	SR-22,Clyde, PA
Sand 3	Sandy subbase	Lab and Field	MI-96, Lansing, MI
Aggregate	Aggregate used for CTB ,I-96	Lab and Field	MI-96, Lansing, MI
Recycled concrete	Untrimmed base and trimmed base	Lab and Field	I-35, IA

Michigan I-94

This pavement study section on I-94 is located in St. Clair and Macomb Counties, Michigan (Figure 13). The in situ testing conducted at this site was performed on a nominal 400 mm thick compacted and trimmed, open-graded steel slag treated base layer. Representative field samples were collected and transported to the laboratory for analysis.

Laboratory testing included: particle-size analysis, specific gravity, percent passing the #200 sieve and large scale aggregate compaction mold permeameter tests. The results of the classification (according to American Association of State Highway and Transportation Officials (AASHTO) and Unified Soil Classification System (USCS)) gradation parameters, specific gravity percent gravel, are provided in Table 16. The materials were classified as GP-GM in accordance with the USCS classification and A-1-a from AASHTO classification (see Figure 14).

Gas permeability test (GPT(B)) were conducted in a grid pattern over 7 m by 7 m test area on 120 test locations. Bag samples (about 1000 g per sample) were directly obtained from the surface of the GPT(B) test locations and transported to the laboratory to determine moisture content, fines content (passing #200 sieve) and gradation.

Table 16. Summary of soil index properties on I-94, Michigan

Parameter	**Value**
USCS Classification	GP-GM
AASHTO Classification	A-1-a
Gravel Content (%) (> 4.75mm)	76
Sand Content (%) (4.75mm-75µm)	17
Silt + Clay Content (%) (< 75µm)	7
D10 (mm)	0.30
D20 (mm)	3.73
D30 (mm)	6.09
D50 (mm)	10.76
D60 (mm)	13.6
D90 (mm)	28.68
Coefficient of Uniformity (c_u)	44.83
Coefficient of Curvature (c_c)	9
Specific Gravity, G_S	2.68

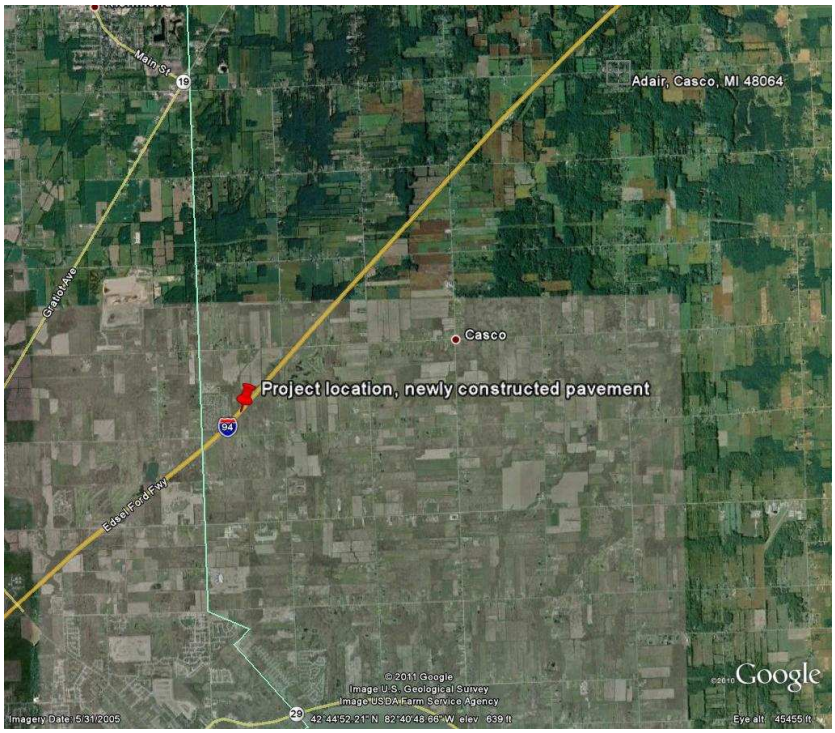

Figure 13. Project location of I-94, Michigan

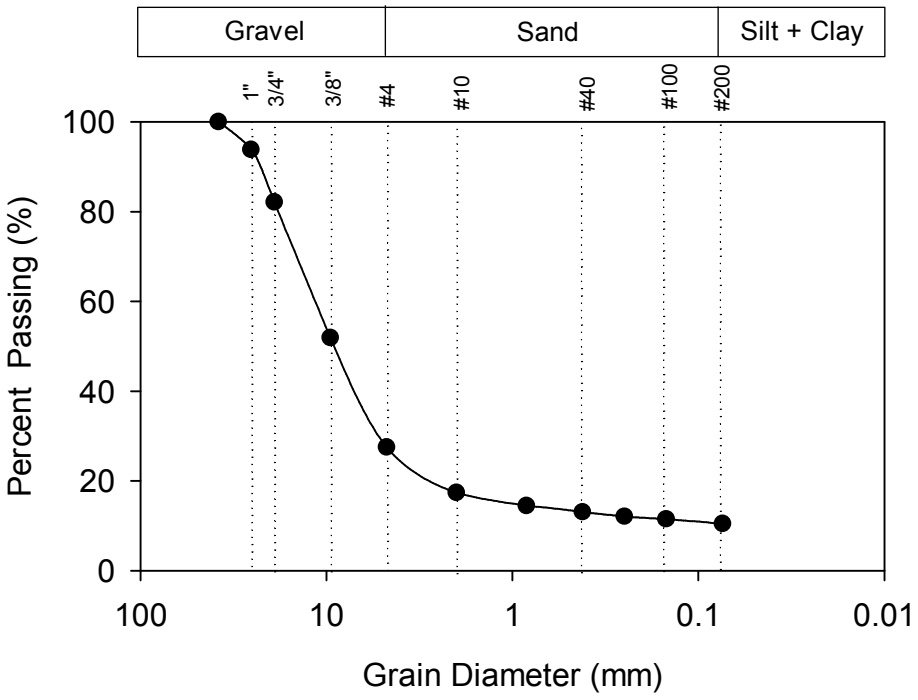

Figure 14.Particle size distribution of steel slag from I-94, Michigan

Michigan I-96

This pavement study section is located on I-96 in Clinton and Eaton County in Michigan (Figure 15). The investigations were performed on an open–graded sandy base and a newly cement treated base (CTB) made from recycled concrete pavement that had been ground and graded. The CTB was underlain by sandy subbase and subgrade.

Laboratory testing included: particle-size analysis of soils, Atterberg limits test, specific gravity, percent passing the #200 sieve, and large scale aggregate compaction mold permeameter tests. The results of the classification (according to American Association of State Highway and Transportation Officials (AASHTO) and Unified Soil Classification System (USCS) gradation parameters, specific gravity percent gravel, are provided in Table 17. Grain size distribution curves for sandy subbase are shown in Figure 16.

GPT measurements were conducted on the sand subbase at 73 points on a 3 ft x 3 ft grid with 9 rows transverse and 10 rows longitudinal with respect to the pavement. Bag samples (1000g) were directly obtained under test locations (0-60 mm) and transported to the laboratory to determine the percentage of fine particles passing the No. 200 sieve.

Table 17. Summary of soil index properties from I-96, Michigan

Parameter	Sandy Subbase	CTB
USCS Classification	SP-SM	—
AASHTO Classification	A-1-b	—
Gravel Content (%) (> 4.75mm)	24	94
Sand Content (%) (4.75mm-75µm)	68	6
Silt Content (%) (75µm-2µm)	9	0
Clay Content (%) (< 2µ)	0	0
Liquid Limit, LL (%)	Non-plastic	—
Plastic Limit, PL (%)	Non-plastic	—
Plasticity Index, PI, (%)	Non-plastic	—
Coefficient of Uniformity (c_u)	13.3	—
D10 (mm)	0.096	—
D15 (mm)	0.18	—
D30 (mm)	0.32	—
D50 (mm)	0.64	—
D60 (mm)	1.27	—
D85 (mm)	8.68	—
Coefficient of Curvature (c_r)	0.8	—
Specific Gravity, G_S (Assumed)	2.6	—

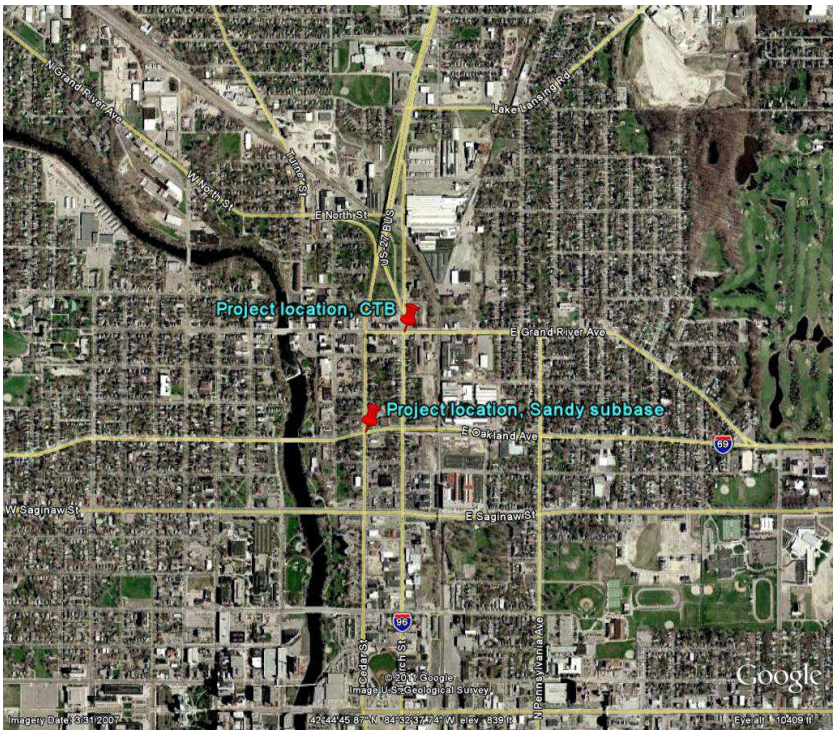

Figure 15. Project location of I-96, Michigan

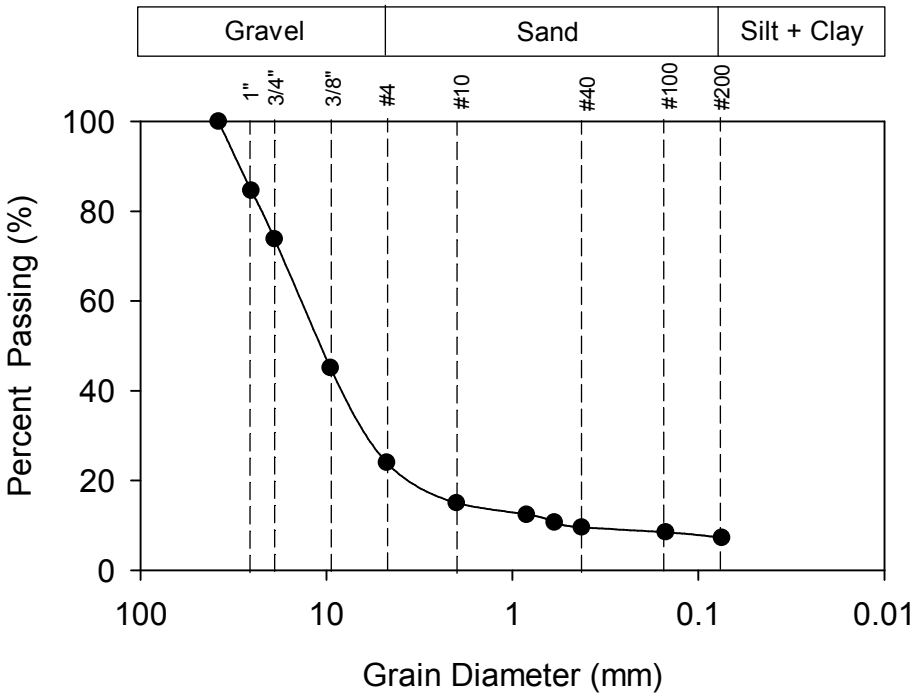

Figure 16. Particle size distribution of existing sand subbase on I-96, Michigan

Pennsylvania SR-22

This pavement study section is located on SR-22 in Blairsville, Pennsylvania (Figure 17). This project involved testing newly constructed cement-treated open-graded crushed AASHTO #57 stone base (CTB), asphalt-treated AASHTO # 57 stone base (ATB), and open-crushed leveling subbase (OSL-PA) layers.

Laboratory testing included: Particle-size analysis of soils, Atterberg limits test, specific gravity, percent passing the #200 sieve, and large scale aggregate compaction mold permeameter test. The results of the classification (according to American Association of State Highway and Transportation Officials (AASHTO) and Unified Soil Classification System (USCS)) gradation parameters, specific gravity percent gravel of the AASHTO#57 stone and the OLS subbase are provided in Table 18. Grain size distribution curves for AASHTO#57 stone and the OLS subbase are shown in Figure 18 and Figure 19.

Table 18. Summary of soil index properties on SR-22, Pennsylvania

Parameter	AASHTO#57	OLS
USCS Classification	GP	GP-GM
AASHTO Classification	A-1-a	A-1-a
Gravel Content (%) (> 4.75mm)	96	49
Sand Content (%) (4.75mm-75µm)	3	41
Silt Content (%) (75µm-2µm)	1	10
D10 (mm)	6.84	0.08
D20 (mm)	8.75	0.71
D30 (mm)	10.21	1.70
D60 (mm)	14.46	6.66
D90 (mm)	21.86	21.30
Coefficient of Uniformity (c_u)	2.11	74.1
Coefficient of Curvature (c_r)	1.10	4.80
Specific Gravity, G_S (Assumed)	2.70	2.70

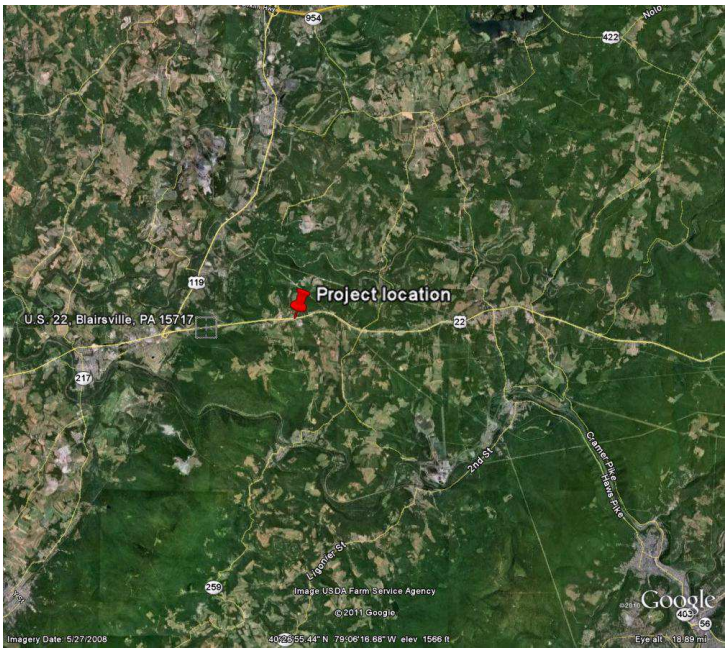

Figure 17. Project location of SR-22, Pennsylvania

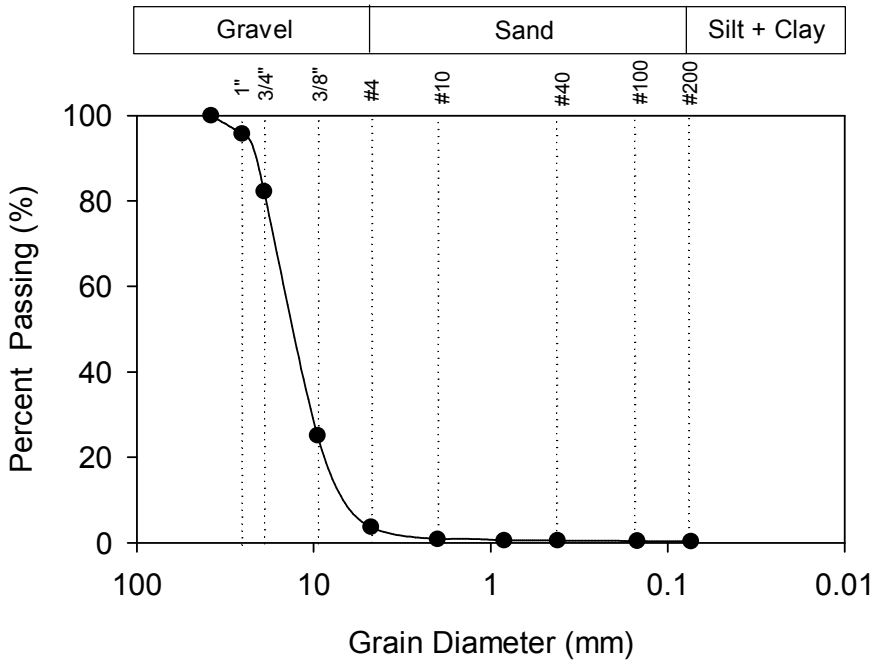

Figure 18. Particle size distribution of AASHTO #57 material from SR-22, Pennsylvania

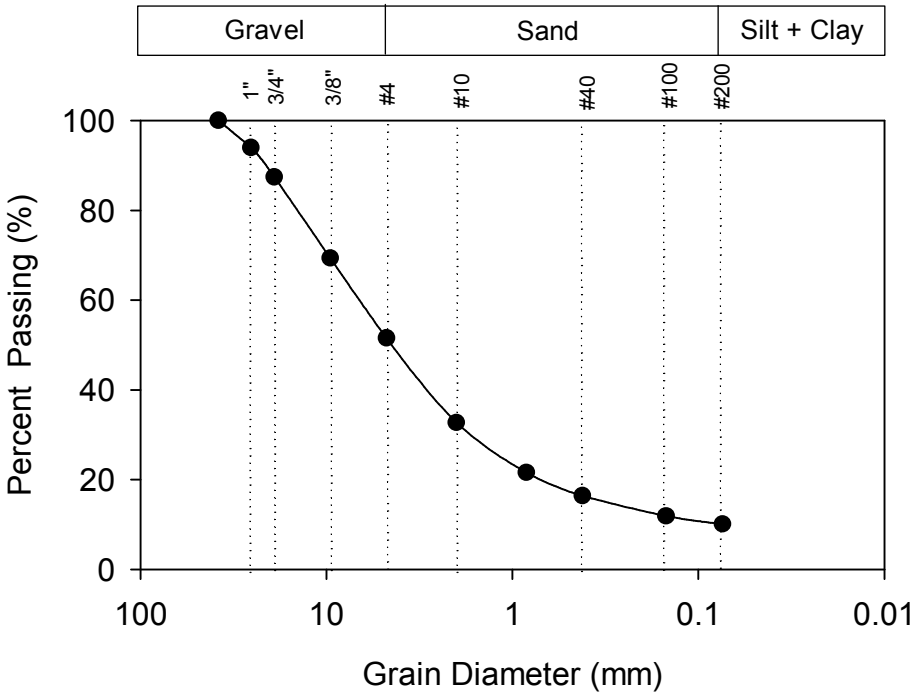

Figure 19. Particle size distribution of open-graded limestone material from SR-22, Pennsylvania

Iowa I-35

This pavement section is located on I-35 in the state of Iowa (Figure 20). There were three test beds: an untrimmed base, a trimmed base, and a virgin mixture bed. Figure 21 shows the strip location and measurement points from GPS.

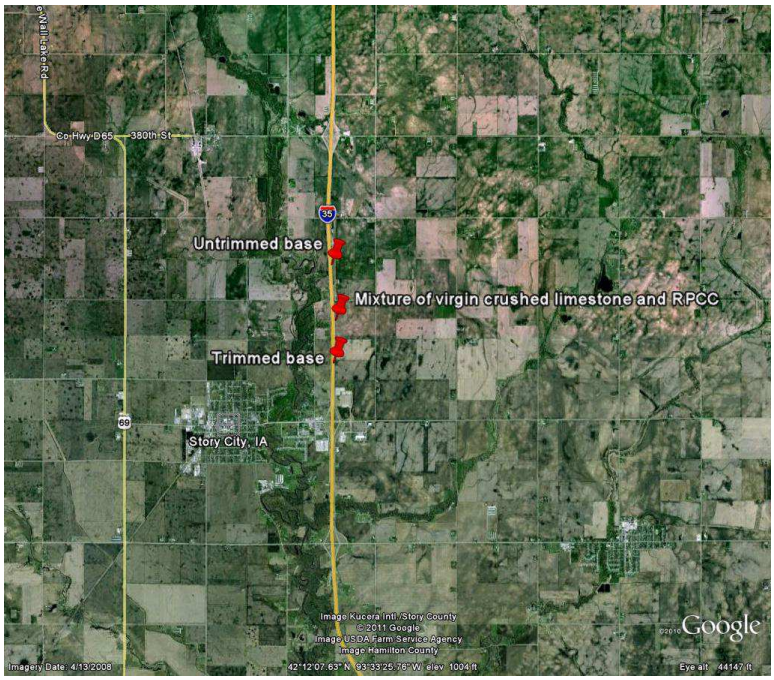

Figure 20. Project location of I-35, Iowa

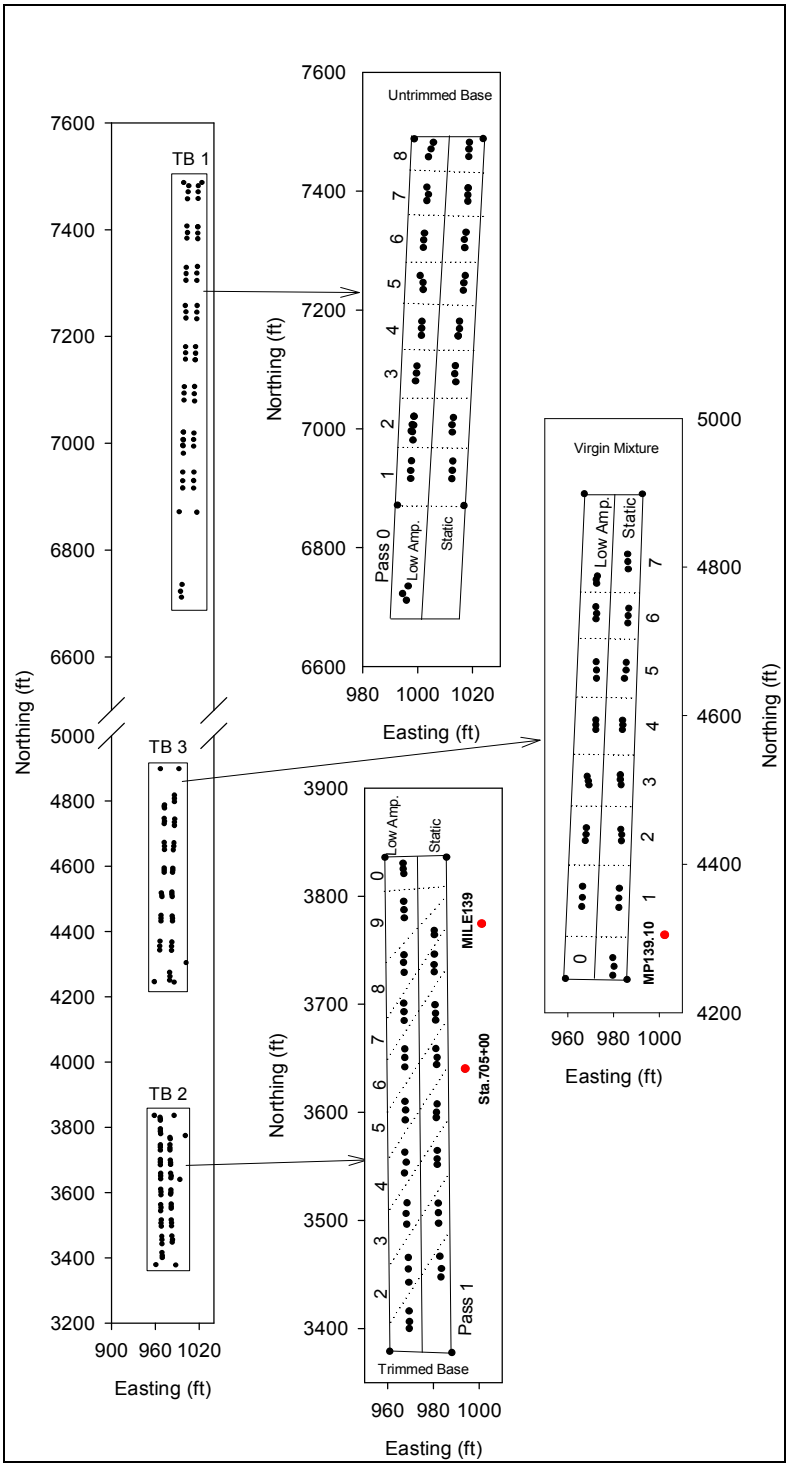

Figure 21. Test strip location and measurement points from GPS for I-35 Iowa test beds

Untrimmed base (Test bed 1)

Test bed 1, the untrimmed base, is approximately 800 ft long by 30 ft wide and is divided into nine sections. The sections are numbered from 0 to 8 indicating the number of roller prior to in situ testing. Soil index properties of low amplitude vibratory and static compaction roller sections are show in Table 19 and Table 20. The material was classified as GW (well graded gravel) and GP (poorly graded gravel) based on USCS classification and A-1-a from AASHTO classification. Grain size distributions of untrimmed base are all within the range of the Iowa DOT limit gradation 4121 recycle granular (range is presented as red bars in Figure 22 and Figure 23).

Table 19. Summary of soil index properties of low amplitude vibratory roller section (1-8) on untrimmed base I-35, Iowa

Parameter	Section 1	Section 2	Section 5	Section 6	Section 7	Section 8
USCS Classification	GW	GW	GP	GP	GP	GW
AASHTO Classification	A-1-a	A-1-a	A-1-a	A-1-a	A-1-a	A-1-a
Gravel Content (%) (> 4.75mm)	82	85	76	67	73	82
Sand Content (%) (4.75mm-75µm)	15	14	22	28	25	17
Silt + Clay Content (%) (< 75µm)	3	1	2	4	2	2
D10 (mm)	2.26	2.97	0.87	0.43	0.66	1.88
D15 (mm)	4.03	4.79	2.12	0.97	1.55	3.68
D30 (mm)	8.0	9.26	6.49	4.13	5.50	8.26
D50 (mm)	13.88	15.55	11.70	8.80	11.91	14.88
D60 (mm)	16.43	18.37	15.11	11.59	15.17	18.26
D85 (mm)6	23.91	28.89	25.04	20.71	23.26	29.10
Coefficient of Uniformity (c_u)	7.28	6.18	17.29	26.69	23.10	9.72
Coefficient of Curvature (c_c)	1.72	1.57	3.19	3.39	3.03	1.99

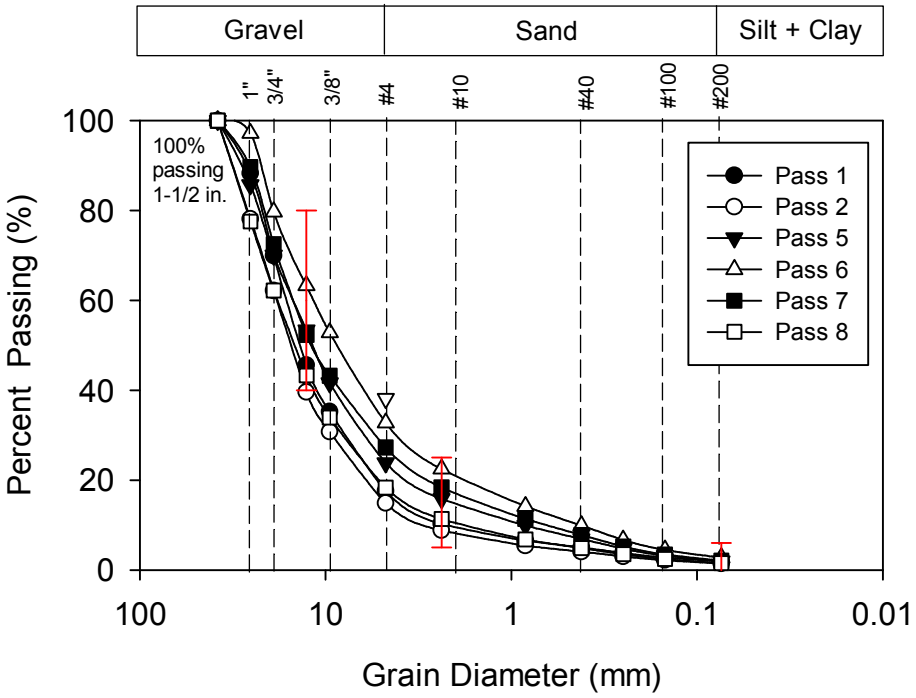

Figure 22. Particle size distribution of low amplitude vibratory roller section on untrimmed base Iowa I-35

Table 20. Summary of soil index properties of static compaction roller section (1-8) on untrimmed base I-35, Iowa

Parameter	Section 1	Section 2	Section 3	Section 4	Section 5	Section 6	Section 7	Section 8
USCS Classification	GW	GW	GW	GP	GW	GW	GW	GW
AASHTO Classification	A-1-a	A-1-a	A-1-a	A-1-a	A-1-a	A-1-a	A-1-a	A-1-a
Gravel Content (%) (> 4.75mm)	82	67	77	69	74	76	58	62
Sand Content (%) (4.75mm-75µm)	17	31	22	28	25	23	39	35
Silt + Clay Content (%) (< 75µm)	1	2	1	4	1	2	2	3
D10 (mm)	2.15	0.50	1.09	0.50	0.82	1.12	0.43	0.44
D15 (mm)	3.96	1.0	2.40	1.70	1.75	2.29	0.80	0.81
D30 (mm)	7.70	4.07	6.38	4.42	5.72	6.13	2.74	2.98
D50 (mm)	13.61	9.10	11.66	9.50	11.83	11.65	6.37	8.23
D60 (mm)	16.22	12.93	13.92	12.83	16.31	14.57	8.48	11.98
D85 (mm)	26.72	24.89	20.16	23.04	24.48	22.85	18.56	21.1
Coefficient of Uniformity (c_u)	7.53	25.93	12.80	25.60	19.88	12.97	19.64	27.43
Coefficient of Curvature (c_c)	1.70	2.57	2.69	3.04	2.45	2.29	2.05	1.70

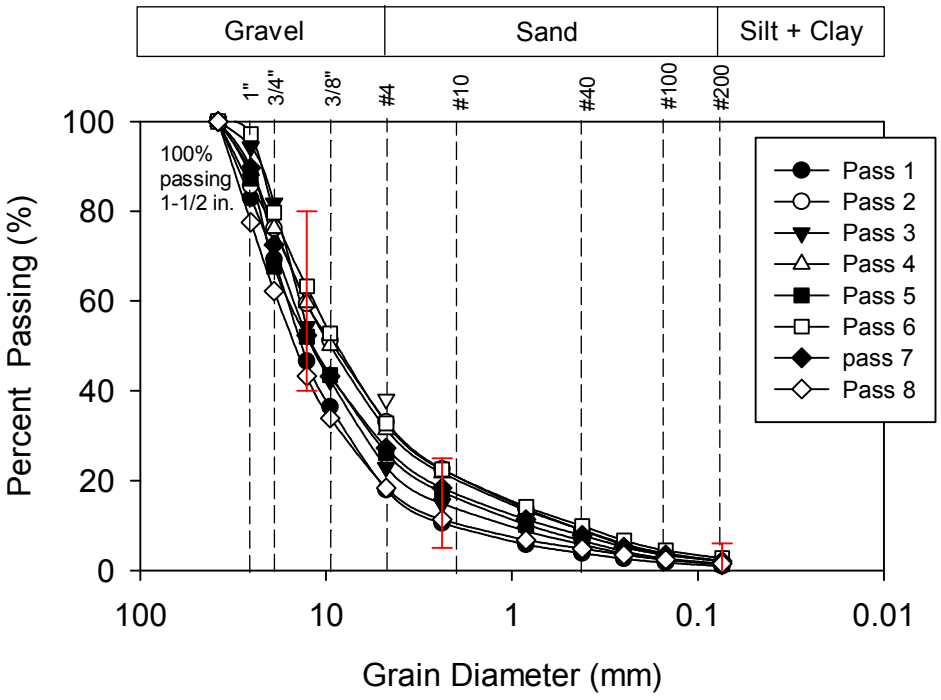

Figure 23. Particle size distribution of static compaction roller section on untrimmed base I-35, Iowa

Trimmed base (Test bed 2)

Test bed 2, the trimmed base, is approximately 500 ft long by 30 ft wide and is divided into ten sections. The sections are numbered from 0 to 9 indicating the number of roller passes prior to in situ testing. Trimmed base included 54 test point locations for 10 sections. 30 test point locations were selected for low-amplitude compaction section. 24 test point locations were selected for static compaction section. Trimmed and untrimmed bases are shown in Figure 24. Trimming process was performed to remove excess base material and meet the required thickness for paving. Figure 25 illustrates the trimming process use a 9500 Geomaco trimmer.

Based on USCS, soil classifications of trimmed base show in Table 21 to Table 22 are from GW-GM (well-graded gravels – silty gravels and gravel-sand-silt mixtures) to GP-GM (poorly-graded gravels - silty gravels and gravel-sand-silt mixtures). More fine contents in the trimmed base compare with the classification of untrimmed base (GW or GP).

The grain size distribution curves are shown in Figure 26 and Figure 27. The Iowa DOT aggregate gradation base requirement is also shown for comparison. Figure 26shows from pass 5 to pass 9 of low amplitude vibratory sections. The grain size distribution has more fine content than the Iowa DOT limit gradation 4121 recycle granular requirement (Iowa DOT specification is presented as red bars in Figure 26 and Figure 27). More fines content is probably due to particle breakage as the result of more compactions.

Figure 24. Trimmed base (left) and untrimmed base (right) for I-35 Iowa

Figure 25. Trimming process for I-35 Iowa

Table 21. Summary of soil index properties of low amplitude vibratory roller sections (1-9) on trimmed base I-35, Iowa

Parameter	Section 1	Section 2	Section 3	Section 4	Section 5	Section 6	Section 7	Section 8	Section 9
USCS Classification	GW-GM	GW-GM	GW-GM	GW-GM	GP-GM	GP-GM	GP-GM	GP-GM	GP-GM
AASHTO Classification	A-1-a	A-1-a	A-1-a	A-1-a	A-1-a	A-1-a	A-1-a	A-1-a	A-1-a
Gravel Content (%) (> 4.75mm)	80	80	80	81	66	61	62	70	60
Sand Content (%) (4.75mm-75µm)	14	14	14	13	25	29	28	22	30
Silt + Clay Content (%) (< 75µm)	6	6	6.0	6	9	10	11	8	10
D10 (mm)	1.94	1.93	1.51	1.44	0.11	0.085	—	0.15	0.08
D15 (mm)	3.64	3.66	3.75	3.86	0.78	0.41	0.25	1.42	0.35
D30 (mm)	6.86	6.70	6.17	6.55	3.95	3.20	3.40	4.82	3.0
D50 (mm)	13.05	11.97	9.66	11.18	8.37	7.13	6.62	11.05	6.95
D60 (mm)	16.06	14.99	12.51	15.26	11.51	10.11	8.62	15.61	9.32
D85 (mm)	26.33	23.07	22.83	27.60	21.01	19.63	15.66	23.56	16.98
Coefficient of Uniformity (c_u)	8.26	7.76	8.26	10.62	107.68	119.55	—	104.4	116.07
Coefficient of Curvature (c_c)	1.51	1.55	2.01	1.95	12.68	11.97	—	9.95	12.05

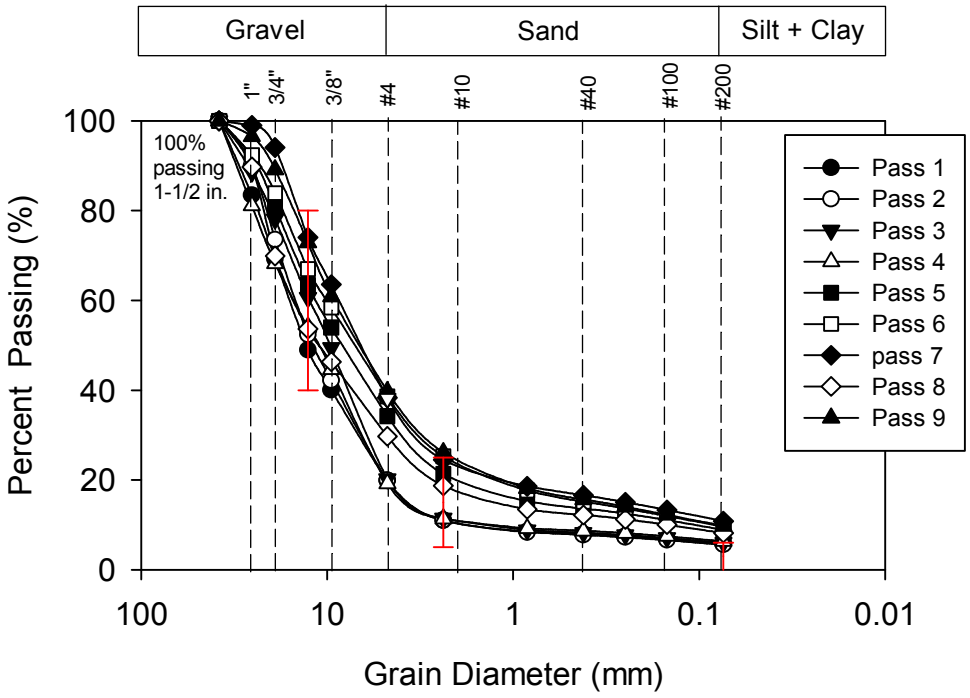

Figure 26. Particle size distribution of low amplitude vibratory roller sections on trimmed base Iowa I-35

Table 22. Summary of soil index properties of static compaction roller sections (1-8) on trimmed base I-35, Iowa

Parameter	Section 1	Section 2	Section 3	Section 4	Section 5	Section 6	Section 7	Section 8
USCS Classification	GP-GM	GW-GM	GP-GM	GP-GM	GW	GP-GM	GP-GM	GP-GM
AASHTO Classification	A-1-a	A-1-a	A-1-a	A-1-a	A-1-a	A-1-a	A-1-a	A-1-a
Gravel Content (%) (> 4.75mm)	73	81	71	69	85	74	68	71
Sand Content (%) (4.75mm-75µm)	19	13	22	23	13	19	23	20
Silt + Clay Content (%) (< 75µm)	8	6	7.0	8	2	7	10	9
D10 (mm)	0.17	1.90	0.43	0.26	2.67	0.29	0.083	0.097
D15 (mm)	1.67	4.0	2.05	1.61	4.65	1.89	0.44	0.63
D30 (mm)	5.13	6.55	4.89	4.62	8.43	5.57	4.32	5.0
D50 (mm)	8.32	10.0	7.87	7.67	11.73	10.04	8.04	9.40
D60 (mm)	11.46	11.47	9.86	9.44	13.73	12.86	10.94	12.36
D85 (mm)	23.15	19.91	18.21	16.11	25.98	20.62	22.86	21.02
Coefficient of Uniformity (c_u)	68.87	6.04	23.11	35.77	5.15	44.79	132.47	127.58
Coefficient of Curvature (c_c)	13.83	1.97	5.67	8.56	1.94	8.40	20.67	20.84

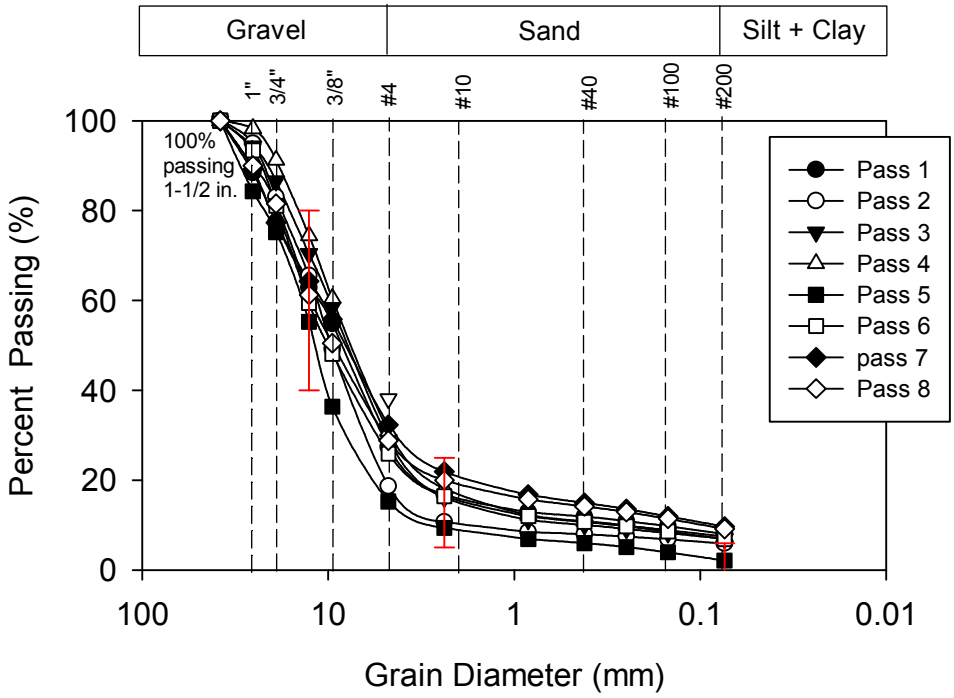

Figure 27. Particle size distribution of static compaction roller sections on trimmed base I-35, Iowa

Mixture of virgin material and RPCC

Test bed 3, the combined mixture of virgin material and RPCC, is approximately 650 ft long by 30 ft wide. This test bed is not subject to any in situ point measurement. Bag samples were collected for full gradation testing at one location from each section for investigation in laboratory. The material was classified as GW-GM to GP-GM (Table 23and Table 24) based on the USCU classification and A-1-a from AASHTO classification in the low amplitude vibratory sections. Static compaction section has more soil classification types (GW, GW-GM, GW-GM and GP-GM) than the low amplitude vibratory.

Grain –size distribution curves for this test bed are presented in Figure 28 and Figure 29. All distribution curves are within the range (red bars presented in Figure 28 and Figure 29 presents the range) of the Iowa DOT limit gradation 4121 recycle granular requirement.

Table 23. Summary of soil index properties of low amplitude vibratory roller sections (0-7) I-35, Iowa

Parameter	Section 0	Section 1	Section 2	Section 3	Section 4	Section 5	Section 6	Section 7
USCS Classification	GW-GM	GW-GM	GP-GM	GP-GM	GP-GM	GP-GM	GP-GM	GP-GM
AASHTO Classification	A-1-a	A-1-a	A-1-a	A-1-a	A-1-a	A-1-a	A-1-a	A-1-a
Gravel Content (%) (> 4.75mm)	86	86	84	82	83	71	79	74
Sand Content (%) (4.75mm-75µm)	9	9	10	11	11	20	14	18
Silt + Clay Content (%) (< 75µm)	5	5	7	7	6	10	7	8
D10 (mm)	2.55	2.07	0.44	0.27	1.04	0.09	0.21	0.14
D15 (mm)	5.46	5.46	4.18	3.30	4.08	0.41	2.57	1.11
D30 (mm)	9.86	10.42	8.42	8.52	8.30	4.86	6.42	5.63
D50 (mm)	14.09	15.61	12.52	12.50	13.11	9.19	10.96	9.92
D60 (mm)	16.53	18.10	14.23	14.46	15.66	11.88	13.66	12.27
D85 (mm)	23.12	23.68	19.50	21.23	21.68	20.45	20.91	19.07
Coefficient of Uniformity (c_u)	6.47	8.76	32.07	53.89	15.08	136.11	63.56	90.34
Coefficient of Curvature (c_c)	2.30	2.90	11.23	18.68	4.24	22.82	14.03	19.02

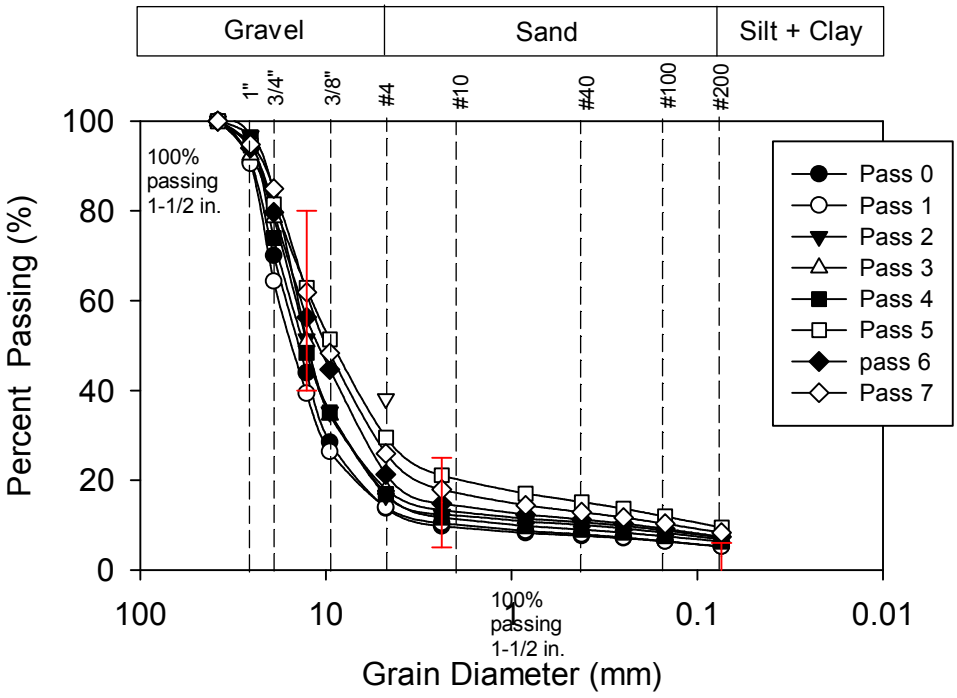

Figure 28. Particle size distribution of low amplitude vibratory sections on mixture of virgin material and RPCC on I-35, Iowa

Table 24. Summary of soil index properties of low amplitude vibratory roller sections (1-7) I-35, Iowa

Parameter	Section 1	Section 2	Section 3	Section 4	Section 5	Section 6	Section 7
USCS Classification	GW	GW-GM	GW-GM	GP-GM	GP-GM	GP-GM	GP
AASHTO Classification	A-1-a	A-1-a	A-1-a	A-1-a	A-1-a	A-1-a	A-1-a
Gravel Content (%) (> 4.75mm)	88	86	87	83	80	81	94
Sand Content (%) (4.75mm-75µm)	8	9	7	11	13	12	3
Silt + Clay Content (%) (< 75µm)	4	5	6	6	7	7	3
D10 (mm)	3.87	1.92	3.40	0.86	0.22	0.51	7.14
D15 (mm)	5.61	4.90	5.35	3.89	2.92	3.69	8.54
D30 (mm)	9.16	8.82	8.63	8.12	6.78	6.95	11.41
D50 (mm)	13.38	13.68	12.58	13.36	10.90	11.02	14.49
D60 (mm)	15.70	15.71	14.41	15.7	13.17	13.05	16.10
D85 (mm)	21.98	21.63	20.54	22.16	23.37	18.38	22.73
Coefficient of Uniformity (c_u)	4.06	8.22	4.24	18.34	60.01	25.34	2.26
Coefficient of Curvature (c_c)	1.38	2.59	1.52	4.91	15.92	7.20	1.13

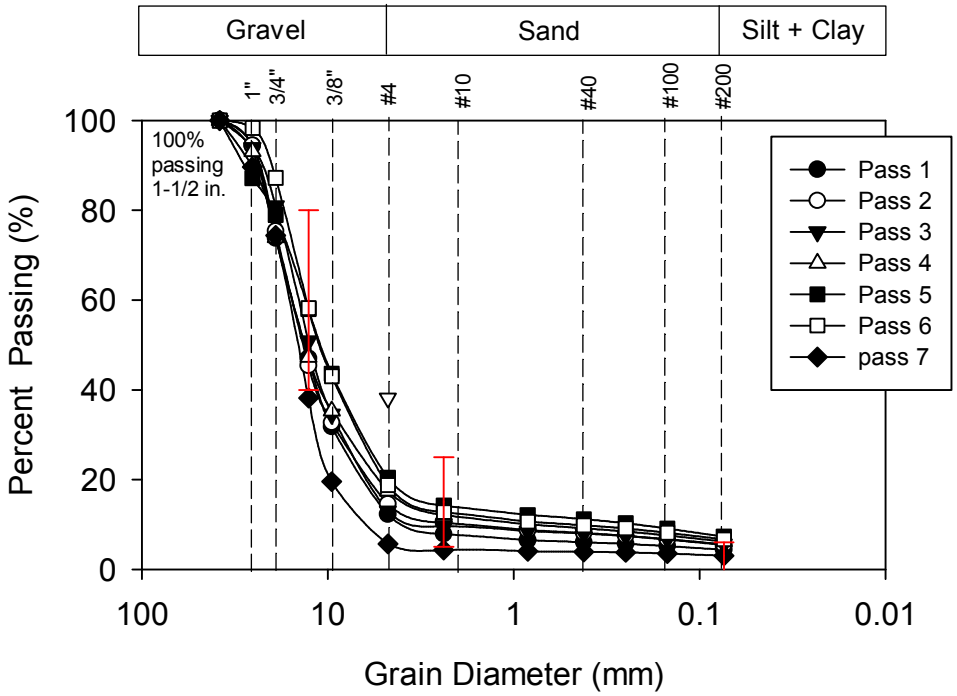

Figure 29. Particle size distribution of static compaction sections on mixture of virgin material and RPCC, I-35, Iowa

Breakage index value

Particle crushing and particle breakage change the particle size distributions. (Itai Einav, 2006). Hardin (1985) showed that defining and adequate measurement of the degree crushing is needed to establish stress-strain models:

"In order to understand the physics of the strength and stress- strain behavior of soils and to devise mathematical model that adequately represent such behaviors, it is important to define the degree to which the particles of an element of soil are crushed or broken during loading."

I-35 studies enrolled different passing which is different loading of particle size distribution in untrimmed base, trimmed base and mixture of virgin materials and RPCC. The breakage index value is the area between two different particle size distribution curves. In order to obtain the breakage index values, the area of each particle size distribution curve with passing 1 curve are calculated, as shown in Table 25.

Table 25. Summary of breakage index values of I-35, Iowa

Passing number	Untrimmed base		Trimmed base		Mixture of virgin material and RPCC	
	Low amplitude vibratory	Static compaction	Low Amplitude vibratory	Static compaction	Low Amplitude vibratory	Static compaction
Section 0-1	—	—	—	—	—	4.19
Section 2-1	7.0	21.32	2.38	8.45	1.43	1.16
Section 3-1	8.26	11.32	6.58	2.39	10.28	3.28
Section 4-1	—	20.82	2.11	6.98	10.04	
Section 5-1	—	10.98	23.24	20.01	6.91	10.52
Section 6-1	23.74	25.33	29.93	2.64	27.90	10.81
Section 7-1	12.38	13.97	35.83	7.63	15.72	14.59
Section 8-1	2.92	1.33	14.06	7.63	22.79	
Section 9-1	—	—	33.92	4.06	—	—

Laboratory Test

Laboratory study involves determination of GPT repeatability, investigation of the effect of thin layer to the hydraulic conductivity use GPT, evaluation of the influence of partial saturation to hydraulic conductivity use GPT and comparison hydraulic conductivity test measurements. Six of materials index properties, which include: classification (according to American Association of State Highway and Transportation Officials (AASHTO) and Unified Soil Classification System (USCS)), gradation parameters, specific gravity, and percent gravel are provided in the Table 26. Other materials index properties are shown in the above. Figure 30 shows the grain-size distribution curve of materials.

Table 26. Summary of material index properties

Parameter	**SAND1**	**SAND 2**	**OLS IA**	**PG**	**WLS-IA**	**OLS-63**
AASHTO Classification	A-1-b	A-1-a	A-1-a	A-1-a	A-1-a	A-1-a
USCS classification	SP	SP	GP	GP	SW-SM	GP-GM
Gravel Content(%) (> 4.75mm)	2	0	93	98	39	73
Sand Content (%) (4.75mm-75µm)	96	100	6	2	50	17
Silt + Clay Content (%) (< 75µm)	2	0	1	0	11	11
D10 (mm)	0.28	0.64	4.88	8.05	0.06	0.07
D20 (mm)	0.43	0.70	5.29	9.60	0.27	2.99
D30 (mm)	0.57	0.74	5.68	10.82	0.60	5.22
D60 (mm)	1.20	0.77	6.92	14.48	4.66	11.52
D90 (mm)	3.00	0.80	8.6	20.73	10.65	22.83
Coefficient of Uniformity (c_u)	4.2	1.2	1.4	1.8	77.6	167.1
Coefficient of Curvature (c_c)	1.0	1.0	1.0	1.0	1.3	34.2
Gs	2.68	2.70	2.71	2.70*	2.68	2.76

*Assumed

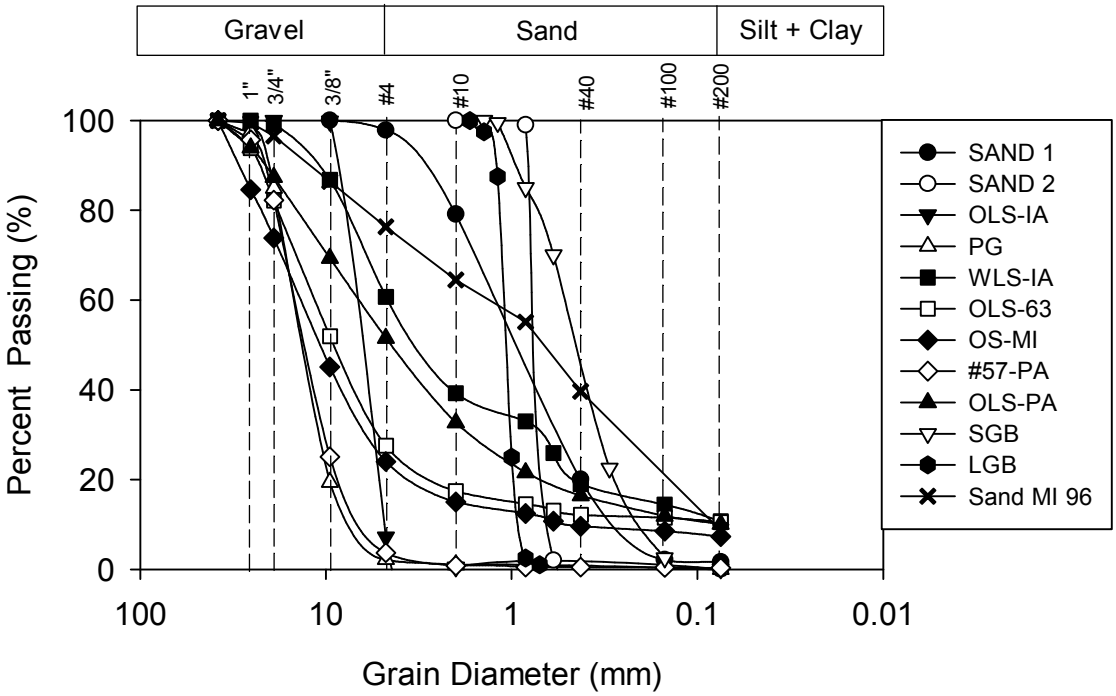

Figure 30. Grain-size distribution curves of materials

CHAPTER 5. RESULTS AND DISCUSSION

This chapter presents and discusses the test results from both in situ and laboratory studies. In situ and laboratory tests include various field base/subbase layers of construction projects (Table 27 and Table 28). Laboratory studies are presented in this order: (a) Drainage analysis use different design devices in the laboratory (b) GPT repeatability and measurement range; (c) GPT thin layers study. In situ study includes measurements of hydraulic conductivity of the four different field sites in four states. This chapter presents and discusses the testing results on samples from I-94, I-96 US-22, and I-35, which include:

- Hydraulic conductivity (k_{sat}) calculated from gas permeability test (GPT) measurements;
- Moisture content (w%) and dry unit weight (γ_d) determined the from Humboldt nuclear gauge (NG) tests;
- Global positioning system (GPS) measurements to obtain spatial northing and easting of each test location.

I-35 study involved other in-situ test methods:

- Dynamic elastic modulus $E_{LWD\text{-}Z23}$ was determined by using a 300 mm diameter plate Zorn light weight deflectometer (LWD);
- Modulus of subgrade reaction was assessed through correlations with California bearing ratio (CBR) and dynamic cone penetration index (DCPI) values;
- Static elastic modulus of subgrade and modulus of subgrade reaction were determined from a static plate load device; and
- Roller intelligent compaction measurements value from a Caterpillar smooth drum vibration roller measuring machine drive power (MDP).

Table 27. Summary of investigated sites and materials

State	Site location	Materials	Date
Michigan	I-94	Existing subbase, base, subgrade	May 27 to June 1,2009
Michigan	I-96	Subbase, subgrade	May 18 to May 20, 2010.
Pennsylvania	US-22	Cement-treated base (CTB),asphalt-treated base (ATB),subbase, subgrade	July 27 to 28, 2009
Iowa	I-35	Trimmed and untrimmed recycled concrete, pavement base	August 27, 30 and 31, 2010

Table 28. Description and source of materials (after NCHRP, 2010)

Material	Description	Lab/Field Study	Source
Sand 1	Concrete sand	Lab	Hallet Materials,Ames, IA
Sand 2	ASTM 20/30 silica sand	Lab	-
WLS-IA	Well-graded crushed limestone	Lab	Martin Marietta Materials, Ames, IA
PG	Open grade pea gravel	Lab	Hallet Materials, Ames, IA
SGB	Small glass beads (0.75 mm spheres)	Lab	—
LGB	Large glass beads (1 mm spheres)	Lab	—
OLS-IA	Open-graded crushed limestone	Lab	Martin Marietta Materials, Ames, IA
OLS-63	Open-graded crushed limestone	Lab	Hwy 63, New Hampton, IA
OS-MI	Open-graded slag	Lab and Field	I-94, St. Clair and Macomb, MI
#57-PA	AASHTO #57 crushed limestone	Lab and Field	SR-22, Clyde, PA
OLS -PA	Open-graded crushed limestone	Lab and Field	SR-22,Clyde, PA
Sand 3	Sandy subbase	Lab and Field	MI-96, Lansing, MI
Aggregate	Aggregate used for CTB ,I-96	Lab and Field	MI-96, Lansing, MI
Recycled concrete	Untrimmed base and trimmed base	Lab and Field	I-35, Story county, IA

In situ Study

Michigan I-94

This in situ study was conducted on a newly constructed pavement on I-94 in St. Clair and Macomb Counties, Michigan. The test bed consisted 40.6 cm compacted and trimmed open-graded aggregate subbase material over an impervious subgrade. Impervious subgrade consisted of a recompacted mixture of sand and silty clay. In situ tests included determination of hydraulic conductivity using a gas permeability device (GPT(B)) and moisture–dry unit weight measurements using NG. GPT(B) was used to obtain various combinations of $P_{o(g)}$ and Q measurements at test locations in a grid pattern over 7 m by 7 m test area (Figure 31). $P_{o(g)}$ and Q measurement range is 1 to 75 mm of H_2O and 250 to 600 cm^3/s, respectively. Bag samples (0-60mm) of materials were obtained directly beneath the GPT location and transported to the laboratory to determine moisture content and fine content (passing #200 sieves). The materials open graded steel slag (OS-MI) was classified as GP-GM (poorly graded gravel and well graded gravel) based on USCS classification and A-1-a from AASHTO classification.

The results from the GPT show a mean hydraulic conductivity of about 4.9 cm/sec, with a coefficient of variation at 119% (Table 29). The hydraulic conductivity values obtained are in the range of about 0.1 to 30 cm/sec. The mean fines content (passing # 200 sieves) is about 3.7% with a coefficient of variation at 37%. The kriged spatial contour maps for hydraulic conductivity and fines contents are shown in Figure 32. Visual interpretation of high fines contents exhibit low hydraulic conductivities. Semi-variogram of fines content shows smaller range (a= 1.8 m) than the k_{sat} range (a= 2.3 m). At the same time, value of sill of fines content is larger than the k_{sat}. Therefore, data of fines content values have more variability than the k_{sat}. Figure 33presents the kriged contour spatial map semivariograms and histogram plots for dry unit weight and moisture content.

Figure 31. Overview for test bed (left) and GPT in situ testing on I-94, Michigan

Table 29. Summary statistics of field measurement on I-94, Michigan

Material	**Steel slag (OS-MI)**
Saturated Hydraulic Conductivity, k_{sat} Statistics	
Number of measurement, N	120
Mean, μ (cm/s)	4.9
Standard Deviation, σ (cm/s)	5.9
Coefficient of Variation, COV (%)	119
Variogram Sill, C+ C_o	0.34
Variogram Range, a (m)	2.3
Minimum value (cm/s)	0.93
Maximum value (cm/s)	30.05
Fines content Statistics	
Number of measurement, N	120
Mean, μ (%)	3.7
Standard Deviation, σ	1.4
Coefficient of Variation, COV (%)	37
Variogram Sill, C+ C_o	2.0
Variogram Range, a (m)	1.8
Minimum value (%)	1.56
Maximum value (%)	8.80
Dry Unit Weight, γ_d Statistics	
Number of measurement, N	120
Mean, μ (kN /m^3)	20.01
Standard Deviation, σ (kN /m^3)	0.62
Coefficient of Variation, COV (%)	3
Minimum value (kN /m^3)	18.5
Maximum value (kN /m^3)	21.3
Moisture Content Statistics	
Number of measurement, N	120
Mean, μ	3.3
Standard Deviation, σ	0.6
Coefficient of Variation, COV (%)	20
Minimum value (%)	1.1
Maximum value (%)	1.9
Degree of Saturation, S Statistics	
Number of measurement, N	120
Mean, μ	24
Standard Deviation, σ	6
Coefficient of Variation, COV (%)	24

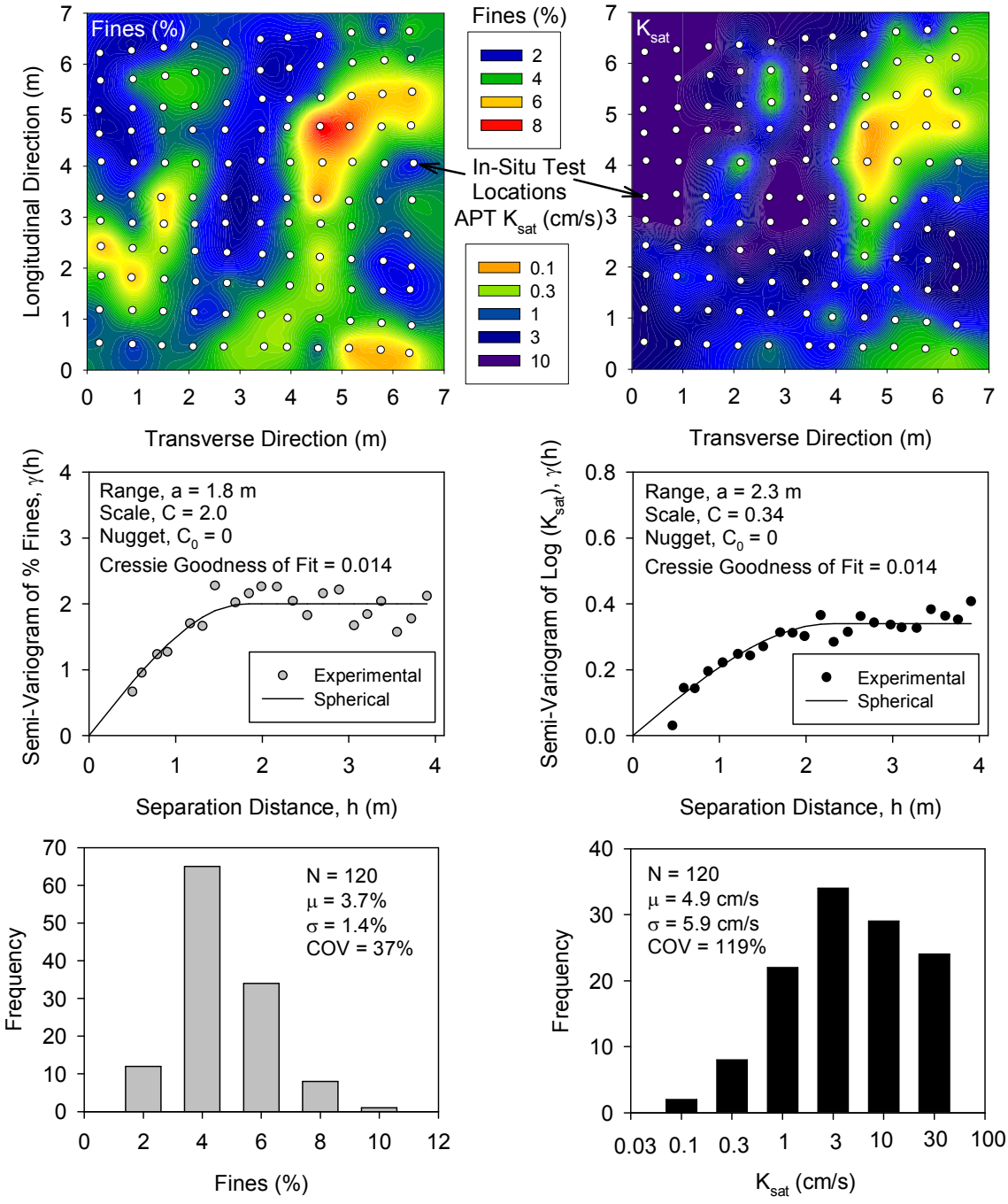

Figure 32. Kriged contour spatial map (top), semivariograms (middle,) and histogram plots (bottom) of fines content and K_{sat} on compacted open-graded steel slag base on I-94, Michigan

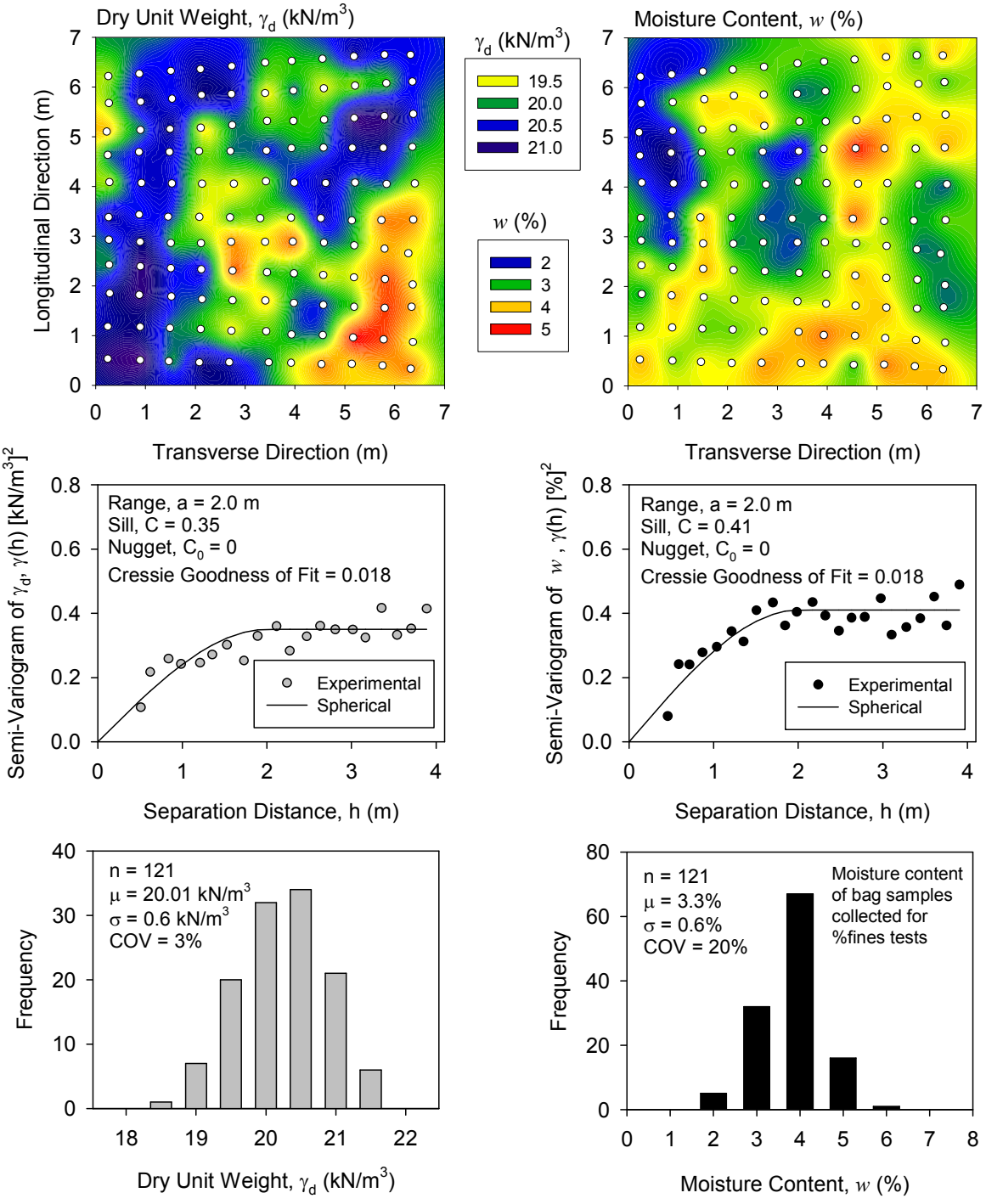

Figure 33. Kriged contour spatial map (top), semivariograms (middle,) and histogram plots (bottom) of dry unit weight and moisture content on compacted open-graded steel slag base on I- 94, Michigan

Michigan I-96

This in situ study data was collected in Lansing, Michigan from May 18 to May 20, 2010. This project involved testing on an open–graded sandy subbase and a newly cement treated base (CTB) made from recycled concrete pavement that has been ground and graded underlain by sandy subbase and clayey subgrade. Michigan DOT used approximately 5 in. of CTB over a geosynthetic separation layer over about 12 in. of a sandy subbase (reused from existing roadway) over the clay subgrade. The material of sandy subbase was classified as A-1-b per AASHTO and SP-SM (poorly graded sand with silt) per USCS classification (see Table 30). Figure 34 shows overview for sandy subbase.

In situ tests include determination of hydraulic conductivity using a gas permeability test device (GPT) and moisture–dry unit weight measurements using NG. Bag samples of untreated base materials were obtained directly beneath the GPT location and transported to the laboratory to determine moisture content and fines content (passing #200 sieve). GPT measurements were conducted on the sand subbase at 73 points on a 3 ft x 3 ft grid with 9 columns across the traffic lanes and 10 rows deep.

Results from the GPT of sandy subbase show a mean saturated hydraulic conductivity of about 1.5 cm/sec, with coefficient of variation at 46%. Hydraulic conductivities range from 0.1 cm/sec to 2.2 cm/sec. The mean of fines content is about 6.5% with a coefficient of variation at 29%. Kriged spatial contour map, semivariograms and histogram plots for hydraulic conductivity and fines contents are presented in Figure 36.Figure 37 also demonstrates the kriged spatial map, semivariograms and histogram plots for dry unit weight and moisture content. Data of kriged spatial contour map generate by geostatistical spatial analysis. GPT results of cement treated base (CTB) show a mean saturated hydraulic conductivity of 2.95 cm/s with a coefficient of variation at 93%. The values obtained were in the range of about 0.1 cm/sec to 816 cm/sec. Figure 35 shows the overview of CTB test bed and segregation of CTB. Kriged spatial map, semivariograms and histogram plots of CTB present in Figure 38.

Table 30. Summary statistics of field measurement on I-96, Michigan

Material	**Sandy subbase**	**CTB**
Saturated Hydraulic Conductivity, k_{sat} Statistics		
Number of measurement, N	64	65
Mean, μ (cm/s)	1.48	2.95
Standard Deviation, σ (cm/s)	0.68	2.7
Coefficient of Variation, COV (%)	46	93
Minimum value (cm/s)	0.47	0.11
Maximum value (cm/s)	4.83	816.0
Fines content Statistics		
Number of measurement, N	69	—
Mean, μ	6.53	—
Standard Deviation, σ	1.9	—
Coefficient of Variation, COV (%)	0.29	—
Minimum value (%)	3.36	—
Maximum value (%)	10.89	—
Dry Unit Weight, γ_d Statistics		
Number of measurement, N	73	118
Mean, μ (kN /m^3)	20.16	14.6
Standard Deviation, σ (kN /m^3)	0.58	0.81
Coefficient of Variation, COV (%)	3	6
Minimum value (kN /m^3)	18.79	12.16
Maximum value (kN /m^3)	21.31	16.29
Moisture Content Statistics		
Number of measurement, N	73	118
Mean, μ	7.82	7.4
Standard Deviation, σ	0.98	1.02
Coefficient of Variation, COV (%)	13	14
Minimum value (%)	6.1	5.6
Maximum value (%)	9.9	12.05
Degree of Saturation, S Statistics		
Number of measurement, N	73	118
Mean, μ	72	26
Standard Deviation, σ	10	5
Coefficient of Variation, COV (%)	14	18

—Data not collected

Figure 34. Overview for sandy subbase test bed (left) and GPT in situ testing on I-96, Michigan.

Figure 35. GPT on cement treated base (left) and segregation of CTB on I-96, Michigan.

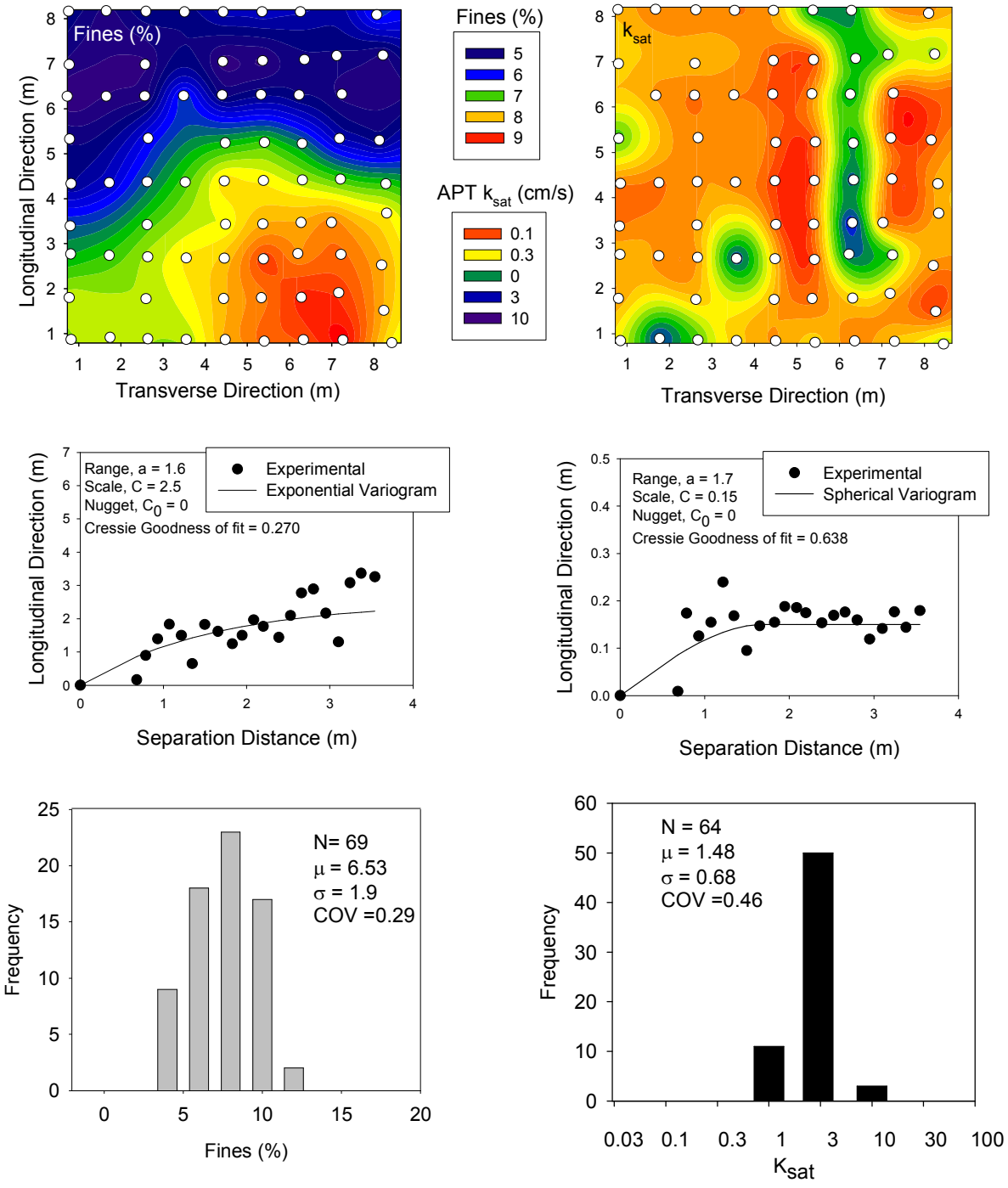

Figure 36. Kriged contour spatial map (top), semivariogram (middle), and histogram plot (bottom) of APT k_{sat} and fines content on sandy subbase on MI-96 project near Lansing, Michigan

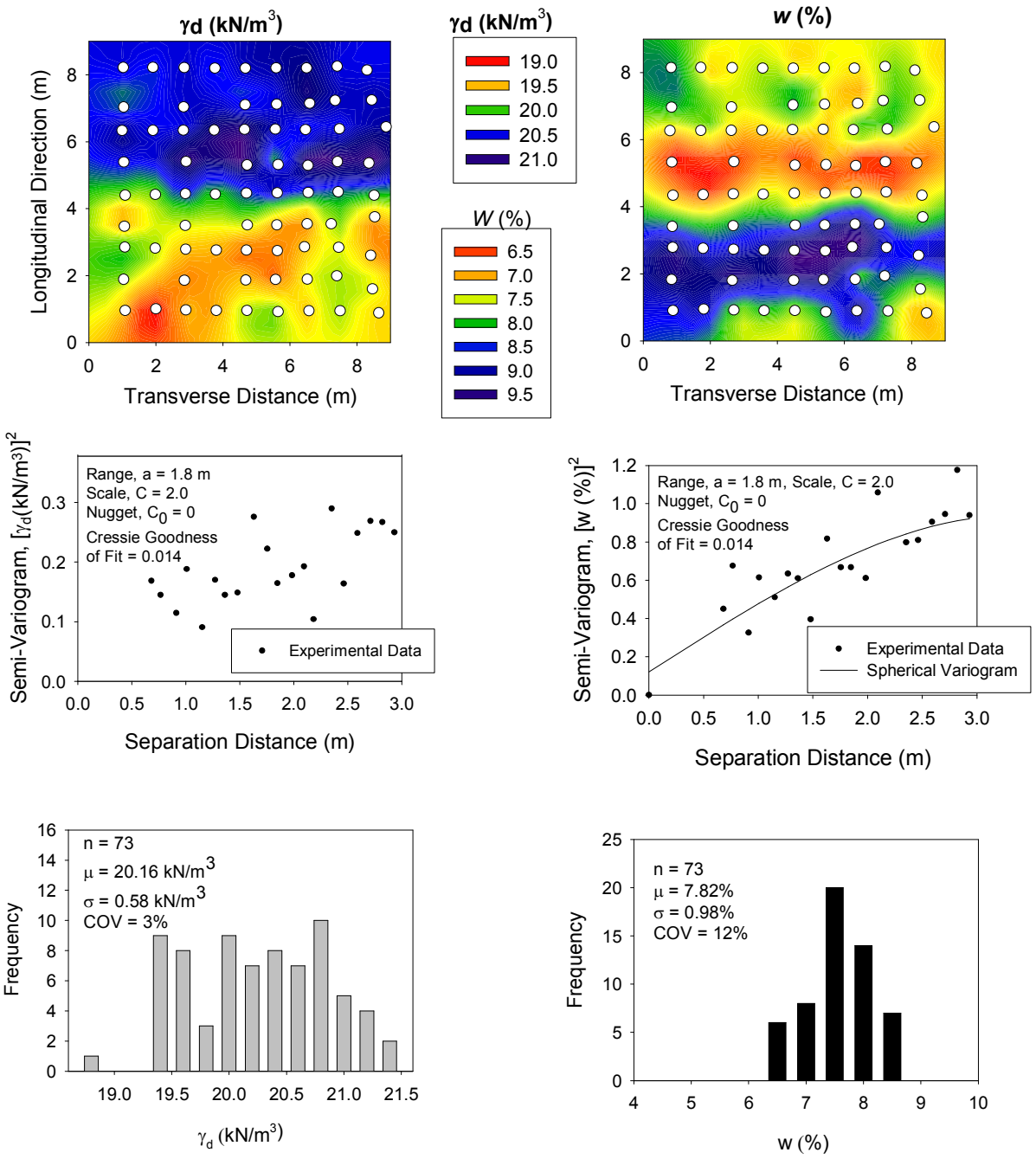

Figure 37. Kriged contour spatial map (top), semivariogram (middle), and histogram plot (bottom) of dry unit weight and moisture content on sandy subbase on MI-96 project near Lansing, Michigan

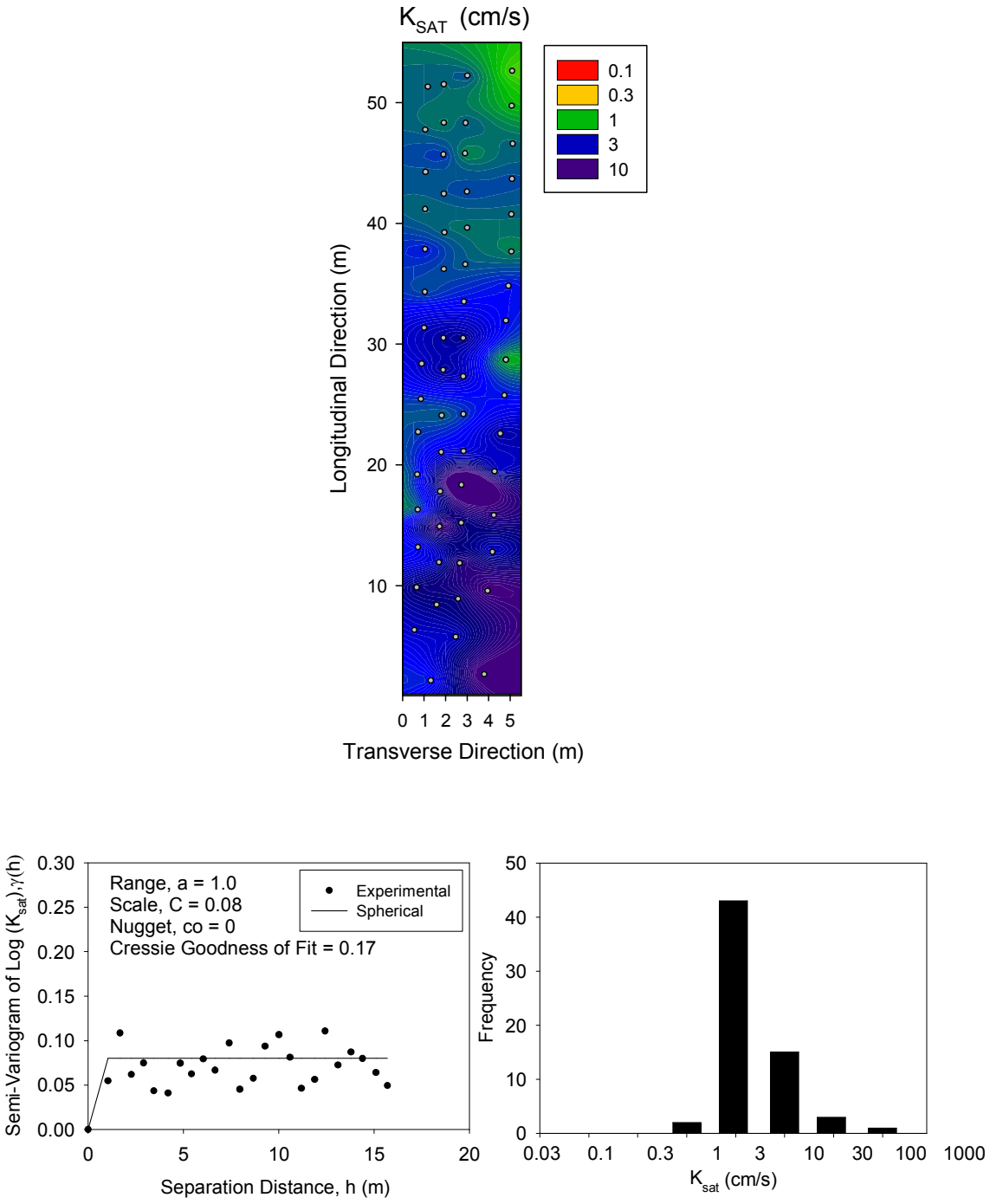

Figure 38. Kriged contour spatial map (top), semivariogram (middle), and histogram plot (bottom) of APT k_{sat} on CTB on MI-96 project near Lansing, Michigan

Pennsylvania SR-22

This field study was conducted at U.S. Highway 22 near Blairsville, PA and Clyde, PA on July 2009. GPT tests involve testing of a newly constructed cement-treated open-graded crushed AASHTO #57 stone base (CTB), a asphalt-treated AASHTO # 57 stone base (ATB), and a open-crushed limestone leveling subbase (OLS-PA) layer.

The CTB layer was approximately 100 mm thick over 50 mm thick crushed limestone and 450 mm of rock cap. CTB tested was performed on the connected shoulder lanes of eastbound and westbound lanes (Figure 39). The eastbound lane base layer was constructed in summer 2009 (Area A) and the westbound lanes base layer was constructed in fall 2008 (Area B). Area B was contaminated with fines. In situ tests include determination of the hydraulic conductivity using a gas permeability device and moisture–dry unit weight measurements using nuclear gauge in an area about 5 m by 9 m. This study includes 49 — locations in Area A and 23 locations in Area B (Figure 40).

GPT tests were performed on the Asphalt Treated permeable base (ATB) and leveling subbase layers. The GPT layer was approximately 100 mm thick over 50 mm of leveling subbase and 450 mm of rock cap. In situ tests includes determination of hydraulic conductivity by GPT and moisture–dry unit weight measurements using nuclear gauge on 99 locations in area 14m by 14 m. Figure 41 shows the area consisted of ATB Layer on the mainline and exposed leveling subbase layer.

GPT(A) and GPT(B) are used to obtain various combinations of $P_{o(g)}$ and Q measurements which range from 5 to 75 mm of H_2O and 250 to 7500 cm^3 on CTB, respectively. High hydraulic conductivity of area A uses GPT(A) and low hydraulic conductivity of area B uses GPT(B). GPT(A) was used to obtain various combinations of $P_{o(g)}$ and Q measurements which range from 5 to 75 mm of H_2O and 200 to 7500 cm^3 on ATB, respectively.

Results (see Table 31) of APT of area A (2009) on cement treated AASHTO # 57 base show saturated hydraulic conductivity of about 7.0 cm/sec with coefficient of variation of 45%. Hydraulic conductivity range is between 1.3 cm/sec and 10.6 cm/sec in this area. However, the area B (2008) have much smaller saturated hydraulic conductivity value than area A which is 0.2 cm/sec and high coefficient of variation of 101%. Hydraulic conductivity

vary from 0.1 cm/sec to 18.3 cm/sec. Kriged spatial contour map (see Figure 42) clearly show the difference between area A and area B. The average k_{sat} value of westbound lane base layer which was constructed in fall 2008 and contaminated with washed out fines is 35 times lower than average k_{sat} value of Area A which was construction in 2009 and without fines. Area A which was constructed in 2009 has more variability than Area B which was constructed in 2008. Because the figures of semi-variogram show the area A has larger values of range and sill than area B.

The average value of hydraulic conductivity of ATB is 4.6 cm/sec with coefficient of variation at 42%. Hydraulic conductivities vary between 0.06 cm/sec to 10.6 cm/sec in this section. The hydraulic conductivity obtained from Open-crushed limestone leveling subbase (OLS-PA) layers is in the range of 0.06 cm/sec to 0.13 cm/sec. ATB have lower hydraulic conductivity values which are similar to the spatial contour map (see Figure 43). Semi-variogram of APT has larger value of range and sill than the leveling subbase (OLS-PA). So, the APT has more variability than the leveling subbase.

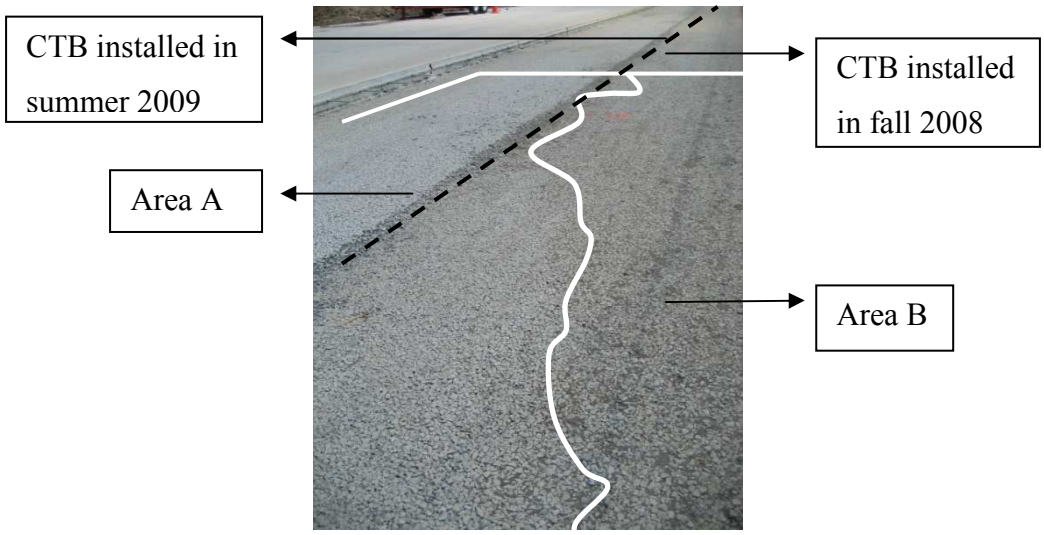

Figure 39. Area A and Area B on cement treated base on SR-22, Pennsylvania

Figure 40. Overview for test bed (left) and GPT in situ testing on cement treated base on SR-22, Pennsylvania

Figure 41. Overview for test bed (left) and subbase test location asphalt treated base on US-22, Pennsylvania

Table 31. Summary of statistical analysis of Pennsylvania US-22 materials on US-22, Pennsylvania

Material	Cement treated AASHTO # 57 base (CTB)		Asphalt treated AASHTO # 57 base (ATB)
	Area A	Area B	
Saturated Hydraulic Conductivity, k_{sat} Statistics			
Number of measurement, N	49	23	99
Mean, μ (cm/s)	7.0	0.2	4.6
Standard Deviation, σ (cm/s)	3.1	0.2	1.9
Coefficient of Variation, COV (%)	45	101	42
Variogram Sill, C+ C_o	0.08	0.04	0.03
Variogram Range, a (m)	3.0	2.5	4.0
Minimum value (cm/s)	0.09		0.06
Maximum value (cm/s)	18.33		10.60
Dry Unit Weight, γ_d Statistics			
Number of measurement, N	49	23	99
Mean, μ (kN /m^3)	16.98	18.25	17.64
Standard Deviation, σ	2.25	0.75	1.88
Coefficient of Variation, COV (%) (kN /m^3)	13	4	11
Minimum value			
Maximum value			
Moisture Content Statistics			
Number of measurement, N	49	23	Not Applicable
Mean, μ	6.2	6.1	
Standard Deviation, σ	0.6	0.7	
Coefficient of Variation, COV (%)	10	11	
Minimum value			
Maximum value			
Degree of Saturation, S Statistics			
Number of measurement, N	49	23	Not Applicable
Mean, μ	31	38	
Standard Deviation, σ	6	4	
Coefficient of Variation, COV (%)	18	11	

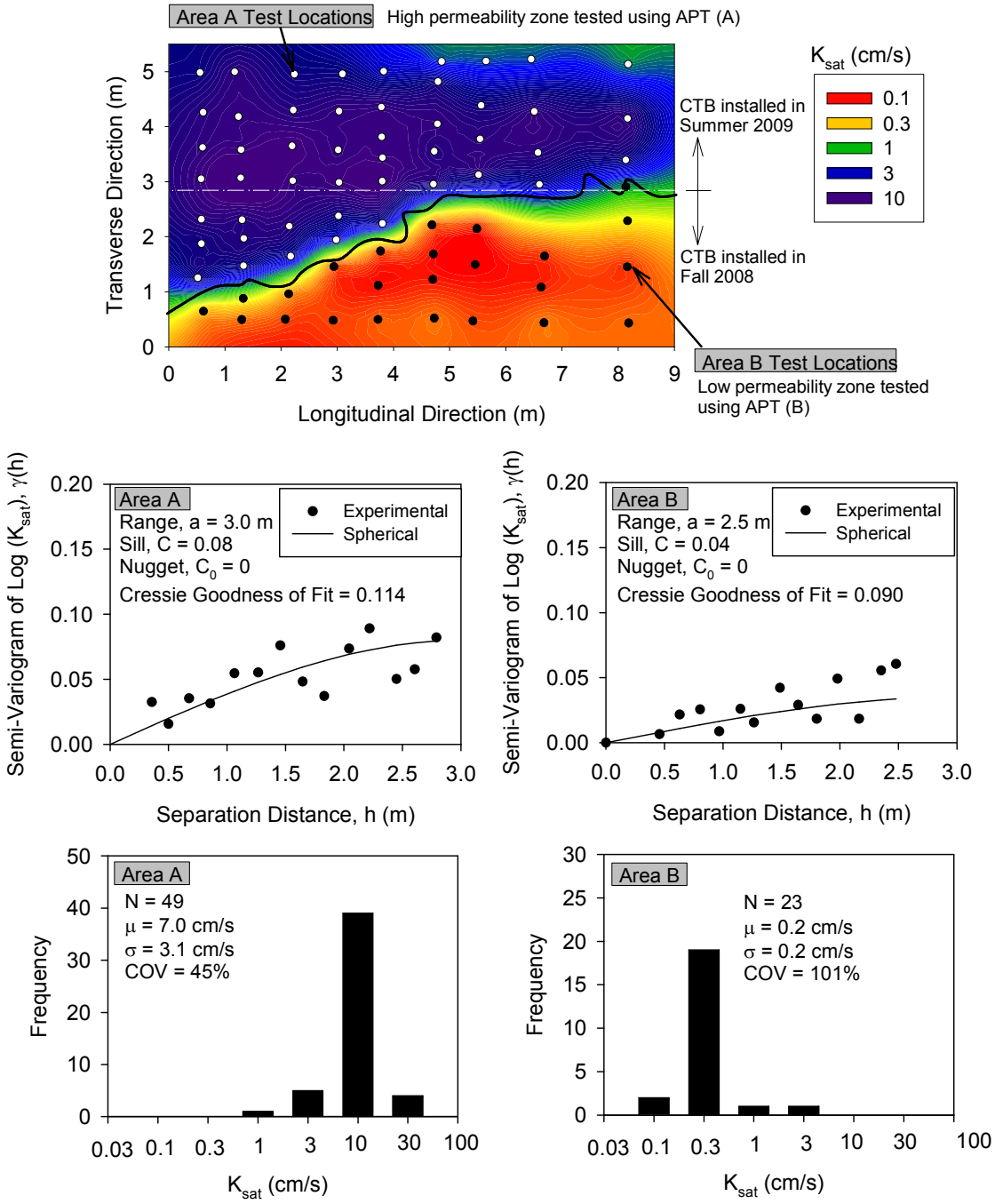

Figure 42. Kriged contour spatial map (top), semivariograms (middle,) and histogram plots (bottom) of CTB ksat on cement treated base on SR-22 project near Clyde, Pennsylvania.

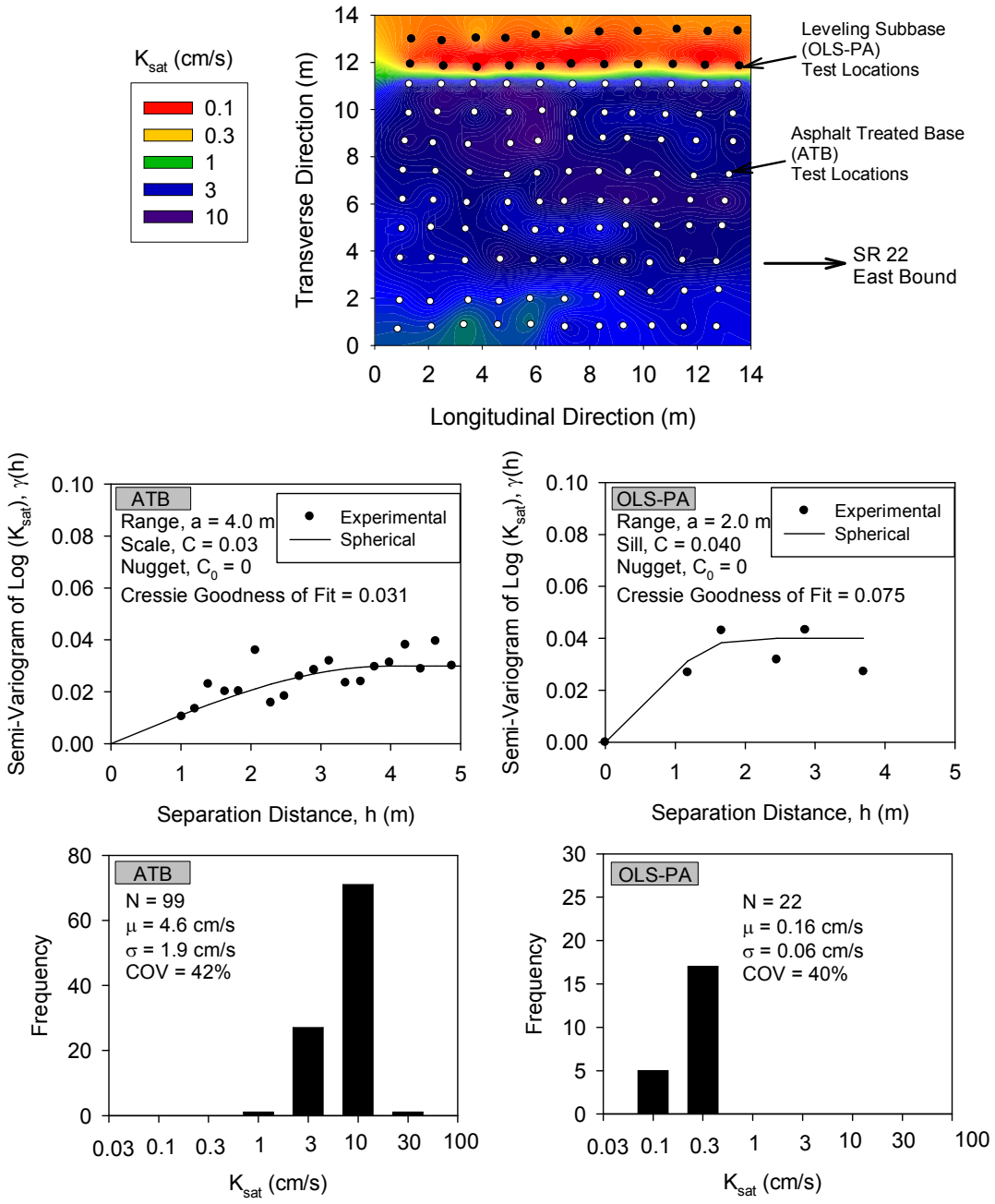

Figure 43. Kriged contour spatial map (top), semivariograms (middle,) and histogram plots (bottom) of APT k_{sat} on cement treated base on SR-22 project near Clyde, Pennsylvania.

MEPDG drainage design calculation

MEPDG (appendix tt) had shown the drainage design calculations. All equations present in this section and Figure 44 show the roadway geometry.

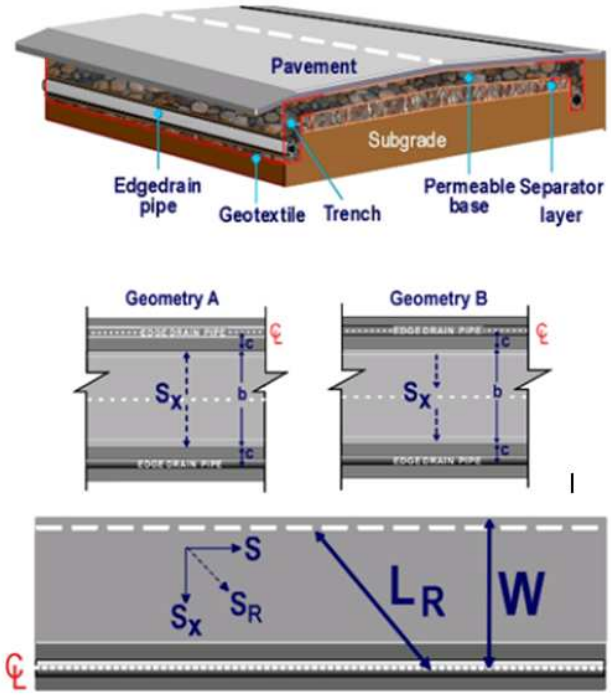

Figure 44.Roadway geometry used in drainage design calculation on MEPDG

MEPDG shows the width of drainage path calculator by the width of pavement surface (b) and the distance from pavement shoulder to the edge of the permeable base(c)

$$W = \frac{b}{2} + c \qquad (5.1)$$

W = Wide of drainage path

c = distance from the pavement shoulder to the edge if the permeable base

b = the width of pavement surface

The resultant length of drainage path is calculated by using the longitude slop and cross as shown below:

$$S_R = \sqrt{S^2 + S^2{}_X}$$

S_R = resultant length of drainage path LR

S = longitudinal slop

S_x = cross slop

LR is the flow path length. W, S and S_X were shown before

$$L_R = W\sqrt{1+\left(\frac{S}{S_X}\right)} \tag{5.2}$$

Inflow (crack infiltration) show in the following equation:

$$q_i = I_C\left(\frac{N_c}{W}+\frac{W_c}{W_P C_S}\right)\times k_p \tag{5.3}$$

Where:

q_i = infiltration rate per unit area ($m^3/day/m^2$)

I_c= infiltration rate of crack ($m^3/day/m^2$)

W_c= length of transverse crack/joints (m)

W_p= width of the drainage layer (m)

N_c = number of contributing traffic lanes (equal to one plus the number of contributing traffic lanes)

C_s = spacing of transverse cracks or joints (m)

k_p =permeability of pavement surface

Barber and Sawyer (1952) showed the capacity of a drainage layer under state flow conditions based on geometry of drainage layer:

$$q = q_i \times W_C = kH\left(S+\frac{H}{2L}\right) \tag{5.4}$$

Where:

q = discharge capacity of the drainage layer ()

k = permeability of the drainage layer (m/day)

S = flow-path gradient (m/m)

H= thickness of the base layer (m/m)

L = flow path length (m)

Casagrande and Shannon (1952) showed a chart to determine the time required for any degree of drainage. As shown in Figure 45.The 50% degree of drainage depends on the time factor T_f and the slop factor S_f were defined as:

$$S_1 = \frac{LS}{H} \tag{5.5}$$

$$T_f = \frac{kHt}{n_e L^2} \tag{5.6}$$

All parameters were shown before except n_e is the effect porosity.

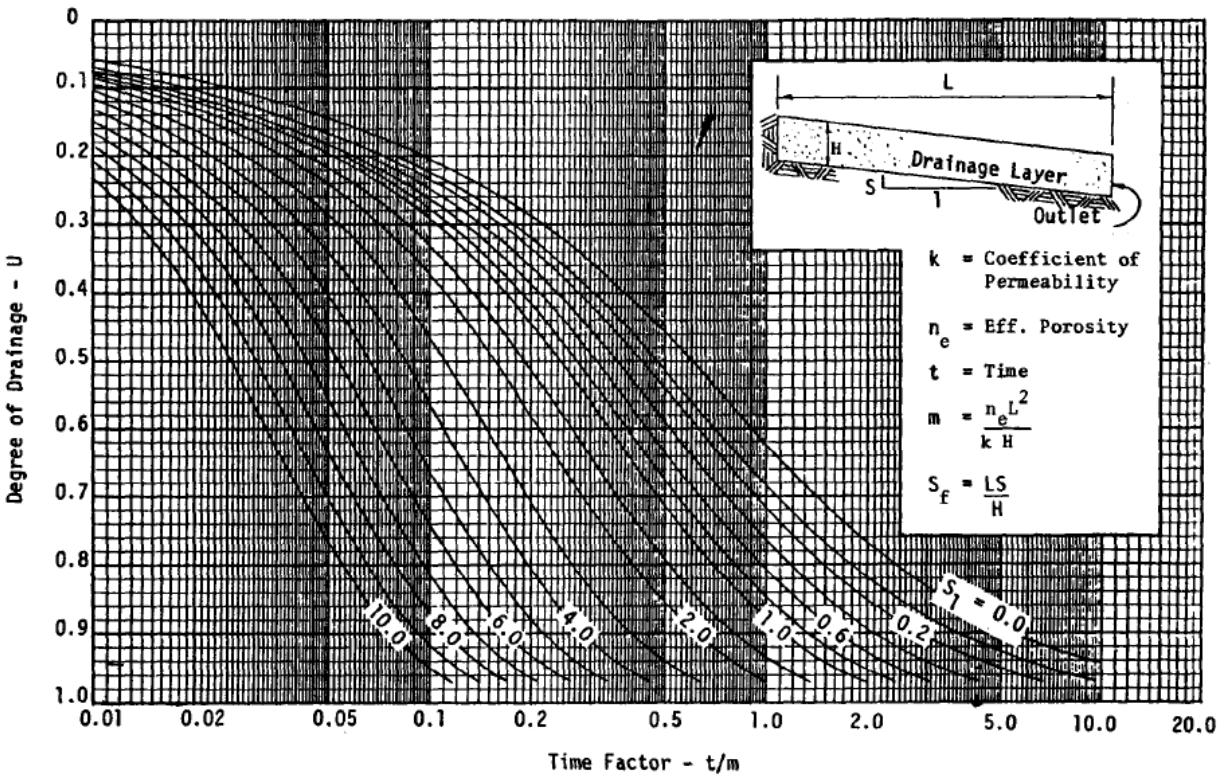

Figure 45. Time –dependent drainage of saturated layer (After Barber and Sawyer (1952))

Sample Calculation:

For the pavement section shown in Figure 46 and for a given set of geometric conditions, calculation for stead and un-steady state flow conditions are provided as follows:

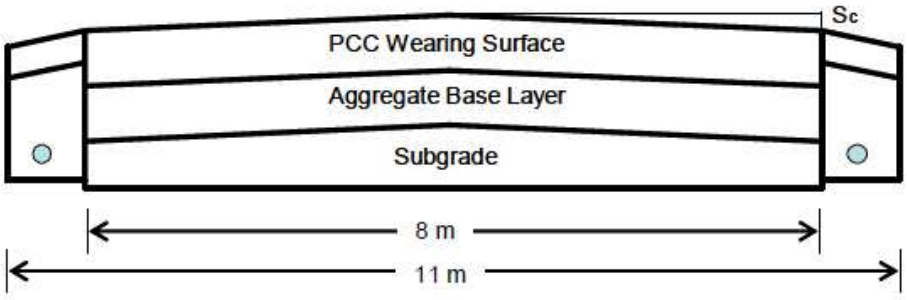

Figure 46. Cross –section pavement

Given data:

Infiltration rate per crack= $I_c = 0.22 m^3/day/m$

Width of the pavement = $W_p = 8$ m

Width of crack = $W_c = 11m$

Spacing of transverse cracks = $C_s = 4m$

No. of lanes = N = 4,

Thickness of base layer = H = 0.15 m,

Effective porosity of the materials = n_e =37%

Cross- slope = $S_c = 2\%$

Longitudinal gradient = g= 1 %

Calculations:

The width of drainage path:

$$W = \frac{b}{2} + c = \frac{8}{2} + 1.5 = 5.5m$$

The infiltration rate per unit area of crack can be calculated using:

$$q_i = I_C\left(\frac{N+1}{W} + \frac{W_c}{W_P C_S}\right) = 0.22 * \left(\frac{4+1}{5.5} + \frac{11}{5.5*4}\right) = 0.31 m^3/day/m^2$$

The infiltration rate per unit width of crack is given by q.

$$q = q_i \times W_C = 0.31 \times 11 = 3.41 m^3 / day / m$$

Flow path gradient and flow path length can be calculated using:

$$S_R = \sqrt{S^2 + S^2{}_X} = \sqrt{0.01^2 + 0.02^2} = 0.0224$$

$$L_R = W\sqrt{1 + \left(\frac{S}{S_X}\right)} = 5.5\sqrt{1 + \left(\frac{0.01}{0.02}\right)^2} = 6.15m$$

The hydraulic conductivity of drainage layer k can be calculated as:

$$k = \left(\frac{q}{(H(S + H/2L))}\right) = \left(\frac{3.41}{0.15(0.0224 + \frac{0.15}{2 \times 6.15})}\right) = 657.13 m/day = 0.76 cm/\sec$$

The time for 50 % degree of drainage may be computed as:

$$S_1 = \frac{LS}{H} = 6.15 \times 0.0224 / 0.15 = 0.92$$

Using U=0.5 and S1=0.92 and T = 0.3

So, the time required for 50% drainage is:

$$t = \left(\frac{n_e L^2}{k \times H}\right) \times T = \frac{0.37 \times 6.15^2}{657.125 \times 0.15} \times 0.3 = 0.4 day = 1 hrs$$

The difference between MEPDG and AASHTO drainage design calculation is the width of the drainage path. MEPDG calculates the width of the drainage path based on the width of a pavement surface and distance between the pavement shoulders to the edge of the permeable base. However, AASHTO considers the pavement width as the width of the drainage path (Vennapusa, 2004). Due to the similar results of MEPDG and AASHTO, Table 32 shows the comparison of in-situ hydraulic conductivity values and its correspondent ratings by using the excel spreadsheet of pavement drainage estimator (PDE) that is developed by Vennapusa (2004). In the PDE program, the longitudinal gradient of base is assumed as 0 %, cross slop is assumed as 2%, and the effective porosity is assumed to be 30%.

Table 32. Comparison of in-situ hydraulic conductivity and the correspondent ratings

Project	**Materials**	**Mean k (cm/sec)**	**Time for 50 drainage**	**Quality of drainage***
I-94, MI	OSL	4.9	< 1	Excellent
I-96, MI	Sandy subbase	1.48	< 1	Excellent
	CTB	2.95	< 1	Excellent
SR-22, PA	CTB (Area A)	7	< 1	Excellent
	CTB (Area B)	0.2	> 2 (2.8 hr)	Good

* Quality of drainage rating according to MEPDG recommendations

Key observation from Michigan I-94, I-96 and Pennsylvania SR-22

- Spatial maps shown in Michigan I-94, Michigan I-96 and Pennsylvania SR-22 studies can be used as QA/QC criteria during base/subbase placement, grading, and compaction to identify field problems such as segregation and particle degradation.
- Spatial maps of fine content and k_{sat} in Michigan I-96, Michigan I-94 and Pennsylvania SR- 22 studies had a good fit between the high fine content zone and lower hydraulic conductivity. For example, Michigan I-94 shows the fine content higher than 6% and then the k_{sat} smaller than 0.1 cm/s. Moulton 1980 indicated the permeability is highly governed by the precentage of fine particles passing the No. 200 sieve for granular materials.
- White et al. (2004) reported that due to segregation of aggregate fines during construction, the in situ k_{sat} of newly constructed base materials has a coefficient of variation (COV) of 50% to 400%. In this study, steel slag materials showed higher COV than that of the cement treated base, asphalt treated base and sandy subbase (Table 33).
- Comparison of hydraulic conductivities between laboratory and field tests is presented in Table 33 and box plots in Figure 47.

Table 33. Summary COV and K_{sat} measurements

Project	Material	COV (%)	Laboratory test cm/s	GPT Field range cm/s
Michigan I-94	Steel slag	119	6.5	0.1 to 30.1
Pennsylvania SR-22	Cement treated base (CTB)	45	11.5	0.1 to 18.3
	Asphalt treated base (ATB)	42	6.5	1.3 to 10.6
Michigan I-96	Sand	46		0.1-2.2
	Cement treated base	93		0.1-60.82

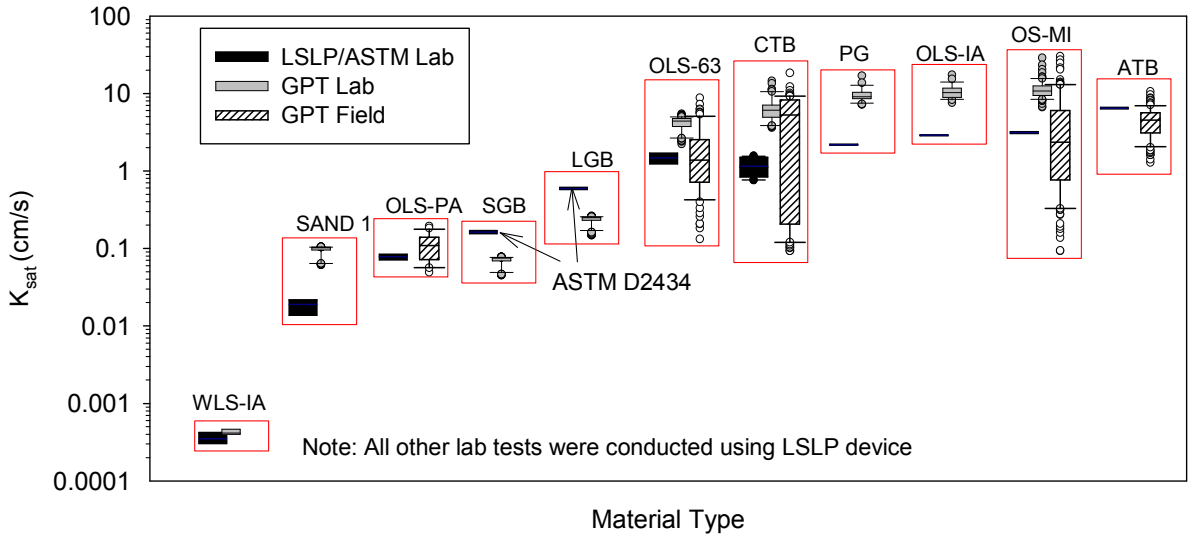

Figure 47. Comparison of saturated hydraulic conductivity determined from large-scale laboratory permeability/ASTM D2434 test measurements using water, APT measurements in lab, and APT measurements in field (after NCHRP 2010)

Iowa I-35

This field study was conducted on I-35, Iowa on 27, 30 and 31 of August, 2011. The test samples were collected from trimmed and untrimmed recycled Portland cement concrete (RPCC) pavement bases supported by reconstructed aggregate subbase, and from a section of pavement base that was a mixture of virgin crushed limestone and RPCC. This section presents the results and analyses of the field investigations. Test bed layouts of trimmed and untrimmed base are shown in Figure 48. The Caterpillar smooth drum roller was operated in low amplitude vibratory and static compaction modes.

Test bed 1, the untrimmed base, is approximately 800 ft long by 30 ft wide and is divided into nine sections. The sections are numbered from 0 to 8 indicating the number of roller prior to in situ testing. GPT and LWD measurements were conducted at all test point locations for the untrimmed base section. Untrimmed base included 51 test point locations for 9 sections. Three test point locations were selected for section 0; 6 test point locations were selected for the other sections. Nuclear gauge (NG), plate load test (PLT), and dynamic cone penetrometer (DCP) were performed only at the center point in longitudinal direction

for each sections. Static and low amplitude vibratory roller compactors were used from sections 1 to 8.

The trimmed base is approximately 500 ft long by 30 ft wide and is divided into ten sections. The sections are numbered from 0 to 9 indicating the number of roller passes prior to in situ testing. GPT and LWD measurements were recorded at all test points locations for the trimmed base. Trimmed base included 54 test point locations for 10 sections. 30 test point locations were selected from low-amplitude compaction sections. 24 test point locations were selected from static compaction section. NG, PLT and DCP were conducted only at the center point in longitudinal direction section. Static and low amplitude roller compactors were used from section 1 to 9. The different of untrimmed base and trimmed base is that excess base material needs to be removed to meet the required thickness for paving.

Tests were conducted on a section made of combined mixture of virgin crushed limestone and RPCC, which is approximately 650 ft long by 30 ft wide. The only in situ point measurement is the machine drive power (MDP) from Caterpillar smooth drum vibration roller, because comparison should be made between trimmed, untrimmed and virgin bases.

Results from particle size analysis, elastic modulus ($E_{LWD\text{-}Z3}$), initial (E_{V1}) and reload modulus (E_{V2}), MDP*, DCP-CBR profiles, hydraulic conductivity, fine content, dry unit weight, moisture content, and comparison of each values are presented separately for each test beds.

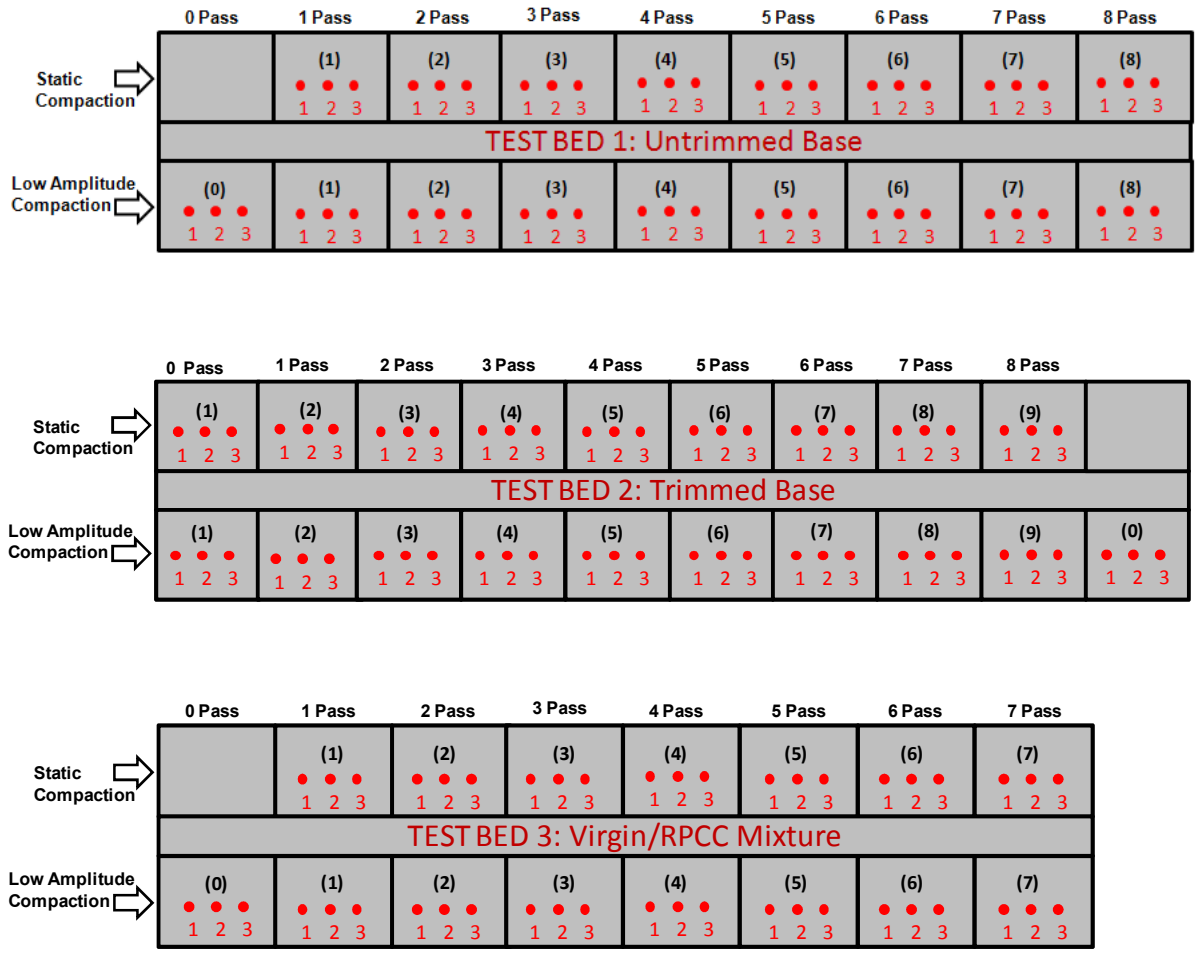

Figure 48. Test bed layout for I-35 Iowa

Particle size analysis

Particle size distribution provided the data for classification in material chapter. Comparisons of D_{10}, $D_{30}$and D_{60} for pass number of untrimmed and trimmed bases are illustrated in this part. D_{10} is grain size corresponding to 10% passing by weight, D_{30} is grain size corresponding to 30% passing by weight, and D_{60} is grain size corresponding 60 % passing by weight. Figure 49, Figure 50 and Figure 51are shown the particle size value of D_{10}, D_{30} and D_{60} on low amplitude vibratory and static compaction sections of trimmed and untrimmed base.

Material of percentage materials passing the #200 sieve were directly collected on each points of untrimmed and trimmed base. Materials were collected from a depth of 0-60 mm and 60-100 mm on untrimmed base, and only 0-60mm on trimmed base. Figure 52 and Figure 53 show the percentage material passing the #200 sieve of low amplitude vibratory and static compaction on untrimmed and trimmed bases.

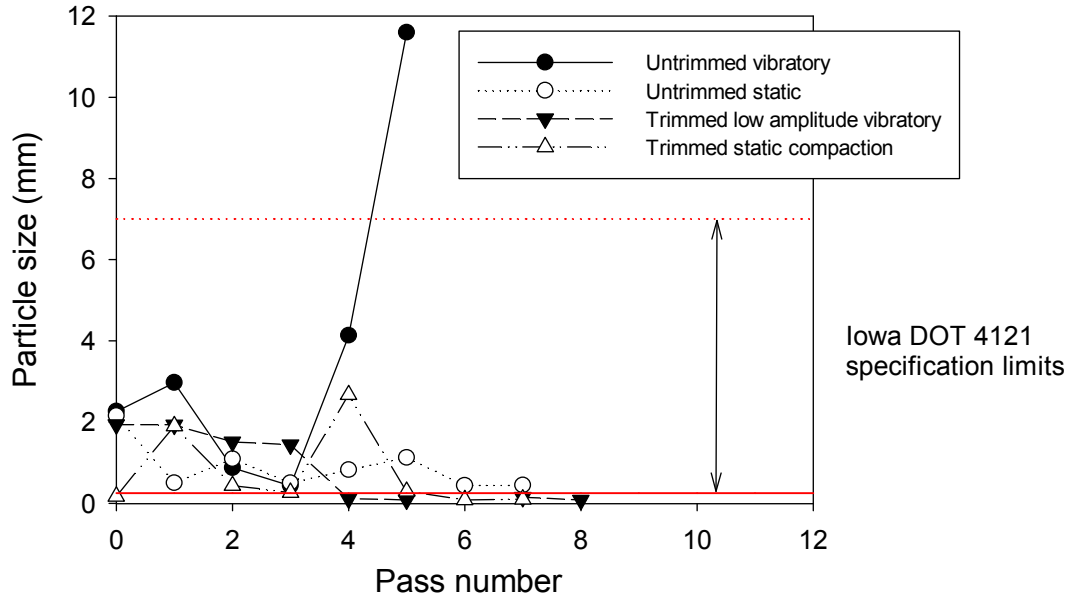

Figure 49. Comparison particle size distribution of D_{10} on trimmed and untrimmed bases of I-35, Iowa

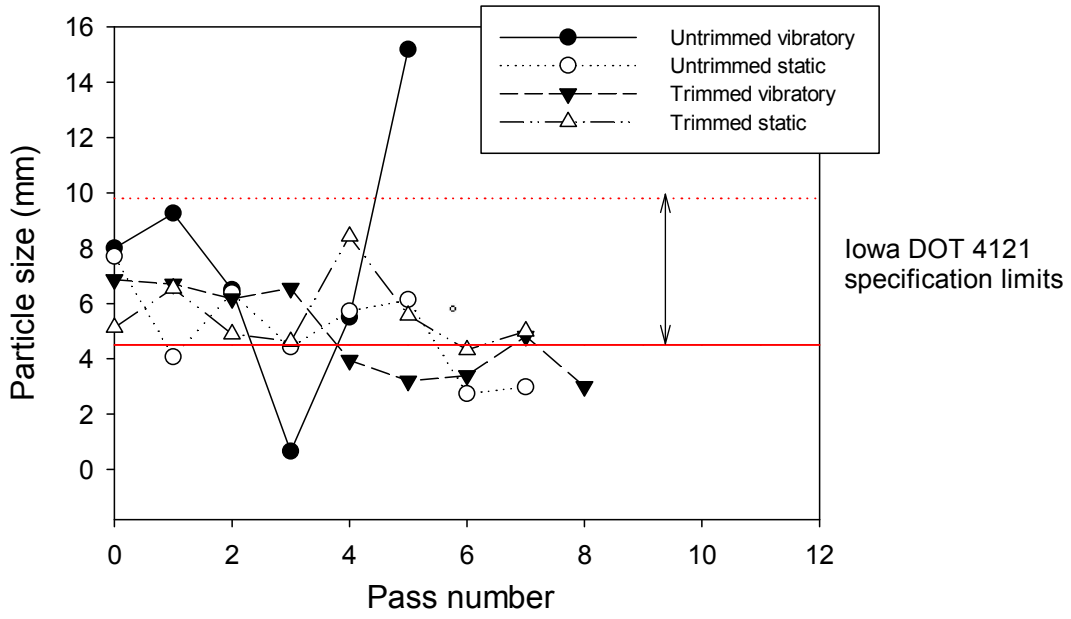

Figure 50. Comparison particle size distribution of D_{30} on untrimmed and trimmed bases of I-35, Iowa

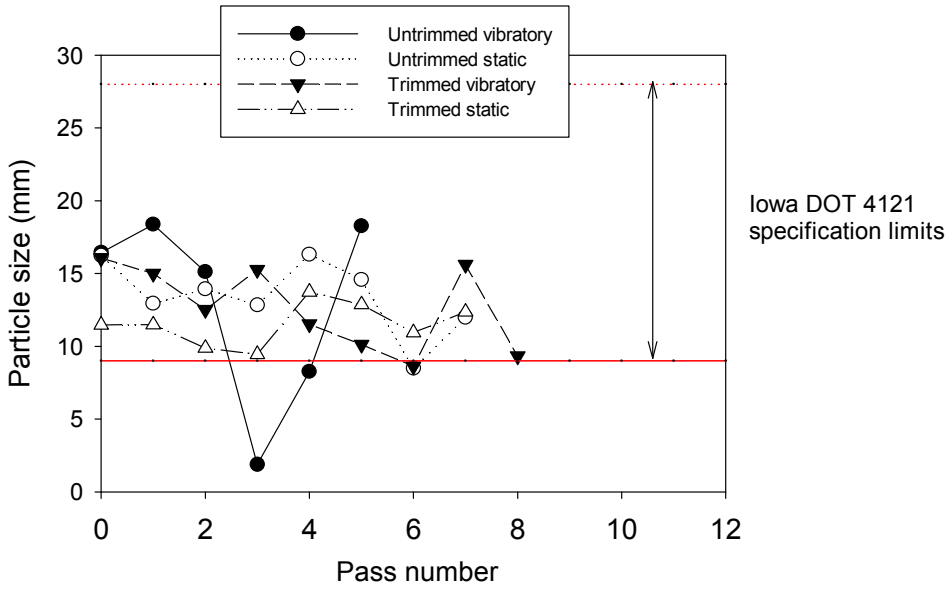

Figure 51. Comparison particle size distribution of D_{60} on untrimmed and trimmed bases of I-35, Iowa

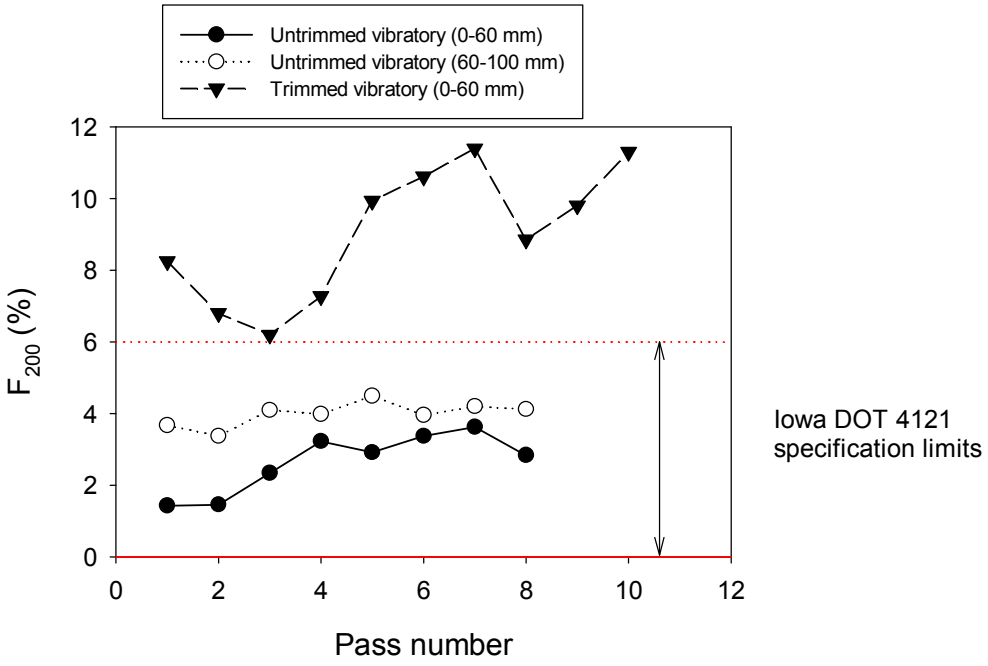

Figure 52. Percentage material passing # 200 sieve of low amplitude vibratory on trimmed and untrimmed base

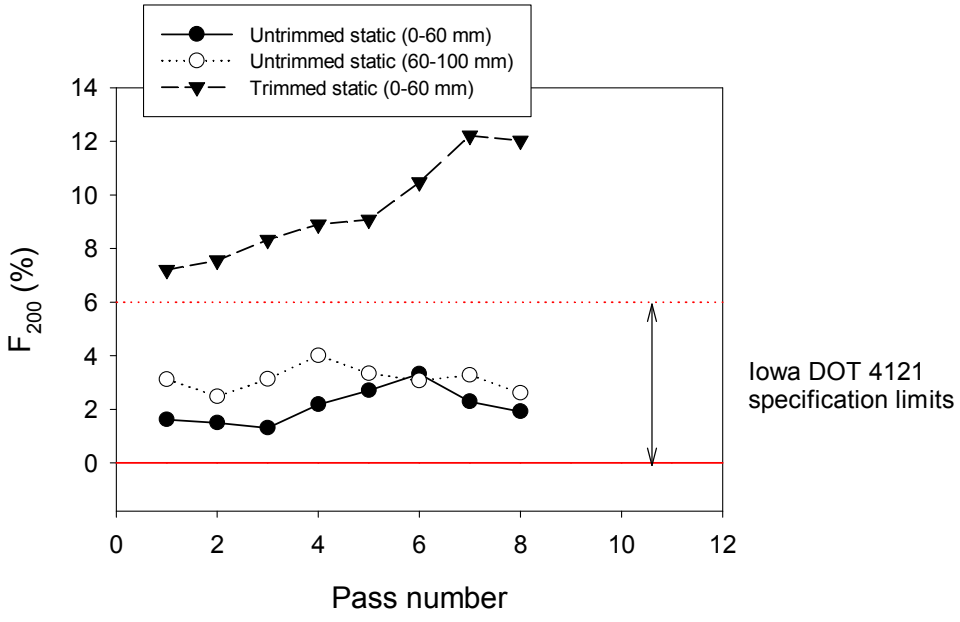

Figure 53. Percentage material passing # 200 sieve of static compaction on trimmed and untrimmed base

Key findings are withdrawn from particle size analysis:

- As shown in Figure 49, all samples meet the requirement of Iowa DOT limits gradation 4121 recycled granular subbase from pass 1 to pass 4. At pass 6, the particle size of untrimmed low amplitude vibratory is higher than the upper bound of requirement. The particle sizes of trimmed low amplitude vibratory under pass number higher than 5 are generally lower than the lower bound of the requirement.
- In Figure 50, the particle size of untrimmed low amplitude vibratory varies a lot at different pass number. For example, at pass 4, the particle size is far below the lower bound of the requirement, while at pass 6, it is far above the upper bound of the requirement.
- The particle sizes of D_{60} on untrimmed and trimmed bases are generally within the range of the Iowa DOT limits gradation 4121 recycled granular subbase except for that of the untrimmed low amplitude vibratory at pass 4 and 5.
- As shown in Figure 49 to Figure 51, pass number has a significant impact on the particle size distribution. There is no clear trend of the particle size distribution at different pass numbers. Among the several samples, untrimmed low amplitude vibratory has the most volatile particle size distribution and its particle size is often outside the range of the Iowa DOT limits gradation 4121 recycled granular subbase.
- As shown in Figure 52, deeper materials (60 to 100mm) have higher fine content than that of the surface materials (0-60mm) on both low amplitude vibratory and static compaction roller sections.
- Trimmed base have almost three times of fine content than untrimmed base on both low amplitude vibratory and static compaction.
- Trimmed base has more influence on passing #4 to #6 on static compaction sections (Figure 53).
- Compared with Iowa DOT limits gradation 4121 recycled granular subbase, both low amplitude vibratory and static compaction sections on trimmed base are over

the upper bounder of the requirement, which means that there are higher fines content on trimmed base.

- Fines content on the untrimmed base which includes low amplitude vibratory and static compaction sections all meet the requirement of Iowa DOT limits gradation 4121 recycled granular subbase. As the fine content on the untrimmed base always meet the Iowa DOT limits gradation 4121 recycled granular subbase requirement and the fine content on the trimmed base always violate the Iowa DOT limits gradation 4121 recycled granular subbase requirement regardless of the pass number, we can conclude that compared to the pass number, whether the base is trimmed or not has more influence on the fine content.

LWD, PLT and MDP analysis*

LWD is used to determine the dynamic elastic modulus of the materials. In this study, a Zorn ZFG 2000 LWD with a 720mm of drop height and 300 mm of plate diameter as used. Three seating drops were performed on the flat areas of the material surface. Three measure drops followed the seating drops and deflections were recorded. The averages of the last three measurements were used to determine the $E_{LWD\text{-}Z3}$. LWD data ($E_{LWD\text{-}Z3}$) increased with the pass number for increased for low amplitude vibratory on the untrimmed base section. The average $E_{LWD\text{-}Z3}$ value for pass 0 is 33 MPa and average value for pass 8 is 54 Mpa for low amplitude of untrimmed base. Maximum $E_{LWD\text{-}Z3}$ data (61Mpa) is produced when passing number is 3. The minimum value of static compaction of untrimmed base is 33 MPa which is in the passing 0 section. Maximum value of 45 psi is produced when passing number is 8. Comparing the modulus value of low amplitude and static compaction, low amplitude section have the maximum value than static compaction sections and both have same minimum value in the section of passing 0. Figure 54 to Figure 57 show that the LWD data ($E_{LWD\text{-}Z3}$) on low amplitude vibratory have wider range (20-70 MPa) than the static compaction (30-50 MPa) of untrimmed test bed. Low amplitude vibratory has higher surface elastic modulus than the static compaction in untrimmed base.

Average LWD modulus values for low amplitude vibratory on trimmed base range are from 55 MPa to 68 MPa. Average value of static compaction section varies from 55 MPa to 61 MPa. Trimmed base (see Figure 56 and Figure 57) is stiffer than untrimmed base (see

Figure 54 and Figure 55). This means surface elastic modulus is more effective in the untrimmed base.

PLT was applied on a 300 mm diameter bearing plate using the weight truck as the reaction force. These tests were performed using a custom apparatus on Freightliner for Geotechnical Mobile Laboratory (White and Gieselman 2009). A data logger continuously recorded the load and deformation during the test. Initial E_{v1} and reload E_{v2} elastic module readings were determined by equation in method chapter. PLT was applied on the center of each section and each stress-strain curves of static plate load tests. Untrimmed base of static elastic modulus in low amplitude vibratory sections (see Figure 58) of initial E_{v1} are between 24 MPa to 53 MPa, reload E_{v2} are between 91MPa and 134 MPa. Static roller compaction (see Figure 59) section of initial E_{v1} from 26MPa to 39 MPa, reload E_{v2} are from 100 MPa to 131 MPa. By comparing the trimmed bases (see Figure 60) of low amplitude vibratory section of initial E_{v1} (54 MPa to 74 MPa) and reload E_{v2} (148 MPa to 231MPa) and static compaction roller section (see Figure 61) of initial E_{v1} (39 MPa to 79 MPa) and reload E_{v2} (122 MPa to182MPa), trimmed base have higher static elastic module than untrimmed base.

Similar to the modulus of subgrade reaction (k_s) (see Figure 62 to Figure 65), there is a higher value of modulus of subgrade reaction (k_s) in the trimmed base compare with untrimmed base. Figure 62 to Figure 65 comparing the actual modulus of subgrade reaction and corrected value for 30 in. diameter pate.

MDP technology relates the mechanical performance of the roller to the properties of the compacted soil during compaction. (White et al, 2010). White and Thompson (2008), Thompson and White (2008), and Vennapusa et al. (2009) verified that the field MDP values are empirically related to the soil compaction characteristics which are density, stiffness and strength. MDP *values range are between 1 and 150. MDP* increase by increasing compaction whereas the original MDP values decrease by increasing compaction.

Figure 66 to Figure 70 present the MDP* value for each low amplitude vibratory compaction and static compaction pass for untrimmed base, trimmed base and virgin crushed limestone and RPCC base. For untrimmed base, low vibratory compaction roller section has a MDP* value ranging between 135 to 139, and static compaction roller has a MDP* value ranging between 139 to142. Static compaction roller has slight higher value than low

amplitude for untrimmed base. Trimmed base of static compaction values of MDP* range from 142 to 144. For virgin crushed limestone and RPCC base, the data obtain of low amplitude vibratory section range from 134 to 136, static compaction has constant MDP*value of 141.

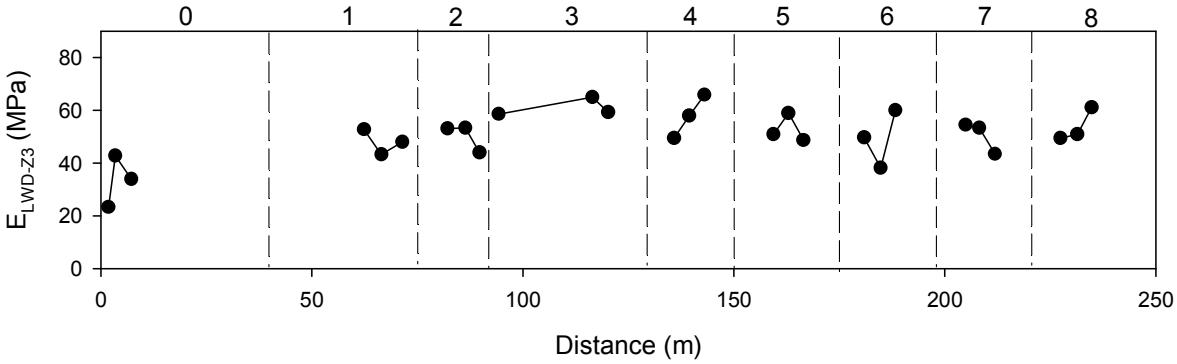

Figure 54. LWD data on low amplitude vibratory untrimmed base I-35, Iowa

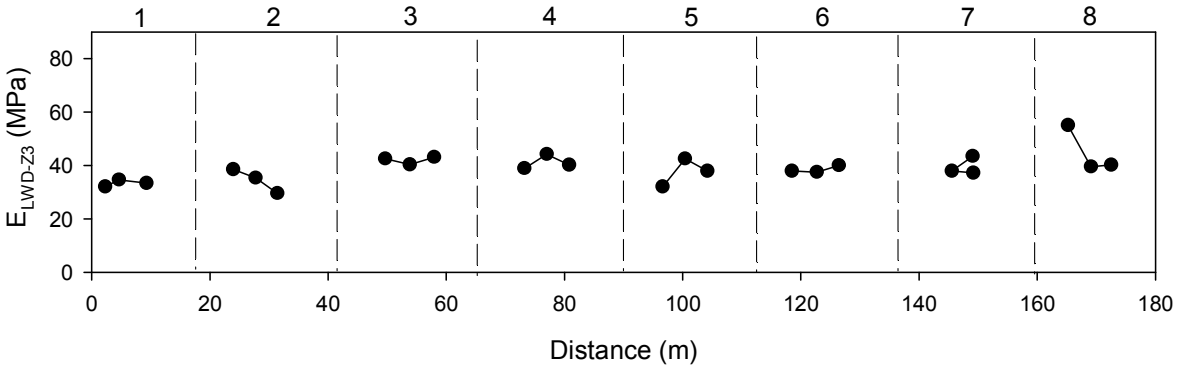

Figure 55. LWD data on static compaction untrimmed base I-35, Iowa

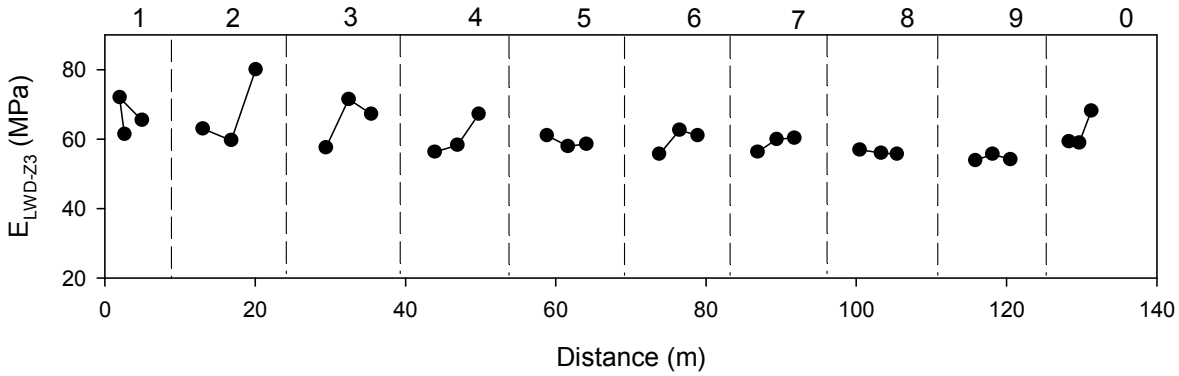

Figure 56. LWD data on low amplitude vibratory trimmed base I-35, Iowa

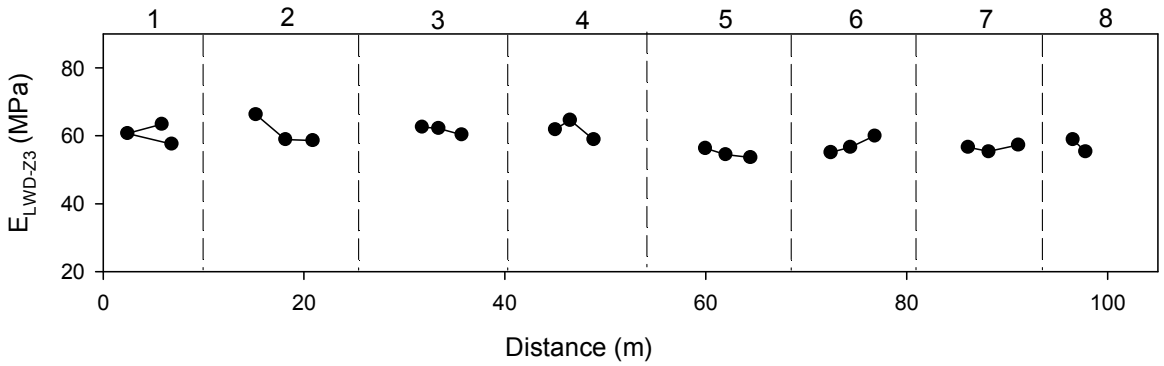

Figure 57. LWD data on static compaction trimmed base I-35, Iowa

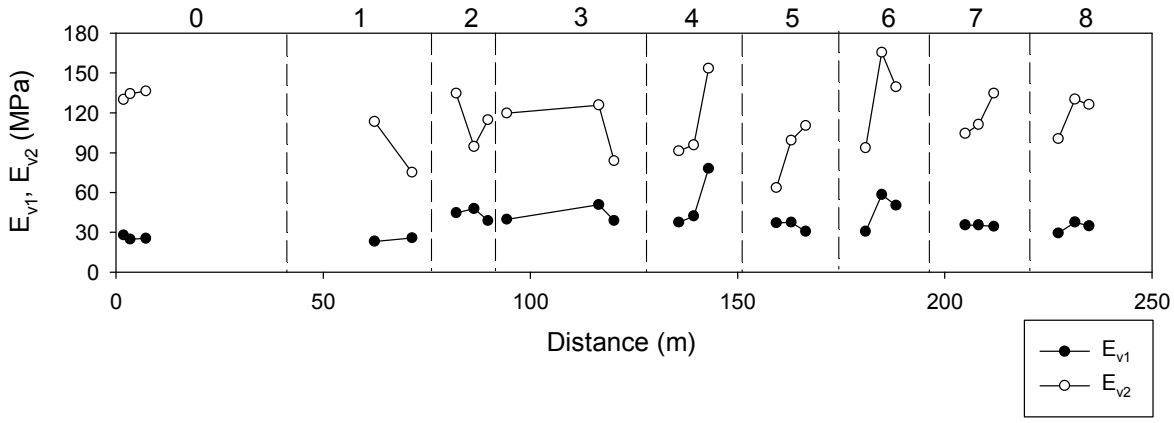

Figure 58. Static elastic modulus of subgrade low amplitude vibratory untrimmed base I-35, Iowa

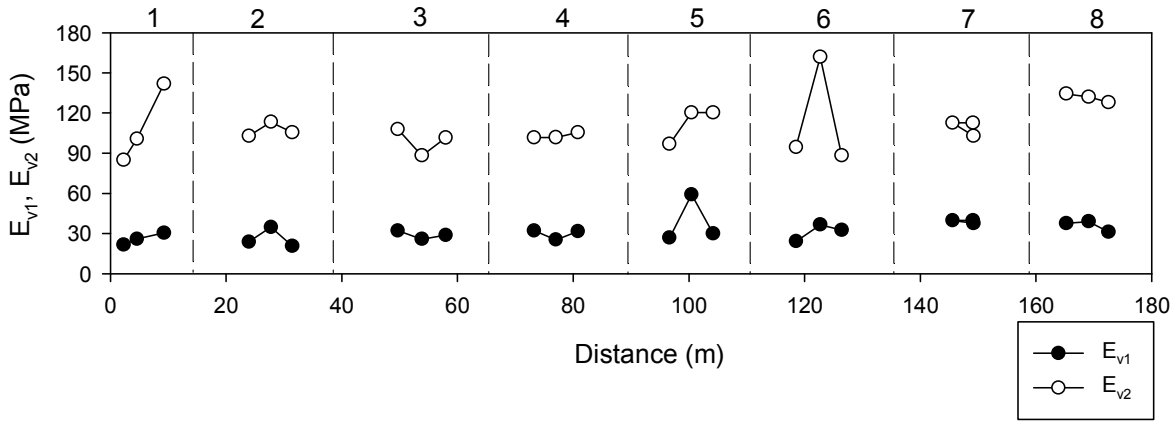

Figure 59. Static elastic modulus of subgrade static compaction untrimmed base I-35, Iowa

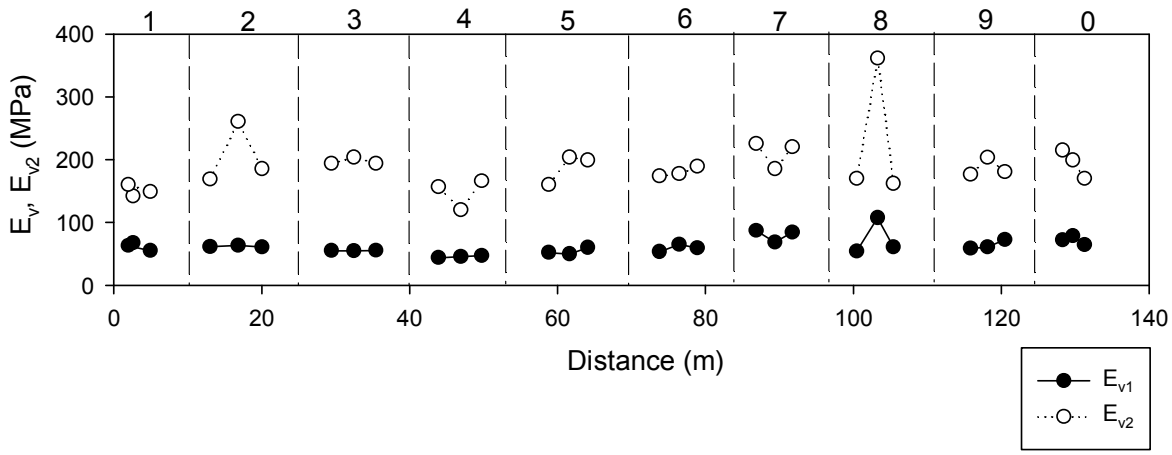

Figure 60. Static elastic modulus of subgrade of low amplitude vibratory trimmed base

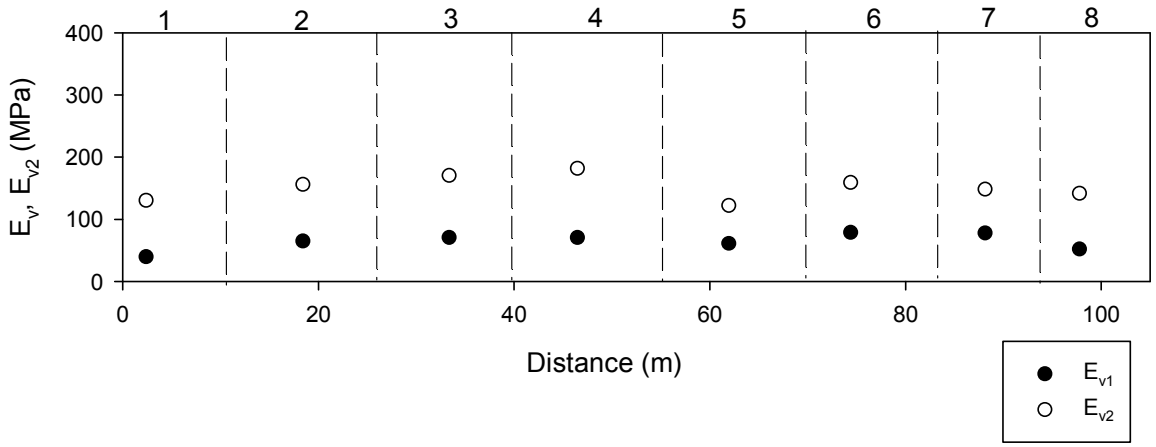

Figure 61. Static elastic modulus of subgrade of static compaction trimmed base

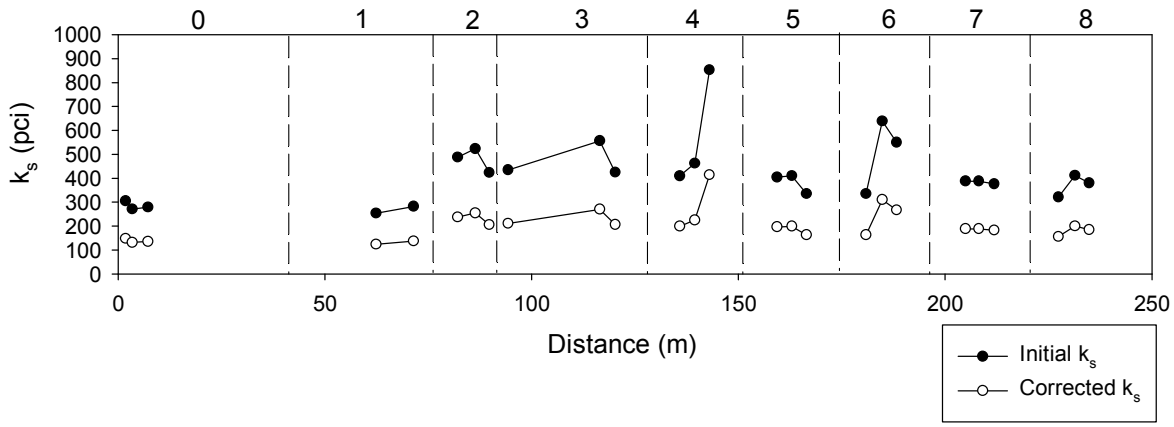

Figure 62. Modulus of subgrade reaction on low amplitude vibratory untrimmed base I-35, Iowa

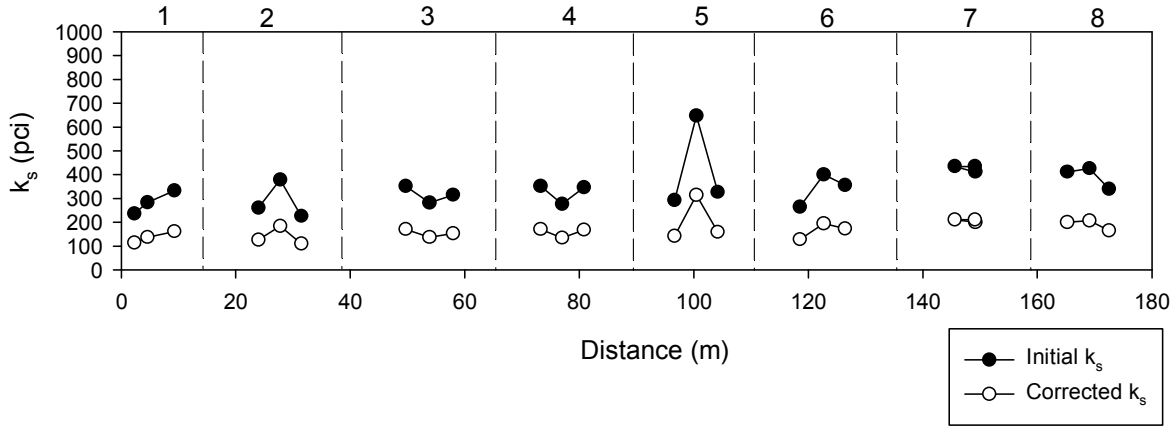

Figure 63. Modulus of subgrade reaction on static compaction untrimmed base I-35, Iowa

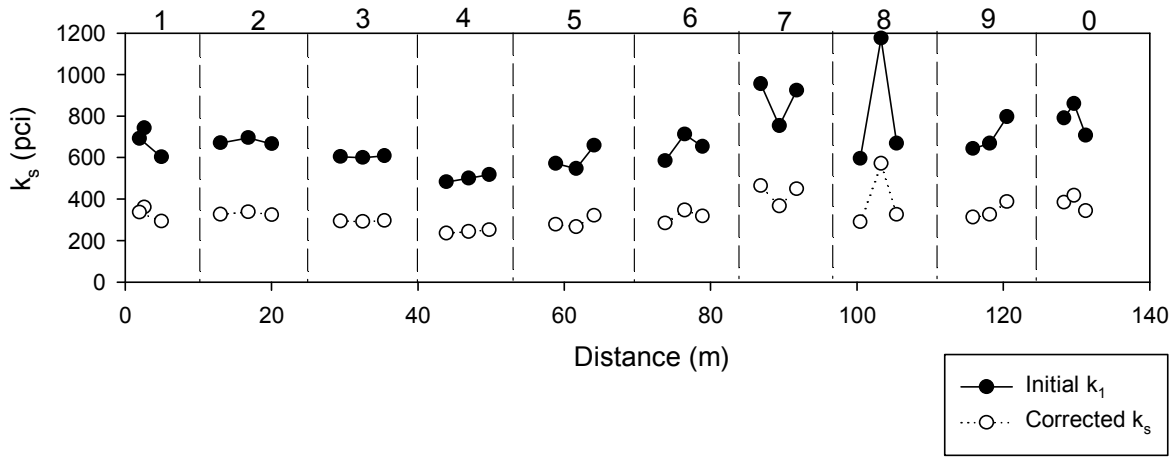

Figure 64. Modulus of subgrade reaction on low amplitude vibratory trimmed base I-35, Iowa

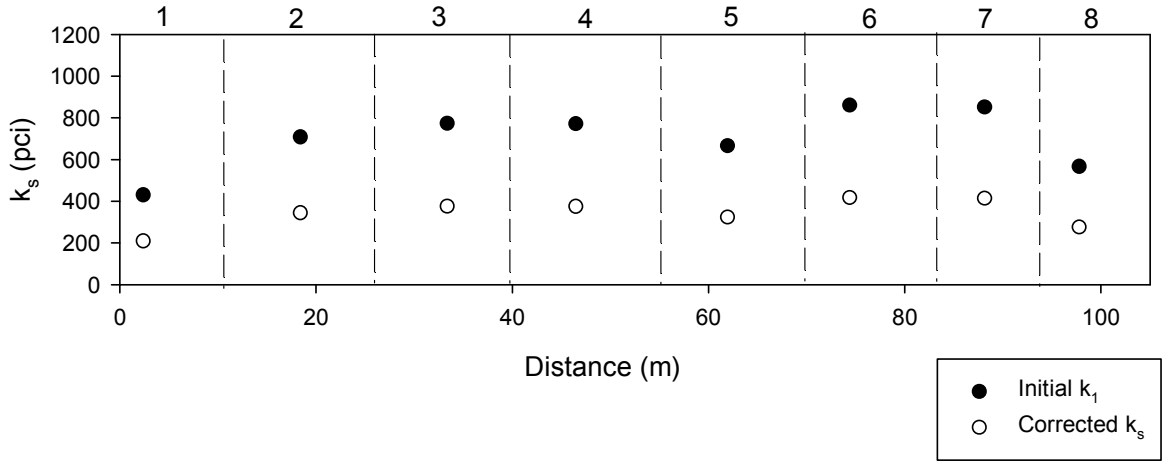

Figure 65. Modulus of subgrade reaction static compaction trimmed base I-35, Iowa

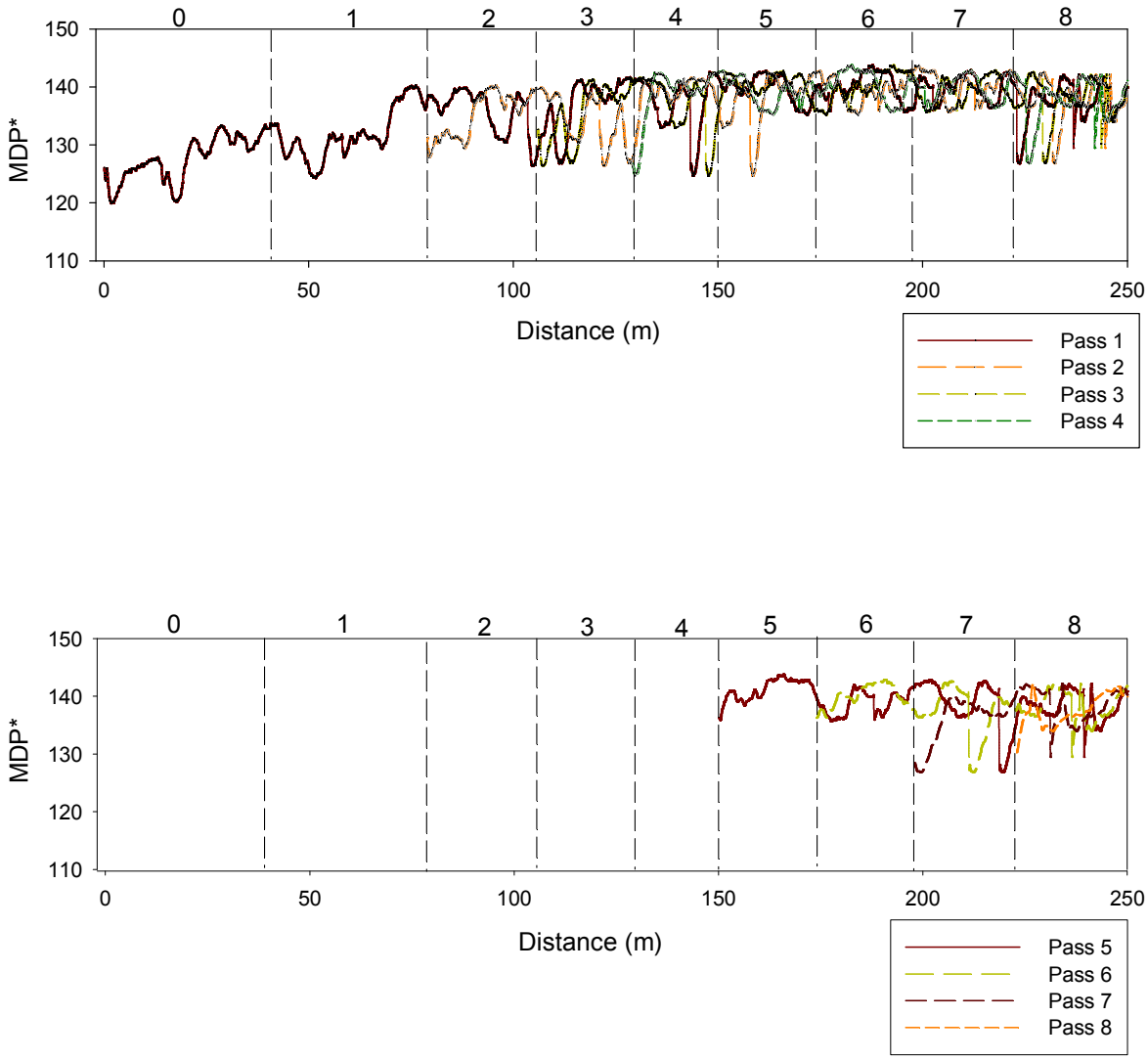

Figure 66. MDP* compaction curves on low amplitude vibratory on untrimmed base of I-35 Iowa

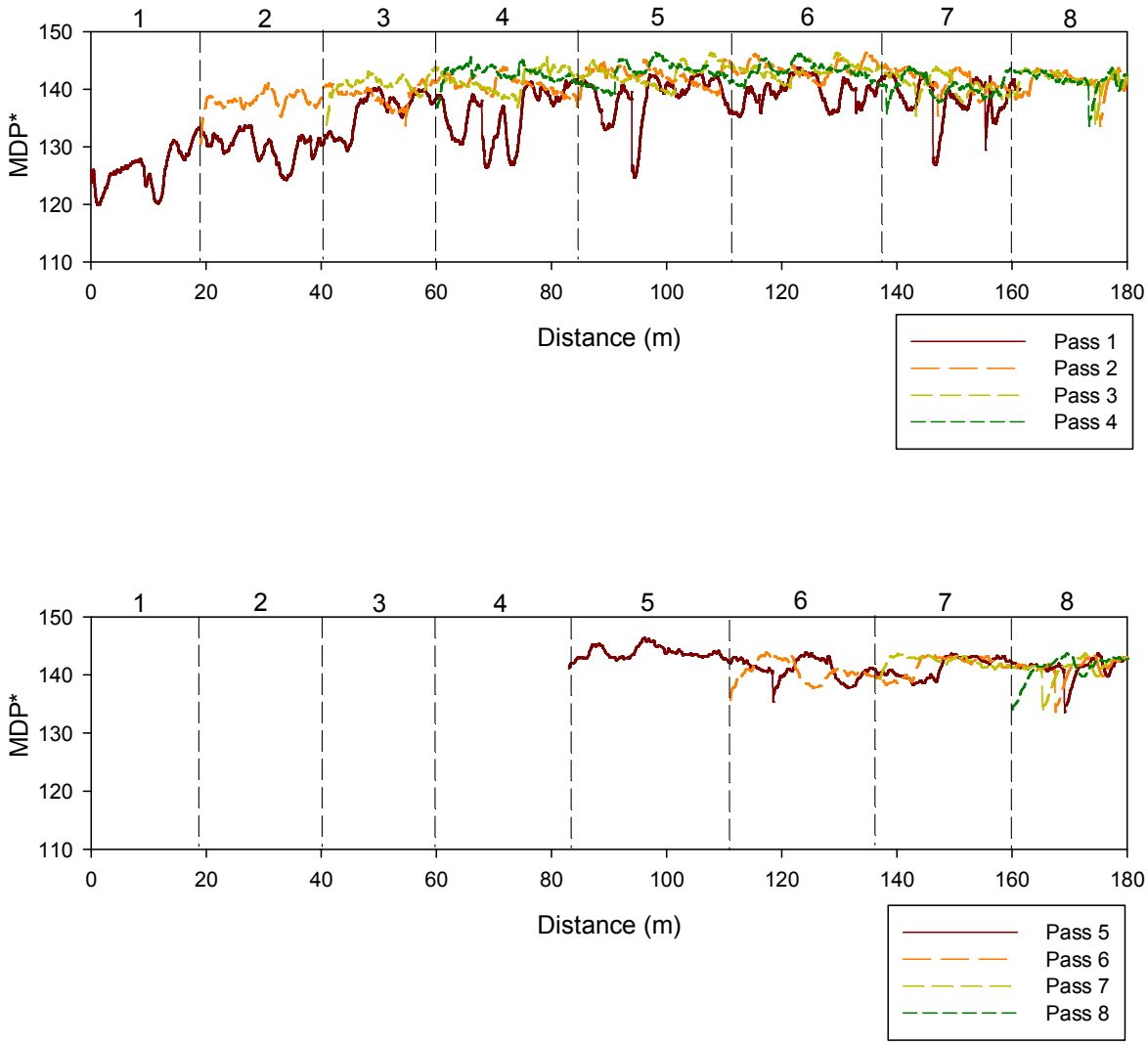

Figure 67. MDP* compaction curves on static compaction on untrimmed base of I-35 Iowa

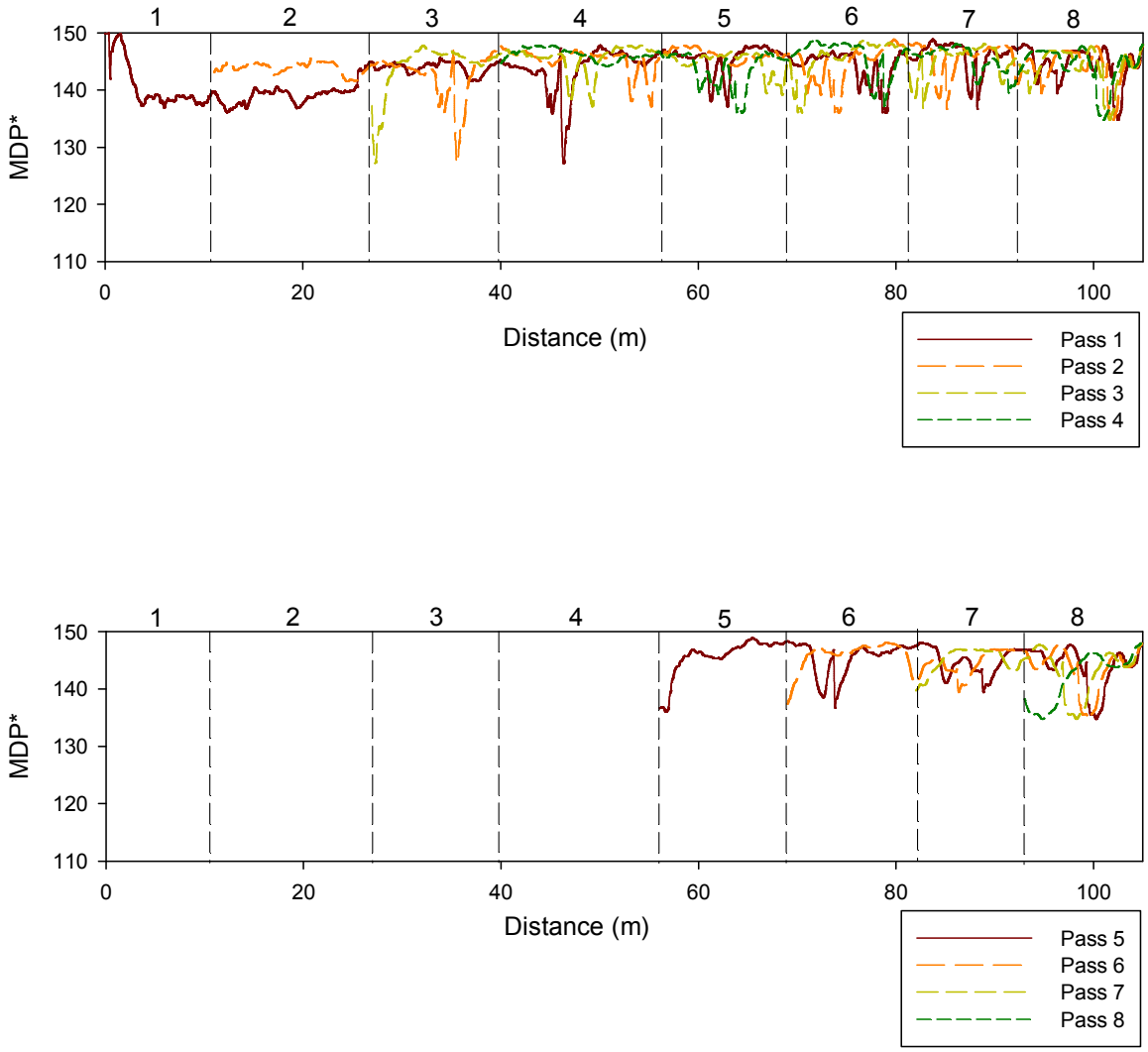

Figure 68. MDP* compaction curves on static compaction on trimmed base of I-35 Iowa

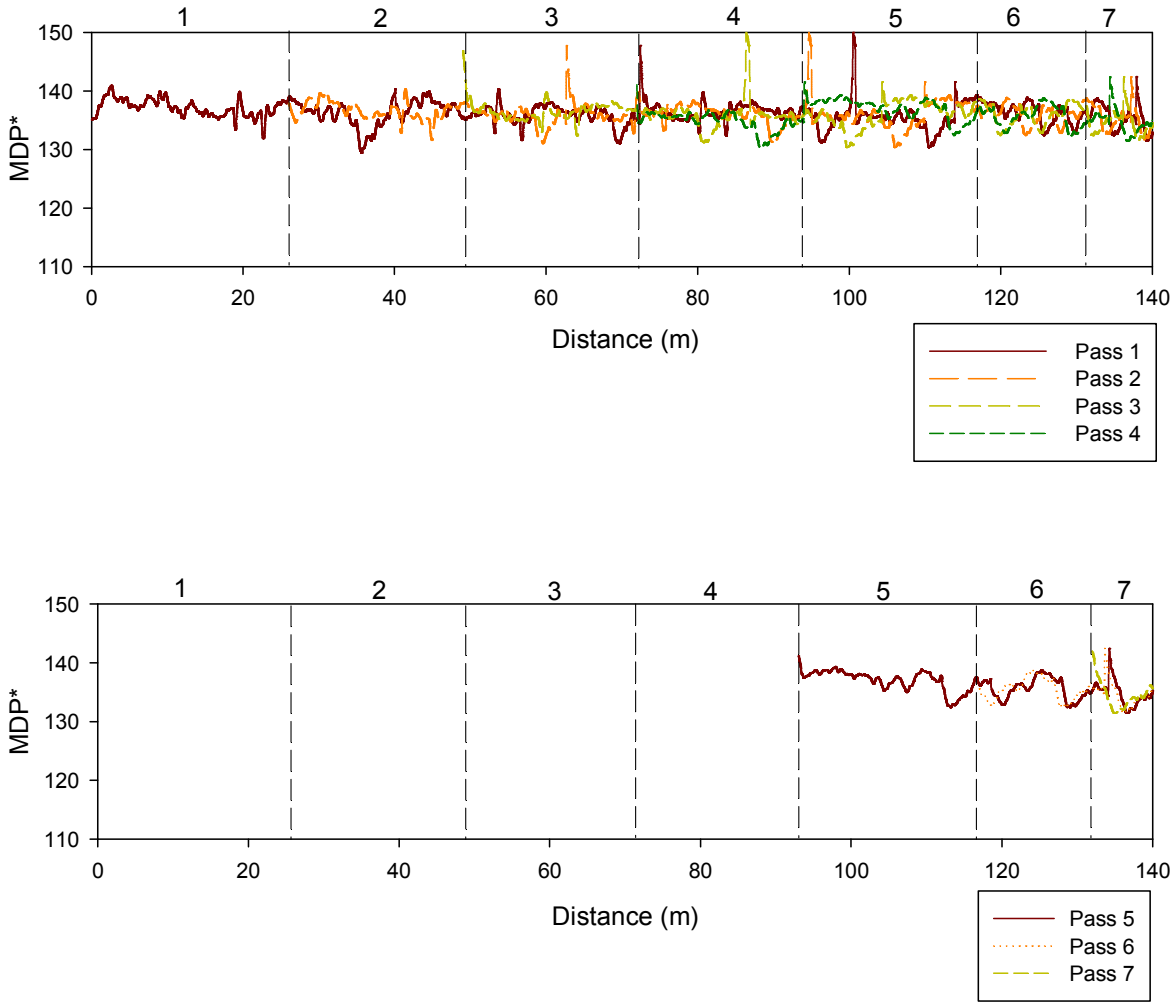

Figure 69. MDP* compaction curves on low amplitude compaction roller on virgin mixture base

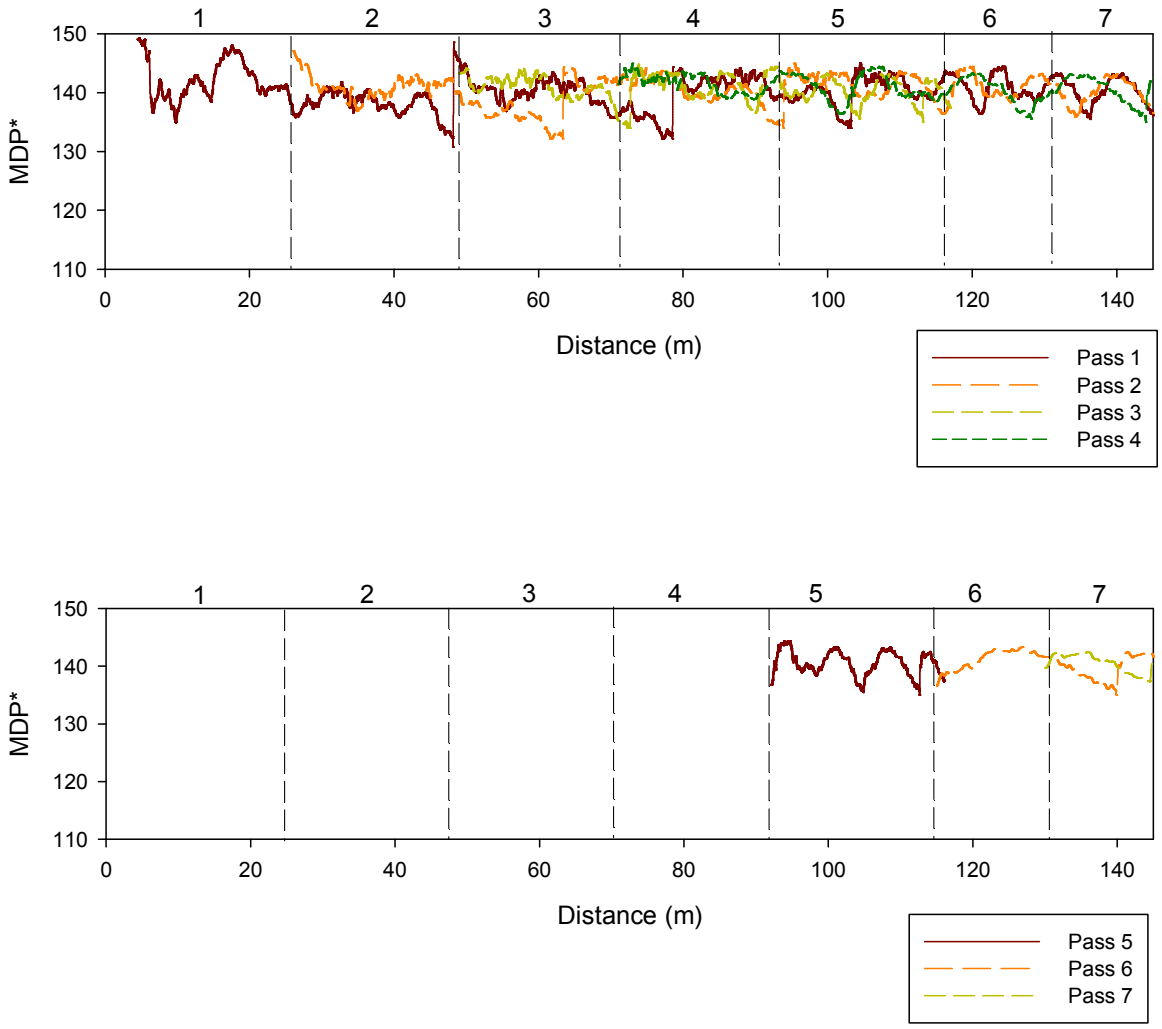

Figure 70. MDP* compaction curves on static compaction on virgin mixture base

Dynamic cone penetrometer (DCP)

DCP works by dropping a 8 kg (17.6 lb) hammer onto a rod with a cone trip from a height of 575 mm (22.6 in) to measure the penetration distance for a given number of blows. DCP tests were performed after GPT, LWD and NG to avoid the disturbance of testing points. DCP test present the thickness of the layer of soil of various profiles. Soil stress was assessed through correlation with California bearing ratio (CBR). The DCP-CBR profiles and CBR value for each layers of low amplitude vibratory and static compaction roller section on untrimmed base and trimmed are shown in Figure 71 to Figure 74. Pavement is typically

comprised of two foundation layers which are base and subbase. Figure 71 to Figure 74 demonstrated higher soil stress in the base layers.

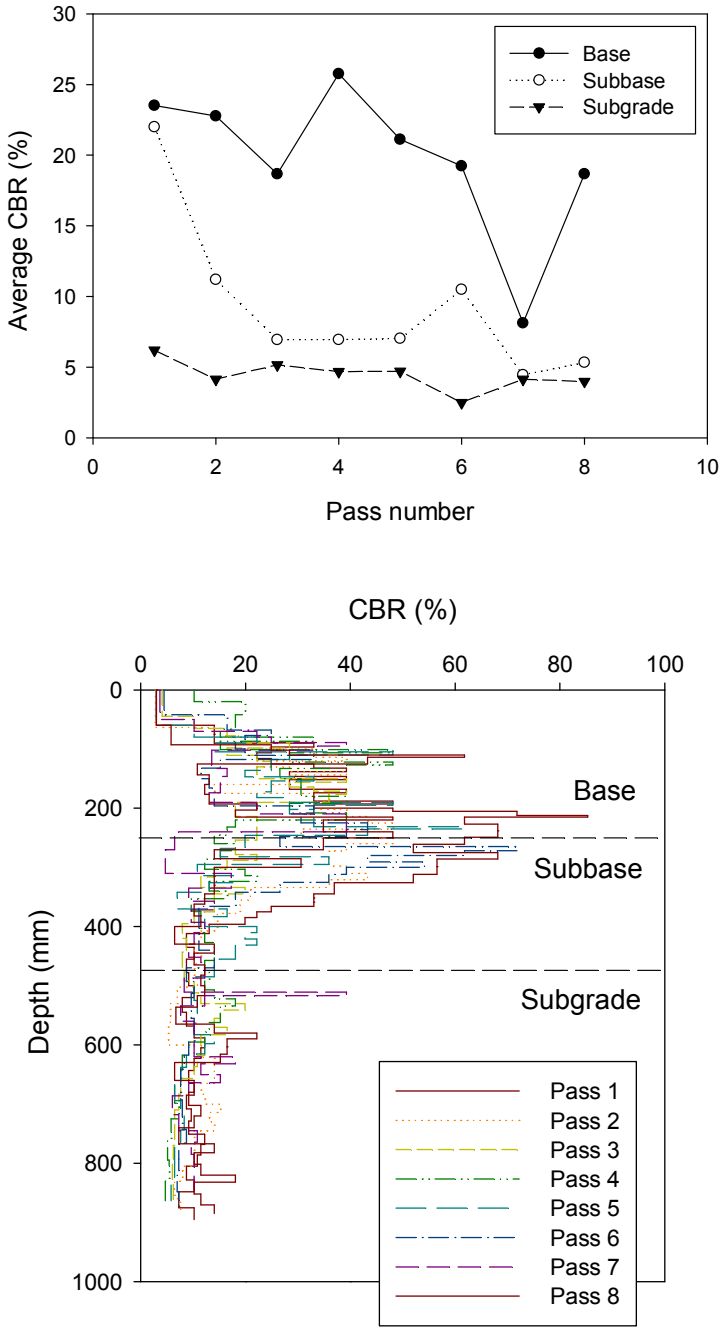

Figure 71. DCP-CBR profiles on low amplitude vibratory compaction on untrimmed base of I-35 Iowa

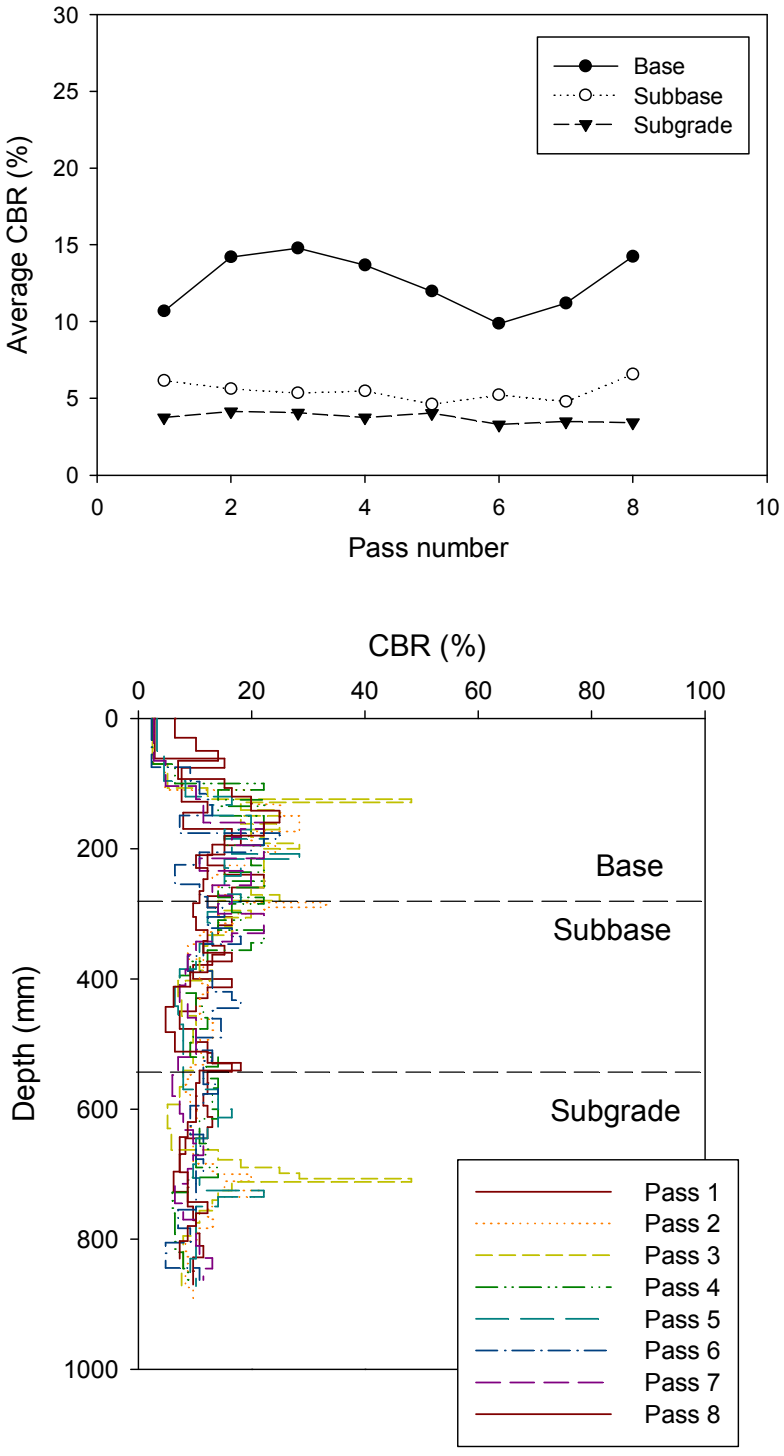

Figure 72. DCP-CBR profiles on static compaction on untrimmed base of I-35 Iowa

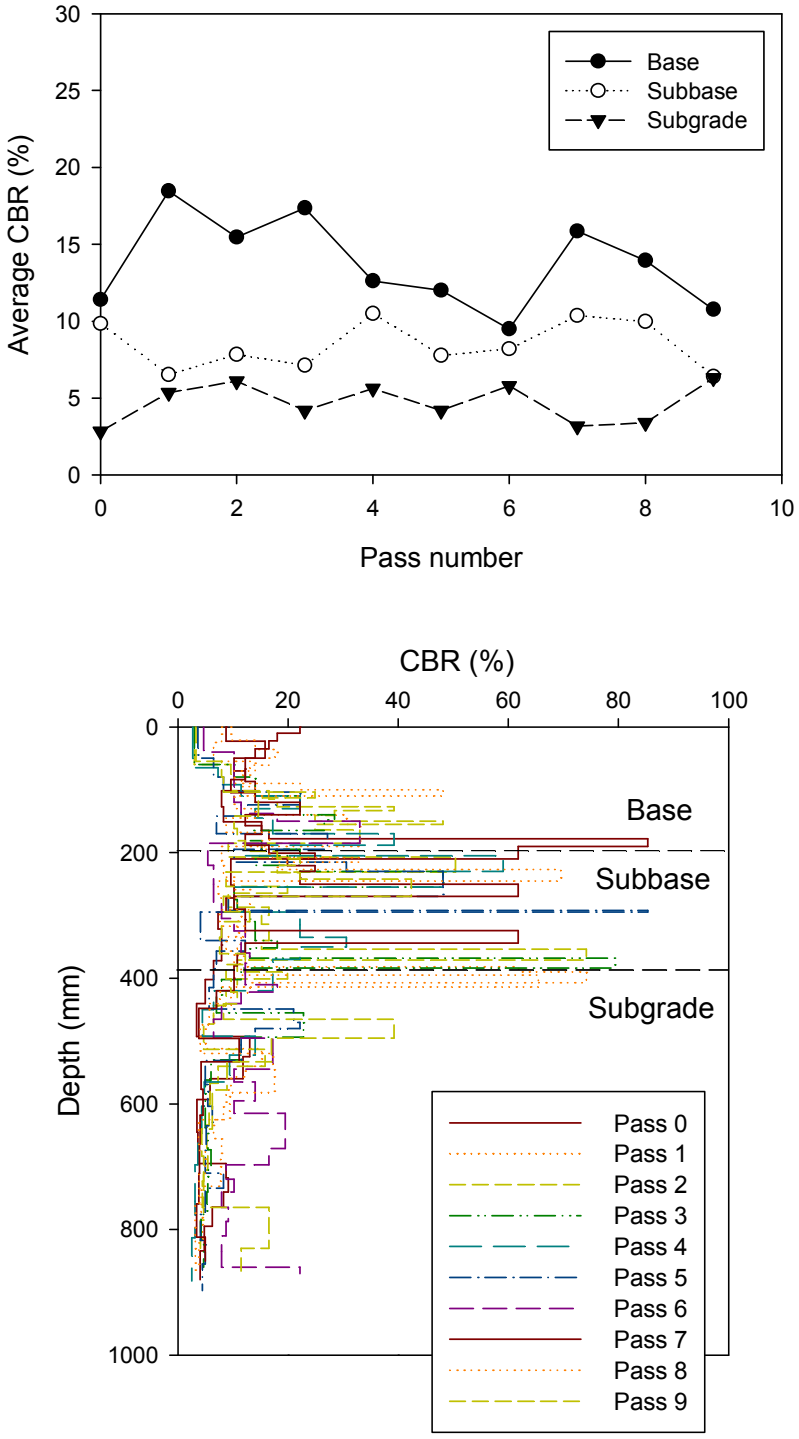

Figure 73. DCP-CBR profiles on low amplitude vibratory compaction on trimmed base of I-35 Iowa

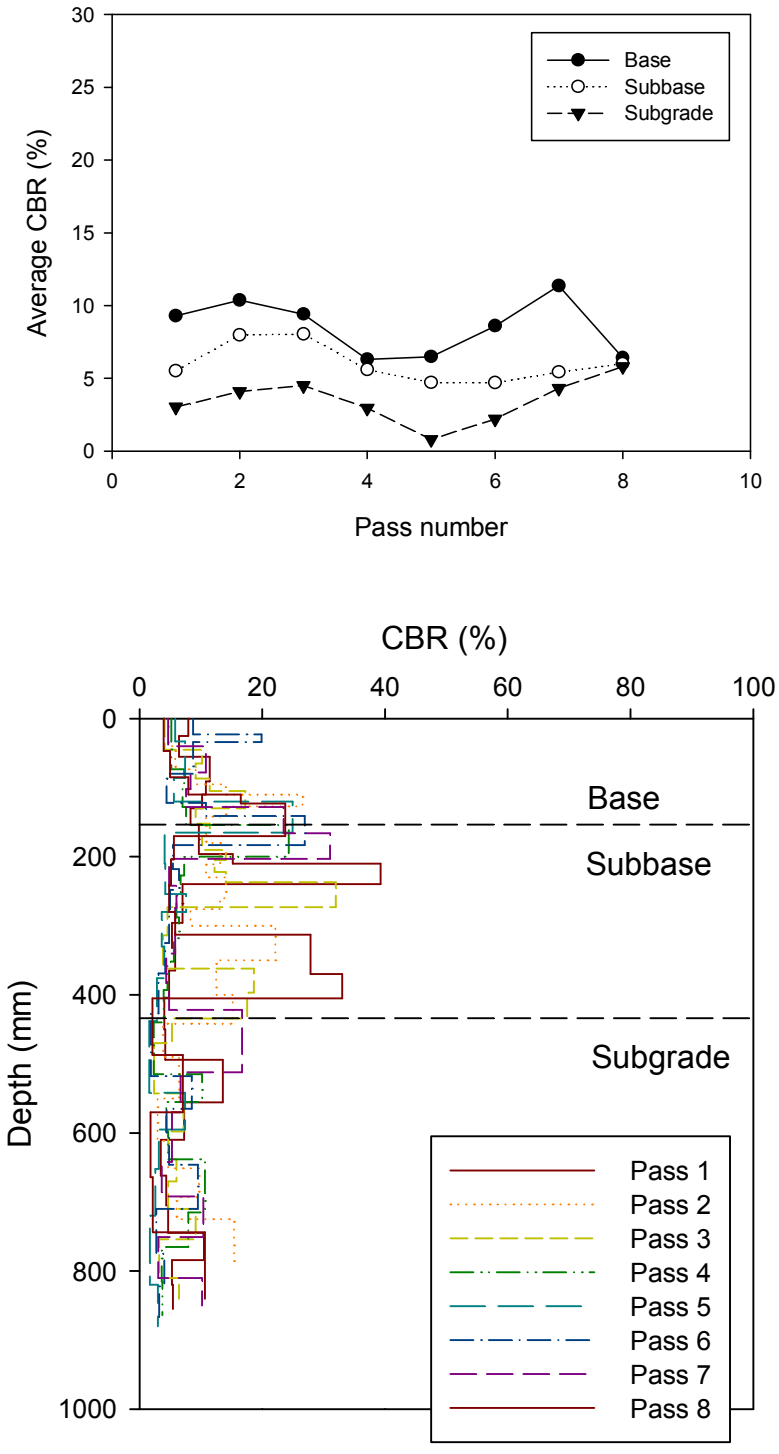

Figure 74. DCP-CBR profiles on static compaction on trimmed base of I-35 Iowa

Hydraulic conductivity and fines content

Air permeability device for quality control (QC) and quality assurance (QA) is used to determine saturated hydraulic conductivity of untrimmed and trimmed bases for each pass. Saturated hydraulic conductivity of low amplitude on untrimmed base varies from 4.1 cm/sec to 158.7 cm/s. The fines content (passing No. 200 sieve) of 0 to 60 mm of base is between 0.82% and 4.69%. Deeper base layer (60 to 100mm) has fines content ranging from 1.4% to 5.3% which is higher than that of the surface of base (see Figure 75). The range of saturated hydraulic conductivity of static compaction roller (see Figure 76) for each pass is from 1.7 cm/sec to 178 cm/sec. The values of fine content were in the range of about 1 to 4.5% for 0 to 60 mm layer and 1.9% to 5.1% for 60 to100 mm layer.

Results of GPT of low amplitude vibratory on trimmed base are from 1cm/sec to 16.5 cm/sec. The fine content of 0 to 60 mm ranges from 4.66% to 12.73%. The data obtained from saturated hydraulic conductivity for static between 0.1 cm/sec to 19.5 cm/sec with fine content from 7.03 cm/sec to14.43 cm/sec. Figure 77 and Figure 78 show the hydraulic conductivity and fine content for each pass of low amplitude vibratory and static compaction sections.

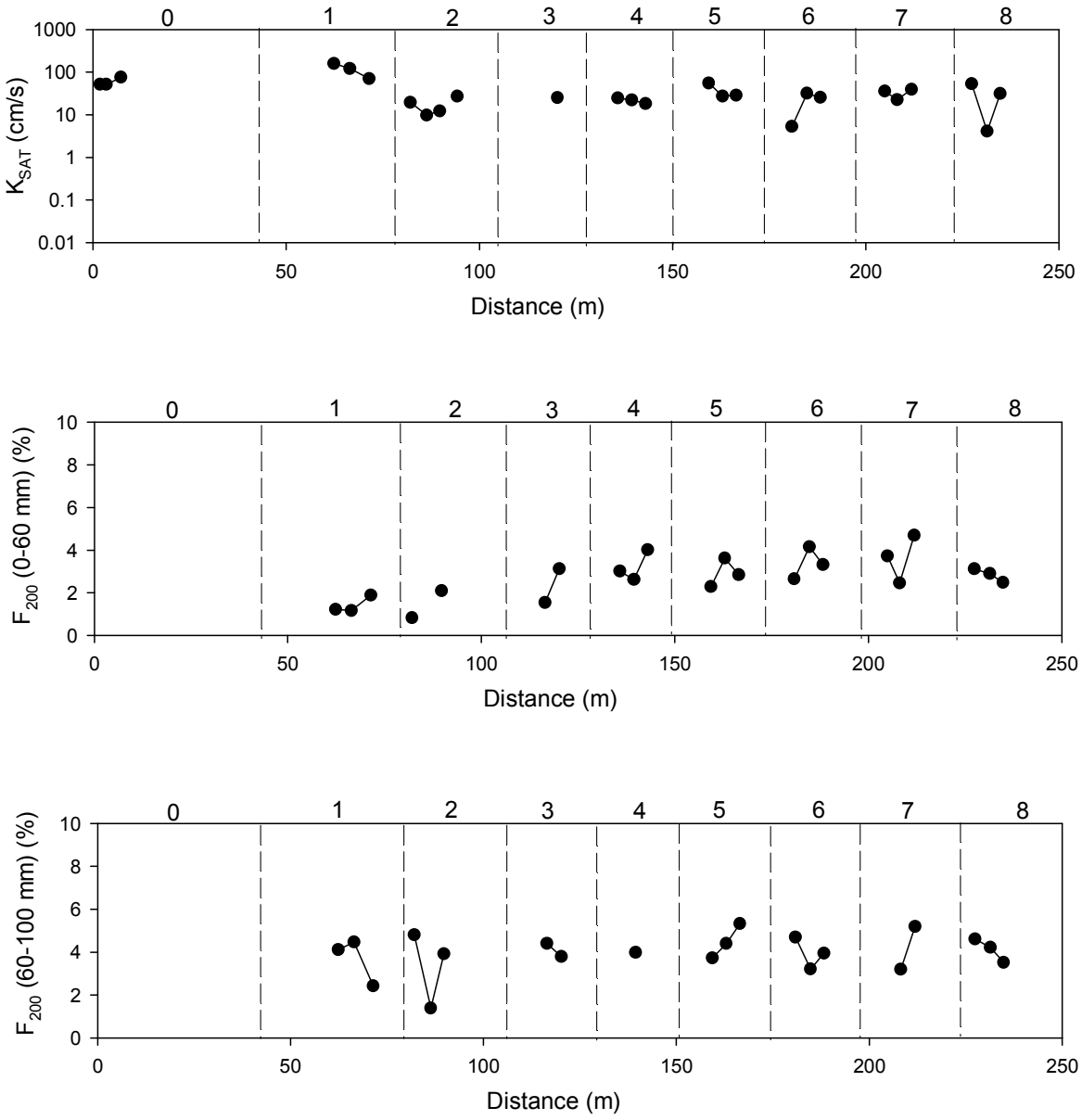

Figure 75. Hydraulic conductivity Ksat and passing #200 fine contents on low amplitude vibratory compaction roller section on untrimmed base of I-35 Iowa

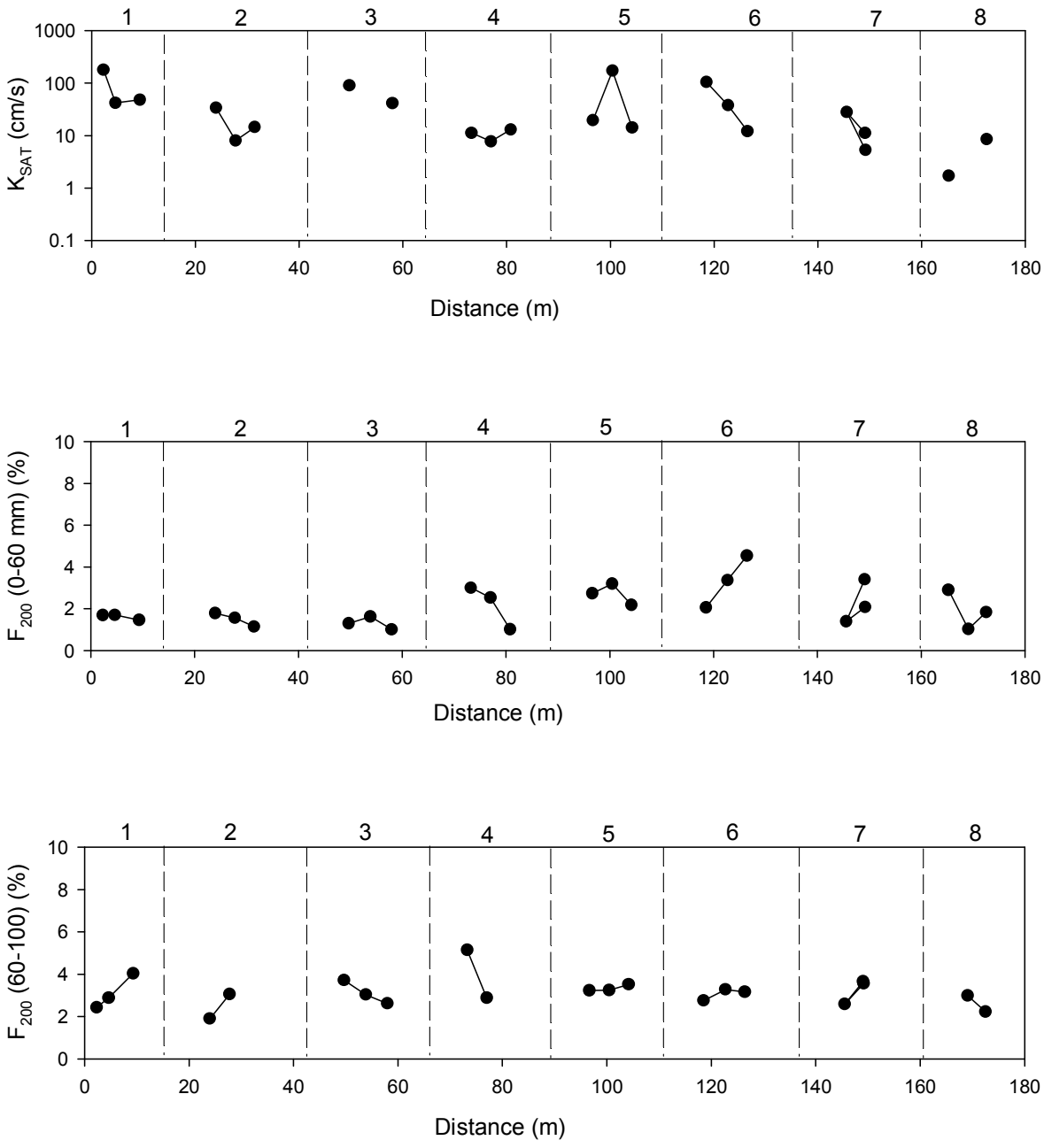

Figure 76. Hydraulic conductivity K_{SAT} and passing #200 fine contents on static compaction roller on untrimmed base of I-35 Iowa

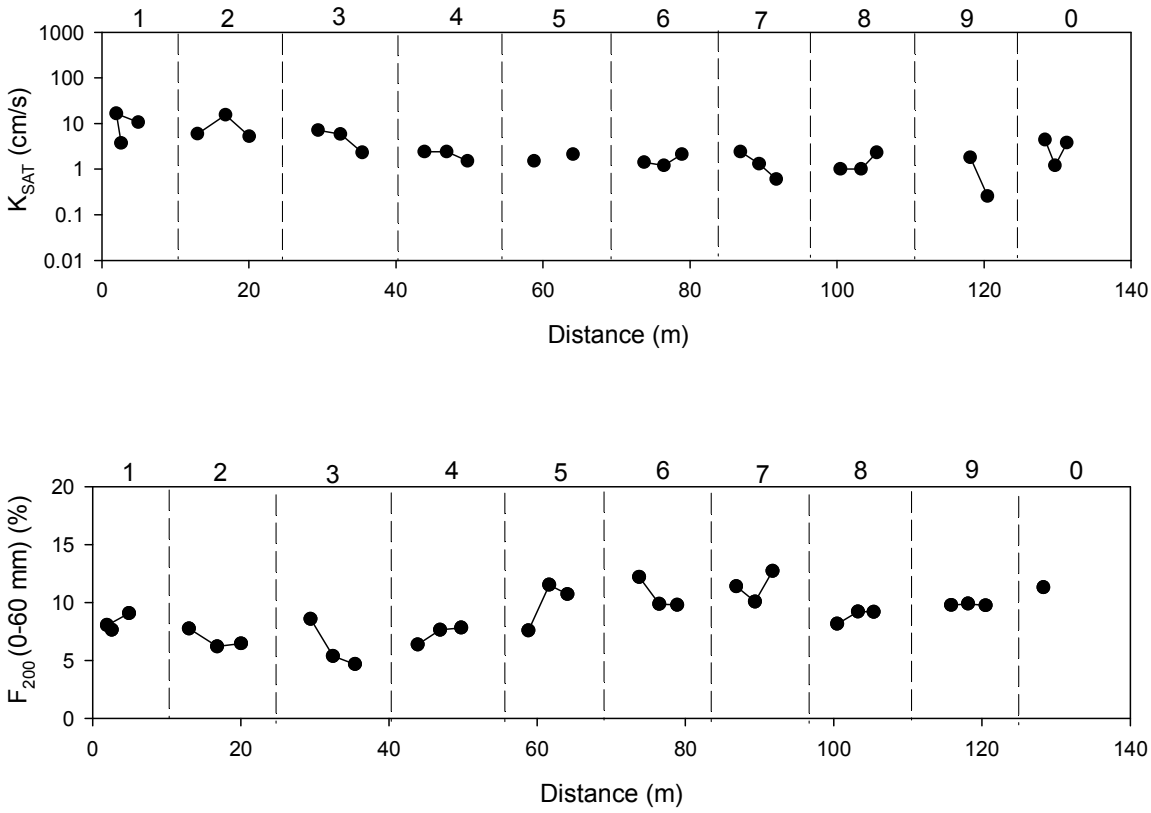

Figure 77. Hydraulic conductivity K_{SAT} and passing #200 fine contents on low amplitude vibratory compaction roller section on trimmed base on I-35 Iowa

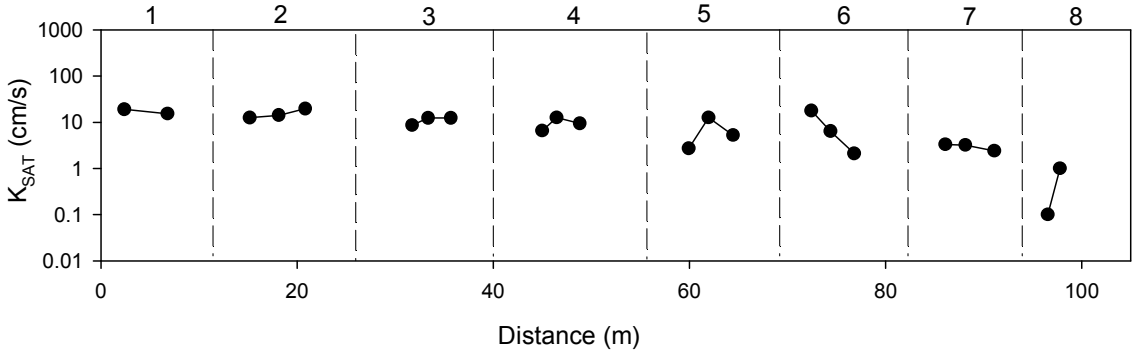

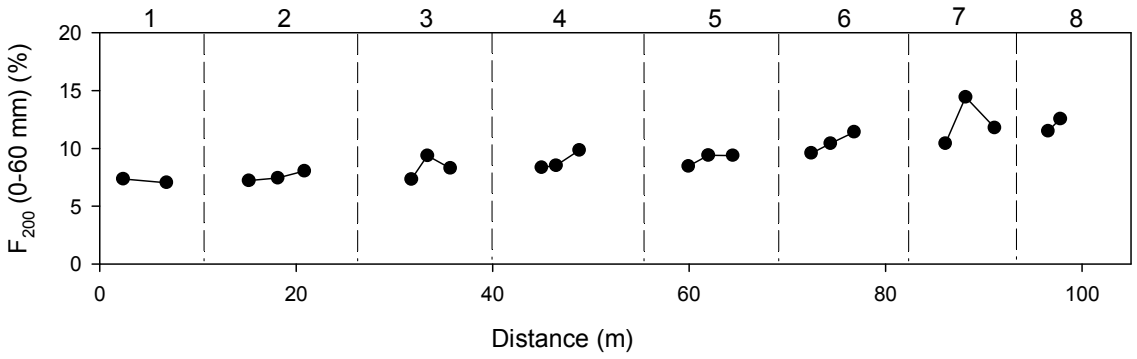

Figure 78. Hydraulic conductivity K_{SAT} and passing #200 fine content on static compaction roller section on trimmed base of I-35 Iowa

Moisture content and density

A calibrated nuclear moisture- density test measures the dry unit weight (γ_d) and moisture content (*w*) at center point of each section. Figure 79 and Figure 80 show the moisture content and density of the untrimmed base low amplitude vibratory and static compaction rollers. Due to different compactions, low amplitude vibratory roller section has higher dry unit weight value (97.5 psi to 106.4 psi) than that of the static compaction sections (90.4 pcf to 100.1 pcf). The moisture range of low amplitude vibratory roller section (6.6% to 8.5%) and static compaction section (7.1% to 8.9%) are similar to each other.

Low amplitude vibratory section (Figure 81) has higher dry unit density (108.3 pcf to 123.4 pcf) than static compaction section (Figure 82) 107.2 pcf to 116.1 pcf. The moisture content of low amplitude vibratory section ranges from 3.8% to 4.9 % and 4.5 % to 6.7 % for static compaction sections.

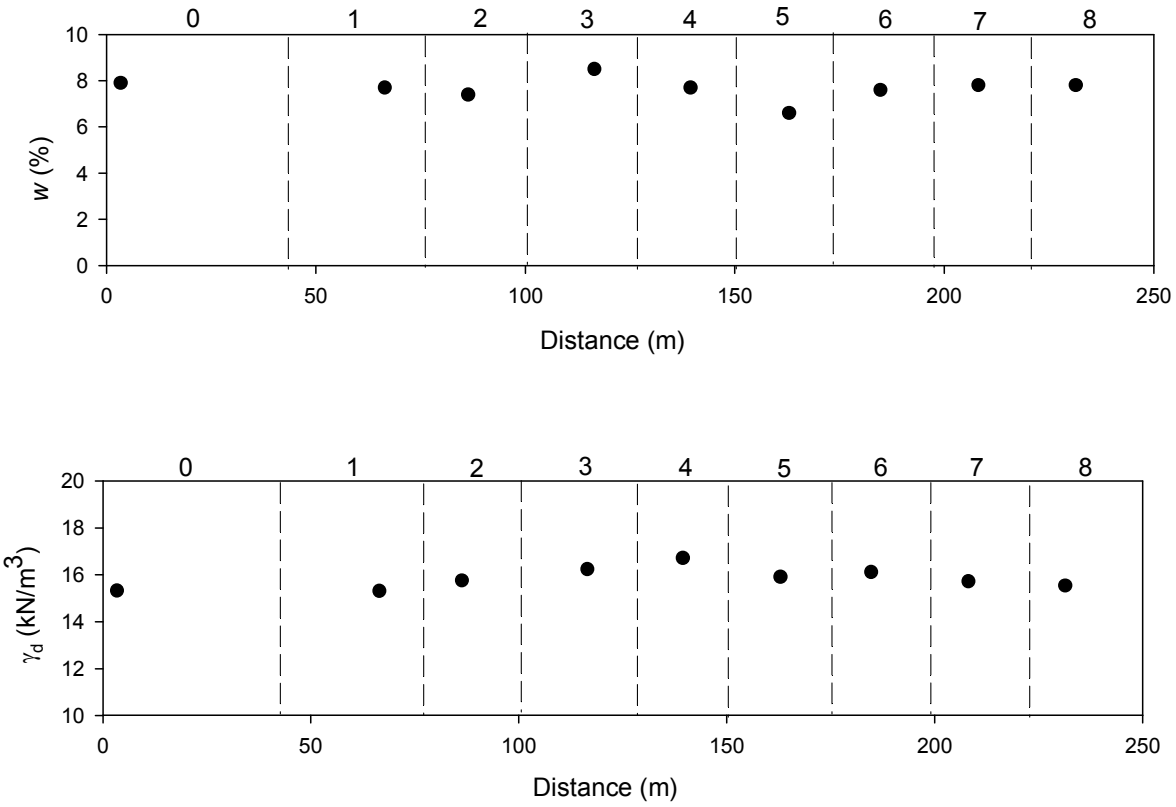

Figure 79. Moisture content, density on low amplitude vibratory roller section on untrimmed base of I-35 Iowa

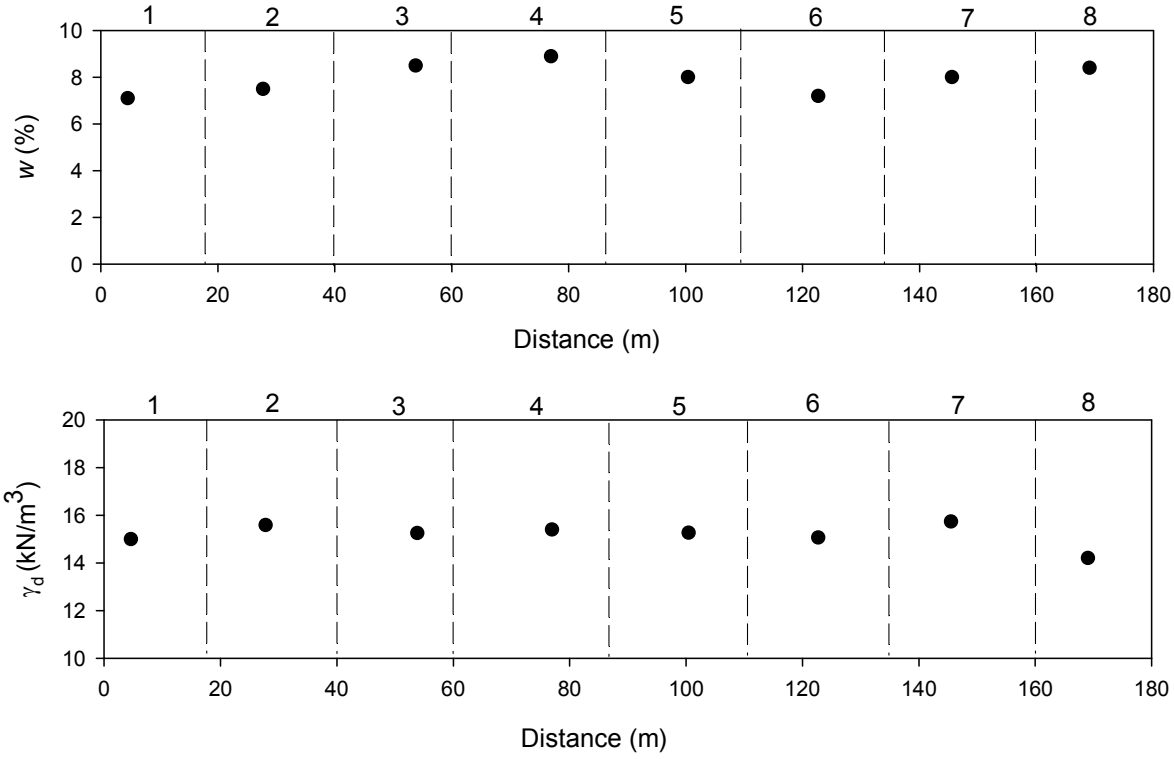

Figure 80. Moisture content, density on static compaction roller section on untrimmed base of I-35 Iowa

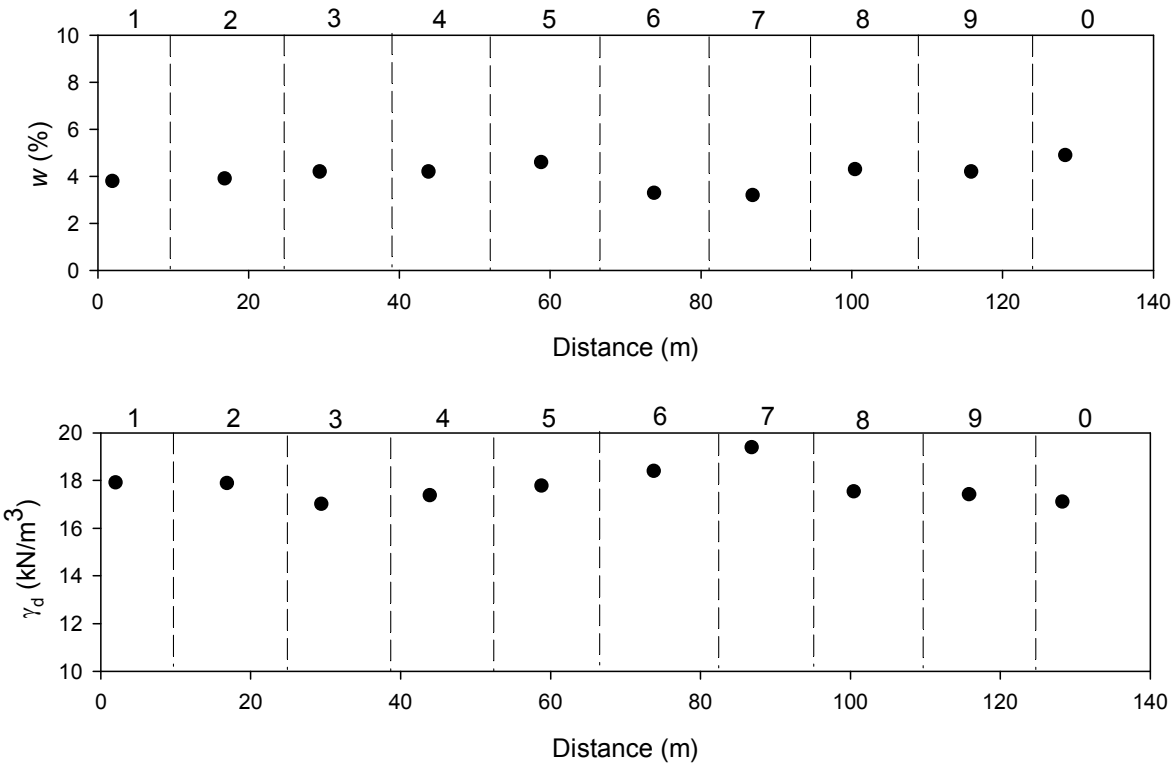

Figure 81. Moisture content, density on low amplitude vibratory roller section on trimmed base of I-35 Iowa

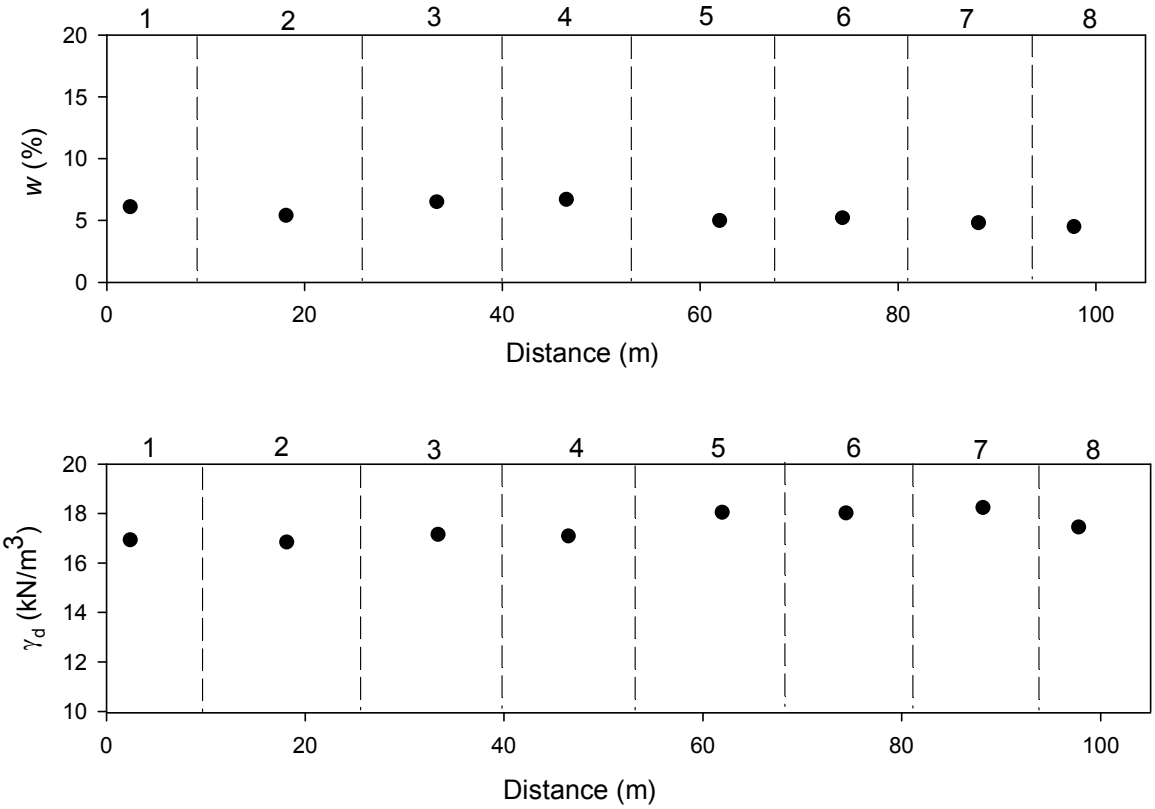

Figure 82. Moisture content, density on static compaction roller section on trimmed base of I-35 Iowa

Average value of measurements on untrimmed base and trimmed base

Average values of GPT, fine content, LWD, NG, PLT, DCP and MDP* of low amplitude vibratory compaction section and static compaction section are illustrated in Figure 83 and Figure 84. Figure 85 compares the average in situ point measurements of low amplitude vibratory roller and static compaction roller on untrimmed base. Static compaction roller section has higher saturate hydraulic conductivity value with lower fine contents. Low amplitude vibratory compaction section has higher elastic modulus, density, and stiffness. In contrary, low amplitude vibratory compaction has lower MDP* values.

Figure 86 and Figure 87 present the average values of GPT, fine content, LWD, NG, PLT, DCP and MDP* of low amplitude vibratory compaction section and static compaction section on trimmed base. Figure 88 compares the average in situ point measurements of low

amplitude vibratory roller and static compaction roller on trimmed base. Same as untrimmed base, static compaction roller section has higher saturated hydraulic conductivity value. Low amplitude vibratory compaction section has higher elastic modulus and stiffness.

Figure 89 compares the average in situ point measurements of low amplitude vibratory roller on untrimmed and trimmed bases. Figure 90 compares the average in situ point measurements of static compaction roller on untrimmed and trimmed bases. Trimmed base has low saturated hydraulic conductivity with high fines contents. Trimmed base has higher elastic modulus and stiffness.

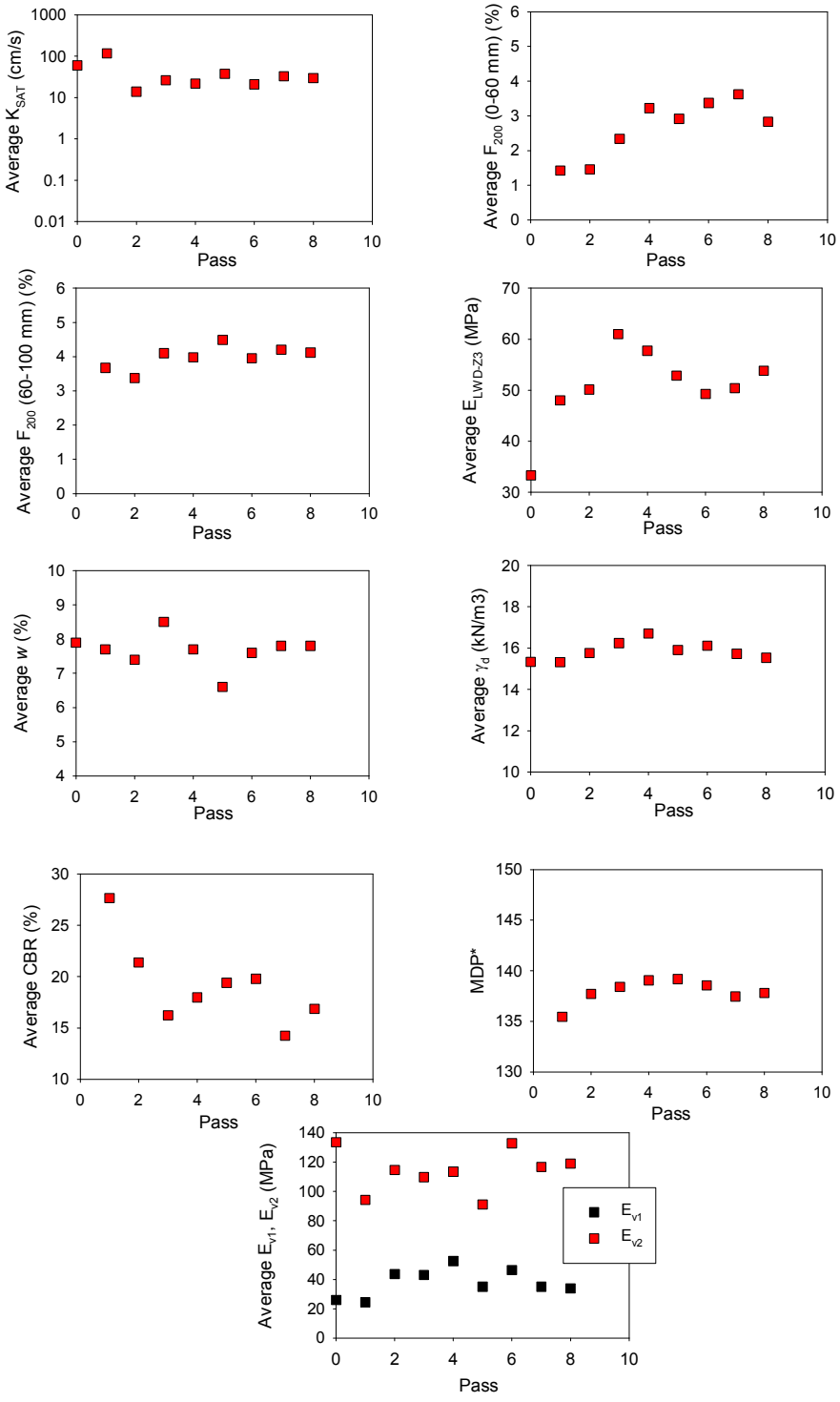

Figure 83. Average in situ point measurements on low amplitude vibratory roller section on untrimmed base of I-35 Iowa

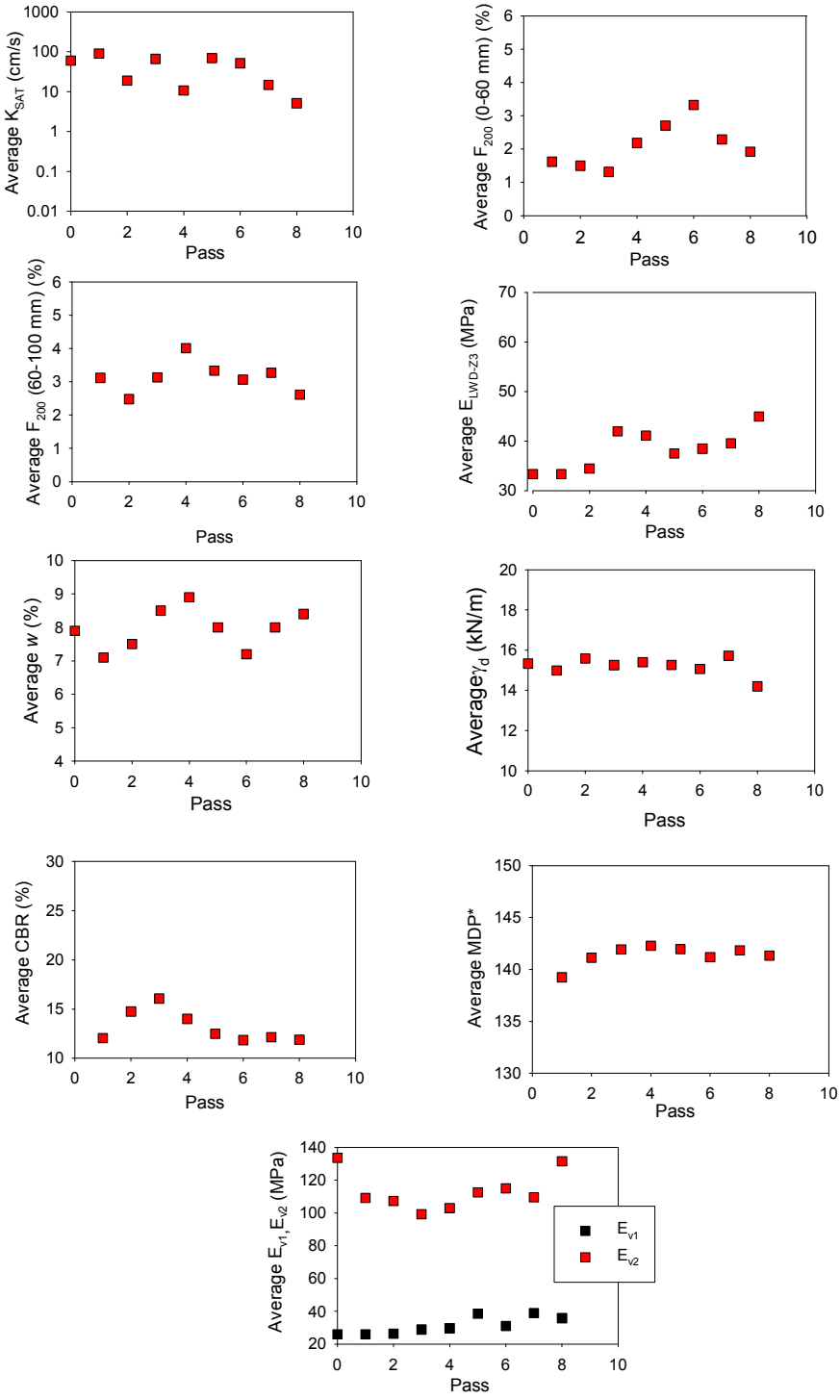

Figure 84. Average in situ point measurements on static compaction roller section on untrimmed base of I-35 Iowa

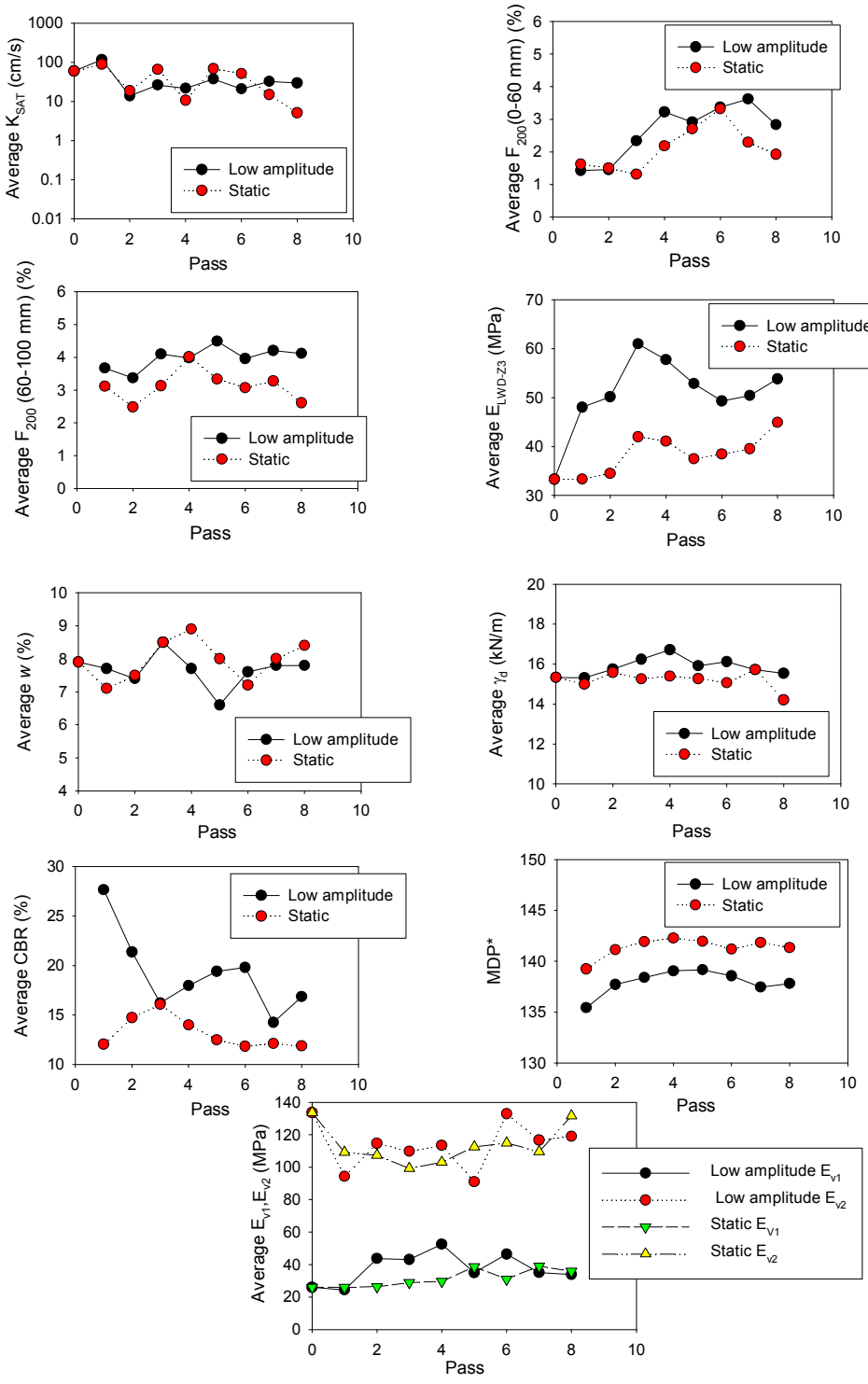

Figure 85. Comparison between in situ point measurements on low amplitude vibratory roller and static roller section on untrimmed base of I-35 Iowa

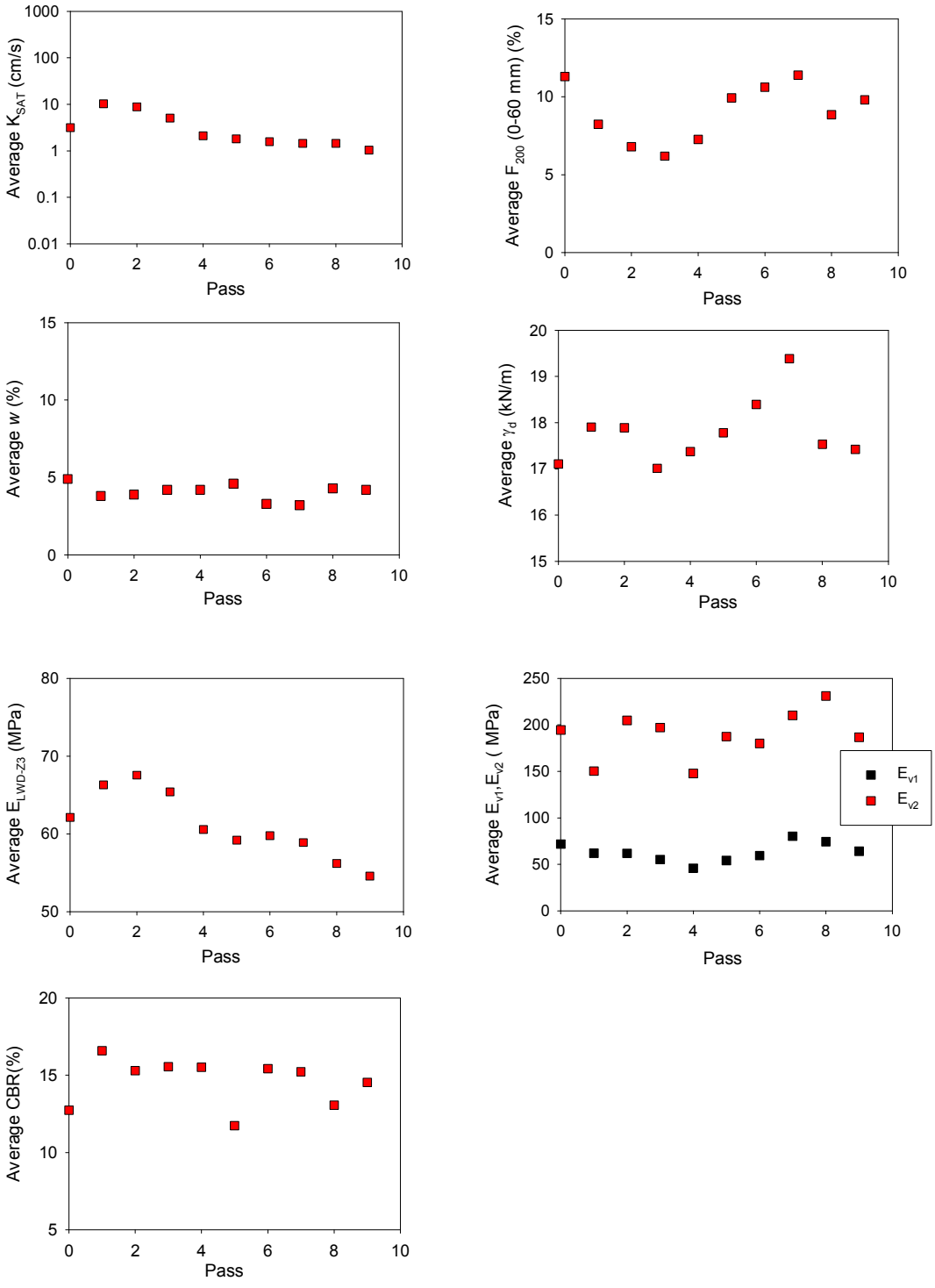

Figure 86. Average in situ point measurements on low amplitude vibratory roller section on trimmed base of I-35 Iowa

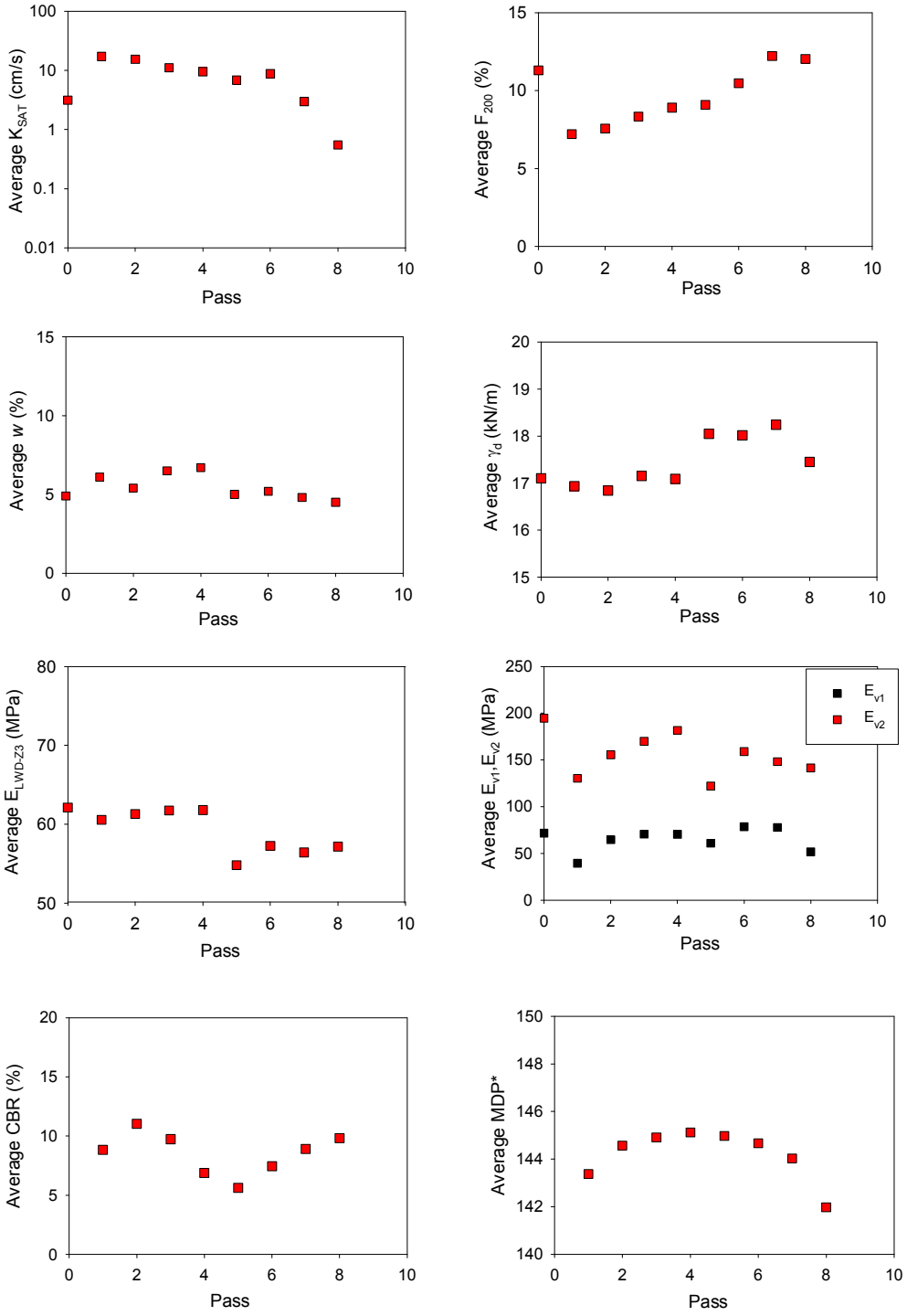

Figure 87. Average in situ point measurements on static compaction roller section on trimmed base of I-35 Iowa

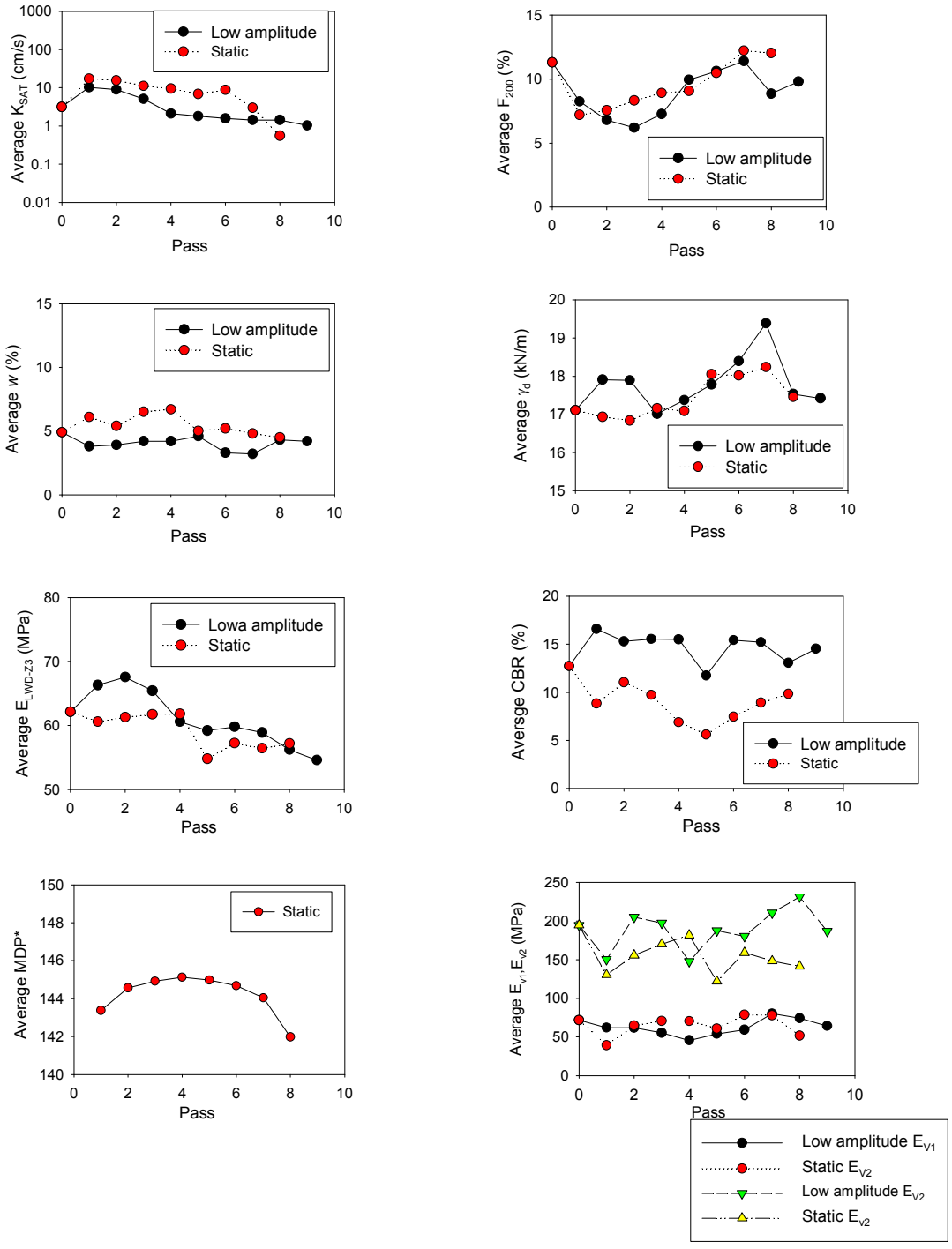

Figure 88. Comparison between in situ point measurements on low amplitude vibratory roller and static roller section on trimmed base of I-35 Iowa

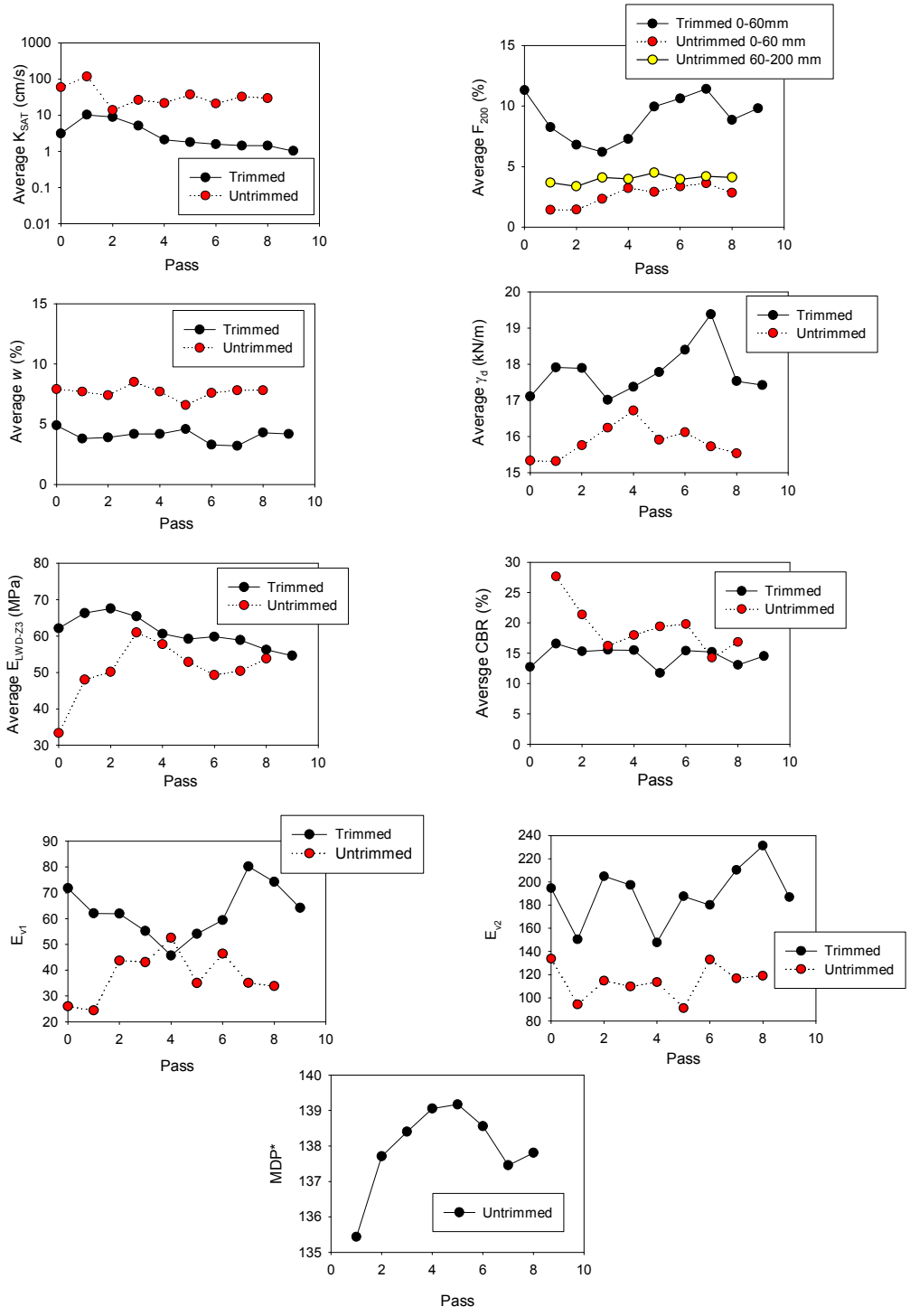

Figure 89. Comparison between in situ point measurements of low amplitude vibratory roller on untrimmed and timed base of I-35 Iowa

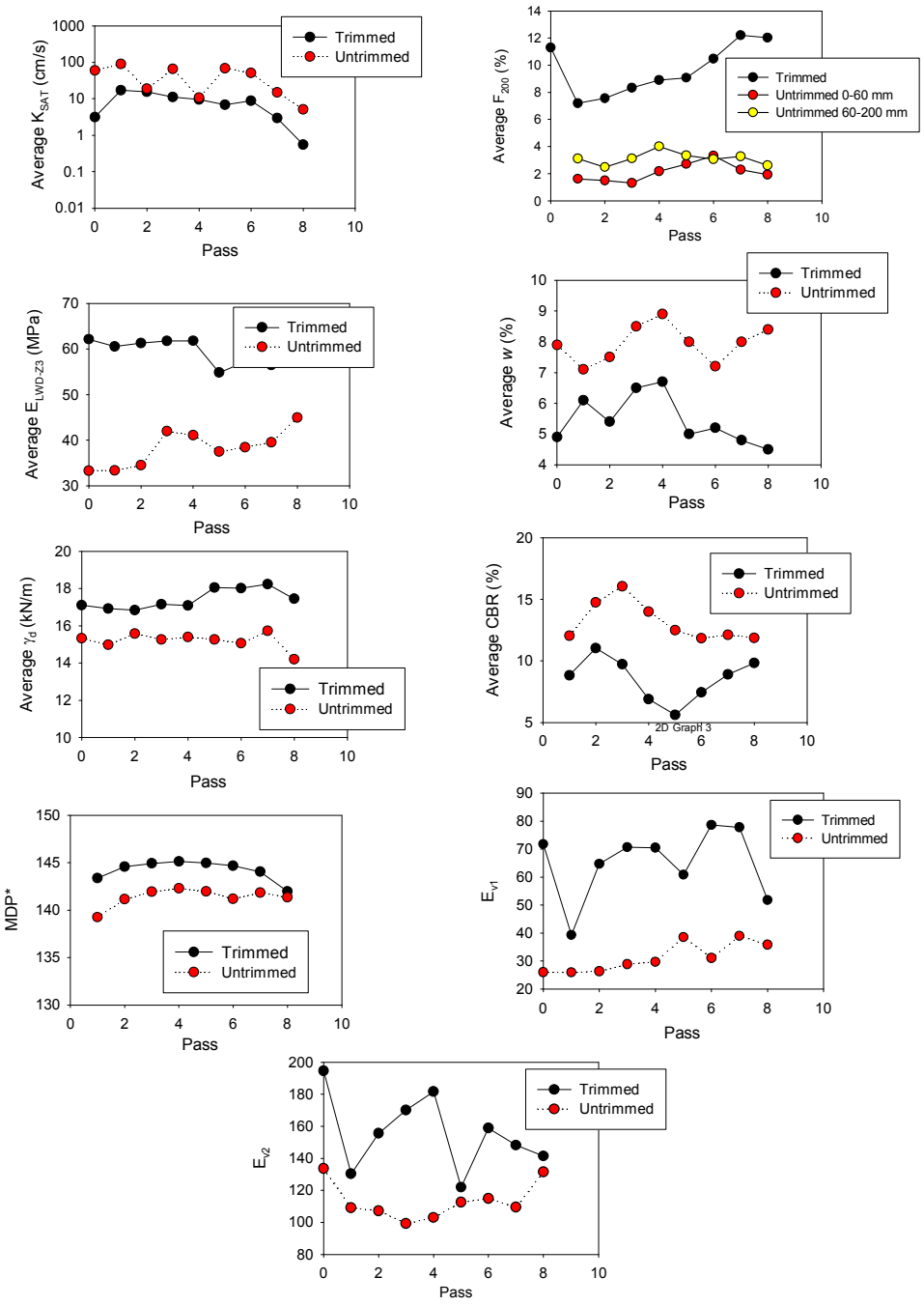

Figure 90. Comparison between in situ point measurements on static compaction roller on trimmed and timed base of I-35 Iowa

Comparison of measurements of each test beds

This section presents the comparison of measurements from GPT, fine content, LWD, NG, PLT, DCP and MDP*. Untrimmed base have higher saturated hydraulic conductivity values than trimmed base (see Figure 91). Oppositely, trimmed base have higher fine content than untrimmed base (see Figure 92). Moulton 1980 reported for granular materials, the saturated hydraulic conductivity is highly governed by its gradation, particularly the percentage of fine particles passing the No. 200 sieve.

Moisture content and dry density values were shown in Figure 93 and Figure 94.Untrimmed base values within the range of maximum and minimum density. Figure 96 was shown average of modulus of subgrade all lower than the Iowa DOT specification. Trimmed base has higher surface elastic modulus ($E_{LWD\text{-}Z3}$) than untrimmed base (see Figure 95). However, Figure 97 shows that trimmed base has lower CBR values. By comparing the static modulus elastic modulus of subgrade, higher values are on trimmed base and low amplitude section (see Figure 98). Figure 99 summarizes the MPD* values of untrimmed base and trimmed base.

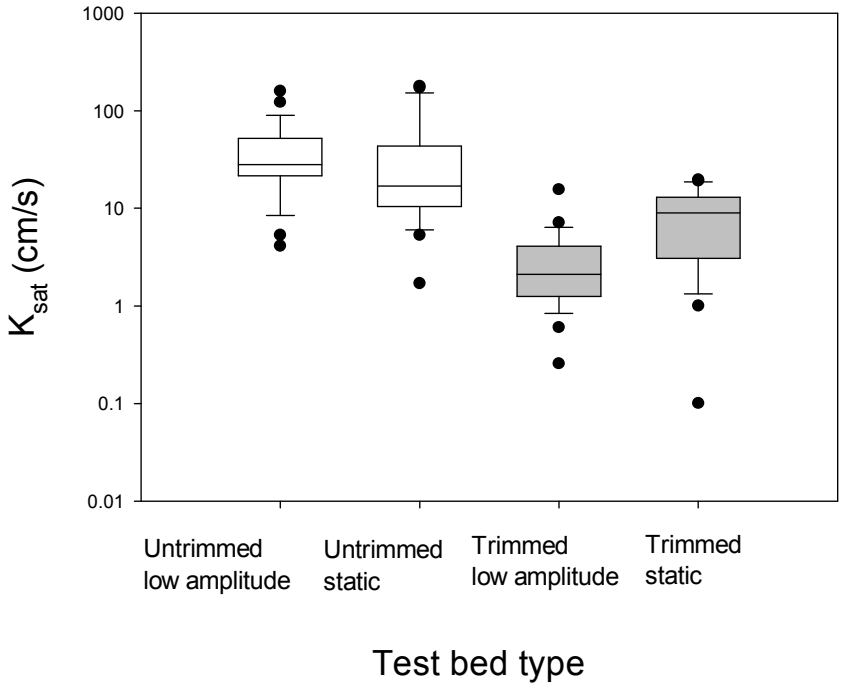

Figure 91. Comparison hydraulic conductivity test measurements for untrimmed base and trimmed bases

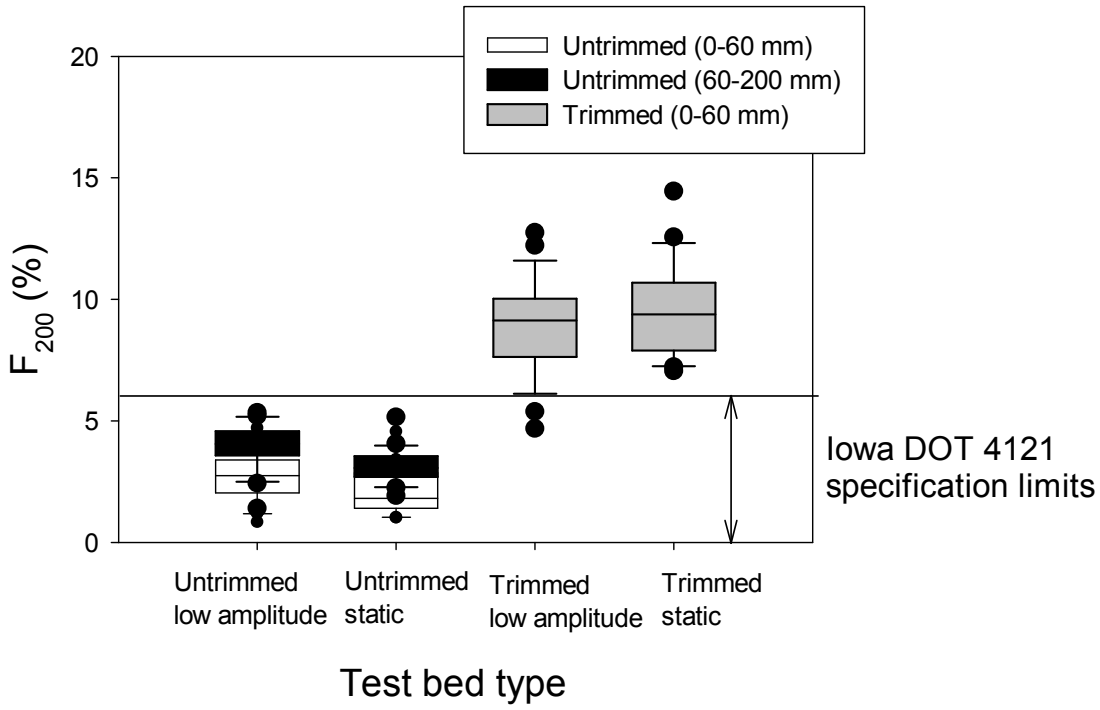

Figure 92. Comparison fines content for untrimmed base and trimmed bases

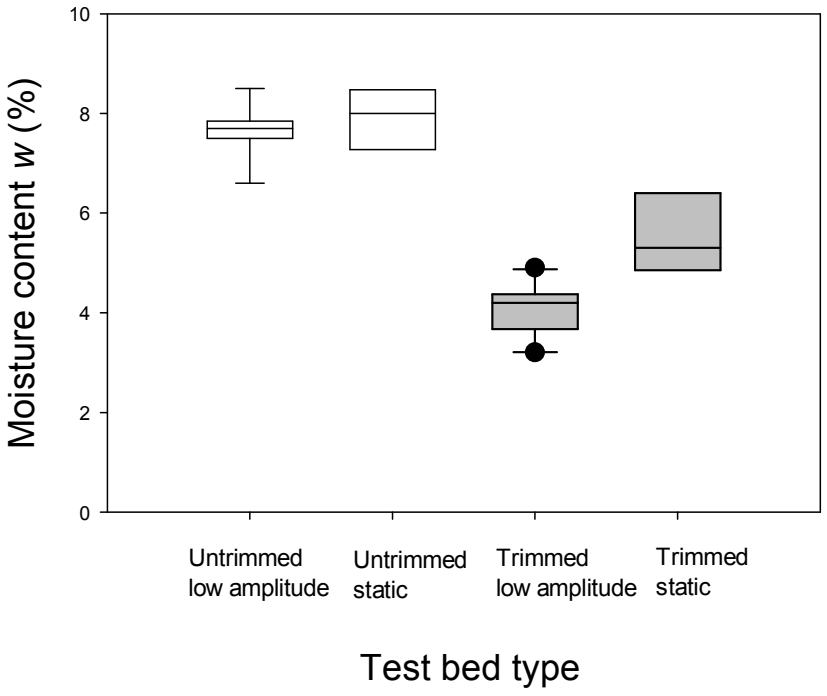

Figure 93. Comparison moisture content for untrimmed base and trimmed bases

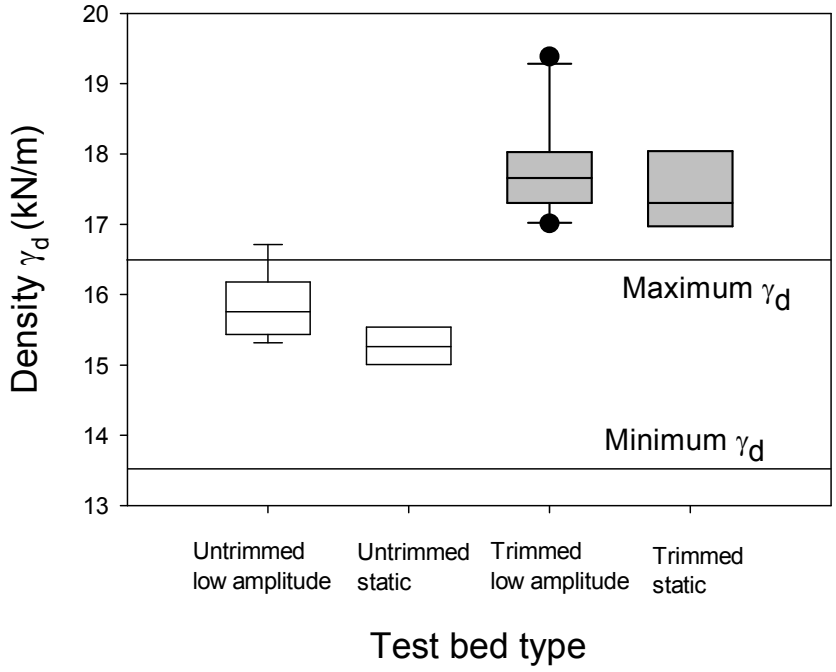

Figure 94. Comparison density for untrimmed base and trimmed bases

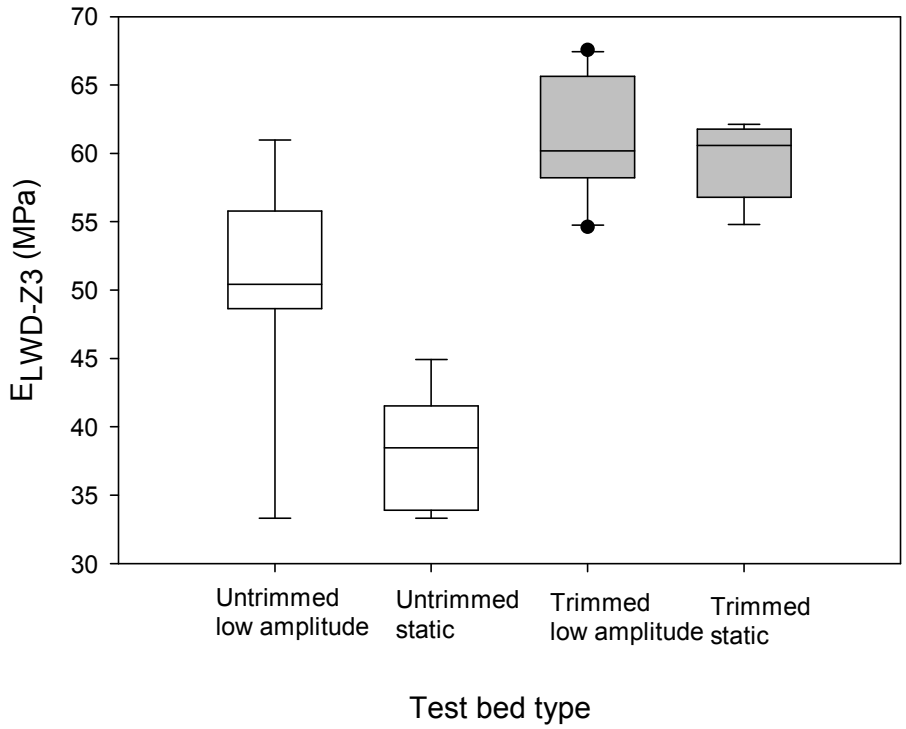

Figure 95. Comparison ELWD-Z3 for untrimmed base and trimmed bases

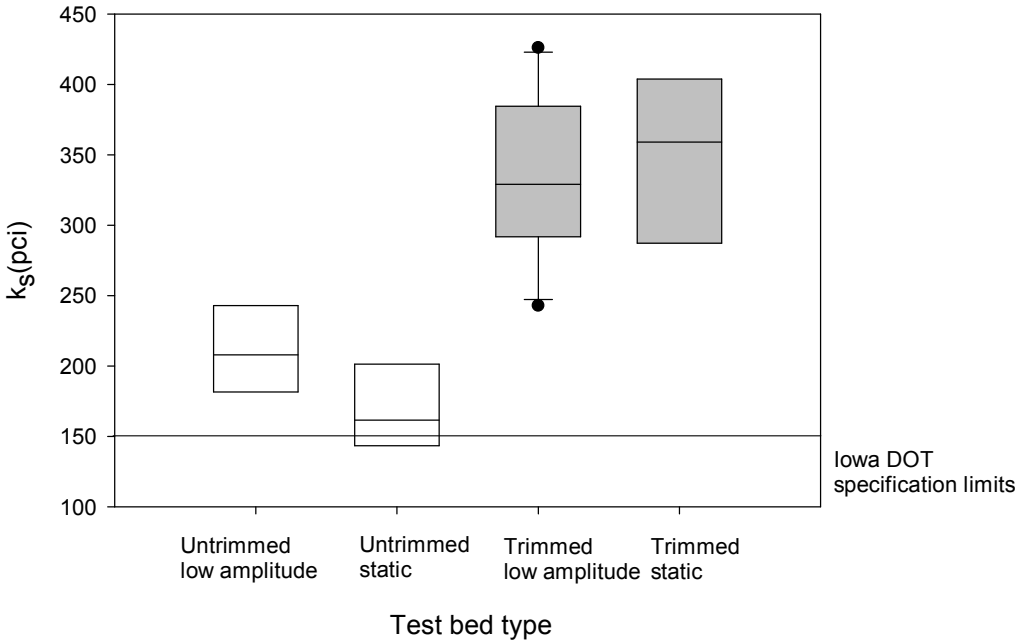

Figure 96. Comparison modulus of subgrade reaction for untrimmed base and trimmed bases

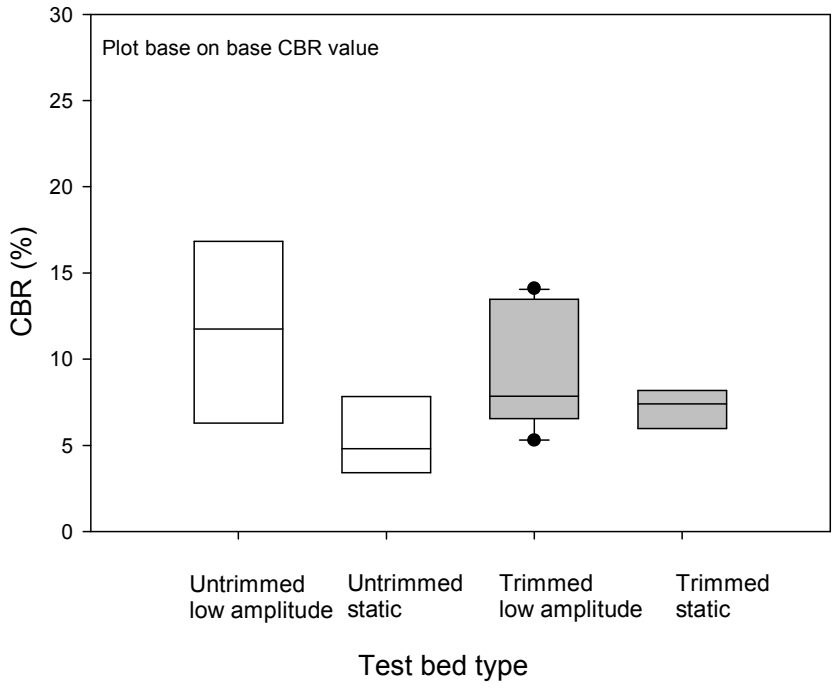

Figure 97. Comparison CBR for untrimmed base and trimmed bases

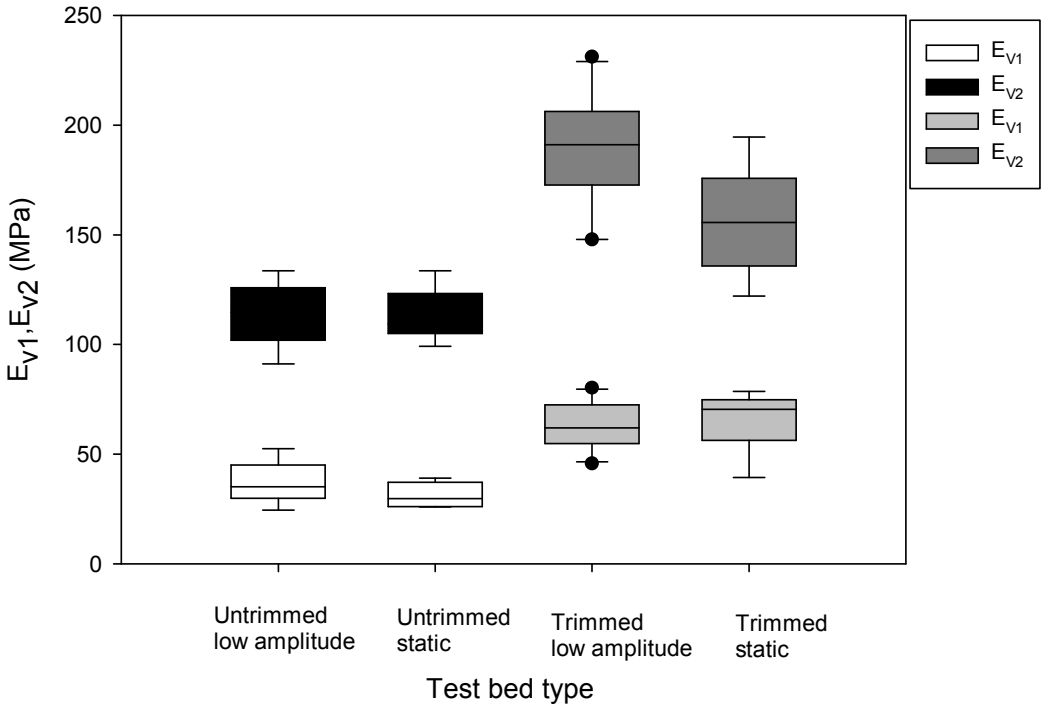

Figure 98. Comparison E_{v1} and E_{v2} for untrimmed and trimmed bases

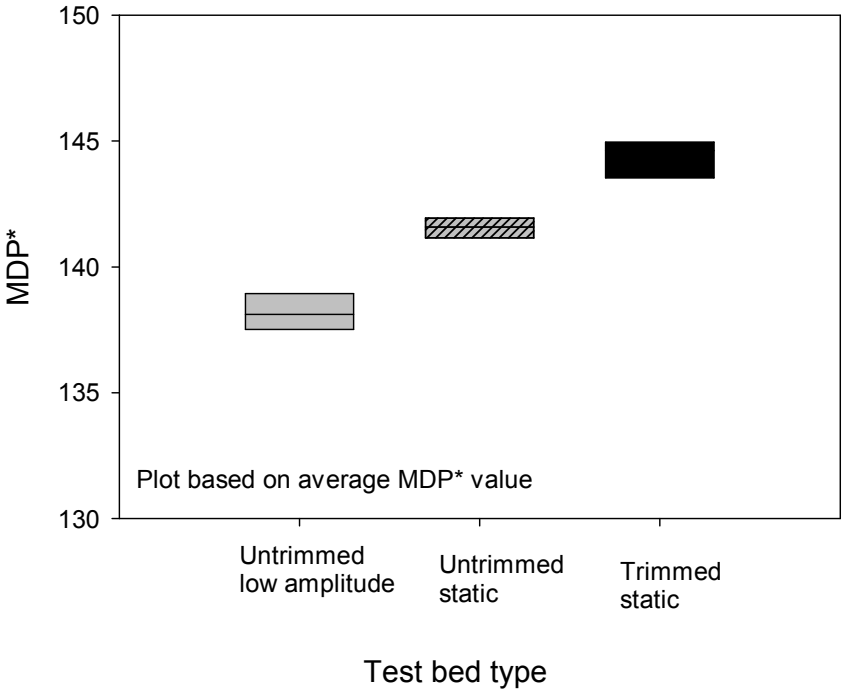

Figure 99. Comparison MDP* for untrimmed and trimmed bases

Laboratory Study

This section presents and discusses the test results laboratory studies in this order:

- Laboratory permeability tests which including use large scale aggregate compaction molds, GPT device and conventional falling head tests apparatus illustrated this section.
- GPT repeatability and measurement range
- Thin layer tests

Laboratory permeability test

Laboratory permeability test was performed using the large scale aggregate compaction mold (LSLP) permeameter and constant head permeability test methods. Sample was compacted using Marshall hammer using 50 blows per layer. Each layer should compact about 150 mm (6 inches) in three lifts of equal thickness. After the sample has been saturated, the decrease in the water level in the reservoir is timed while the water flows through the sample. Based on water head level drop with time, average K_{sat} vale is calculate. The thickness of materials varies between 0.15 m and 0.3 m.

GPT measurement was collected on the uniformly mixed and compacted materials in the 0.57 m square by 0.15 m height box and diameter of 0.95 m and height of 0.31 m of ring. The thickness of materials varies between 0.08 m and 0.3 m.

The GPT and Laboratory permeability test results vary from 0.2 to 5.0. According to NCHRP 2010, the reason for the wide range of test results are: (a) The significantly higher pressure head of laboratory permeability tests by comparing with the inlet gauge pressure ($P_{o(g)}$) in the GPT. High pressure head caused the non-laminar flow condition for high permeability materials in the laboratory permeability test. (b) By comparing the GPT three dimensional flow conditions with the one-dimensional LSLP laboratory permeability test, GPT measurements would be expect high hydraulic conductivity value than LSLP laboratory tests. Because more permeability pathway will control the drainage capacity which means gas flows through the high permeability to low permeable locations. Due to assumptions implicit to the k_{sat} derivation from GPT measurements, the difference between LSLP laboratory tests and GPT measurement is acceptable.

NCHRP 2010 found the empirical equation proposed by Moultom (1980). MEPDG EICM used the k_{sat} model and equation show in Equation 11 and Equation 12. Equation 11 was used for granular base and subbase materials with $P_{200} > 0$ and Equation 12 was used for granular non-plastic soils with k_{sat} between 10^{-6} and 10^{-2} cm/s (note that this correlation is based on limited measurements and showed significant scatter in the data). Result of LSLP laboratory and GPT hydraulic conductivity measurements for all materials are summarized in the. Table 34 summarized k_{sat} determined from GPT, laboratory permeability tests, and empirical relationship.

$$K_{sat}\ (\text{ft/day}) = \frac{6.214\times10^{5} D_{10}^{1.478} n^{6.654}}{P_{200}^{0.597}} \tag{5.7}$$

$$K_{sat}\ (\text{cm/s}) = 10^{-6}\times10^{\left(5.3D_{10}+0.049D_{60}+0.0092\frac{D_{60}}{D_{10}}-0.1P_{200}+1.5\right)} \tag{5.8}$$

Table 34. K_{sat} determined from GPT, Laboratory permeability tests, and empirical relationship (after NCHRP 2010)

Material	Laboratory Permeability Test Measurements			GPT Measurements				Ratio of GPT and lab K_{sat} (cm/s)	Empirically estimated K_{sat} (cm/s)
	Range of h_w (mm)	γ_d (kN/m^3)	K_{sat} (cm/s)	Range of $P_{o(g)}$ (mm)	Range of Q (cm^3/s)	γ_d (kN/m^3)	K_{sat} (cm/s)		
WLS-IA	900 to 620	19.05	3.5E-04†	53 to 77	22 to 30	18.90	4.4E 04***	1.3	1.8E-04‡, 4.6E-05‡‡
SAND 1	900 to 600	17.96	0.02†	13 to 65	80 to 720	17.60	0.10**	5.0	0.01‡, 7.62E-04‡‡
OLS-PA	900 to 500	19.50	0.08†	—§					1.9E-04‡, 1.0E-04‡‡
SGB	360 to 50	14.77	0.16††	15 to 73	80 to 720	14.78	0.07**	0.4	NA‡, NA‡‡
LGB	170 to 50	15.57	0.59††	4 to 22	520 to 2070	15.56	0.13*	0.2	NA‡, NA‡‡
				40 to 94	520 to 2070	15.56	0.24**	0.4	
OLS-63	900 to 500	15.92	1.47†	3 to 12	1020 to 6260	16.45	4.16*	2.8	2.1E-03‡, NA‡‡
CTB	177 to 51	17.03	1.53†	5 to 15	1020 to 6260	16.73	6.49*	4.2	4.9‡, NA‡‡
PG	900 to 500	15.15	2.17†	1 to 7	2160 to 6500	16.12	9.69*	4.5	NA‡, NA‡‡
OLS-IA	900 to 500	17.35	2.89†	4 to 6	4620 to 6260	17.40	10.09*	3.5	1.9‡, NA‡‡
OS-MI	900 to 500	14.77	3.14†	< 1 to 6	1040 to 6260	14.77	11.49*	3.7	0.08‡, NA‡‡
ATB	900 to 700	—§	6.46†	—§	—§	—§	—§	—§	4.9‡, NA‡‡

*GPT(A), **GPT(B), ***GPT(C), †Laboratory permeability tests using LSLP,††Laboratory permeability tests following ASTM D2434 procedure, §Not measured ‡calculated using equation 1, ‡‡calculated using equation 2, NA-not applicable.

Laboratory study of cement treat base (CTB)

This cement treat base (CTB) collected from field work in I-96 Lansing, Michigan. CTB specimens were obtain from a newly cement treated base (CTB) made from recycled concrete pavement that has been ground and graded underlain by sandy subbase and subgrade. CTB specimens are cylindrical that have different diameter and height, as illustrated in Figure 100 and Table 35. The samples are numbered from 1 to 5 from left to right.

Figure 100. Compaction of specimens of CTB I-96 Michigan

Table 35. Height and Diameter of specimens of CTB I-96 Michigan

Sample Number	Height (in)	Diameter (in)
1	5.26	5.93
2	3.27	5.71
3	3.07	5.91
4	2.35	5.87
5	3.98	5.93

The permeability of cylindrical specimens is collected by conventional falling head test. Figure 102 shows falling head permeability test. Each specimen of CTB was enclosed in a rubber sleeve, and directly attached to the pipe. Flexible sealing gum used around the top perimeter of the sample to prevent from leaking along the side of sample. The sample were confined in a member and sealed in the rubber sleeve, and surrounded by the adjustable hose clamps. Time *t* was recorded for the water head level to drop. Calculation based on the water head level for this test is from 20 to 2 in. and from 10 to 2 in. for specimens 1 to 3. Specimens 4 and 5 used water level head between 10 and 2 in. Average values are reported in Table 36. The maximum hydraulic conductivity value is 1.66 cm/sec, which is obtained from specimen 1.

Table 36. Porosity and permeability coefficients of falling head test (vertical) CTB, I-96 Michigan

Sample number	Hydraulic conductivity		Porosity (%)	Reynold's number
	cm/sec	(ft/day)		
1	1.66	4698.80	34.95	308.42
2	1.52	4303.10	20.61	415.28
3	0.78	2225.04	29.68	256.81
4	0.48	1365.05	35.95	162.68
5	0.7	1984.25	31.29	109.40

In this study falling head test was modified to measure the horizontal permeability. The bottom of each sample was sealed by using epoxy to bind the cement treated soil. As the result of these modifications, the boundary condition and the direction of flow are changed (see Figure 101 and Figure 102).

Based on the height of the specimens, tests performed on the specimens1 and 5 and results shows in Table 37. Hydraulic conductivity of specimen 1 is 0.23 cm/sec which is one seventh of the initial vertical value for specimen 1. However, specimen 5 has same hydraulic conductivity value for vertical flow and horizontal flow which is 0.7 cm/sec. The reason of same hydraulic conductivity may caused by the height of specimens. Specimen 1 is 1.3 in lower than the specimen 5.

Laboratory falling head test of CTB from both vertical and horizontal flow have lower values than the average hydraulic conductivity value (2.95 cm/sec) with average 5 in. thick in situ tests. Laboratory falling head tests has higher water head which is significantly higher than the inlet pressure during GPT tests.

Figure 101. Sealing the bottom of CTB of I-96 Michigan

Figure 102. Falling head permeability test of vertical flow (left) and horizontal flow (middle and right) of CTB, I -96 Michigan

According to (Bloomquist, 2007), for horizontal flow, the permeability could be calculated by the following equation in this boundary condition:

$$K_{sat} = \frac{\Pi d^2}{4F\Delta T} \ln \frac{H_1}{H_2} \qquad (5.9)$$

Where

d = the diameter of the sample diameter used

L = effective length of the slot

F = shape factor for which the device is used and it could be calculated by

$$F = \frac{2\Pi L}{\ln\left(\frac{L}{D} + \sqrt{1 + \left(\frac{L}{D}\right)^2}\right)} - 2.75D \qquad (5.10)$$

In equation 3, D is the same as d in equation 3.

Table 37. Permeability Coefficients of falling head test (horizontal) CTB, I-96 Michigan

Sample Number	Range of water head		Hydraulic conductivity	
	in.	cm	cm/sec	(ft/day)
1	24 to 3	61 to 7.6	0.23	644.73
5	12 to 3	30.5 to 7.6	0.7	1984.25

GPT repeatability and measurement range

Laboratory tests use four different orifice diameters size (GPT(A), GPT(B), GPT(C), GPT(D)) to obtain repeated measurements on nine different materials. Diameter of 0.95 m and height of 0.31 m of ring and 0.57 m square by 0.15m height boxes are used to uniformly mix and compact materials (see Figure 103). Table 38 summarized the $\sigma_{repeability}$ and K_{sat} value. The results indicate that repeatability in the calculated K_{sat} (i.e., COV ≤ 1%) is achievable with a minimum $P_{o(g)}$ = 10 mm of H_20 and Q = 100 cm^3/s. $P_{o(g)}$ = 10 mm of H_20 was not possible to match the high hydraulic conductivity and COV in the range of 5 to 18%. $P_{o(g)}$ = 10 mm of H_20 was not possible to match for GPT(D) and COV in the range of 23% (NCHRP 2010).

Figure 103. Laboratory GPT tests in 0.95 m diameter by 0.31 m height ring (left) and 0.57 m square by 0.15 m height box (right)

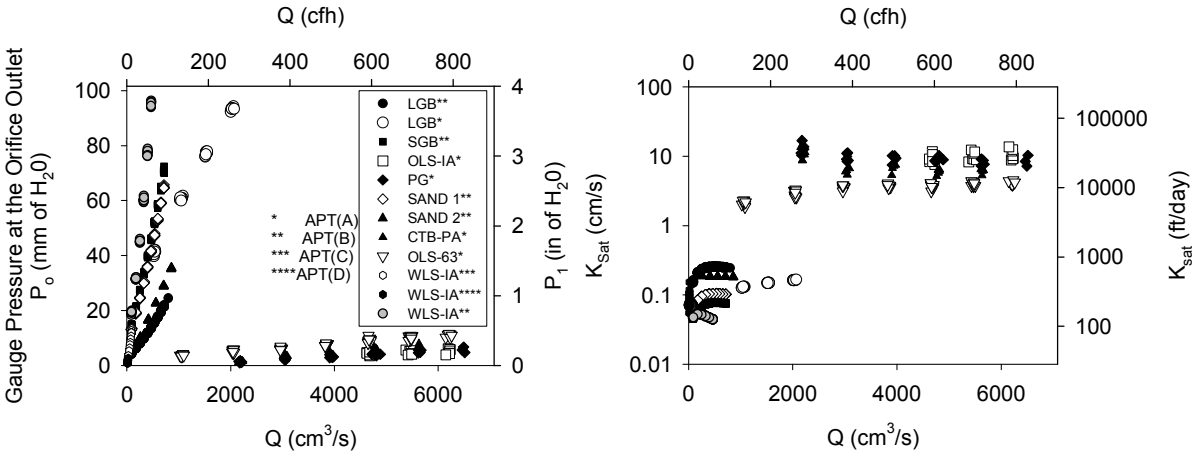

Figure 104. GPT repeatability on different materials [Note: P1 (Pa) = Po (mm of H20)*250 + 101325] (Adapted by NCHRP)

Table 38. Repeatability of GPT K_{SAT} measurement (Adapted by NCHRP)

Material	GPT ID	N	P_o Range (mm of H_20)	Q Range (cm^3/s)	K_{sat} Range (cm/s)	K_{sat} $\sigma_{repeatability}$ (cm/s)	COV (%)	Remarks
LGB	GPT(A)	47	39.8 to 94.3	520 to 2070	0.10 to 0.17	0.0001	≤ 1	Approximate target minimum: $P_{o(g)}$ = 10 mm of H_20 Q = 100 cm^3/s for COV ≤ 1%
SGB	GPT(B)	100	14.5 to 72.5	80 to 720	0.05 to 0.08	0.0004	≤ 1	
WLS-IA	GPT(B)	66	18.3 to 96.3	84 to 470	0.04 to 0.05	0.0004	≤ 1	
SAND1	GPT(B)	95	13.1 to 65.7	80 to 720	0.06 to 0.10	0.0005	≤ 1	
SAND2	GPT(B)	30	6.8 to 35.6	170 to 860	0.18 to 0.20	0.0014	≤ 1	
LGB	GPT(B)	99	4.1 to 21.9	80 to 720	0.15 to 0.26	0.0015	≤ 1	
WLS-IA	GPT(C)	70	3.0 to 15.1	30 to 105	0.06 to 0.07	0.0008	≤ 1	
OLS-63	GPT(A)	70	3.3 to 9.5	1020 to 6260	1.85 to 4.54	0.1857	5	$P_{o(g)}$ did not achieve the target minimum
OLS-IA	GPT(A)	21	3.5 to 6.1	4620 to 6260	7.59 to13.62	1.3264	13	
PG	GPT(A)	26	1.0 to 6.7	2160 to 6500	7.19 to16.94	1.5816	16	
CTB-PA	GPT(A)	24	1.1 to 7.9	1020 to 6260	5.16 to14.53	1.3382	18	
WLS-IA	GPT(D)	19	0.8 to 2.7	12 to 25	0.05 to 0.15	0.0201	23	$P_{o(g)}$ and Q did not achieve the target minimum

Figure 105 presented the measurement range of GPT device using different orifices. MEPDG recommended the minimum hydraulic conductivity value of permeable value is 0.35 cm/s (1000 ft/day). Christopher et al. (2006) also report the same hydraulic conductivity as MEPDG. American Concrete Paving Association (ACPA) recommended the target of hydraulic conductivity values is 50 to 150 ft/day.

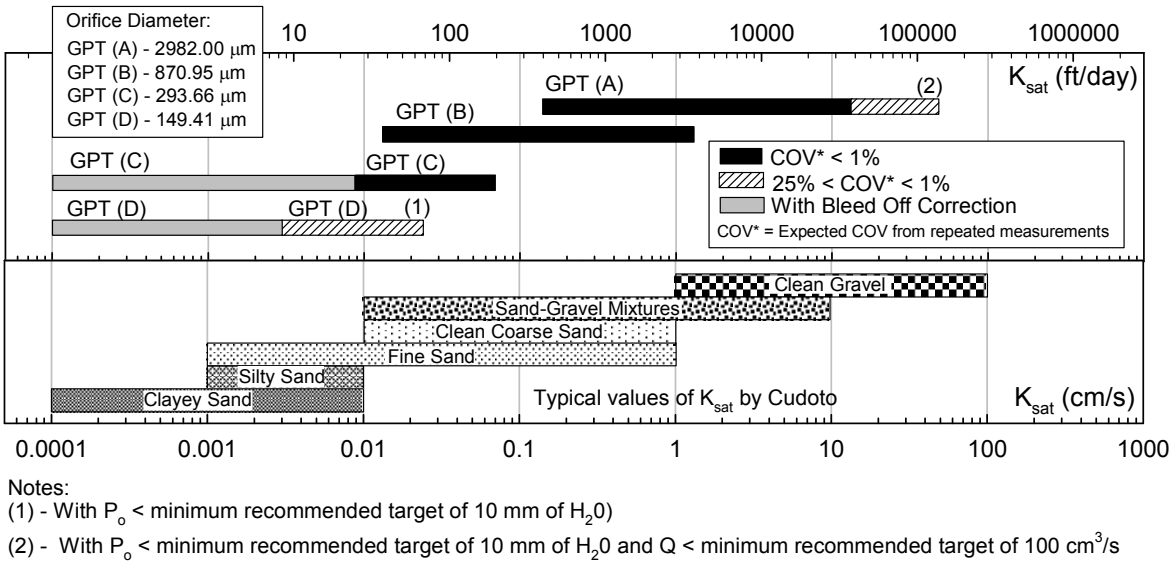

Notes:
(1) - With P_o < minimum recommended target of 10 mm of H_20)
(2) - With P_o < minimum recommended target of 10 mm of H_20 and Q < minimum recommended target of 100 cm^3/s

Figure 105. Measurement range of the GPT device using different orifice configurations (Adapted by NCHRP)

Thin layers study

Thin layer tests determined by measurements on three different material types using the GPT device setup with different orifice diameter sizes (GPT(A)),(GPT(B)). The materials were mixed in the laboratory in a 0.57 m square by 0.15m height box. GPT were performed on 10 layers of materials and each layer was 1 cm (see Figure 107). Therefore, the materials thickness were from 1 to 10 cm. GPT measurements were obtained at various combinations of $P_{o(g)}$ and Q measurements on silica sand, big glass beads (BGB) and small glass beads (SGB).

The geometric factor (G_o) was developed for steady state gas flow considering the GPT device geometry, sample geometry, and three dimensional flow conditions using an approach proposed by Goggin et al. (NCHRP 2010). Derivation the relationship of saturated hydraulic conductivity from the gas flow and pressure measurement is expressed as

$$\Rightarrow K_{sat} = \left[\frac{2\mu_{gas} Q P_1}{r G_o \left(P_1^2 - P_2^2\right)}\right] \times \frac{\rho g}{\mu_{water}\left(1 - S_e\right)^2 \left(1 - S_e^{((2+\lambda)/\lambda)}\right)} \qquad (5.11)$$

where: k_{sat} = saturated hydraulic conductivity (cm/s); μ_{gas} = kinematic viscosity of the gas (PaS); Q = volumetric flow rate (cm^3/s); P_1 = absolute gas pressure on the soil surface (Pa) $P_{o(g)}$ x 9.81 + 101325; P_2 = atmospheric pressure (Pa); r = radius at the outlet (4.45 cm); G_o= Geometric factor (dimensionless factor see Figure 106), S_e = effective water saturation [S_e = $(S - S_r)/(1-S_r)$]; λ = Brooks-Corey pore size distribution index; S_r = residual water saturation; S = water saturation; ρ = density of water (g/cm^3); g = acceleration due to gravity (cm/s^2); μ_{water} = absolute viscosity of water (gm/cm-s).

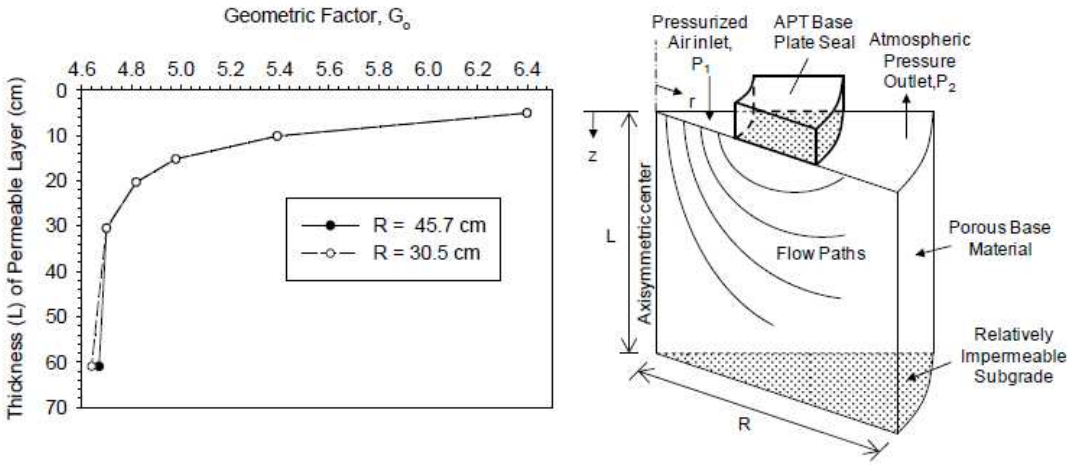

Figure 106. Graph to determine the geometric factor G0 for K_{sat} calculation

Graph (Figure 106) determined G_0 for calculation applied for thickness of permeable layer greater than 5 cm. Since the limitation of G_0 when permeable layer smaller than 5 cm, this experiments use three materials to study G_0 effect on the thin layers.

Figure 108 to Figure 110 present the GPT measurements at various of gauge pressures at the orifice outlet ($P_{0(g)}$) and volumetric flow rate (Q), constant $P_{0(g)}$ and Q change with the thickness, and constant Q verse various $P_{0(g)}$ of silica sand, BGB and SGB. The trend of Q is shown in the figure of constant $P_{0(g)}$ and Q change with the thickness. After target thickness is read, Equation 15 is used to calculate the G_0. In the same way, the target thickness layers read from trend of $P_{0(g)}$ on the constant Q with change $P_{0(g)}$ to calculate the G_0.

Figure 111 to Figure 113 compare the G_0 reading from Figure 106 and G_0 values calculate by constant Q and constant $P_{0(g)}$. Figure 106 shows that G_0 decrease with thickness

of permeable layer increased. Oppositely, G_0 increases with higher thickness of permeable layer in experiment tests (Figure 111 to Figure 113).

Figure 107. Gas permeability test of thin layers test

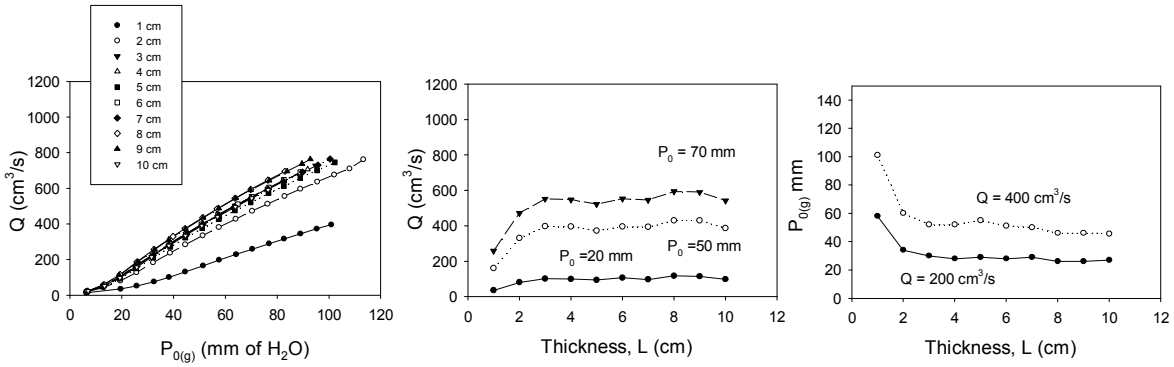

Figure 108. Gas permeability tests on silica sand

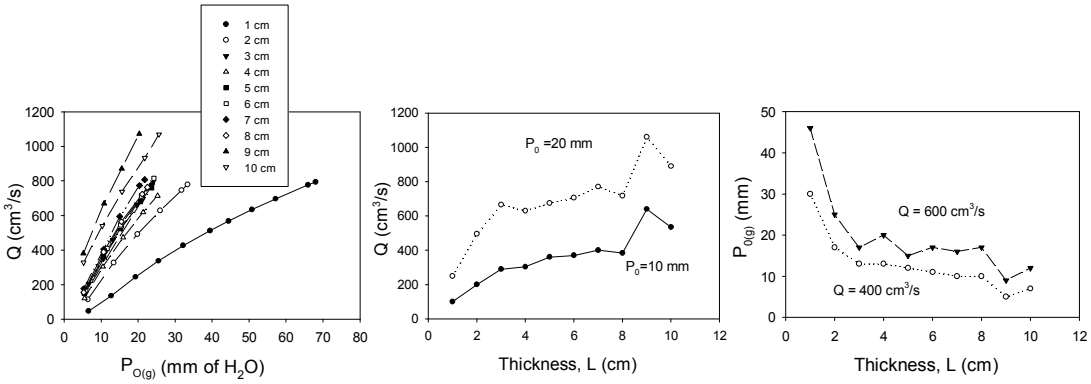

Figure 109. Gas permeability tests on big glass beads (1 mm spheres)

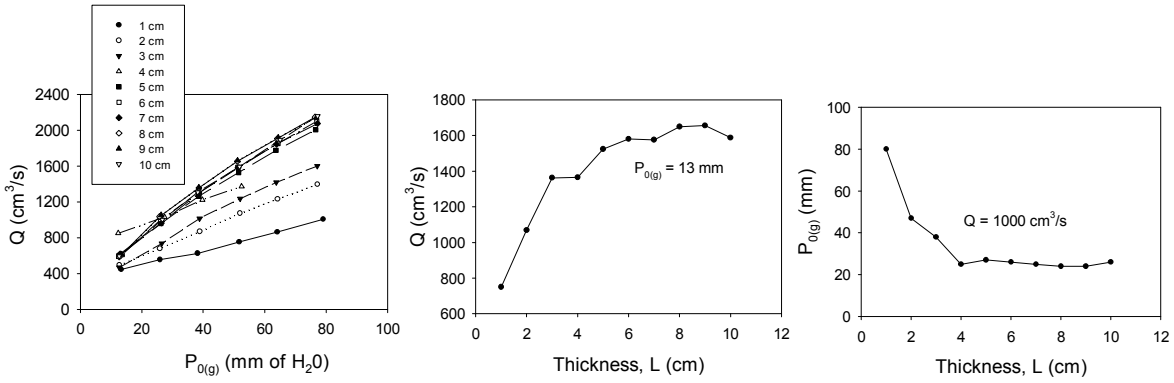

Figure 110. Gas permeability tests on small glass beads (0.75 mm spheres)

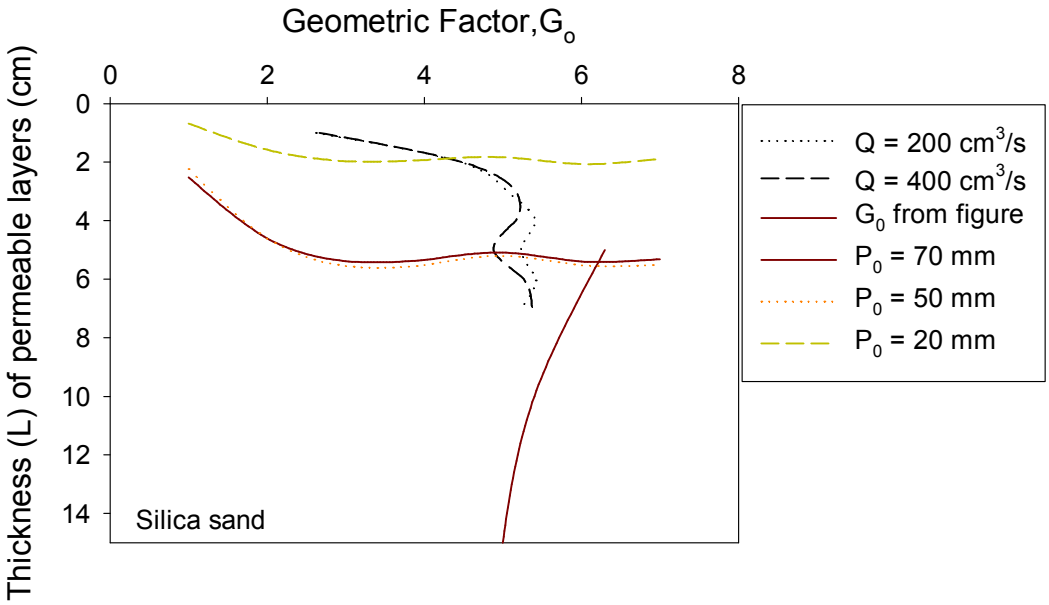

Figure 111. Geometric factor (G_0) on silica sand

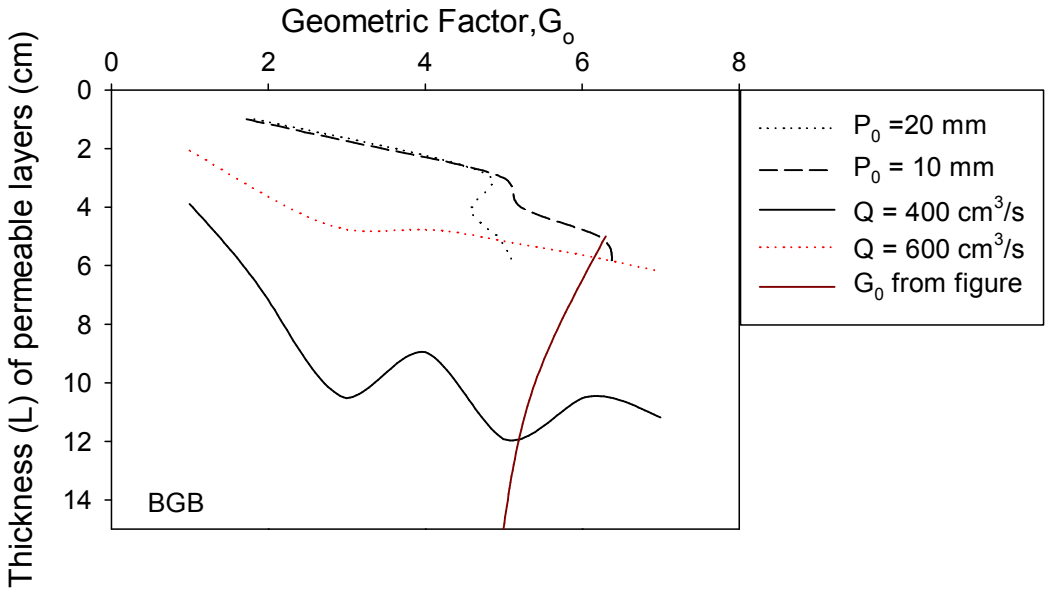

Figure 112. Geometric factor (G_0) on big glass beads (1 mm spheres)

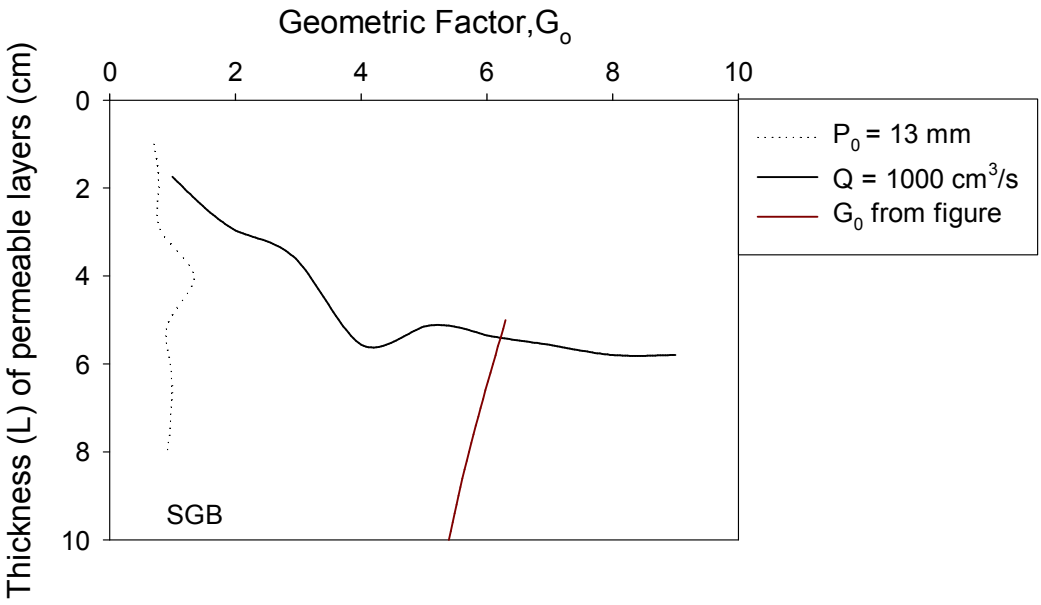

Figure 113. Geometric factor (G_0) on small glass beads (0.75 mm spheres)

CHAPTER 6. CONCLUSIONS

This chapter presents conclusions derived from in situ and laboratory study from this study. One of the objectives of this research was to provide new insights into new testing methods to effectively measure k_{sat} of pavement drainage layers both in laboratory and in situ . This research was built on work conducted for the Iowa DOT and NCHRP-IDEA research projects (White et al. 2010). This research also studies field construction operation for placement of granular subbase and the relationship between compaction and permeability.

Some of conclusions obtained from this research are:

- From the in situ and laboratory studies, GPT is proven to be a repeatable and rapid in situ permeameter test devise that take less than 30 seconds per test to determine saturated hydraulic conductivity of pavement base/ subbase materials. Spatial analysis of a small area at a short time can be used as QA/QC criteria to identify field problems such as segregation and particle degradation. The device also can be used effective in situ QA tool to verify the design assumptions.
- Laboratory studies about permeability of cement treated base (CTB) from I-96 Michigan are conducted by falling head test. Result shows thickness of specimens is an important parameter effect the hydraulic conductivity of vertical flow and horizontal flow. Hydraulic conductivity of vertical flow is eight times higher than that of the horizontal flow of a specimen which is 5.26 in. high and 5.93 in. in diameter. However, hydraulic conductivity values of vertical and horizontal flow are the same for a specimen which is 3.98 in. high and 5.93 in. in diameter.
- As more passes are considered (from 0 to 4), the average MDP* result increases. For real-time quality control, pass 4 has the maximum value for low amplitude and static on untrimmed bases and static compaction on trimmed base.
- Particle size distribution curve meets the Iowa DOT aggregate gradation base requirement except low amplitude vibratory of passing 5 to passing 9 on trimmed base. More fine content of particle size distribution than Iowa DOT limits per gradation on low amplitude vibratory of passing 5 to passing 9 of trimmed base. More fine content is probably due to particle breakage as the result of more compaction.

- Compared to untrimmed base, trimmed base has lower CBR, low amplitude vibratory has higher CBR value on both untrimmed and trimmed bases. Compared with static compaction, CBR of low amplitude vibratory on untrimmed base is higher than the static on trimmed base.
- Trimmed base has higher MDP*, dynamic elastic modulus ($E_{LWD\text{-}Z3}$), static elastic modulus of subgrade (E_{v1} and E_{v2}) and density that those of the untrimmed base.
- Hydraulic conductivity values of trimmed base are lower than those of the untrimmed base for both static and low amplitude vibratory compaction.
- Fine content of trimmed base are almost three to four times higher than the untrimmed base on the depth of 0 to 60 mm. Two to three times higher than the untrimmed base of depth of 60-200 mm.
- The findings from research study as guidance for marking informed decision about how pavement base/subbase construction and specifications can be used in improve construction operations (compaction, and trimming operations).

Future Research Recommendations

- Comparison of the hydraulic conductivity of GPT and large scale aggregate compaction mold permeameter tests (LSLP) are used for this study. However, the pressure head of LSLP uses relatively high water head (> 1 ft of water) which is significantly higher than the inlet pressure of $P_{o(g)}$ during GPT test. Further research will use horizontal laboratory permeability which maintains water head (< 75 mm) levels that are similar to the GPT tests.
- Significant segregation and increase in fines contents were clearly shown in three in situ studies. In order to build better performing pavement structures, the constructor should follow proper construction guidelines to reduce segregation of fines and, in turn, the variability of k_{sat} of the drainage base layers. Further research should be conducted by using the same testing procedure to test additional materials and the GPT device can be used as a forensic tool to investigate the "problem" site. Specifications should be written that require k_{sat} measurement as a QA/QC value. A test standard should be established for the GPT.

- Falling head tests was conducted on the cement treat base (CTB) specimens from I-96 in Michigan. However, this tests method applies to one-dimensional, laminar flow of water with porous materials such as soil and rock. A new device better suited for testing CTB specimens should be developed.
- The geometric factor (G_0) which is a parameter to calculate the saturated hydraulic conductivity is obtained from figure. However, the geometric factor for layers thinner than 5cm cannot be obtained directly from the figure. In this study, permeable layers thinner than 5cm were assumed to have a geometric factor of 6.4. More studies are needed to better predict G_0 at thinner layers.

REFERENCES

AASHTO. (1993) *Guide for design of pavement structures*, American Association of State Highway and Transportation Officials, Washington, D.C.

ACPA. (2008a) "Drainage in concrete pavement structures" American Concrete Pavement Association. Skokie, IL.

ACPA. (2008b) "Permeable subbases: reasons to avoid their use" American Concrete Pavement Association. Skokie, IL.

ACPA. (2008c) "Stabilized subbases" American Concrete Pavement Association. Skokie, IL.

Allen, D.L., Schultz, D.B., and Fleckenstein, L.J. (2001). "Development and Proposed Implementation of a Field Permeability Test for Asphalt Concrete." Kentucky Transportation Center, University of Kentucky. Lexington, KY.

Amoozegar, A., and Warrick, A.W. (1986) "Hydraulic Conductivity of Saturated Soils – Field Methods."American Society of Agronomy, Madison, WI.

Andrew D (2008) "Water in road structures " Nottingham Transportation Engineering Centre, University of Nottingham, UK.

ASTM C 136-01 "Standard test methods for Sieve Analysis of Fine and Coarse Aggregates." American Standard for Testing Methods (ASTM), West Conshohocken, PA.

ASTM D854-06. "Standard test methods for specific gravity of soil solids by water pycnometer." American Standard for Testing Methods (ASTM), West Conshohocken, PA.

ASTM D1196-93. "Standard Test Method for Nonrepetitive Static Plate Load Tests of Soils and Flexible Pavement Components, for Use in Elcaluation and Design of Airport and Highway Pavement." American Standard for Testing Methods (ASTM), West Conshohocken, PA.

ASTM D2434-68. "Standard test method for permeability of granular soils (Constant Head)", American Standard for Testing Methods (ASTM), West Conshohocken, PA.

ASTM D2422-63. "Standard test method for particle-size analysis of soild", American Standard for Testing Methods (ASTM), West Conshohocken, PA.

ASTM D2922. "Test method for density of soil and soil aggregate inplace by nuclear methods (shallow depth)." American Standard for Testing Methods (ASTM), West Conshohocken, PA.

ASTM D4318. "Test methods for liquid limit, plastic limit, and plasticity index of soils." American Standard for Testing Methods (ASTM), West Conshohocken, PA.

ASTM D6951-03. "Standard Test Method for Use of the Dynamic Core Penetrometer in Shallow Pavement Application." American Standard for Testing Methods (ASTM), West Conshohocken, PA.

Allen, D.L., Schultz, D.B., and Fleckenstein, L.J. (2001). "Development and Proposed Implementation of a Field Permeability Test for Asphalt Concrete." Kentucky Transportation Center, University of Kentucky. Lexington, KY.

Amoozegar, A., and Warrick, A.W. (1986) "Hydraulic Conductivity of Saturated Soils – Field Methods."American Society of Agronomy, Madison, WI

Andrew D (2008) "Water in road structures " Nottingham Transportation Engineering Centre, University of Nottingham, UK.

Beckemeyer, C.A., Khazanovich, L., Yu, H.T. (2002). "Determining amount of built-in culring in jointed plain concrete pavement." *Transportation Research Record No. 1089,* Transportation Research Board, Washington, D.C., 85-92.

Cedergren, H. R. (1988), "Why all Important Pavement Should be Well Drained." Transportation Research Record. 1188, pp.56-62.

Cuelho, E., Perkins.S. (2009). Fields Investigation of geosynthetics used for subgrade stabilization. Montana State University, Bozeman, Montana.

Clyne, T.R., Voller, V.R., and Birgisson, B, July 2001. *Evaluation of a Fields Permeameter to Measure Saturated Hydraulic Conductivity of Base/Subgrade Materials*. Minnesota Department of Transportation , St. Paul, Minnesota.

Christopher, B.C., Zhao, A. (2001) "Design Manual for Roadway Geocomposite Underdrain Systems". Christopher Consultanta, 210 Boxelder Lane Rosewell, GA.

Elsayer, A.D., and Lindly, J.K. (1996). "Estimation Permeability of Untreated Roadway Base". Transportation Research Record, Washing , D.C.11-18.

Forsyth, R. A., Wells, G.K., and Woodstrom J.H. (1978). "Economic impact of pavement subsurface drainage". Transportation Research Record. 1121. Transportation Research Board, Washing, D.C.77-85.

Krstulovich, J.M, Pierce, L.M., Smith, K.D, and Peshkin, D.G. (2010). *Review of State Highway Materials for Concrete Airfield Pavement Construction*. Iowa Highway Materials- concrete Airfield Pavement, IPRH Project 01-G-002-05-3. Airport Concrete Pavement Technology Program. Skokie, IL.

Hung, Y.H., (1993). *Pavement analysis design*, University of Kentucky

Itai Einav (2006). "Breakage mechanics-Part 1: Theory" Journal of the mechanics and physics of solids, 55 (2007) 1274-1297.

Moulton, L.K (1980). *Highway Subdrainage Design.* Report No. FHWA-TS-80-224. Federal Highway Administration, Washington, D.C.

Moulton, L.K., and Seals, K.R. (1979). Determination of the In-situ permeability of Base and Subbase courses. Final Report No. FHWA-RD-79-88, Department of Civil Engineering, West Virginia University, West Virginia.

Mallela, J., Titus-Glover L., and Darter, M. (2001). Appendix SS: Hydraulic design, maintenance, and construction details of subsurface drainage systems. National Cooperative Highway Research Program. Champaign, Illinois.

Kozeliski, F. A., (1992). Permeable Base Help Solve Pavement Drainage Problem. Aberdeen's Concrete Construction Vol. 37 no. 9 pp. 660–2.

Vennapusa, P., White, D.J. and Morris, M. (2010). Geostatistical analysis of spatial referenced roller-integrated compaction measurements. *Journal of Geotechnical and Geoenvironmental Engineering*, ASCE, 136(6), 813–822

Vennapusa, P., and White, D. J. (2009). "Comparison of light weight deflectometer measurements for pavement foundation materials." *Geotech.Test. J.*, ASTM, 32(3), 239-251.

Vennapusa, P., White, D. J., and Jahren, C. T. (2006). "In-situ permeability of unbound granular bases using the air permeameter test," *Proceedings of 85th Annual Transportation Research Board Conference*, CD-ROM Paper No. 06–1729, Transportation Research Board, Washington, D.C.

White, D. J., Vennapusa, P., and Janhren, C.T. (2004). Determination of the Optimum Base Characteristics for Pavements. Geotechnical Testing Jounal, ASTM International, Vol. 30, No. 4.

White, D. J., Vennapusa, P., and Suleiman, M.T. (2007). *An In situ Device for Rapid Determination of Permeability for Granular Bases.* Final Report, Iowa DOT Project TR–482, Centre of Transportation Research and Education Project 02-119, Iowa State University, Ames, Iowa.

White, D.J., Vennapusa, P., Eichner, D., Gieselman, H., Zhao, L., and Jahren, C. (2010). Rapid, self-contained in-situ permeameter for field QA/QC of pavement base/subbase materials. Iowa State University, Ames, IA.

White, D.J., and Gieseman, H. (2009). "Plate Load Test Device" Tech Brief, Earthworks Engineering Research Center, Iowa State University, Ames. IA.

Standiford, D.L., Graul,R.A., and Lenke,L.R., (1985) Permeability Equipment for Porous Friction Surface" Interim Report

Guide for mechanistic-empirical design of new and rehabilitated pavement structures. Part 2. Design inputs, Chapter1. Subgrade/foundation design input. National Cooperative Highwat Research Program Transportation Research Board. National Research Council. Champaign, Illinois.

White, D.J., Vennapusa, P., Eichner, D., Gieselman, H., Zhao, L., Jahren, C.T. (2010). *Rapid, self-contained in-situ permeameter for field QA/QC of pavement base/subbase*

materials. NCHRP 1-130 IDEA Project, Transportation Research Board, Washington, D.C.

White, D.J., Vennapusa, P., Gieselman, H., Zhang, J., Goldsmith, R., Johanson, L., Quist, S. (2010b). *Accelerated Implementation of Intelligent Compaction Monitoring Technology for Embankment Subgrade Soils, Aggregate Base, and Asphalt Pavement Materials* TPF-5(128) – *New York IC Demonstration Field Project*, ER10-01, Report submitted to The Transtec Group, FHWA, January.

White, D.J., Vennapusa, P., Gieselman, H., Johanson, L., Goldsmith, R. *Accelerated Implementation of Intelligent Compaction Monitoring Technology for Embankment Subgrade Soils, Aggregate Base, and Asphalt Pavement Materials* TPF-5(128) – *Texas IC Demonstration Field Project*, Report submitted to The Transtec Group, FHWA, November 2008.

White. D.J., Vennapusa, P., Gieselman, H., Zhang, J., Goldsmith, R., Johanson, L., Quist, S. *Accelerated Implementation of Intelligent Compaction Monitoring Technology for Embankment Subgrade Soils, Aggregate Base, and Asphalt Pavement Materials* TPF-5(128) – *Texas NY Demonstration Field Project*, Preliminary Data Report submitted to The Transtec Group, FHWA, June 2009.

Zorn, G. (2003). *Operating manual: Light drop-weight tester ZFG2000*, Zorn Stendal, Germany**.**

David Bloomquist, Adrian Albert Viala, Mike Gartner. *Development of a Field Permeability Apparatus: the Vertical and Horizontal Insitu Permeamter (VAHIP).* Gainesville, FL: Florida Department of Transportation, 2007.

Thomas J. Van Dam, James M. Krstulovich, Linda M. Pierce, Kurt D. Smith, David G. Peshkin. *Highway Materials-Concrete Airfield Pavement IPRF Project 01-G-002-05-3.* Skokie, IL: Innovative Pavement Research Foundation, 2010.

APPENDIX A. Raw data form I-35 iowa

Table 39. Summary moisture content and density on untrimmed base Iowa I-35

Compaction Method	Roller Passes	Sections	Point #	w_1	γ_{d1}	w_2	γ_{d1}
No compaction	0	0	2	8.0	97.2	7.8	97.9
Static Compaction	1	1	1	6.9	95.2	7.6	94.4
			2	7.3	96.5	6.6	95.6
	2	2	2	7.2	99.4	7.7	98.9
	3	3	2	9.0	91.3	8.0	102.9
	4	4	2	9.1	98.0	8.6	97.9
	5	5	2	7.8	97.2	8.2	97.2
	6	6	2	6.2	96.6	8.1	95.1
	7	7	2	8.9	99.1	7.1	101.1
	8	8	2	8.1	90.7	8.6	90.0
Low amplitude	1	1	1	8.0	96.6	8.1	98.8
			2	7.3	96.5	7.5	97.9
	2	2	1	6.4	101.4	8.4	99.2
	3	3	2	8.2	103.9	8.8	102.9
	4	4	2	7.8	106.3	7.6	106.5
	5	5	2	6.4	101.2	6.8	101.3
	6	6	2	7.5	102.2	7.7	102.9

Table 40. Summary moisture content and density on untrimmed base Iowa I-35

Compaction Method	Roller Passes	Sections	Point #	w_1	γ_{d1}	w_2	γ_{d2}
No compaction	0	0	0	4.7	108.9	5.0	108.8
Static Compaction	1	1	2	5.8	108.1	6.4	107.4
	2	2	2	5.6	107.2	5.1	107.2
	3	3	2		110.2	6.5	108.1
	4	4	2	6.8	108.8	6.6	108.8
	4	4	2	6.8	105.5	6.3	106.9
	5	5	2	5.5	112.6		114.2
	5	5	2	5.3	114.2	4.7	115.5
	6	6	2	5.6	115.1	4.7	114.2
	7	7	2	4.6	116.2	5.0	116.0
	8	8	2	4.1	111.7	4.8	110.4
Low amplitude	1	1	2	3.7	113.6	3.8	114.3
	2	2	2	3.8	114.2	4.0	113.5
	3	3	2	4.5	107.9	3.8	108.6
	4	4	2	4.2	110.7	4.2	110.4
	5	5	2	4.1	113.4	5.1	112.9
	6	6	2	3.0	117.2	3.6	117.0
	7	7	2	3.2	123.6	3.1	123.1
	8	8	2	4.5	111.1	4.0	112.0
	9	9	2	4.1	110.7	4.2	111.0

Table 41. Summary of dynamic elastic modulus subgrade for LWD test

Section	Test number	Untrimmed base E_{LWD-Z3} (MPa)		Trimmed base E_{LWD-Z3} (MPa)	
		Low Amplitude vibratory	Static compaction	Low amplitude vibratory	Static compaction
0	1	23.28	—	59.29	—
	2	42.71	—	58.94	—
	3	33.93	—	68.11	—
1	1	52.77	32.0	61.46	57.6
	2	43.26	34.64	72.0	60.72
	3	48	33.38	65.45	63.40
2	1	53.05	38.47	63.0	66.32
	2	53.33	35.37	59.64	58.95
	3	44.02	29.56	80.0	58.60
3	1	58.60	42.53	57.6	62.61
	2	65.03	40.32	71.49	62.22
	3	59.29	43.08	67.20	60.36
4	1	49.41	38.92	56.31	61.84
	2	57.93	44.21	58.27	64.62
	3	65.88	40.16	67.20	58.95
5	1	50.90	32.0	61.09	56.31
	2	58.94	42.53	57.93	54.49
	3	48.7	37.89	58.60	53.62
6	1	49.66	37.89	55.69	55.08
	2	38.18	37.47	62.61	56.63
	3	60	40.0	61.09	60.0
7	1	54.49	37.20	56.31	56.63
	2	53.33	37.89	60.0	55.38
	3	43.45	43.45	60.36	57.27
8	1	49.41	55.08	56.95	58.95
	2	50.91	39.53	56.0	55.38
	3	61.09	40.16	55.69	—
9	1	—	—	53.90	—
	2	—	—	55.69	—
	3	—	—	54.19	—

Table 42. Summary of static elastic modulus subgrade for PLT test

Section	Test number	Untrimmed base PLT(MPa)				Trimmed base PLT(MPa)			
		Low Amplitude vibratory		Static compaction		Low amplitude vibratory		Static compaction	
		E_{v1}	E_{v2}	E_{v1}	E_{v2}	E_{v1}	E_{v2}	E_{v1}	E_{v2}
0	1	27.85	129.98	—	—	72.18	214.7	—	—
	2	24.72	134.4	—	—	78.52	198.88	—	—
	3	25.44	136.38	—	—	64.55	170.02	—	—
1	1	—	—	21.53	85.01	67.81	141.97		
	2	23.16	113.37	25.86	100.6	63.21	160	39.3	130.23
	3	25.76	75.14	30.42	141.77	55.04	148.86	—	—
2	1	44.59	134.67	23.76	102.86	61.28	168.99	—	—
	2	47.8	94.51	34.59	113.32	63.52	260.37	64.67	155.56
	3	38.71	114.71	20.67	105.47	60.83	185.2	—	—
3	1	39.69	119.61	32.12	107.84	55.21	193.85	—	—
	2	50.8	125.84	25.77	88.19	54.72	203.64	70.63	170.02
	3	38.8	83.78	28.74	101.54	55.56	194.02	—	—
4	1	37.44	91.24	32.14	101.66	44.12	156.86	—	—
	2	42.25	95.73	25.27	101.82	45.65	120	70.46	181.62
	3	77.97	153.36	31.68	105.47	47.29	166.19	—	—
5	1	36.96	63.52	26.71	96.83	52.15	160	—	—
	2	37.47	99.26	59.1	120.21	49.9	203.64	60.83	121.96
	3	30.65	110.34	29.87	120.43	60.16	198.82	—	—
6	1	30.64	93.58	24.13	94.51	53.41	173.79	—	—
	2	58.33	165.52	36.54	161.93	65.05	177.29	78.57	158.87
	3	50.22	139.42	32.51	88.19	59.68	189.3	—	—
7	1	35.46	104.35	37.63	102.86	87.27	225.43	—	—
	2	35.44	111.12	39.68	112.72	68.84	185.2	77.78	148.14
	3	34.36	134.67	39.68	112.72	84.42	220.33	—	—
8	1	29.28	100.45	37.6	134.4	54.37	170.02	—	—
	2	37.6	130.18	38.91	132.13	107.35	361.29	51.77	51.77
	3	34.72	126.23	31.04	128	61.04	161.93	—	—
9	1	—	—	—	—	58.7	176.38	—	—
	2	—	—	—	—	61.04	203.34	—	—

Table 43. Summary of static modulus subgrade reaction for PLT test

Section	Test number	Untrimmed base PLT(MPa)				Trimmed base PLT(MPa)			
		Low Amplitude vibratory		Static compaction		Low amplitude vibratory		Static compaction	
		K1	K2	K1	K2	K1	K2	K1	K2
0	1	304.77	1422.41	235.66	930.30	789.89	2349.54		
	2	270.52	1470.79	282.0	1100.90	859.27	2176.42		
	3	278.40	1492.46	332.90	1551.44	706.39	1860.59	—	—
1	1			260.01	1125.63	742.07	1553.63		
	2	253.45	1240.65	378.53	1240.10	691.73	1750.94		
	3	281.90	822.28	226.20	1154.20	602.32	1629.03	430.07	1425.15
2	1	487.96	1473.74	351.50	1180.13	670.61	1849.32		
	2	523.09	1034.26	282.01	965.10	695.12	2849.32		
	3	423.62	1255.31	314.51	1111.2	665.68	2026.71	707.71	1702.35
3	1	434.34	1308.94	351.72	1112.50	604.18	2121.37		
	2	555.92	1377.11	276.54	1114.25	598.82	2228.51		
	3	424.60	916.84	346.69	1154.20	608.01	2123.23	772.93	1860.59
4	1	409.72	998.48	292.30	1059.65	482.82	1716.58		
	2	462.36	1047.61	646.75	1315.50	499.56	1313.20		
	3	853.25	1678.27	326.88	1317.91	517.51	1818.68	771.07	1987.53
5	1	404.47	695.12	264.06	1034.26	570.69	1750.94		
	2	410.05	1086.24	399.87	1772.06	546.07	2228.51		
	3	335.41	1207.49	355.77	965.10	658.35	2175.76	665.68	1334.65
6	1	335.30	1024.08	411.80	1125.63	584.48	1901.85		
	2	638.32	1811.35	434.23	1233.54	711.86	1940.15		
	3	549.58	1525.72	434.23	1233.54	653.10	2071.58	859.82	1738.57
7	1	388.051	1141.94	411.47	1470.79	955.02	2466.96		
	2	387.83	1216.03	425.81	1445.95	753.34	2026.71		
	3	376.01	1473.74	339.68	1400.75	923.84	2411.15	851.17	1621.15
8	1	320.42	1099.26	—	—	594.99	1860.59		
	2	411.47	1424.61	—	—	1174.77	3953.73		
	3	379.95	1381.38	—	—	667.99	1772.06	566.54	1547.39
9	1	—	—	—	—	642.38	1930.19		
	2	—	—	—	—	667.98	2225.22		
	3	—	—	—	—	796.79	1976.92	—	—

Table 44. Summary k_{sat} and fine content on untrimmed base Iowa I-35

Section	Test number	Untrimmed base					
		Static compaction			Low Amplitude vibratory		
		K_{sat} (cm/s)	Fine content (%)		K_{sat} (cm/s)	Fine content (%)	
			0-60 mm	60-200 mm		0-60 mm	60-200 mm
0	1	—	—	—	51.75	—	—
	2	—	—	—	51.60	—	—
	3	—	—	—	75.77	—	—
1	1	178.4	1.69	2.43	158.67	1.22	4.12
	2	41.7	1.70	2.88	121.80	1.17	4.47
	3	48.1	1.46	4.04	70.50	1.89	2.42
2	1	33.77	1.79	1.90	19.52	0.82	4.81
	2	8.0	1.57	3.06	9.8		1.40
	3	14.4	1.14		12.30	2.09	3.92
3	1	89.73	1.31	3.72	27.22		
	2		1.62	3.04		1.55	4.41
	3	41.30	1.01	2.63	25.22	3.13	3.79
4	1	11.20	3.0	5.14	24.50	3.02	—
	2	7.7	2.53	1.55	22.20	2.62	3.98
	3	13.0	1.02		18.30	4.02	—
5	1	19.5	2.74	3.23	55.40	2.29	3.72
	2	172.0	3.20	3.25	27.40	3.62	4.40
	3	14.2	2.18	3.51	28.90	2.84	5.33
6	1	104.2	2.06	2.76	5.30	2.65	4.70
	2	37.60	3.36	3.28	31.90	4.15	3.21
	3	12.1	4.54	3.16	25.60	3.32	3.95
7	1	5.3	2.08	3.57	35.70	3.73	—
	2	27.9	1.39	2.59	22.50	2.46	3.18
	3	11.10	3.40	3.66	39.40	4.69	5.20
8	1	1.7	2.89		53.20	3.12	4.61
	2	66.90	1.03	2.99	4.10	2.90	4.22
	3	8.5	1.84	2.23	31.40	2.48	3.52

Table 45. Summary k_{sat} and fine content on trimmed base Iowa I-35

Section	Test number	Trimmed base			
		Low amplitude		Static compaction	
		K_{sat}	% fine	K_{sat}	% fine
section 0	1	4.4	11.30	—	—
	2	1.2	—	—	—
	3	3.8	—	—	—
section 1	1	3.7	7.63	15.30	7.04
	2	16.5	8.04	19.00	7.36
	3	10.6	9.06		
section 2	1	5.9	7.74	12.50	7.20
	2	12.8	6.19	14.20	7.43
	3	15.5	6.46	19.50	8.03
section 3	1	5.2	8.57	8.60	7.33
	2	7.1	5.37	12.30	9.37
	3	5.8	4.66	12.30	8.28
section 4	1	2.3	6.36	6.50	8.34
	2	2.4	7.63	12.60	8.52
	3	2.4	7.82	9.40	9.85
section 5	1	1.5	7.57	2.70	8.45
	2	1.5	11.52	12.60	9.40
	3		10.71	5.20	9.38
section 6	1	2.1	12.20	17.70	9.58
	2	1.4	9.86	6.40	10.44
	3	1.2	9.79	2.10	11.40
section 7	1	2.1	11.40	3.30	10.43
	2	2.4	10.07	3.20	14.43
	3	1.3	12.73	2.40	11.78
section 8	1	0.6	8.16	0.10	11.50
	2	1	9.22	1.00	12.55
	3	1	9.19	—	—
section 9	1	2.3	9.77	—	—
	2	8.5	9.89	—	—
	3	1.8	9.75	—	—

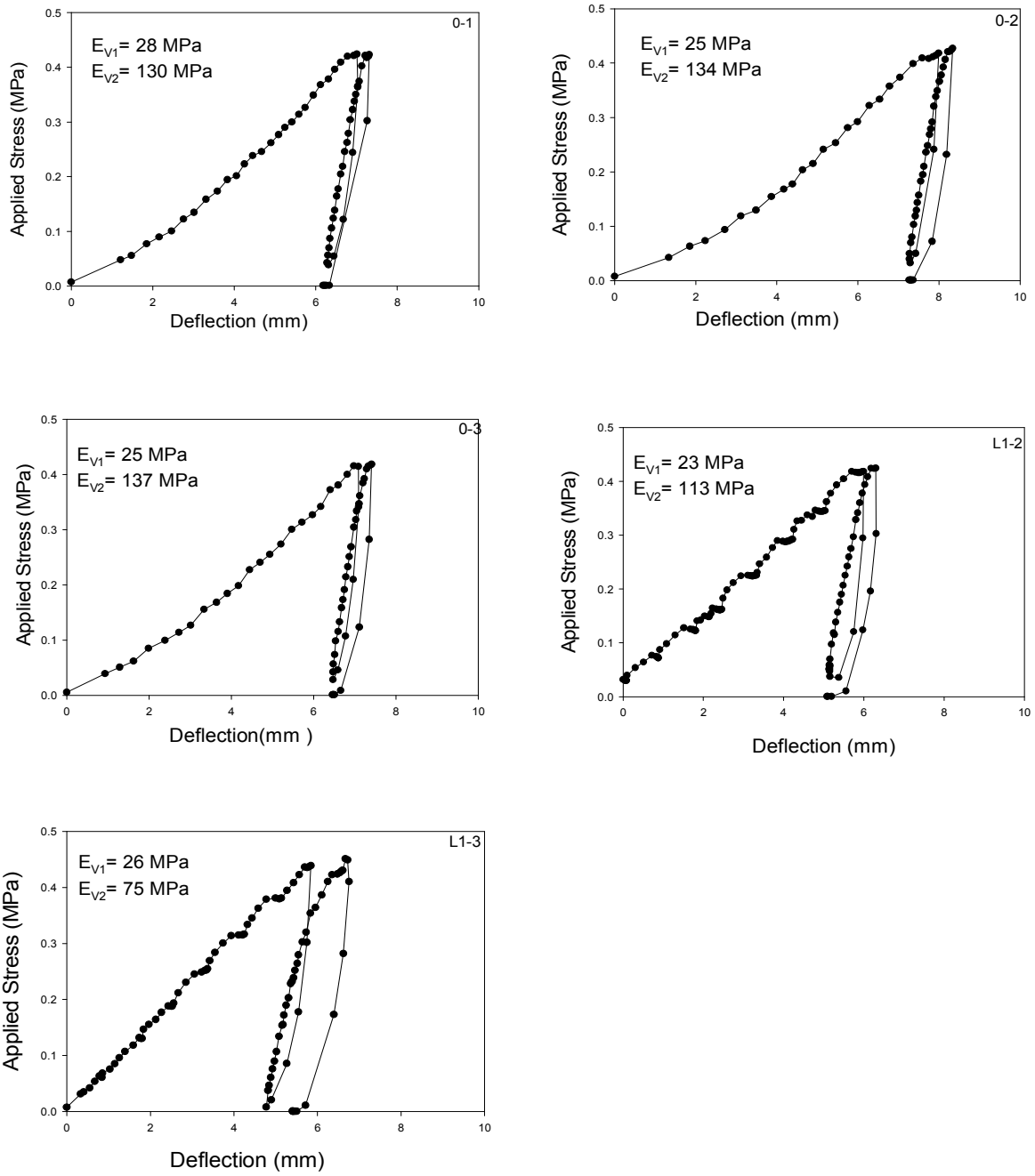

Figure 114. Stress-strain curves on low amplitude vibratory compaction roller section (0, 1) untrimmed base on I-35 Iowa

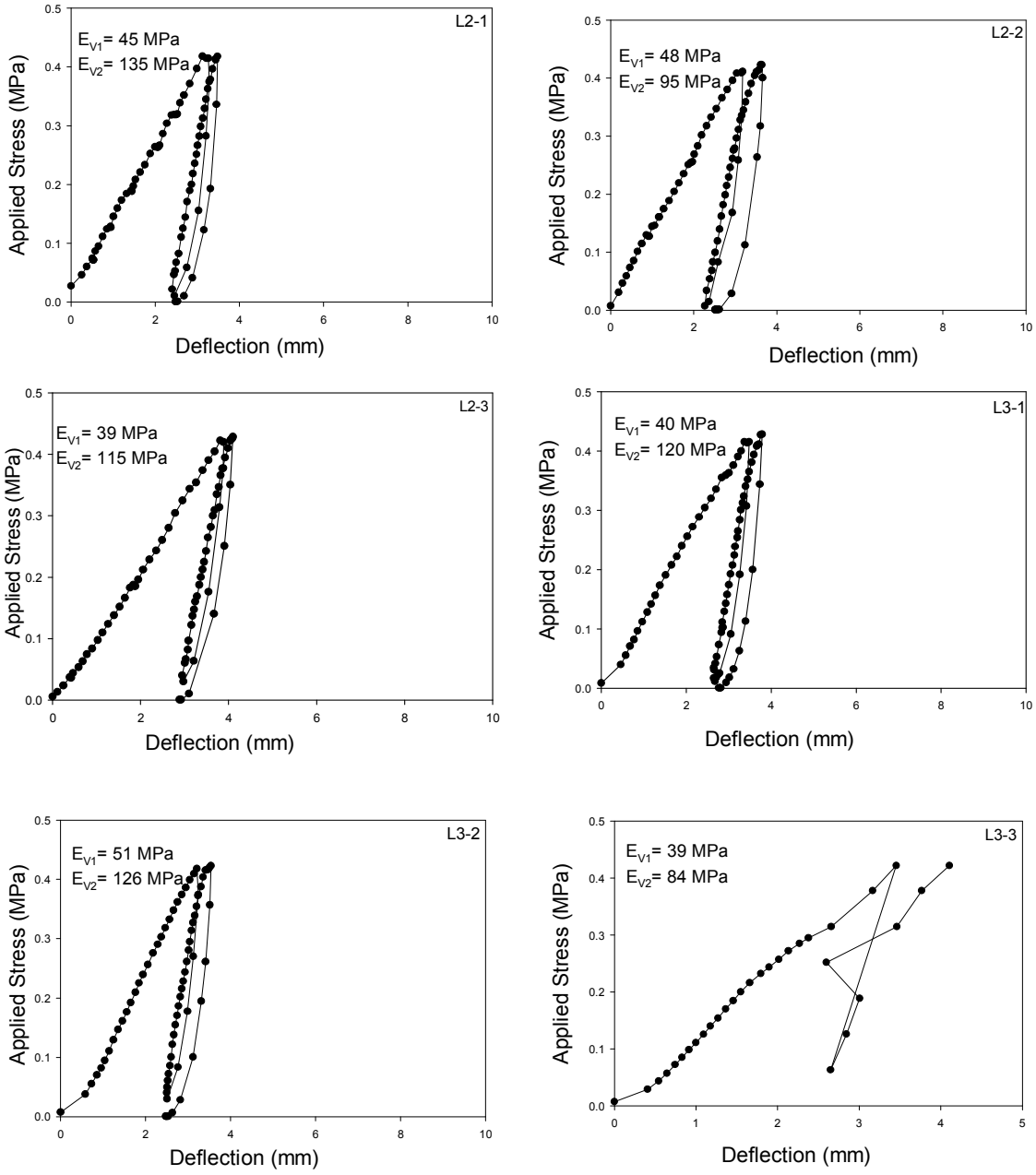

Figure 115. Stress-strain on low amplitude vibratory compaction roller section (2, 3) untrimmed base on I-35 Iowa

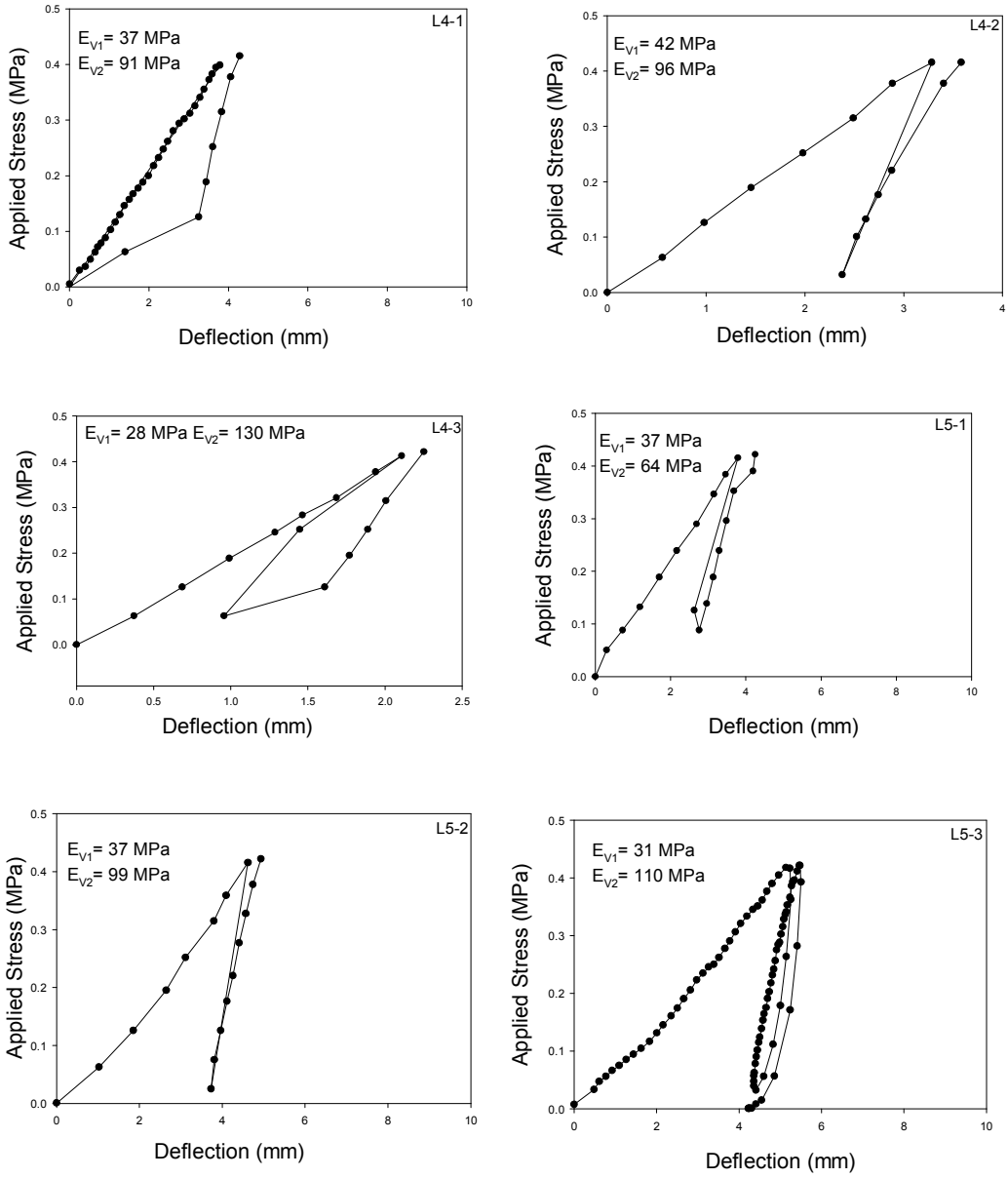

Figure 116. Stress-strain curve on low amplitude vibratory compaction roller section (4, 5) untrimmed base on I-35 Iowa

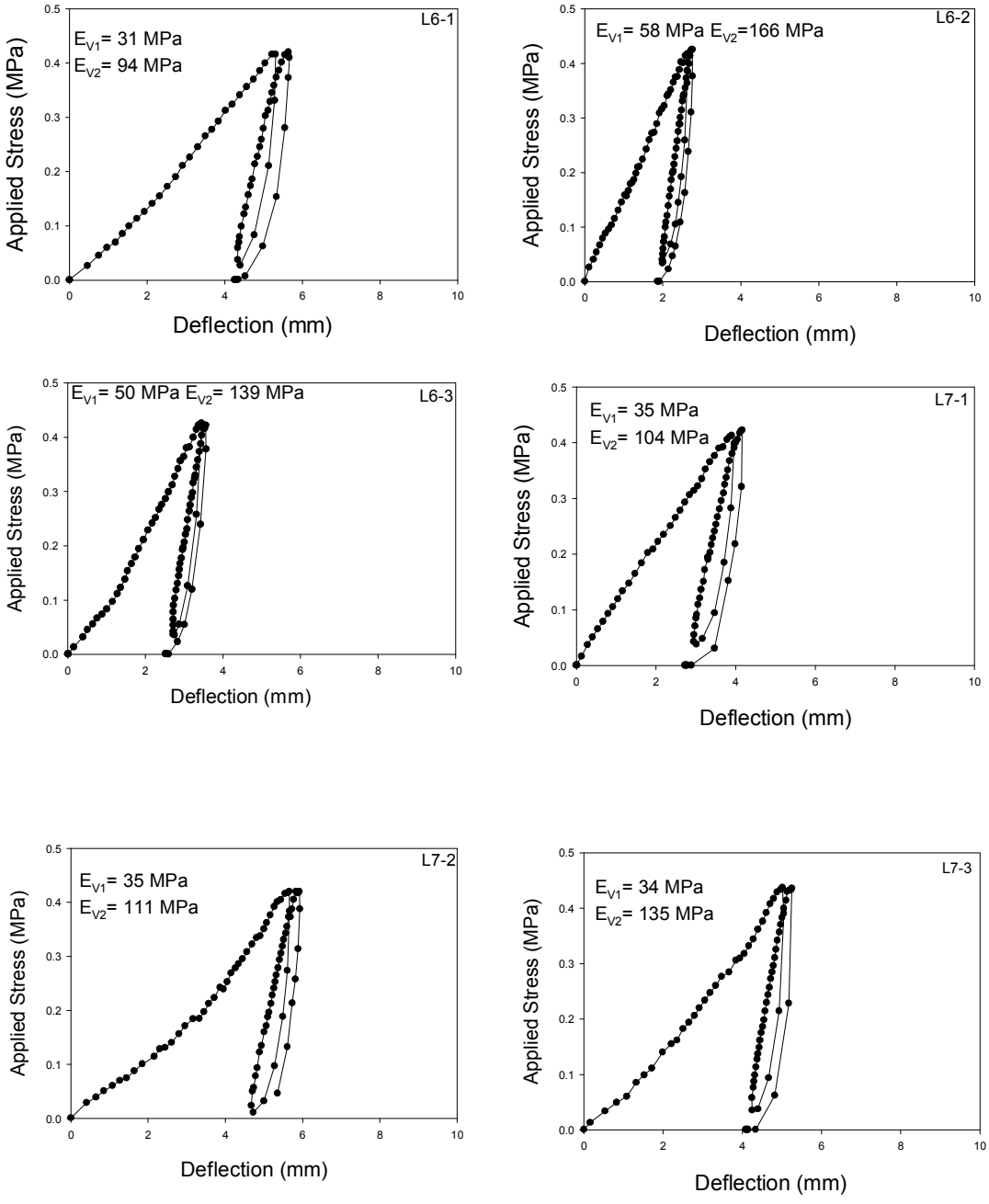

Figure 117. Stress-strain on low amplitude vibratory compaction roller section (6, 7) untrimmed base on I-35 Iowa

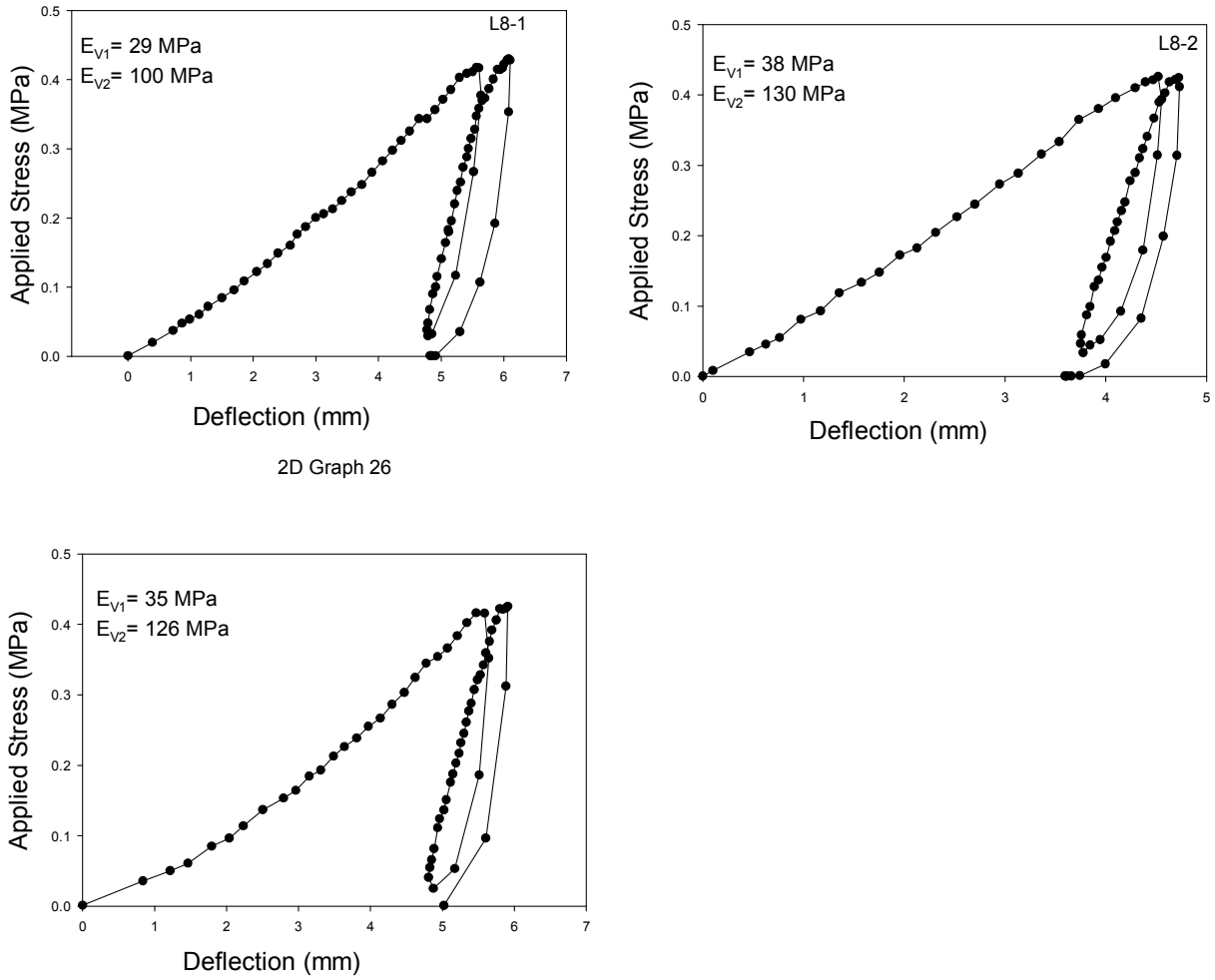

Figure 118. Stress-strain curve on low amplitude vibratory compaction roller section (8, 9) untrimmed base on I-35 Iowa

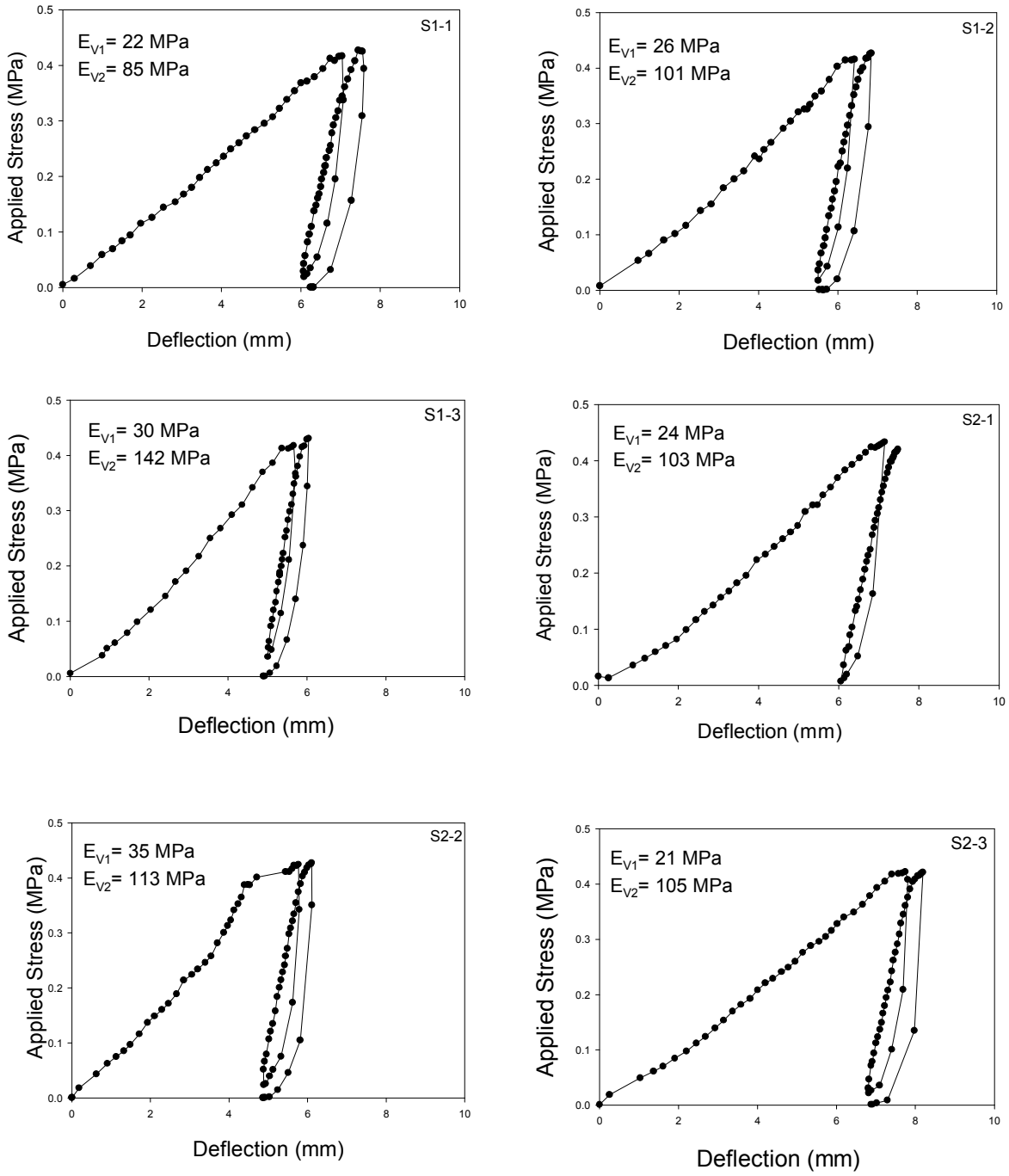

Figure 119. Stress-strain curve on static compaction roller section (1, 2) untrimmed base on I-35 Iowa

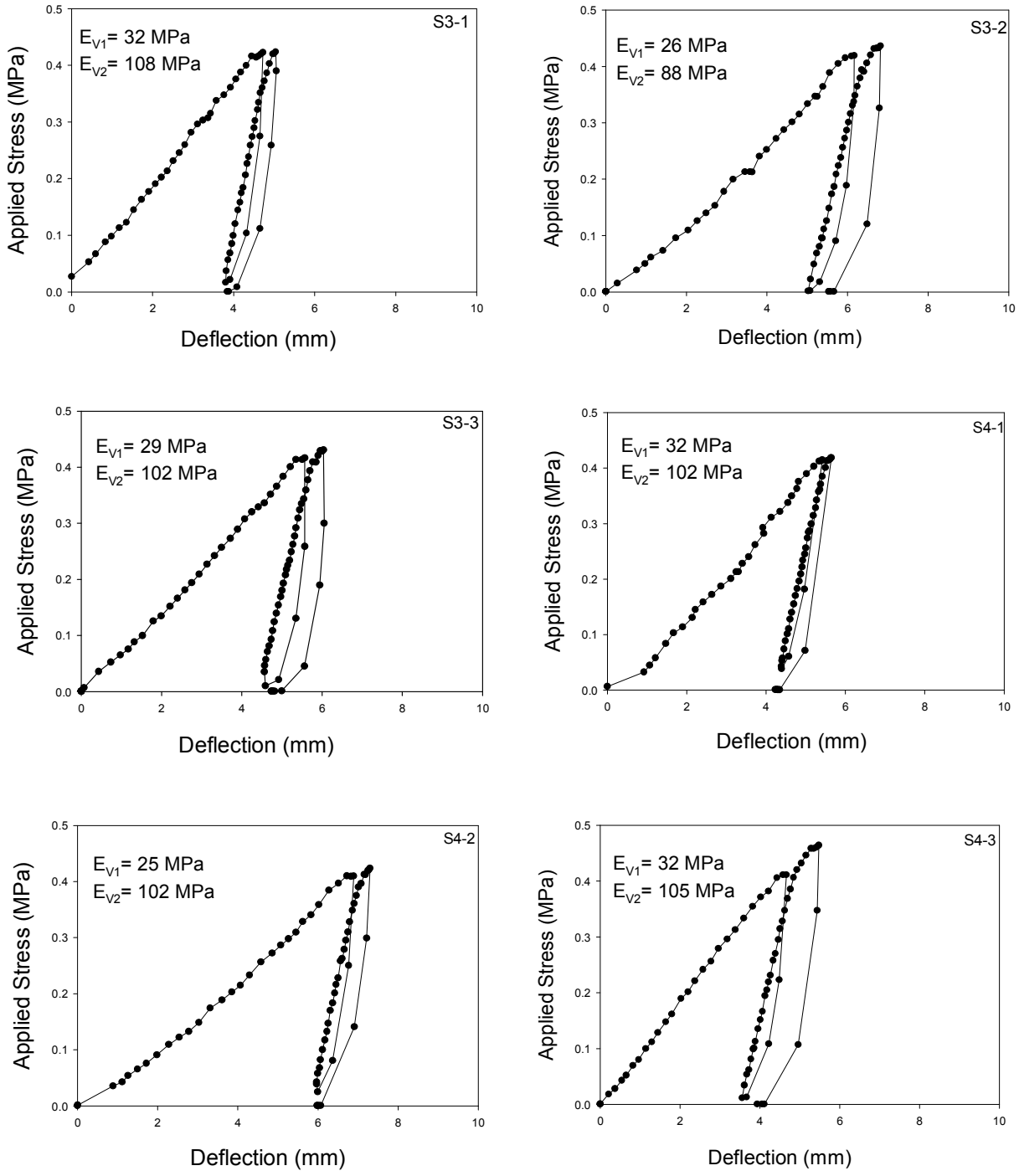

Figure 120. Stress-strain curve on static compaction roller section (3, 4) untrimmed base on I-35 Iowa

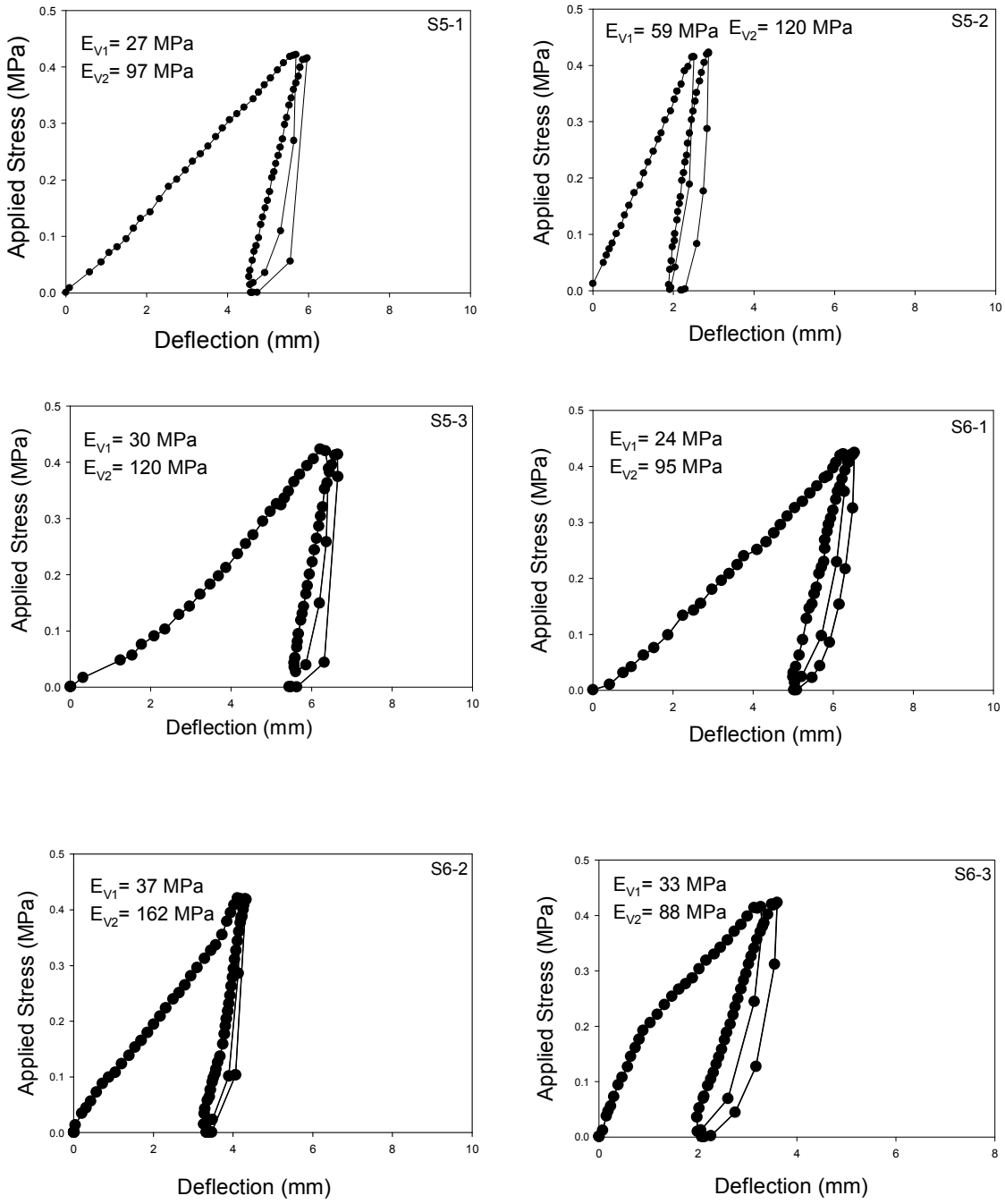

Figure 121. Stress-strain curve on static compaction roller section (5, 6) untrimmed base on I-35 Iowa

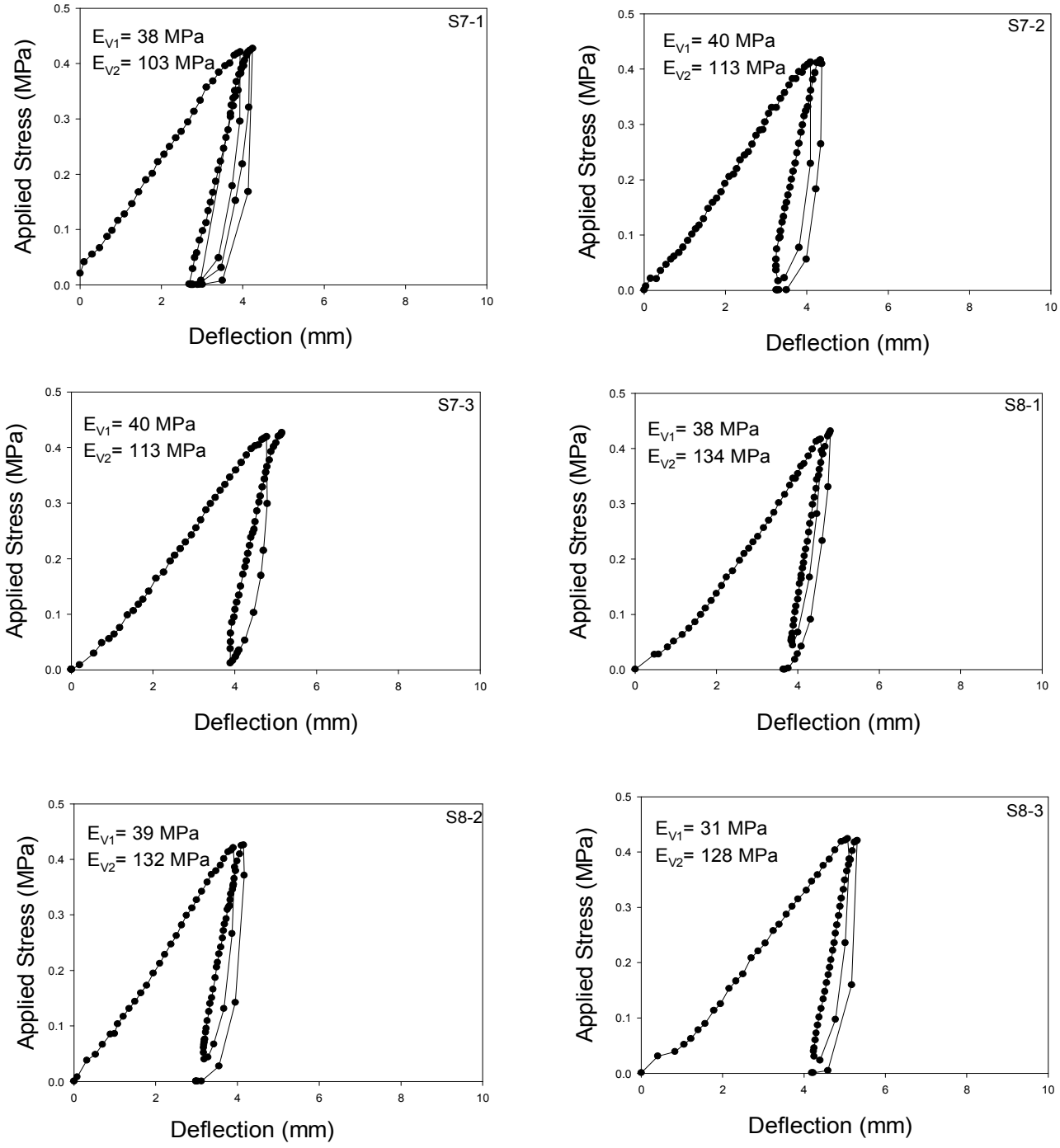

Figure 122. Stress-strain curve on static compaction roller section (7, 8) untrimmed base on I-35 Iowa

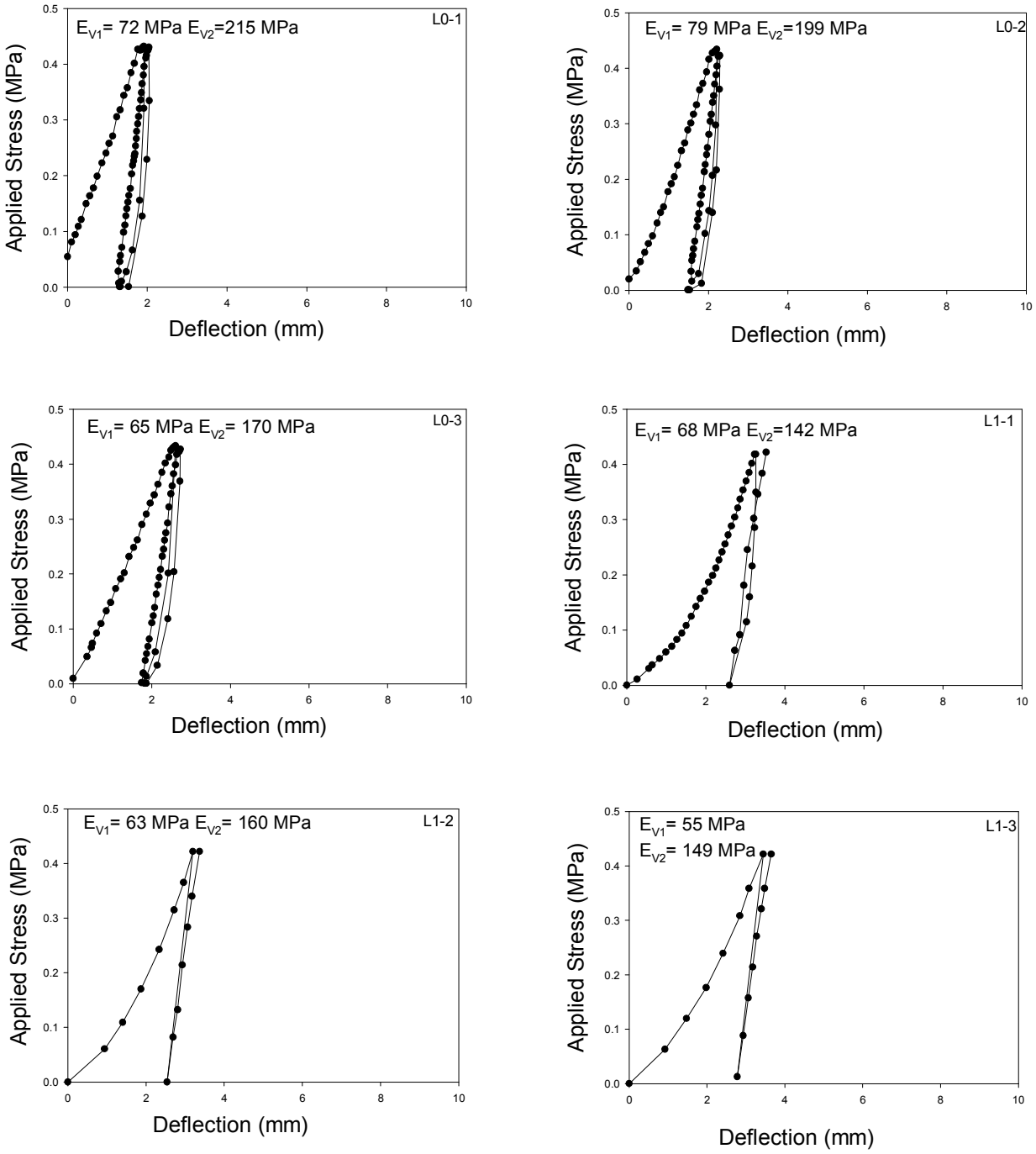

Figure 123. Stress-strain curves on low amplitude vibratory compaction roller section (0, 1) trimmed base on I-35 Iowa

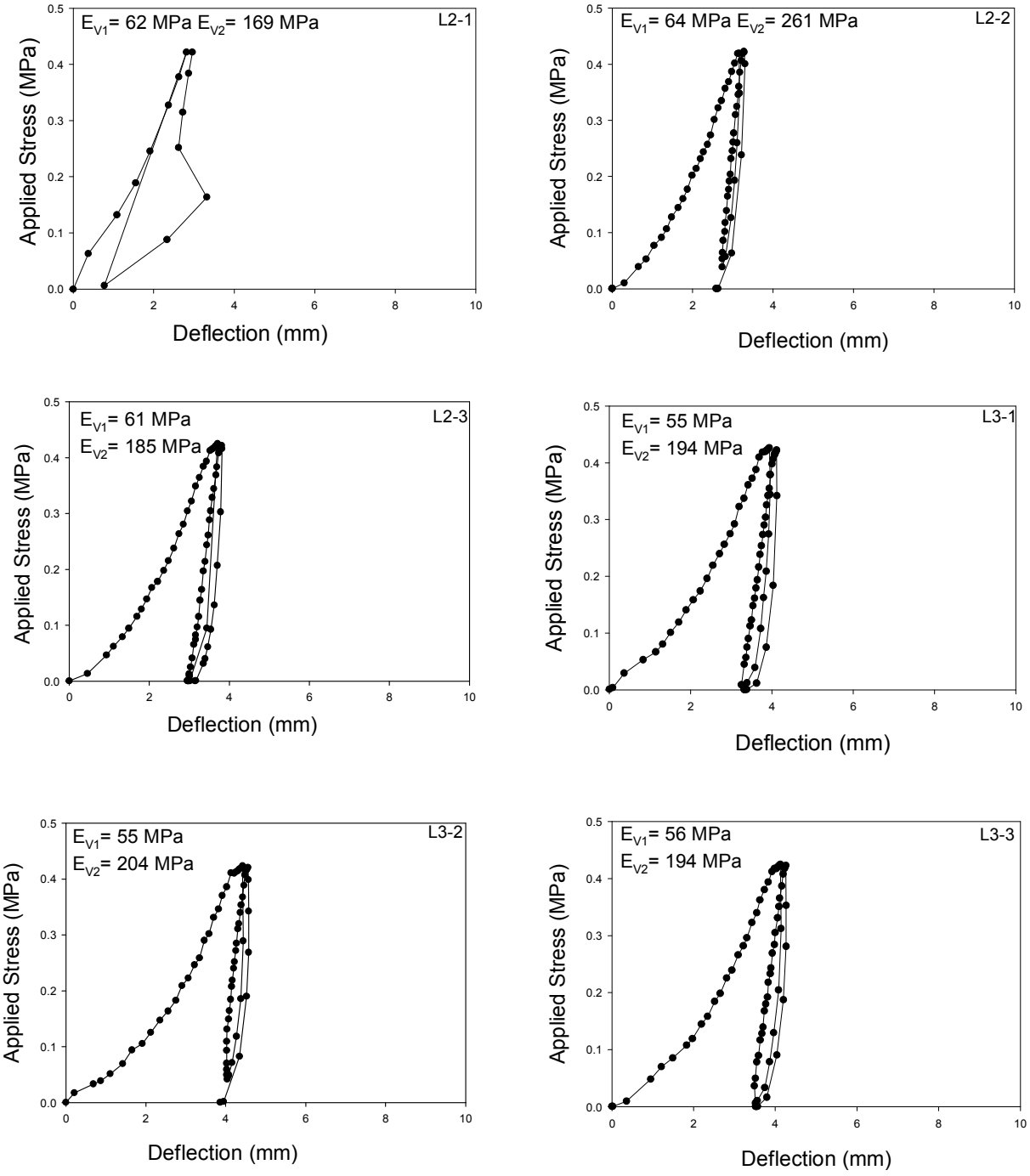

Figure 124. Stress-strain curves on low amplitude vibratory compaction roller section (2, 3) trimmed base on I-35 Iowa

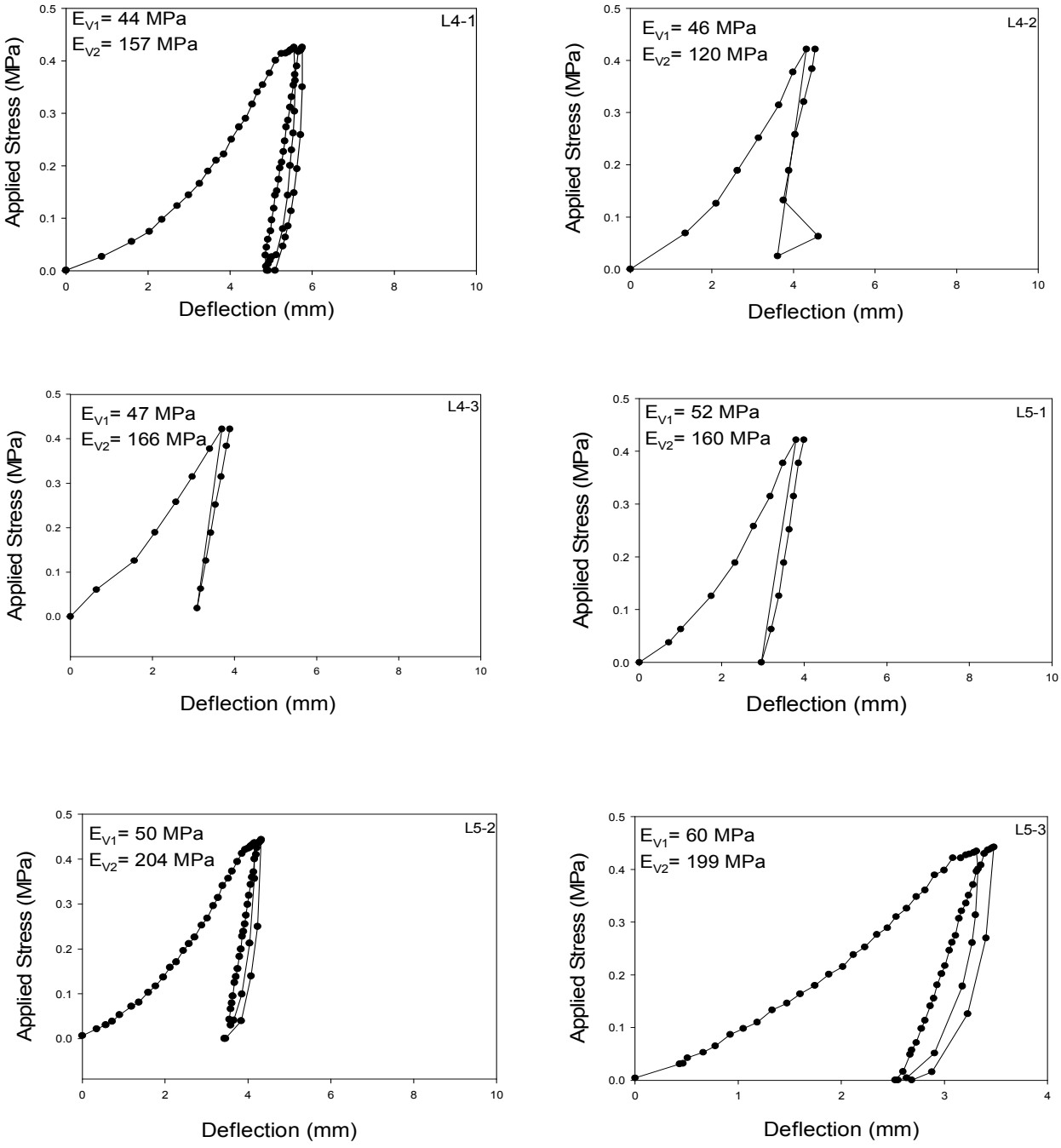

Figure 125. Stress-strain curves on low amplitude vibratory compaction roller section (4, 5) trimmed base on I-35 Iowa

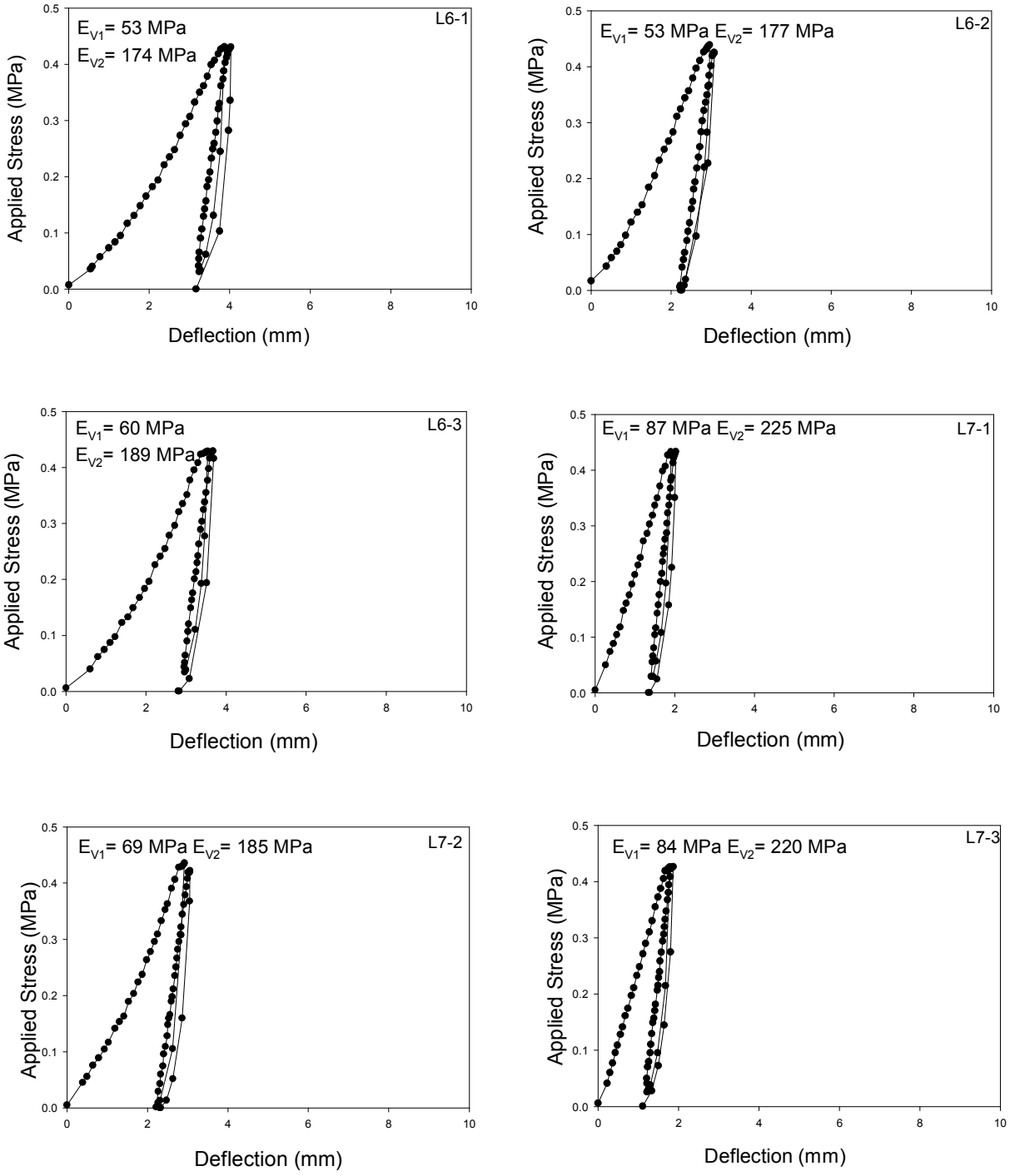

Figure 126. Stress-strain curves on low amplitude vibratory compaction roller section (6, 7) trimmed base on I-35 Iowa

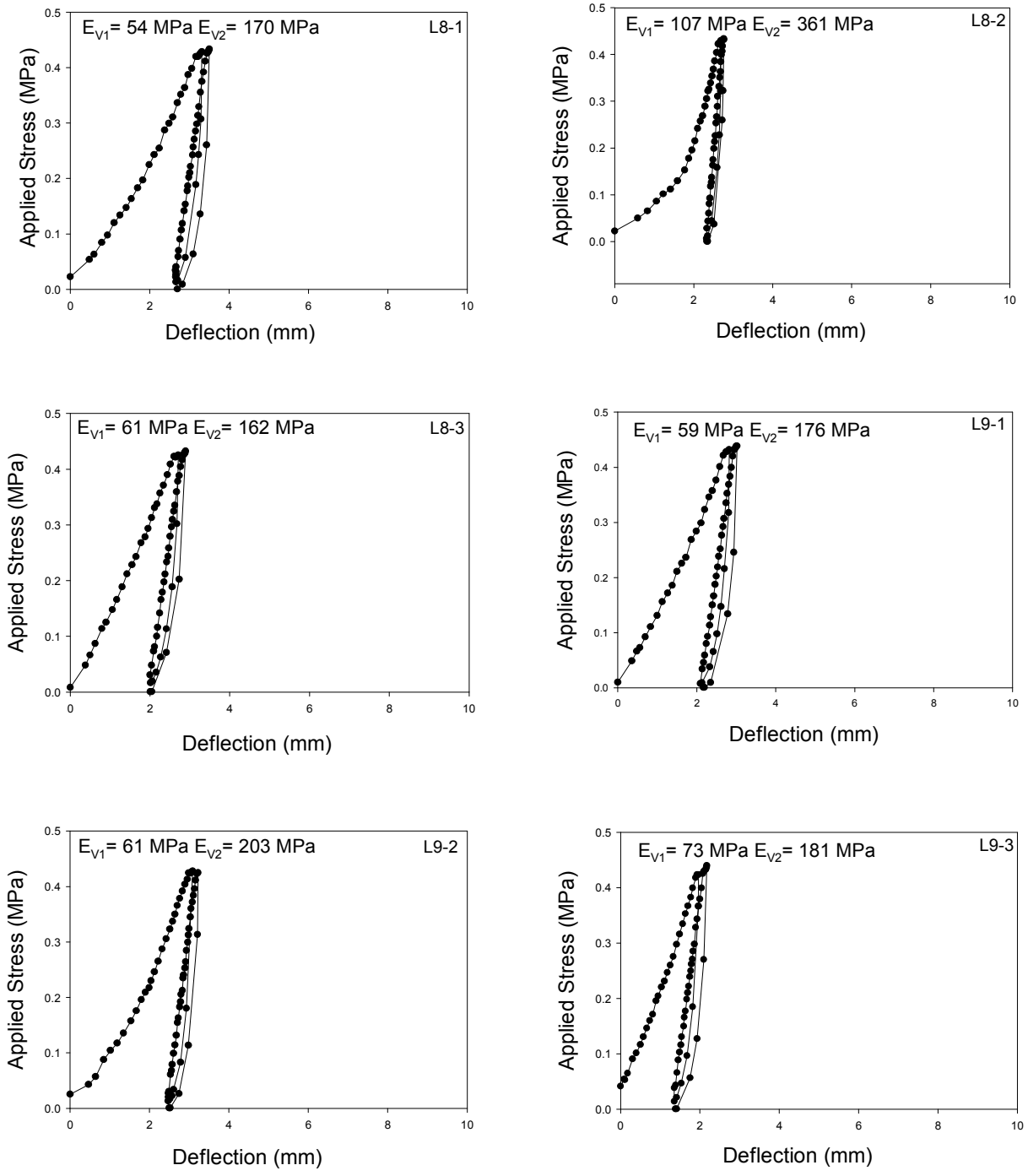

Figure 127. Stress-strain curves on low amplitude vibratory compaction roller section (8, 9) trimmed base on I-35 Iowa

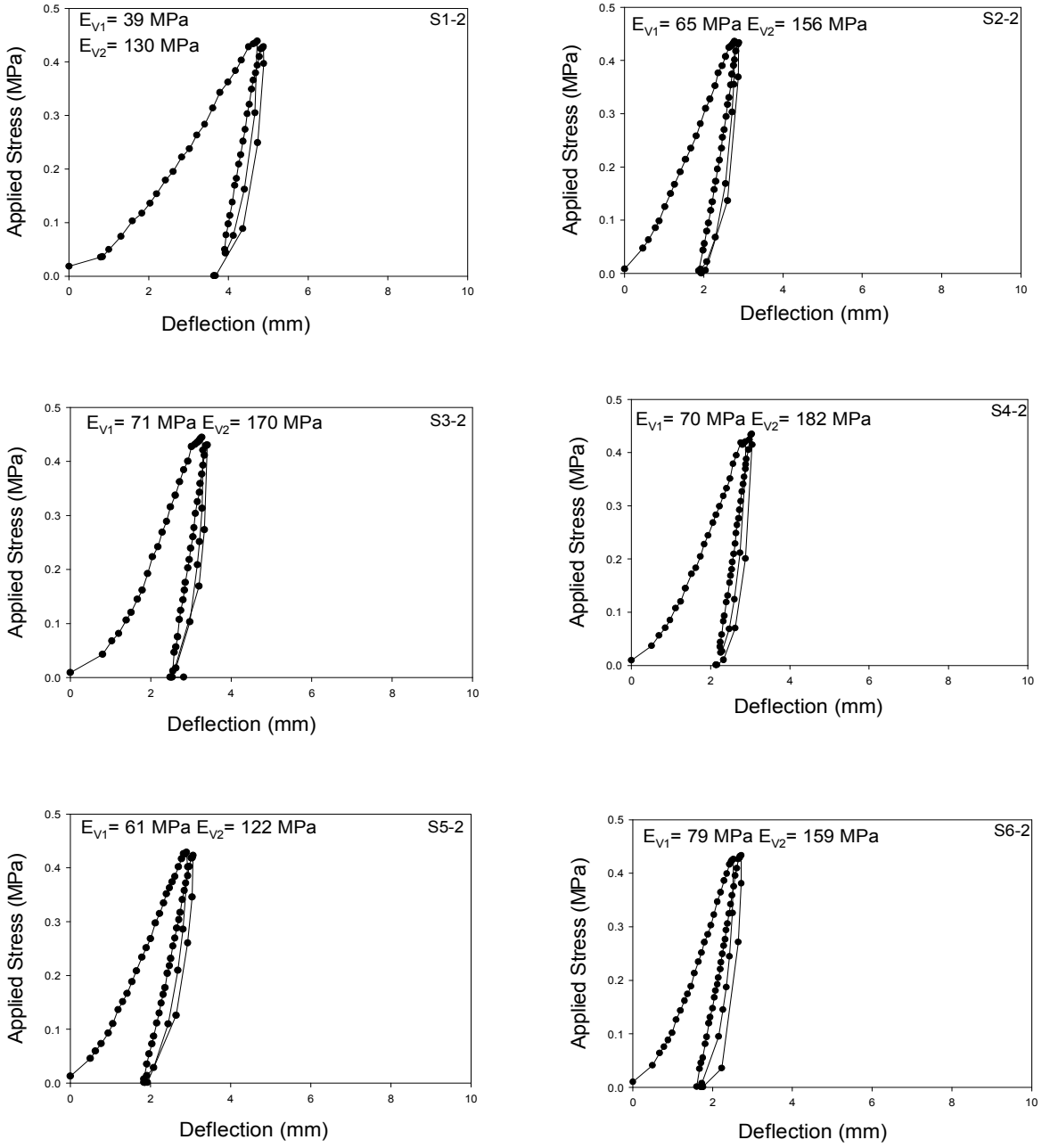

Figure 128. Stress-strain curves on low amplitude vibratory compaction roller section (1, 6) trimmed base on I-35 Iowa

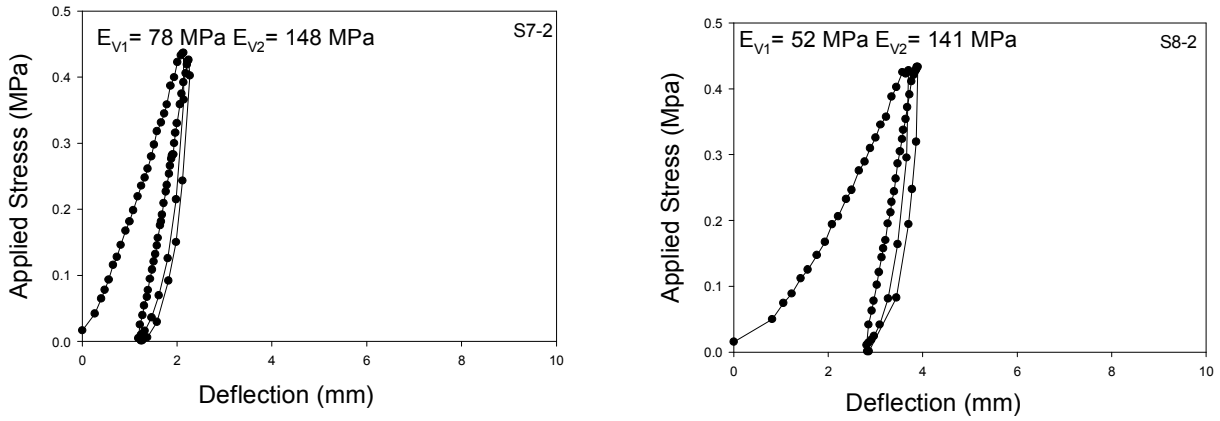

Figure 129. Stress-strain curves on low amplitude vibratory compaction roller section (7, 8) trimmed base on I-35 Iowa

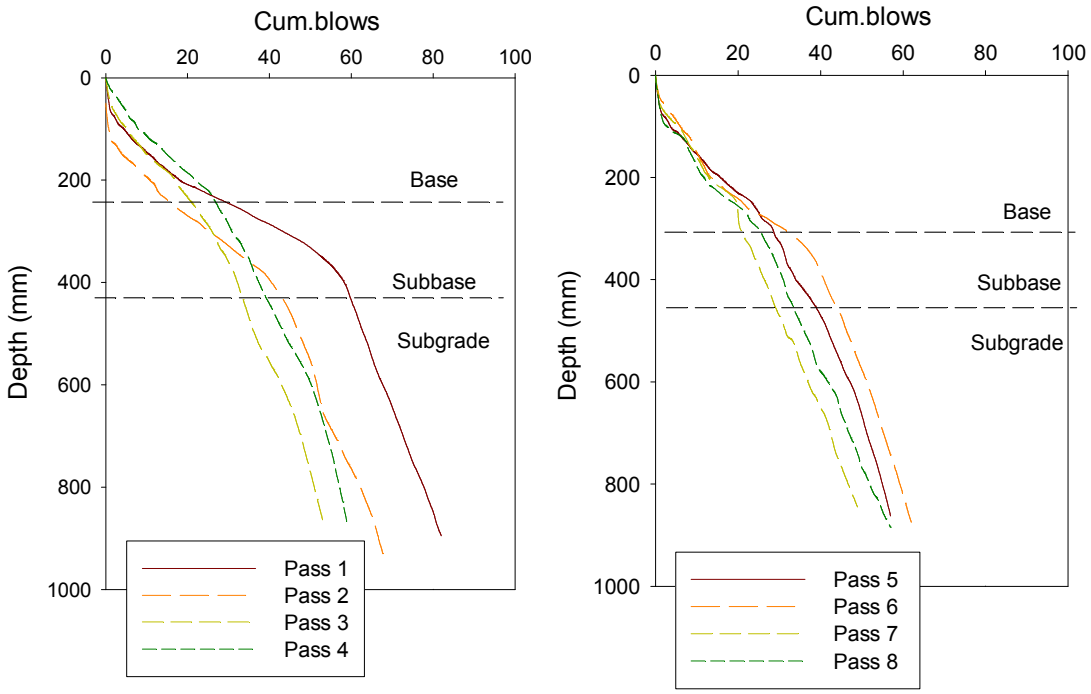

Figure 130. DCP profiles for low amplitute vibratory on untrimmed base of I-35 Iowa

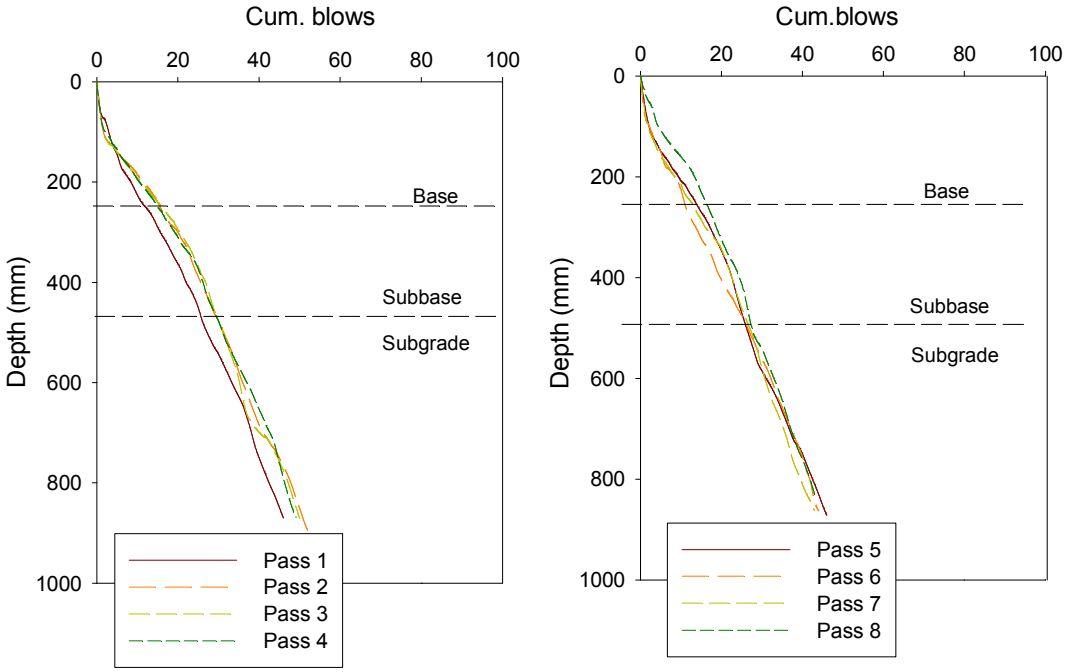

Figure 131. DCP profiles for static compaction on untrimmed base of I-35 Iowa

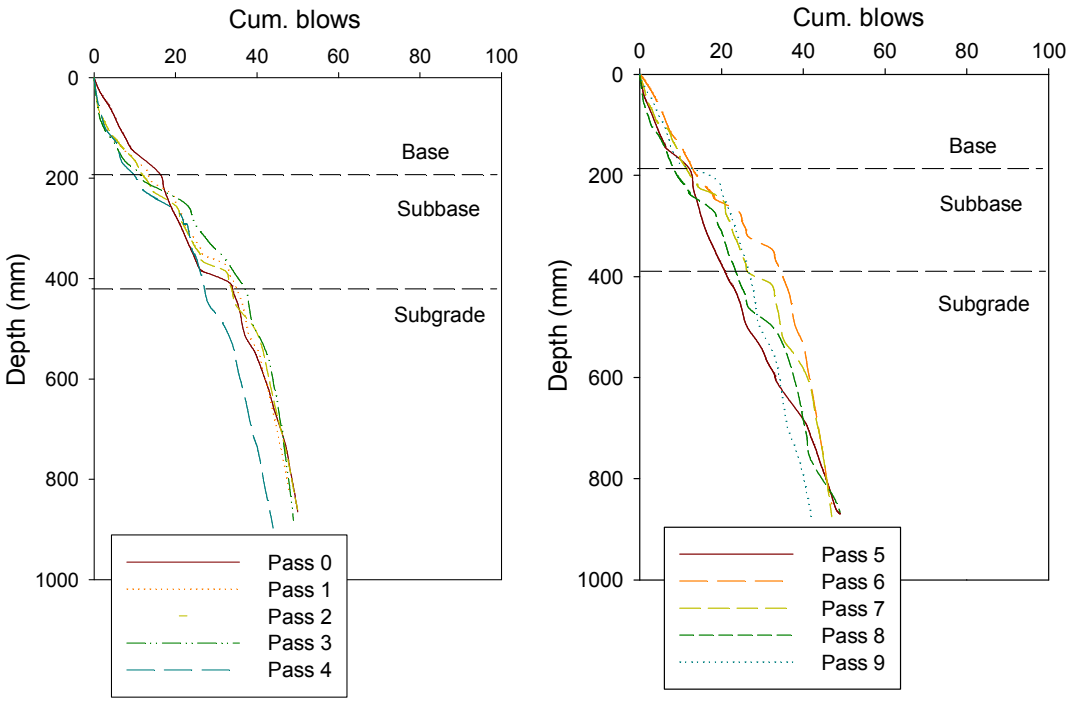

Figure 132. DCP profiles for low amplitute vibratory on trimmed base of I-35 Iowa

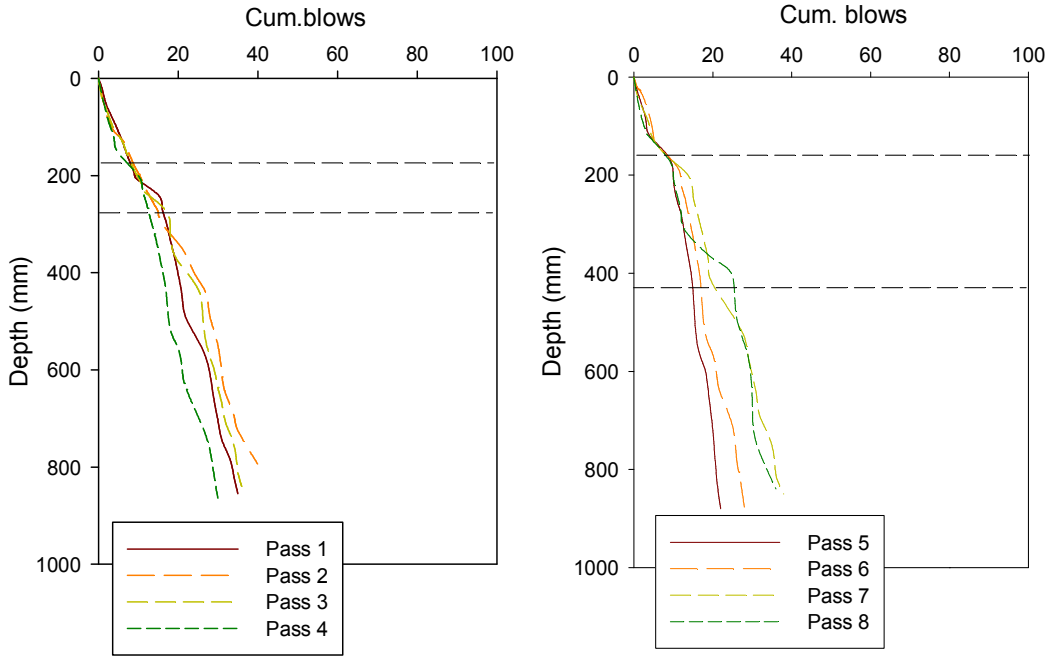

Figure 133. DCP profiles for static compaction on trimmed base of I-35 Iow

METHOD OF TEST

APPENDIX B GPT

IN-SITU GAS PERMEAMETER TEST FOR PAVEMENT BASE AND SUBBASE MATERIALS (ADOPTED FROM NCHRP 2010)

SCOPE

This test method describes the procedure for determining the in-situ saturated hydraulic conductivity of pavement base/subbase materials using the gas permeameter test [GPT] device. Measurements are limited to materials with hydraulic conductivity between 10^{-4} to 10 cm/s.

DEFINITION

Gas Permeability – It is defined as a factor of proportionality between the rate of gas flow and the pressure gradient along the flow distance.

Saturated Hydraulic Conductivity – It is defined as the rate of discharge of water at 20°C under conditions of laminar flow through a unit cross-sectional area of a soil medium under a unit hydraulic gradient.

APPARATUS

The GPT device is shown in Figure 1. The GPT unit is self-contained with two compressed gas cylinders attached to the wheel cart. With two carbon dioxide (CO2) cylinders, more than 50 tests can be performed before refilling the cylinders. The unit can be mounted on to a wheel cart on large rubber wheels to allow for easy transporting and handling in the field. The gas flow is controlled using a regulator and a replaceable precision orifice located inside the ruggedized housing. The gauge pressure at the inlet and the outlet of the orifice are monitored using digital pressure transducers to calculate flow rate. The use of precision orifice to calculate flow rate allows for high precision even at low pressures (i.e., < 1 in of water pressure). The inlet pressure transducer is of 0 to 250 psi range and the outlet pressure transducer is of 0 to 3 in of water [H20] range. The inlet and outlet gauge pressures and calculated flow rate measurements are displayed on a programmable digital display panel attached to the top cover plate. The digital display panel is connected to a rechargeable battery mounted inside the ruggedized housing. Data obtained during the test can be transferred to a computer via the RS-232 port and the auxiliary switch on the top cover plate.

The base plate is fabricated using an abrasive resistant polymer and is replaceable if needed. A polyurethane base seal is attached to the base plate. The test is performed by placing the GPT unit on closed-cell compressible foam to effectively seal the base and prevent gas leakage.

Figure 134. Gas Permeameter Test (GPT) Device

EQUIPMENT

A. GPT Unit
B. Compressed air or CO_2 or nitrogen tank and regulator,
C. ½ in. hose with quick connections at both ends,
D. A wrench to fix the regulator to the compressed air tank,
E. 1 in. thick closed cell compressible foam of 11.5 in. diameter with a 3.5 in. diameter hole in the center.

TEST PROCEDURE

There are several steps required to use the GPT effectively in the field but first, the basic information for using the GPT is listed below (Quick Startup and use of the GPT). Following that will be a more detailed description of the programming details for the device.

The APT device is usually attached to a two-wheeled cart that allows it to be moved quickly into position and lowered onto the surface. Once lowered onto the surface, a "free-float" mechanism on the cart insures the GPT is sitting firmly on the subbase material, kept in place by its own weight. The two-wheeled cart also carries a pair of 20-pound CO_2 cylinders of gas. A step down regulator feeds gas to the GPT faceplate via a flexible hose and quick-connect coupler.

Quick Setup and use of the GPT in the field:

- Assemble the GPT two-wheeled cart; attach CO_2 cylinders and the regulator with the flexible "quick-connect" hose.
- Remove the GPT device from the carrying case and place on the "free-float" pins.
- Attach the CO_2 hose using the "quick-connect" fitting
- Open the CO_2 cylinder valve
- Roll the cart and GPT device to the appropriate location and lower the GPT on the subbase surface (note- the surface is smoothed reasonably flat prior to placement) and make sure it is "free floating" from the cart.

1. Turn on the GPT device, allow for warm-up and start the measuring procedure as follows:
2. Read and record the values for P1, P2 and Flow at a "Zero" P1 level. Note that the P1 and P2 values displayed on the device are $P_{i(g)}$ and $P_{o(g)}$, respectively in the calculations.
3. Turn the Pressure/Flow regulator knob to raise the P1 value and take readings at various points – allow the P1 pressure to stabilize prior to recording P2 or Vol.

General Data Collection Procedure:

The GPT is currently set up to collect and store the data using the following procedure.

1. Connect the APT to a computer using HyperTerminal (a standard Windows program)

2. Test the connection by turning on the GPT while the serial cable is connected and the following message will appear on the screen

   HI-Q by OTEK
   Ver. 3.03
   Address: '01'
   Warming up...done
   *

Data Collection Procedure:

1. Start up HyperTerminal (using the PUFF2 program to connect)

2. Go to the TRANSFER option on the Menu (Upper portion of the screen)

3. Select Capture Text

4. A "Capture Text" box will open

5. Name the file and provide a location

6. Select START

7. The box will close and the system is ready to start collecting data

8. Press the MENU button on the meter panel face to Reset the Counter/Timer to Zero and collect the 1st data set

9. Turn up the regulator as required

10. Press the ENTER button to collect the 2nd set of data and all subsequent data at a particular location.

11. When done collecting data at a particular location, there are 2 options to consider for additional locations.

Option #1 – saving each data set in a separate File

At this point you can either STOP the data collection by going to the Menu/ Capture Text and choosing STOP. This will stop the data collection process

and save the data file to your original file name.

Option #2 – saving data continuously in a single file with the data separated by a ZERO in the Time Line

Go to the next test point

Press the MENU button the meter panel (this generates the 1st data set for that location and places a ZERO in the TIME Line location (use this to help separate data sets)

Press the ENTER button to collect the 2nd set of data and all subsequent data at a particular location.

Collect data – make notes on what you have done to keep track.

HIQ-126 OTEK Digital Meter Setup and Programming Notes:

The HIQ-126 OTEK Digital Meter is programmable using Hyper Terminal software. The device will need to be programmed whenever the orifice diameter, type of gas (e.g., Air, CO_2, or Nitrogen), units of measure or decimal point location is changed. In some cases the program may need to be reloaded if the battery is allowed to run too low on power. If the digital meter display starts blinking, it may be a sign of low battery voltage. Shut the unit OFF and plug in the AC charger. Check to see if the program and sub-routines are still in place before additional use. It will require reprogramming if the internal algorithms are modified. Internal algorithms determine how input data is manipulated or used for other inputs.

Programming the HIQ-126 (OTEK Digital Meter) requires a computer for communication with the digital meter via the Hyper Terminal program (which is a standard Microsoft Windows interface program). Communication is handled via a panel mounted RS-232 interface plug (DB-9 connector) on the device faceplate. In addition, the following programs or hardware will be needed or useful:

- Text Editor - Note Pad, TextPad or Word – used to write new programs, review or edit data
- HIQ-126 (OTEK Digital Meter OTEK) manual. Refer to the HIQ-126 manual for details.

- Excel spreadsheet program - an effective way to analyze and graph data.
- Laptop computer - used for collection of field data.

The HIQ –126 meter uses 3 digital meters to display the information from the GPT.

- Display # 1 – Top - displays the Input value of Pressure P1 – PSIG ($P_{i(g)}$ in the calculations)
- Display # 2 – Middle - displays the Chamber Back Pressure P2 Inches of Water ($P_{o(g)}$ in the calculations)
- Display # 3 – Bottom - displays the Flow Rate of the test gas Cubic Feet/Hour – Calculated (Q in the calculations)

The program codes developed for GPT (A)(B)(C)(D) and air, nitrogen, and CO_2 gases are provided in Appendix B. These codes are transferred to the HIQ-126 OTEK Digital Meter using the Hyper Terminal program. The steps involved in the programming are as follows:

1. Save the appropriate program codes provided in Appendix B as a *.txt file
2. Start the HyperTerminal (using the PUFF2 program to connect)
3. Go to the TRANSFER option on the Menu (Upper portion of the screen)
4. Select Send Text File and select the text file saved as part of Step 1

The program code will appear in the hyper terminal program. After the programming is finished, the GPT device is ready for measurements.

CALCULATIONS

Determine the Geometric Factor (G_o) based on the estimated thickness of the aggregate layer (L) at the test location using Figure 135.

Use the range of saturation values provided in Table 46 to estimate S for the calculations. For better accuracy, determine the in-situ dry density and moisture contents at each test location and calculate S using equation A.

$$S = \frac{G_s w}{\left(\frac{G_s \gamma_w}{\gamma_d} - 1\right)} \qquad [A]$$

Where:

S = Degree of saturation

G_s = Specific gravity (Assume 2.70 if unknown)

w = Moisture content

γ_w = Unit weight of water (62.4 pcf)

γ_d = Dry unit weight of the material (pcf)

A. Calculate the saturated hydraulic conductivity K_{sat} (cm/sec) using equation B:

$$K_{sat} = \left[\frac{2\mu_{gas} Q P_1}{r G_o \left(P_1^2 - P_2^2\right)}\right] \times \frac{\rho g}{\mu_{water}\left(1 - S_e\right)^2 \left(1 - S_e^{((2+\lambda)/\lambda)}\right)} \qquad [B]$$

where:

K_{sat} = Saturated hydraulic conductivity (cm/sec)

μ_{gas} = Kinematic viscosity of the gas (Pas) (CO_2: 1.48E-05, Air: 1.83E-05, Nitrogen: 1.78E-05)

P_1 = Absolute gas pressure on the soil surface (Pa) = $P_{o(g)}$ * 250 + 101325

$P_{o(g)}$ = Gauge pressure at the orifice outlet (inches of H_20)

P_2= Atmospheric pressure (Pa) = 101325

Q = flow rate (cm^3/s)

r = radius at the outlet (cm) = 4.45

G_0 = Geometric factor determined from Figure 135

μ_{water} = Absolute viscosity of water (g/cm-s) = 0.01

ρ = Density of water (g/cc) = 1

g = Acceleration due to gravity (cm/s^2) = 981

S_e = Effective saturation [$S_e = (S - S_r)/(1-S_r)$]

S = Field saturation (from step B)

S_r = Residual saturation (determine based on soil type from Table 47)

λ = Brooks-Corey pore size distribution index (determine based on soil type from Table 47)

A sample calculation sheet and an example calculation are provided below.

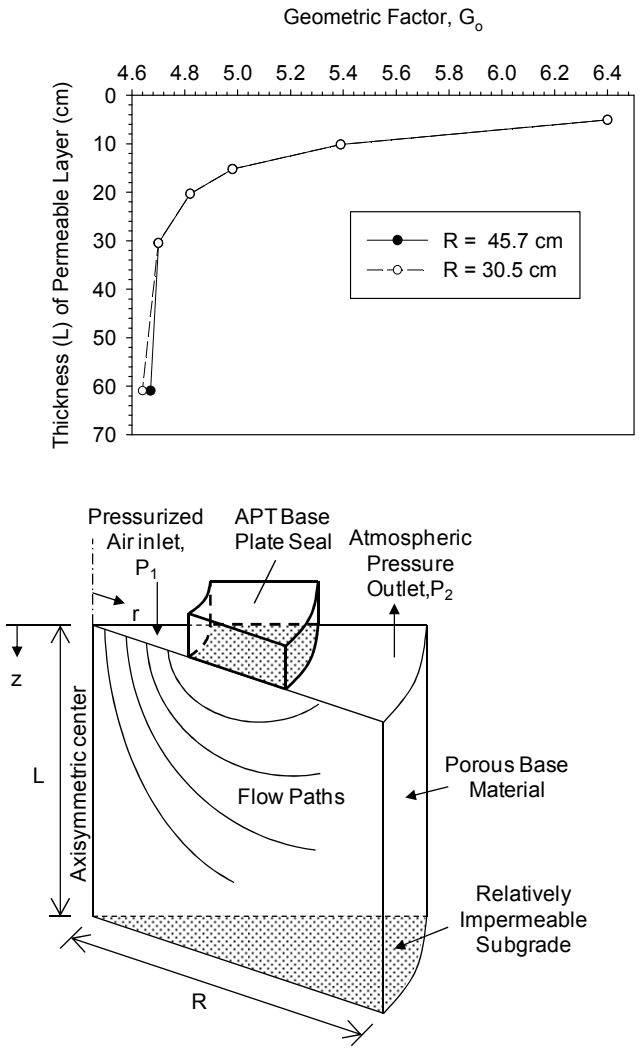

Figure 135. Graph to determine Geometric factor G_o for GPT Device

Table 46. Summary of typical field saturation values reported in the literature for granular base/subbase materials

Material Type	Classification (USCS, AASHTO)	Field Saturation, S (%)†	
		Mean	COV (%)
Crushed Lime Stone	GP-GM, A-1-a	16	20
Reclaimed Asphalt	GP-GM, A-1-a	28	49
Crushed Recycled Concrete	GW-GM, A-1-a	45	9
Crushed Lime Stone	GP-GC, A-1-a	19	17
Crushed Recycled Concrete	GP, A-1-a	37	19
Crushed Gravel	SP-SM, A-1-b	53	9
Crushed Gravel	SP-SM, A-1-b	44	31
Flex Base Material	GP-GM, A-1-a	58	15
Crushed Sandstone	GW	62	9
Crushed Limestone	GP-GM, A-1-a	36	19
Crushed Slag	GP-GM, A-1-a	24	24
Cement Treated Base	GP, A-1-a	35	15

†field saturation values determined from in-situ moisture and density measurements using a nuclear gauge.

Table 47. Summary of residual saturation and pore size distribution index values reported in the literature and typical values calculated for granular materials

Material Type or USCS Classification	Residual Saturation (S_r)	Pore Size Distribution Index, λ
Touchet Silt Loam[1]	18 to 22	1.02 to 1.70
Columbia Sandy Loam[1]	18 to 22	1.27 to 1.70
Unconsolidated Sand[1]	8 to 9	4.02 to 4.75
Volcanic sand[2]	16	2.29
Fine sand[2]	17	3.7
Glass beads[2]	9	7.3
Natural Sand Deposits[2]	—	4
Crushed Granite[2]	—	0.33 to 0.36
Crushed Shale[2]	—	0.23 to 0.27
Crushed Limestone[2]	—	0.22 to 0.31
Range of values for typical filter materials and open graded bases (5)		
SW (Filter Materials)	10 to 11	0.65 to 2.15
SP (Filter Materials)	10	11.15
GP (Open Graded Bases)	1 to 2	17.26 to 18.20
Range of values determined for granular materials used in this study		
SP	10	2.20 to 4.08
SW-SM	11	0.54
GP	2 to 5	3.65 to 4.62
GP-GM	11 to 15	0.59 to 0.98

(1) G.E. Laliberte, A.T. Corey, and R.H. Brooks. Properties of Unsaturated Porous Media. Hydrology Papers, No. 17, Colorado State University, Fort Collins, Colorado, 1966.

(2) R.H. Brooks and A.T. Corey. Hydraulic Properties of Porous Media. Hydrology Papers, No. 3, Colorado State University, Fort Collins, Colorado, 1964.

(3) S.F. Averjanov. About Permeability of Subsurface Soils in Case of Incomplete Saturation," Engineering Collection, Vol. 7, as Quoted by P. Ya Palubarinova, 1962. The Theory of Ground Water Movement (English Translation by I. M. Roger DeWiest. Princeton Univer

(5) H.R. Cedergren, J.R. Arman, and K.H. O'Brien. *Development of Guidelines for the design of Subsurface Drainage Systems for Highway Structural Systems.* Final Report, Federal Highway Administration, Washington, D.C., February 1973.sity Press, Princeton, NJ), pp. 19–21. 1950.

ACKNOWLEDGEMENTS

I would like to thank all the people who have helped and inspired me during my master's study, to only some of whom it is possible to give particular mention here.

First and foremost I offer my deepest appreciation to my advisor, Dr. David White, who has supported me throughout my master's study with his stimulating suggestions and encouragement. The completion of this project would not have been possible without his contributions of time, ideas, and funding. The enthusiasm he has for research motives me throughout my study. I would also like to express my gratitude to my committee members Dr. Vennapusa, Dr. Schaefer, and Dr. Gu, for their valuable suggestions and constructive comments on my work.

I would like to thank Dr. Vennapusa, Heath Gieselman, Dr. C. White, and all the other members of Dr. White's research team for their cooperation and invaluable help. I am grateful to all my friends in Iowa State University for all the emotional support, entertainment, and caring they provided.

Finally, I want to express my appreciation to my parents, Tieshuan Zhao and Juanli Du, my brother Chen Zhao, and my boyfriend Yang Gu for their love, understanding, patience, endless support, and never failing faith in me. To them I dedicate this thesis.